

5. SITE 689¹

Shipboard Scientific Party²

HOLE 689A

Date occupied: 15 January 1987; 1552 local time
Date departed: 16 January 1987; 0800 local time
Time on hole: 16 hr, 8 min
Position: 64°31.009'S; 03°05.996'E
Bottom felt (rig floor: m, drill pipe): 2091
Distance between rig floor and sea level (m): 11
Water depth (drill-pipe measurement from sea level, m): 2080
Penetration (m): 11.8
Number of cores: 1
Total length of cored section (m): 9.5
Total core recovered (m): 9.35
Core recovery (%): 98
Oldest sediment cored:
Depth sub-bottom (m): 11.8
Nature: Diatom ooze
Age: middle Pliocene

HOLE 689B

Date occupied: 16 January 1987; 0800 local time
Date departed: 18 January 1987; 0445 local time
Time on hole: 44 hr, 45 min
Position: 64°31.009'S; 03°05.996'E
Bottom felt (rig floor: m, drill pipe): 2091
Distance between rig floor and sea level (m): 11
Water depth (drill-pipe measurement from sea level, m): 2080
Penetration (m): 297.3
Number of cores: 33
Total length of cored section (m): 297.3
Total core recovered (m): 229.44
Core recovery (%): 77
Oldest sediment cored:
Depth sub-bottom (m): 297.3
Nature: Chert
Age: late Campanian
Measured velocity (km/s): 2.040

HOLE 689C

Date occupied: 18 January 1987; 0445 local time
Date departed: 18 January 1987; 1215 local time

Time on hole: 7 hr, 30 min
Position: 64°31.009'S, 03°06.026'E
Bottom felt (rig floor: m, drill pipe): 2091.3
Distance between rig floor and sea level (m): 11
Water depth (drill-pipe measurement from sea level, m): 2080
Penetration (m): 27.6
Number of cores: 3
Total length of cored section (m): 27.6
Total core recovered (m): 20.54
Core recovery (%): 74
Oldest sediment cored:
Depth sub-bottom (m): 27.6
Nature: Diatom ooze
Age: late Miocene

HOLE 689D

Date occupied: 18 January 1987; 1215 local time
Date departed: 19 January 1987; 0935 local time
Time on hole: 21 hr, 20 min
Position: 64°31.009'S; 03°06.026'E
Bottom felt (rig floor: m, drill pipe): 2091.3
Distance between rig floor and sea level (m): 11
Water depth (drill-pipe measurement from sea level, m): 2080
Penetration (m): 133.8
Number of cores: 12
Total length of cored section (m): 115.7
Total core recovered (m): 115.97
Core recovery (%): 100
Oldest sediment cored:
Depth sub-bottom (m): 133.8
Nature: Nannofossil ooze
Age: late Eocene

Principal results: Site 689, near the crest of Maud Rise, was occupied from 15 to 19 January 1987. Four holes were drilled: Hole 689A consists of a single advanced piston corer (APC) core from 2.3 to 11.8 mbsf (meters below seafloor); Hole 689B consists of 21 APC cores from 0 to 197.5 mbsf and 12 extended core barrel (XCB) cores from 197.5 m to 297.3 mbsf; Hole 689C consists of 3 APC cores from 0 to 27.6 mbsf; and Hole 689D consists of 12 APC cores from 18.1 to 133.8 mbsf. The quality of the cores is generally excellent with marked disturbance only in the uppermost cores of each hole. Hole 689B was abandoned at an estimated 25–45 m above basement, when progress in drilling cherty layers became too slow.

The sedimentary sequence is exclusively pelagic, biogenic in origin, and ranges in age from late Campanian?–early Maestrichtian (~75 Ma) at the base to Quaternary at the top. The preliminary biostratigraphy and the magnetostratigraphy indicate the presence of brief sedimentary hiatuses or highly condensed sequences throughout the section. These occur in the upper Danian (calcareous nannofossil Zones CP4 and CP6); uppermost Paleocene to Eocene (CP9–

¹ Barker, P. F., Kennett, J. P., et al., 1988. *Proc. ODP, Init. Repts.*, 113: College Station, TX (Ocean Drilling Program).

² Shipboard Scientific Party is as given in the list of participants preceding the contents.

CP11); uppermost Eocene (CP15b); tentatively uppermost Oligocene to lowermost Miocene; and upper Pliocene to Quaternary. Site 689 provides a fine biostratigraphic sequence that will form, in conjunction with Site 690, the southernmost anchor for Atlantic biostratigraphy, biogeography and isotopic stratigraphy. This is the first sequence to be cored in the Antarctic that provides a late Mesozoic-Cenozoic calcareous nannofossil and planktonic foraminiferal biostratigraphy. Mixed assemblages of calcareous and siliceous microfossils from the late Eocene through the Neogene have allowed the first biostratigraphic calibration to be carried out between these groups in the Antarctic region. Sedimentation across the Cretaceous/Tertiary (K/T) boundary was continuous in Site 689, and the boundary is associated with a 40-cm interval of vitric ash and clay of apparent volcanic origin.

The section sampled 297.3 m of almost pure siliceous and calcareous oozes to chalk, with chert layers at the top and bottom of the sequence. Three units have been recognized: Unit I extends from 0 to 31 mbsf, is of late Miocene to Quaternary age, and is represented by biosiliceous ooze. Unit II extends from 31 to 149.1 mbsf and is dominated by a mixture of biosiliceous and calcareous oozes ranging in age from late Eocene to late Miocene. The calcareous component is almost totally dominated by calcareous nannofossils. Unit III extends from 149.1 mbsf to the bottom of the hole (297.3 mbsf), is of late Campanian-early Maestrichtian to late Eocene age, and consists of nannofossil ooze and chalk, lacking biosiliceous sediments and containing varying amounts of foraminifers. The siliceous intervals are dominated by diatoms, although radiolarians and silicoflagellates become important elements in several intervals. The carbonate sediments are dominated by calcareous nannofossils throughout, with planktonic foraminifers forming an abundant element in the lower part of the sequence (Upper Cretaceous through upper Eocene).

Sediments and microfossil diversity and assemblages clearly reflect a sequential cooling of the Antarctic water mass, inferred to be related to Antarctic glacial development. The siliceous biogenic facies progressively replaced the carbonate facies during the Cenozoic, with initial siliceous sedimentation in the latest Eocene-earliest Oligocene, a major increase in siliceous sedimentation beginning near the base of the Neogene, and exclusively siliceous sedimentation from the upper Miocene. The rate of sediment accumulation was always low for biogenic sediments compared with many other oceanic areas and apparently quite uniform over long intervals of time. During the Eocene, sedimentation rates were about 4 m/m.y. For the Oligocene and Neogene, sedimentation rates between hiatuses are double that (7–9 m/m.y.). Site 689, located just south of the Antarctic Divergence, has always lain well to the south of the high productivity biogenic belt of the Polar Front. During the Cenozoic, this was an oceanic backwater.

BACKGROUND AND OBJECTIVES

Site 689 lies in 2080 m of water near the crest of Maud Rise, an isolated elevation in the eastern Weddell Sea (Fig. 1). This site was selected to obtain a high-quality (APC-XCB), continuously-cored pelagic biogenic sequence through Upper Cretaceous, Paleogene, and Neogene sediments in the area of the present-day Antarctic water mass. It is also the shallower of two sites on Maud Rise that form part of a depth transect for studies of the history of vertical water-mass stratification, the other site being Site 690, located on the southwestern flank of Maud Rise in 2914 m of water.

Multichannel seismic reflection and 3.5-kHz pinger profiles (Figs. 2–4) indicate the presence of a relatively thin (0.4-s two-way traveltime—*twt*) sequence of draped and mounded, weakly reflective sediments inferred to be pelagic oozes. The presence of distinct reflection horizons, especially in the uppermost and lowermost parts of the sequence, suggested that a number of hiatuses might interrupt a continuous sequence. The profiles also indicate a sequence of lavas or volcanoclastic sediments underlying the pelagic sequence. Regional tectonic considerations suggested a Late Cretaceous (possibly Cenomanian) age for basement at this location. Maud Rise, an aseismic ridge, was presumed to have an oceanic basement and, like similar features (the Rio Grande Rise and Walvis Ridge, for example), to have

formed by the interaction of a spreading ridge with a hot-spot. It was therefore possible that its early history was subaerial and that a major basement unconformity would be present.

Site 689 is located in the present-day Antarctic surface water mass 1000 km south of the Polar Front, 100 km north of the Antarctic Divergence, and 700 km north of the East Antarctic continent. Compared with other parts of the Weddell Sea, the area around Site 689 is marked by reduced sea-ice coverage and hence high annual biotic productivity. This is because it lies within or close to the Weddell polynya, a very large area of water that remains ice-free during many winter seasons (De Felice and Wise, 1981; Martinson et al., 1981). The site is located toward the eastern end of the Weddell Gyre, which extends to about 20°–30°E (Deacon, 1937) or even 40°E (Gordon et al., 1981) and dominates the oceanic circulation of the Weddell Sea. Because of the location of Site 689 in this part of the gyre, within the zone of eastward surface circulation, yet away from the Antarctic coast, it sees few icebergs. Thus, ice-rafted detritus within the sediments was expected to be sparse.

There were three main reasons why Site 689 was chosen:

1. There is almost no information about the Cenozoic paleoceanography and biostratigraphy of the Antarctic water mass.
2. Maud Rise is one of the few topographic highs within Antarctic waters where it might be possible to obtain sedimentary sequences in the open ocean at depths shallow enough to preserve calcareous sediments. The site was also considered isolated from terrigenous sediment supply from the nearby continent that could complicate the sedimentary record.
3. Seismic profiles (Fig. 3) indicated that the drilling was likely to recover a reasonably continuous Cenozoic and Late Cretaceous sequence.

Because Site 689 is located in relatively shallow water, it could provide one of the best opportunities in the Antarctic region to sample calcareous oozes above or close to the carbonate compensation depth (CCD) and the foraminiferal and calcareous nannofossil lysoclines. Foraminiferal and calcareous nannofossil assemblages should be well-preserved and provide an excellent paleoceanographic and paleoclimatic record. Furthermore, the location of the site in Antarctic waters should also provide a siliceous biogenic record that would allow, for the first time, calibration of the calcareous and siliceous biostratigraphies. According to Gersonde (pers. comm., 1987), piston cores from Maud Rise of Miocene, Pliocene, and Quaternary age contain both calcareous and siliceous microfossil assemblages.

Studies of the Site 689 sequence were of a pioneering nature because this is the first calcareous biogenic sequence to be drilled at such high southern latitudes and in Antarctic waters. Previously drilled sites in the Antarctic region were either in deeper waters where carbonate preservation had been poor, or were in shallow regions dominated by terrigenous sedimentation (such as the Ross Sea). For several reasons, the site was considered of particular importance as the first APC-XCB sequence to be drilled in the Antarctic:

1. It could yield the first Antarctic planktonic foraminiferal and calcareous nannofossil biostratigraphies. Previously drilled sequences lack sufficient calcareous microfossils in most stratigraphic intervals to be of much value.
2. It could be the first site in the Antarctic to provide the potential of producing oxygen and carbon isotopic stratigraphies for the Cenozoic and Late Cretaceous. The most useful existing record from the Southern Ocean is from the northern Subantarctic region of the Southwest Pacific (Shackleton and Kennett, 1975).
3. It could also be the first Antarctic site capable of yielding an integrated siliceous and calcareous biostratigraphy, magneto-

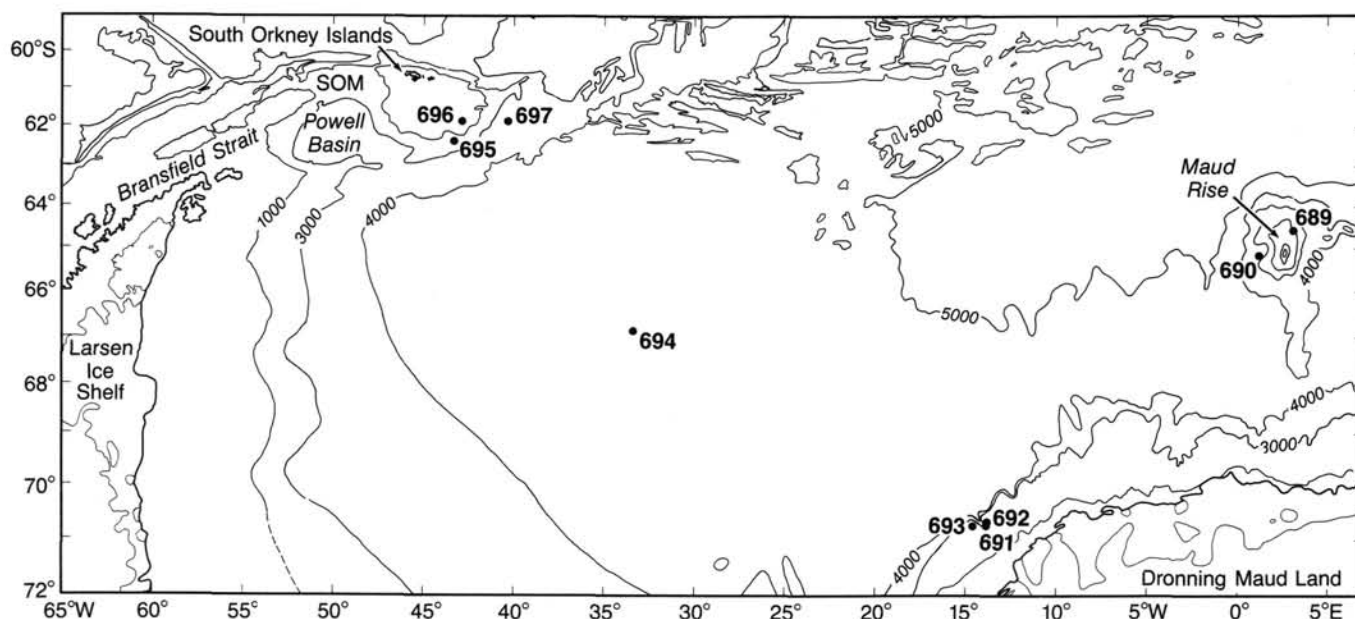


Figure 1. Location map showing positions of Sites 689 and 690 on Maud Rise and other Leg 113 sites. Bathymetric contours at 2000-m intervals from Tectonic Map (1985) and GEBCO sheet 5.16. SOM = South Orkney microcontinent.

stratigraphy, and oxygen, carbon, and strontium isotopic stratigraphy.

4. It should provide the first relatively complete sequence of sediments of any facies through the Paleogene. There has been a long-standing need to obtain Paleogene sediments from the Antarctic region.

Site 689 should provide us with important information about the paleoceanographic and paleoclimatic development of the Antarctic region. In particular, changes in the dominance of calcareous relative to siliceous sediments through the Cenozoic should mark the evolution of the nutrient-rich upwelling regime associated with the development of the modern surface and intermediate water circulation of the Antarctic Ocean. The stratigraphic distribution of ice-rafted detritus should provide evidence of the glacial history of the continent, although the present-day position of the site in an area largely free of icebergs indicates that the other Leg 113 sites will be better located for such an investigation.

The hoped-for presence of both planktonic and calcareous benthic foraminifers in the sequence would provide an unprecedented opportunity for studies of oxygen and carbon isotopic stratigraphy, which bear on the glacial evolution of Antarctica, the development of latitudinal (in conjunction with anticipated results from Leg 114) and vertical temperature gradients, and changes in the vertical water-mass structure and biotic productivity through the Cenozoic.

An abundance of both siliceous and calcareous microfossils would also provide a strong basis for studies of the evolution of species, assemblages, and biogeographic patterns in relation to the development of the Antarctic water mass.

The drilling plans for Site 689 were to drill two APC holes to refusal and to continue drilling with the XCB continuously through the remainder of the section to basement.

OPERATIONS

Punta Arenas, Chile, to Site 689

At 1110 on the morning of 5 January 1987, *JOIDES Resolution* departed for Antarctica from Punta Arenas, Chile, toward

the northeast through the Magallanes Strait. The *Maersk Master*, our sister ship and ice-management vessel, remained behind to wait for essential spare parts. The pilot on *JOIDES Resolution* disembarked at 2015 during unexpectedly calm weather.

Good progress was made during 6 and 7 January. Between 1600 and 2000 hr on 7 January, the Antarctic Convergence was crossed, and the seawater temperature dropped from 44° to 37°F. This temperature change was to cause future trouble in the form of fog. On the morning of the 8th, the first iceberg was sighted at 56°21'S, 49°34'W.

Near noon on the 8th, warm northerly winds passing over cold water created fog, resulting in reduced visibility and necessitating a reduction in ship speed. The underway geophysical gear was pulled aboard each time the ship slowed in case it was necessary to reverse the engines to avoid ice. The average speed for the 24 hr of the 9th was only 8.9 kt. The *Maersk Master* caught up on the 10th and began leading the way, resulting in an increase in speed. The 13th was marked by heavy fog, and only 200 nmi were made at 8.3 kt. By the 14th, the wind had moved to the east providing some relief from the fog.

The approach to Site 689 began on the afternoon of 14 January with the streaming and testing of the underway geophysical gear. After about 3 hr of operation the air guns froze. A temporary solution to this problem was to pour antifreeze down the air-gun hose. A prototype venturi device was built which allowed the adding of antifreeze to the air-gun supply system. No further freezing occurred.

Hole 689A

Site 689 (64°31'S, 03°06'E) was reached at 1552 hr on 15 January after streaming 2467 nmi from Punta Arenas in 241.5 hr, at an average speed of 10.2 kt. There was only one small piece of ice in the area that the *Maersk Master* broke up with propwash. The beacon (frequency 16.5 kHz) was dropped. The geophysical gear was recovered, thrusters lowered, station-keeping established, and the bottom-hole assembly (BHA) made up. The bit selected was an RBI rebuilt type C-3. The BHA was for the APC/XCB bit and consisted of a long bit sub, seal bore drill collar, landing sub, long top sub, head sub, five 8 1/4" drill collars, torque jars, one 8 1/4" drill collar, one 7 1/4" drill collar, XO, and two stands of 5 1/2" drill pipe.

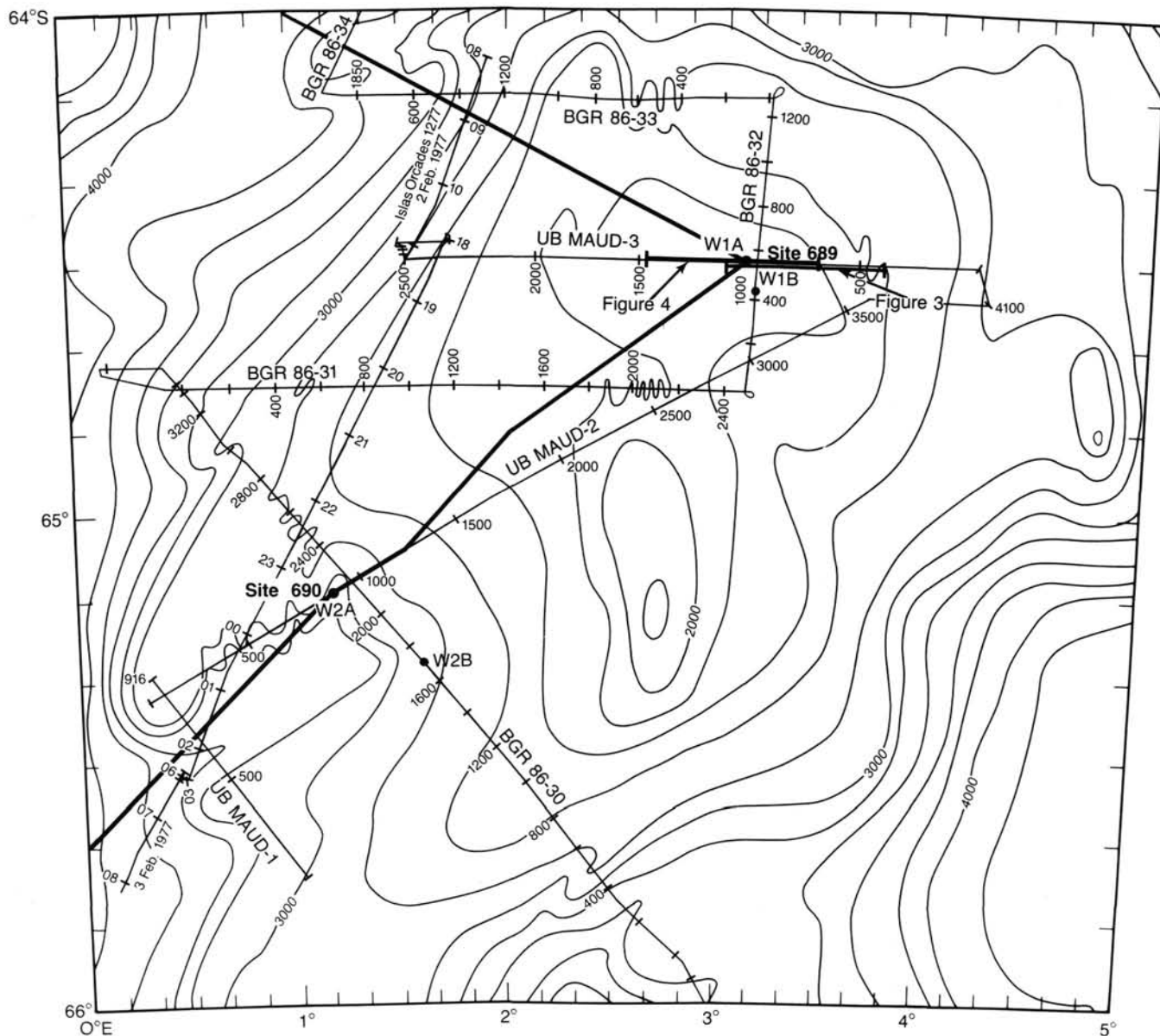


Figure 2. Approach and departure, Site 689. Also positions of Norwegian (NARE 85) multichannel seismic reflection and 3.5-kHz profiles (UB Maud-3), illustrated in Figures 3 and 4.

The precision depth recorder (PDR) water depth at Site 689 was 2084.8 m or 2095 m dual elevator stool (DES). The mud-line core was shot with the bit at 2093.6 m. The barrel was full, indicating that the bit had been below the mud line. It was therefore necessary to begin Hole 689B with our second core to obtain the mud line.

Hole 689B

The second shot was with the bit held at 2087.1 m, and the mud line was obtained and established to be at 2091.3 m (rig-floor depth). A surprising discovery was a thin layer of chert at the top of the core. Twenty-one APC cores were taken to 197.5 mbsf (Table 1). Coring was essentially trouble-free and recovery was near 100% until the last two cores. There were indications that the tool was not obtaining full stroke, although maximum pull-out was about 35,000 lb. A total of 197.5 m was cored, with 183.29 m recovered, providing 92% recovery.

Following APC to refusal, the XCB coring system was deployed for Cores 113-689B-22X to 113-689B-33X (197.5–297.3 mbsf). Core recovery was generally high, except for Cores 113-689B-24X and 113-689B-27X, where chert was penetrated that seriously disturbed the surrounding matrix of firm calcareous ooze. Core 113-689B-31X encountered a significant quantity of chert that could not be penetrated with the XCB sawtooth cutting shoe. The shoe was worn down about 1/2 in. during the 50 min of rotating while laboriously advancing the bit only 6.3 m. The next two cores were attempted using Acker Amalgamated cutting shoes. The first was partially successful in advancing 3.5 m with 0.82 m recovery (mostly chert). The second Amalgamated shoe was destroyed while advancing the hole only 3.0 m in 48 min. At this point it became evident that further penetration with the XCB would probably result in damage to the coring system because of the chert. The hole was abandoned and filled with seawater.

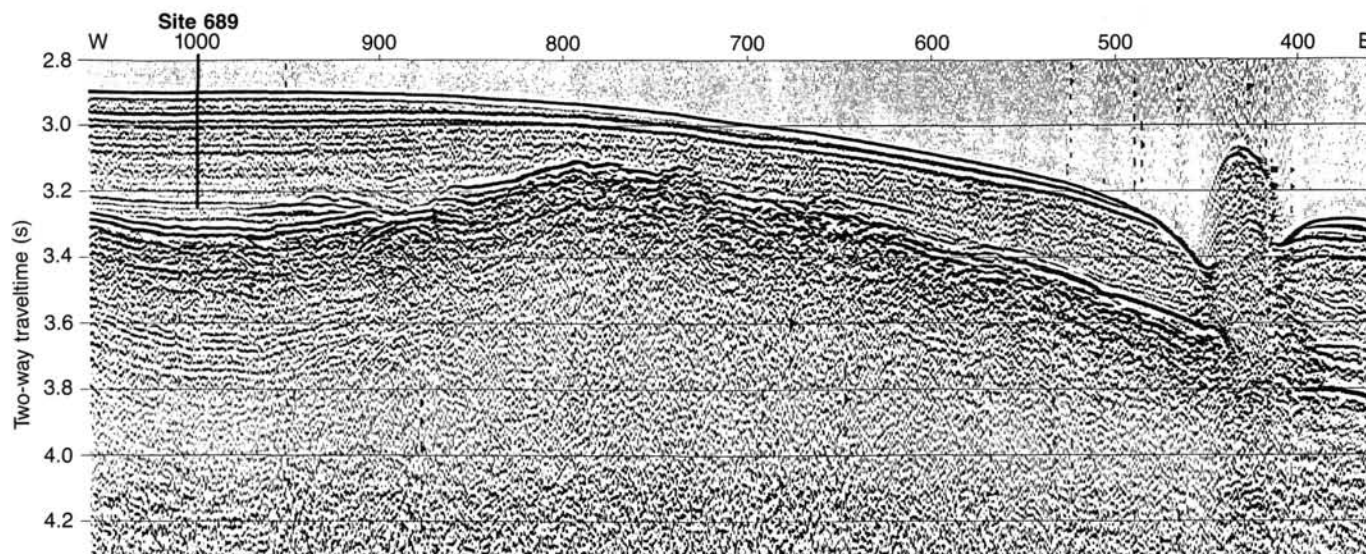


Figure 3. Norwegian (NARE 85) multichannel seismic reflection profile (UB Maud-3) showing location of Site 689, located in Figure 2.

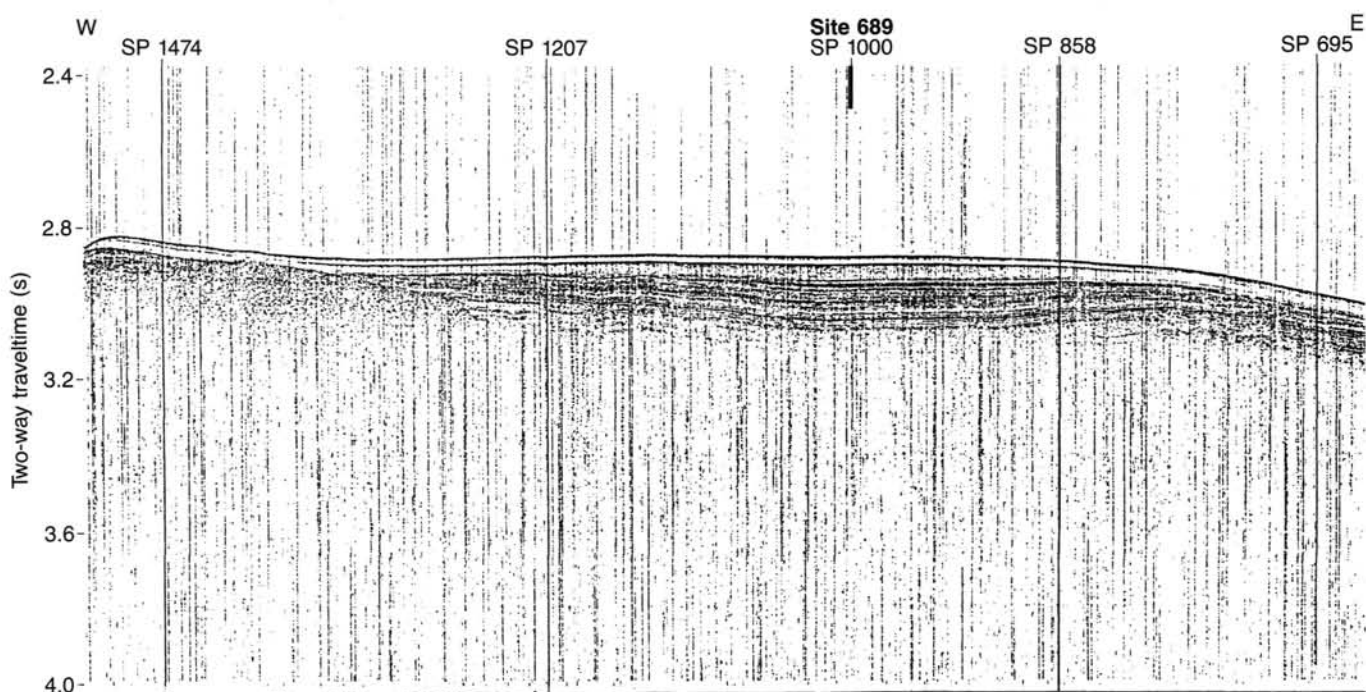


Figure 4. Norwegian (NARE 85) 3.5-kHz pinger profile (UB Maud-3) showing location of Site 689, located in Figure 2.

Hole 689C

The ship was moved about 20 m for an overlap APC hole. The first shot was with the bit at 2090.4 m, considered to be about 1 m above the seafloor. The core barrel was completely full, and it is believed that the core was taken with the ship on the bottom of the heave cycle. Rather than shoot again from a higher position it was felt the time would be better utilized by assuming the seafloor was at the same depth as Hole 689B and to continue coring (Table 1). On the second shot, the piston lock head pin in the APC sheared and the recovery was only 0.75 m. The third core recovered a full 9.5 m, but the wire-line pack-off rams in the line wiper had begun to leak badly. Rather than

leave the bit heaving in the open hole and risk its plugging, it was pulled up above the seafloor while the rams were changed.

Hole 689D

The bit was washed to 18.1 mbsf to a depth equivalent to the base of Hole 689C. Coring continued with 100% recovery (Table 1). Heat-flow measurements were taken in conjunction with Cores 113-689D-3H and 113-689D-6H. A third heat-flow measurement was planned, but since the second heat-flow core required an additional 50,000 lb overpull, to avoid the risk of becoming stuck, the third heat-flow measurement was abandoned. At the planned tenth and last core the operation was going so

Table 1. Coring summary, Site 689.

Core no.	Date (Jan. 1987)	Time (local)	Depth (mbsf)	Cored (m)	Recovered (m)	Recovery (%)
113-689A-						
1H	16	0800	2.3-11.8	9.5	9.35	98.4
113-689B-						
1H	16	0930	0.0-5.3	5.3	5.34	101.0
2H	16	1030	5.3-14.8	9.5	9.49	99.9
3H	16	1130	14.8-24.3	9.5	9.38	98.7
4H	16	1245	24.3-33.8	9.5	9.48	99.8
5H	16	1530	33.8-43.3	9.5	9.42	99.1
6H	16	1645	43.3-52.9	9.6	9.54	99.4
7H	16	1745	52.9-62.5	9.6	9.59	99.9
8H	16	1845	62.5-72.1	9.6	9.43	98.2
9H	16	2045	72.1-81.7	9.6	8.56	89.1
10H	16	2115	81.7-91.3	9.6	8.79	91.5
11H	16	2200	91.3-101.0	9.7	7.66	78.9
12H	16	2245	101.0-110.6	9.6	9.62	100.0
13H	16	2330	110.6-120.2	9.6	9.63	100.0
14H	17	0045	120.2-129.9	9.7	9.56	98.5
15H	17	0130	129.9-139.4	9.5	9.87	104.0
16H	17	0215	139.4-149.1	9.7	9.69	99.9
17H	17	0300	149.1-158.8	9.7	9.80	101.0
18H	17	0345	158.8-168.5	9.7	8.05	83.0
19H	17	0430	168.5-178.1	9.6	8.55	89.0
20H	17	0530	178.1-187.8	9.7	6.36	65.5
21H	17	0615	187.8-197.5	9.7	4.48	46.2
22X	17	0900	197.5-207.2	9.7	7.93	81.7
23X	17	1045	207.2-216.9	9.7	5.65	58.2
24X	17	1215	216.9-226.6	9.7	1.66	17.1
25X	17	1345	226.6-236.3	9.7	8.91	91.8
26X	17	1515	236.3-246.0	9.7	1.91	19.7
27X	17	1630	246.0-255.6	9.6	4.18	43.5
28X	17	1830	255.6-265.2	9.6	6.41	66.8
29X	17	2000	265.2-274.9	9.7	4.57	47.1
30X	17	2200	274.9-284.5	9.6	4.55	47.4
31X	18	0000	284.5-290.8	6.3	0.14	2.2
32X	18	0145	290.8-294.3	3.5	0.82	23.4
33X	18	0445	294.3-297.3	3.0	0.42	14.0
				297.3	229.44	
113-689C-						
1H	18	0900	0.0-8.6	8.6	9.85	114.0
2H	18	1100	8.6-18.1	9.5	0.75	7.9
3H	18	1215	18.1-27.6	9.5	9.94	104.0
				27.6	20.54	
113-689D-						
1H	18	1540	18.1-27.6	9.5	9.71	102.0
2H	18	1700	27.6-37.3	9.7	9.97	103.0
3H	18	1830	37.3-47.0	9.7	9.36	96.5
4H	18	1930	47.0-56.7	9.7	9.87	102.0
5H	18	2015	56.7-66.4	9.7	9.53	98.2
6H	18	2130	66.4-76.0	9.6	9.81	102.0
7H	18	2230	76.0-85.6	9.6	9.91	103.0
8H	18	2300	85.6-95.2	9.6	9.67	101.0
9H	19	0000	95.2-104.8	9.6	9.88	103.0
10H	19	0115	104.8-114.4	9.6	9.96	104.0
11H	19	0215	114.4-124.1	9.7	10.11	104.2
12H	19	0315	124.1-133.8	9.7	8.19	84.4
				115.7	115.97	

well it was decided to take two more cores, which were successful. The hole was abandoned and filled with seawater.

Summary

In summary, the coring conditions at Site 689 were excellent. APC recovery was essentially 100% (Table 1), pullouts were in the 15,000-30,000 lb range for long sections and increased gradually downhole. XCB recovery, as expected, was lower but was still high at low pump rates. Two minor coring problems were

encountered. The first was an inability to determine the seafloor depth from PDR readings. It is suspected the Carter tables used to correct for water density (Carter, 1980) produce a depth to seafloor which is about 3 m too shallow in this area of the Weddell Sea. The second problem was chert. As expected, the XCB can drill only small thicknesses of material with so low drillability, such as chert.

The weather at Site 689 was good and never hampered the operation. Ice was rare in the region. On 19 January the bit was clear of the seafloor at 0455 and the thrusters were secured by 0930. As the ship left the site, the geophysical gear was streamed and a final pass was made over the location. Full ahead for Site 690 was ordered at 1110.

LITHOSTRATIGRAPHY AND SEDIMENTOLOGY

Introduction

The sedimentary sequence drilled at Site 689 is of purely pelagic origin. The sediments recovered have been divided into three lithologic units (Fig. 5) based upon composition (Fig. 6) and diagenetic maturity. Siliceous components (diatoms, silicoflagellates, and radiolarians) decrease with increasing depth in the sequence whereas calcareous components such as nannofossils and foraminifers increase. Terrigenous and volcanic detritus as well as authigenic minerals occur only as minor components. The abundance of sediment components is based on smear slide analyses.

Lithostratigraphic Unit I is composed of biogenic siliceous ooze ranging in age from late Miocene to Quaternary. Unit II is dominated by a mixture of biogenic siliceous and calcareous oozes of late Eocene to late Miocene age. This unit can be further divided into two subunits; Subunit IIa of late Oligocene to late Miocene age shows a decreasing proportion of biogenic siliceous components with core depth. Subunit IIb of late Eocene to late Oligocene age is dominated by calcareous nannofossil oozes but with diatomaceous horizons. Unit III consists of foraminifer nannofossil oozes and chalk and can be divided into two subunits; Subunit IIIa, of late Maestrichtian to late Eocene age, contains a semilithified calcareous ooze to chalk sequence; Subunit IIIb is composed of pelagic chalk with interbedded thin chert layers and is of late Maestrichtian to probable late Campanian-early Maestrichtian age.

Sediments of Site 689, Holes 689A, 689B, 689C, and 689D are generally only slightly to moderately disturbed by the drilling process. Soupy structures occur only in the uppermost cores of each hole. Additional sediment disturbance is common at the top of each APC core and in the ooze-to-chalk transition. Recovery decreased significantly in the chert-bearing sequences of Subunit IIIb.

Unit I (Depth 0-31.0 mbsf; Age late Miocene-Quaternary)

Core 113-689A-1H; depth 2.3-11.8 mbsf; thickness 9.5 m; age Pliocene; Cores 113-689B-1H to 113-689B-4H-5, 70 cm; depth 0-31.0 mbsf; thickness 31.0 m; late Miocene through Quaternary in age; Cores 113-689C-1H to 113-689C-3H, CC; depth 0-27.6 mbsf; thickness 27.6 m; late Miocene through Quaternary in age; and Cores 113-689D-1H to 113-689D-2H-3, 30 cm; depth 18.1-29.4 mbsf; thickness 11.3 m; late Miocene through Quaternary? in age.

A complete lithologic sequence of Unit I has been recovered only from Hole 113-689B.

Unit I is composed mainly of white (2.5Y 8/2, 10YR 8/2) to light gray (2.5Y 7/2) radiolarian-bearing and radiolarian diatom oozes, white (10YR 8/1, 8/2, 2.5Y 8/2) silicoflagellate-bearing diatom ooze and white (10YR 8/2), pale yellow (5Y 7/3, 8/3), and light gray (2.5Y 7/2, 5Y 7/1, 7/2) silicoflagellate diatom ooze.

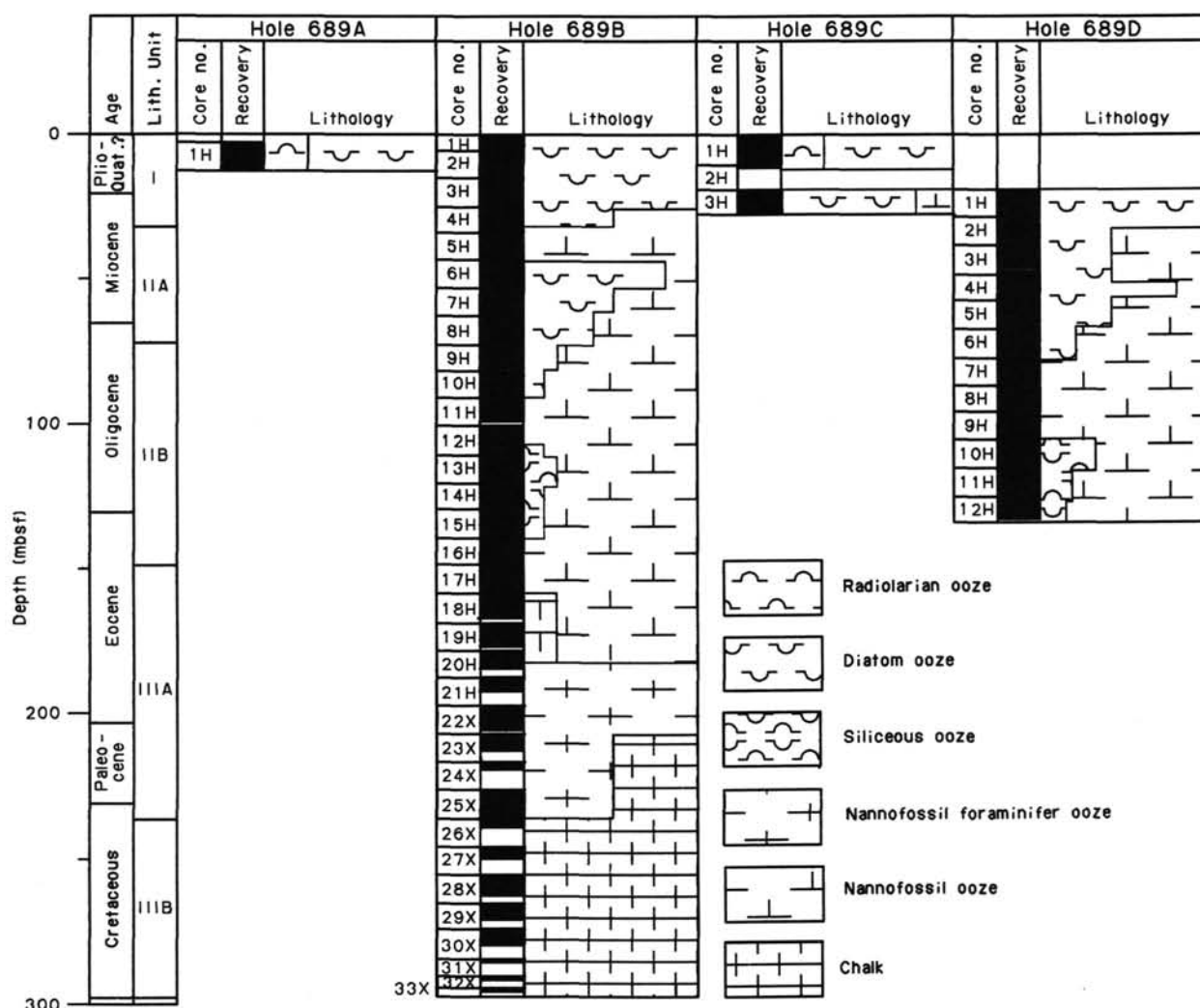


Figure 5. Lithostratigraphic summary log of Site 689, Maud Rise.

As a minor lithology, thin (less than 10 cm) chert layers occur at the top of Cores 113-689A-1H and 113-689B-2H. The light gray (10YR 7/1) and dark yellowish brown (10YR 4/4) cherts were broken and partly displaced during drilling and cutting operations. At Core 113-689A-1H it could not be determined if there were two chert layers or only one which had been partly fragmented and displaced by coring. The latter is more probable. The chert is very young (middle Pliocene; about 3 Ma) and may be the youngest ever recovered from the marine environment (see "Biostratigraphy" section, this chapter).

Glacial marine dropstones occur in Samples 113-689A-1H-4, 118 cm, 113-689A-1H-5, 8 and 37 cm, 113-689C-3H-1, 43 cm, 113-689D-1H-1, 120 cm, and 113-689D-1H-2, 58 cm (Fig. 7) and represent the only source of coarse terrigenous detrital input besides volcanic ash derived from the Antarctic Peninsula, the South Shetland Islands, or South Sandwich Islands.

Smaller pieces of ice-rafted detritus are probably represented by fine sand and silt-sized "accessory" minerals identifiable in smear slides (Fig. 6). The petrography of the ice-rafted detritus is discussed at the end of this section.

The sediment sequence of Unit I is slightly to moderately bioturbated. Only a few sections show clearly definable biotur-

bation structures mostly of the halo burrow and Planolites type (Fig. 8).

An apparent color cyclicity on a meter as well as decimeter scale is present in Unit I. In most cores color changes are gradational and slight, however, some sharp color contacts occur (Fig. 9). The gradational color changes are commonly too subtle to be detected with the Munsell color scale and cannot be correlated with compositional changes based on smear slide analyses.

Unit II (Depth 31.0–149.1 mbsf; Age late Eocene-late Miocene)

Sample 113-689B-4H-5, 70 cm, to Core 113-689B-17H; depth 31.0–149.1 mbsf; thickness 118.1 m; late Eocene to late Miocene in age; and Sample 113-689D-2H-3, 30 cm, through Section 113-689D-12H, CC; depth 29.4–133.8 mbsf; thickness 104.4 m; late Eocene to late Miocene in age.

Unit II is characterized by a wide variety of pure and mixed biogenic siliceous and biogenic calcareous sediment types. The top of Unit II is marked by a very white (10YR 8/0) diatom nannofossil ooze giving a sharp color contrast to Unit I. The base of Unit II is marked by the disappearance of biogenic siliceous sediment components and the simultaneous increase of zeolite

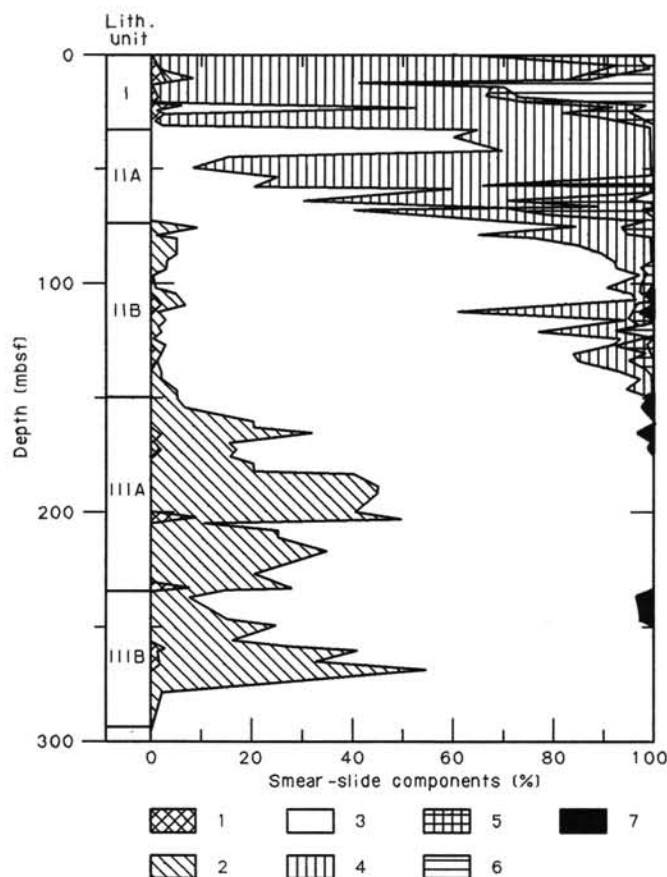


Figure 6. Sediment composition of Hole 689B, Maud Rise, from ship-board smear slide data. 1 = terrigenous quartz and clay, 2 = foraminifers, 3 = calcareous nannofossils, 4 = diatoms, 5 = radiolarians, 6 = silicoflagellates, 7 = zeolites.

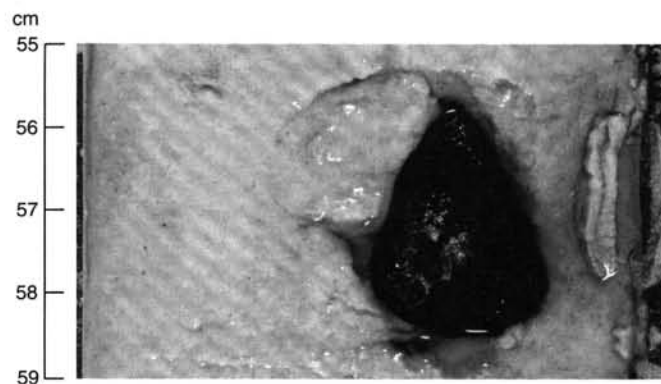


Figure 7. Glacial marine dropstone in Pliocene diatom ooze (113-689D-1H-2, 55-59 cm).

content. Unit II is divided into two subunits based mainly on the abundance of diatoms, on the appearance of foraminifers, and the disappearance of radiolarians.

Subunit IIA (Depth 31.0-72.1 mbsf)

Cores 113-689B-4H-5, 70 cm, to 113-689B-9H; depth 31.0-72.1 mbsf; thickness 41.1 m; late Oligocene to late Miocene in age; and Cores 113-689D-2H-3, 30 cm, to 113-689D-6H-4; depth 29.4-70.9 mbsf; thickness 41.5 m; late Oligocene-early Miocene to late Miocene in age.

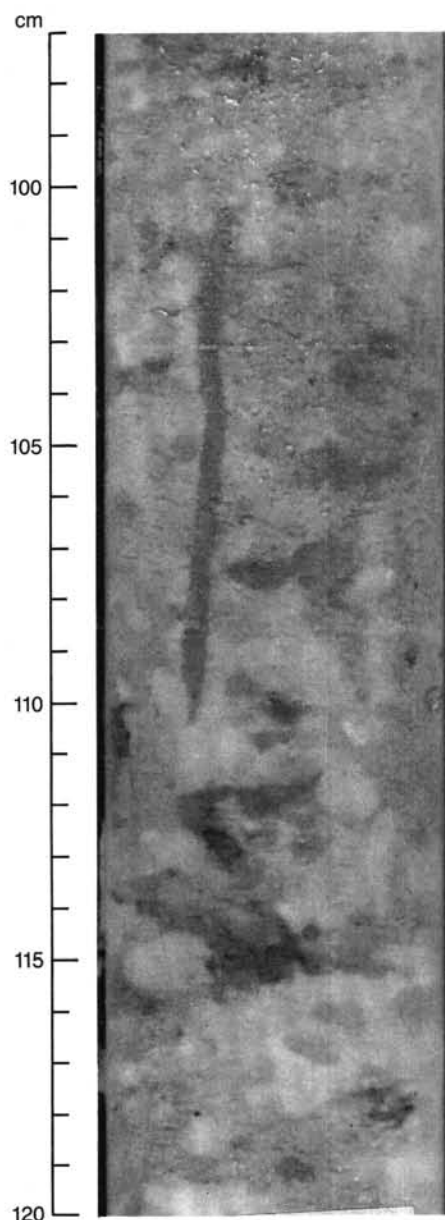


Figure 8. Well-preserved burrow structures mainly of *Planolites* type from unconsolidated Pliocene diatom ooze (113-689B-1H-3, 97-120 cm).

The main sediment types of Subunit IIA are very white (10YR 8/0) to white (2.5Y 8/1) diatom nannofossil ooze, light gray (2.5Y 7/2, 8/2) diatom-bearing nannofossil ooze, varicolored white (2.5Y 8/2), light gray (2.5Y 7/2, 7/1), light brownish gray (2.5Y 6/2), and pale brown (2.5Y 6/3) nannofossil diatom ooze, light gray (2.5Y 7/2, 8/2) to very white (10YR 8/0) nannofossil ooze, and very white (10YR 8/0) to pale olive (5Y 6/4) diatom ooze.

Minor sediment types are represented by very white (2.5Y 8/0) to light gray (2.5Y 7/2) radiolarian-bearing diatom nannofossil ooze, light gray (10YR 7/2) to light brownish gray (10YR 6/2) nannofossil-bearing radiolarian diatom ooze, and light gray (2.5Y 7/1) radiolarian diatom ooze.

Glacial marine dropstones are observed in Samples 113-689B-7H, 60 cm, and 113-689D-5H, 105 cm, representing a time as early as the early Miocene.

Bioturbation is slight to moderate throughout Subunit IIA. In general, burrows are well preserved even in unconsolidated

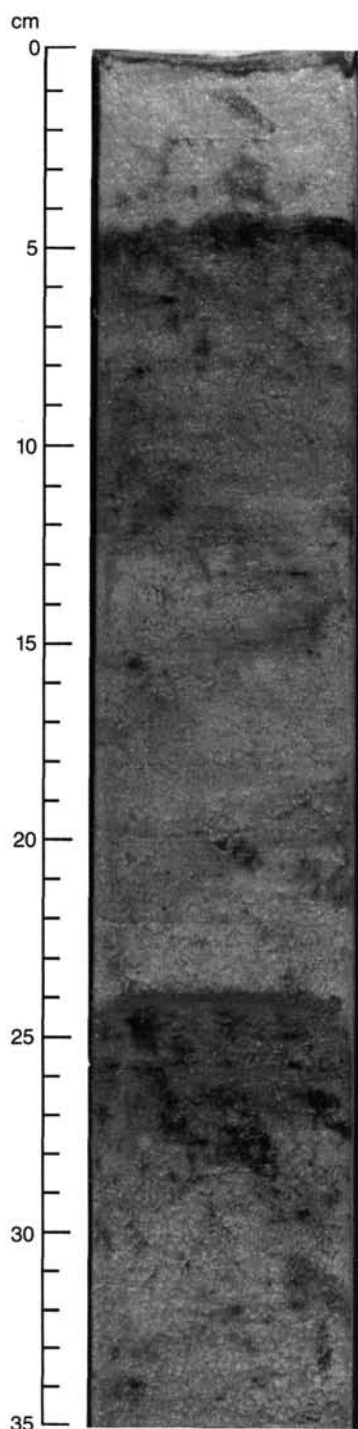


Figure 9. Sharp color contact in upper Miocene diatom ooze (113-689B-4H-2, 0–35 cm), colors are light gray (2.5Y 7/2) at 0–4 cm, light brownish gray (2.5Y 6/2) at 4–5 cm, grading into light gray (2.5Y 7/2) at 20–24 cm, sharp contact and changes into light brownish gray (2.5Y 6/2) at 24–25 cm grading downward into white (2.5Y 8/2).

Subunit IIB (Depth 72.1–149.1 mbsf)

Cores 113-689B-9H to 113-689B-17H; depth 72.1–149.1 mbsf; thickness 77.0 m; late Eocene to late Oligocene in age; and Core 113-689D-6H-4 through Section 113-689D-12H, CC; depth 70.9–133.8 mbsf; thickness 62.9 m; late Eocene to late Oligocene-early Miocene in age.

The sediments of this subunit are dominated by calcareous nannofossils. Radiolarians decrease downward to insignificant numbers whereas foraminifers become an additional but still minor sediment component.

The major lithologies of Subunit IIB are very white (10YR 8/0), white (10YR 8/1, 8/2), light gray (2.5Y 7/2, 7/1) to light brownish gray (2.5Y 6/2) nannofossil ooze, white (10YR 8/1, 8/2) to light gray (10YR 7/1) diatom nannofossil ooze, and white (10YR 8/1, 8/2), and light gray (2.5Y 7/2) to brownish gray (10YR 6/2) diatom-bearing nannofossil ooze.

Minor lithologies are white (10YR 8/1) diatom and radiolarian-bearing nannofossil oozes and diatom and foraminifer-bearing nannofossil oozes.

Glacial marine dropstones, 4–5 mm in size, were found in Cores 113-689B-10H-1, 70 cm, and 113-689B-10H-5, 118 cm, and Section 113-689B-10H, CC, which is late Oligocene in age. This implies that icebergs drifted over the Maud Rise as early as the late Oligocene.

Unit III (Depth 149.1–297.3 mbsf, Age Campanian(?)–late Eocene)

Cores 113-689B-17H through 113-689B-33X, CC; depth 149.1–297.3 mbsf; thickness 148.2 m; Campanian to late Eocene in age.

Sediments of Unit III consist mainly of nannofossil ooze and chalk with varying amounts of foraminifers (Fig. 6). The abundance of foraminifers increases significantly downward through this unit. Unit III can be divided into two subunits mainly based on induration of calcareous oozes into chalk and the occurrence of chert layers.

Subunit IIIA (149.1–236.3 mbsf)

Cores 113-689B-17H to 113-689B-26X; depth 149.1–236.3 mbsf; thickness 87.2 m; late Maestrichtian to late Eocene in age.

Subunit IIIA represents a semilithified ooze to chalk sequence. Firm chalk layers, 2–3 cm in thickness, first occur in Core 113-689B-21H (190 mbsf), rapidly increasing downhole in abundance and thickness (5–8 cm). The sediments are composed predominantly of very white (10YR 8/0), white (10YR 8/1, 8/2), light gray (10YR 7/1) to very pale brown (10YR 8/3, 8/4) foraminiferal nannofossil ooze, very white (10YR 8/0) nannofossil ooze, and foraminiferal nannofossil ooze.

As minor lithologies, altered volcanic-ash-bearing layers are present in Core 113-689B-22X and Sections 113-689B-23X-4 (Fig. 10), 113-689B-25X-1, and 113-689B-25X-5.

The thickness of the ash-bearing layers varies from 4–5 cm (Samples 113-689B-23X-4, 71–75 cm; 113-689B-25X-1, 5–10 cm) to about 35 cm (Sample 113-689B-25X-5, 50–85 cm). Ashes in these layers are finely dispersed by bioturbation (Fig. 10).

Bioturbation in the sediments of Unit IIIA is slight to moderate, showing well-preserved burrows of the pelagic types Planolites, Chondrites, and Zoophycos.

Subunit IIIB (Depth 236.3–297.3 mbsf)

Cores 113-689B-26X through 113-689B-33X, CC; depth 236.3–297.3 mbsf; thickness 61.0 m; late Campanian(?)–early Maestrichtian to late Maestrichtian in age.

Subunit IIIB is an indurated lithified calcareous sequence. Its major lithologies are very white (2.5Y 8/0), white (2.5Y 8/1) and light gray (5Y 7/1) nannofossil chalk, white (5Y 8/1) to

sequences. Most common are halo burrows; other identified burrows belong to Planolites, Zoophycos, Chondrites, and Teichichnus types. Vertical burrows as long as 35 cm are common.

Bedding structures other than bioturbation, such as bedding planes, are rarely observed and then only where highlighted by color changes. Overprinting of primary structures by horizontal burrowing commonly forms beddinglike patterns.

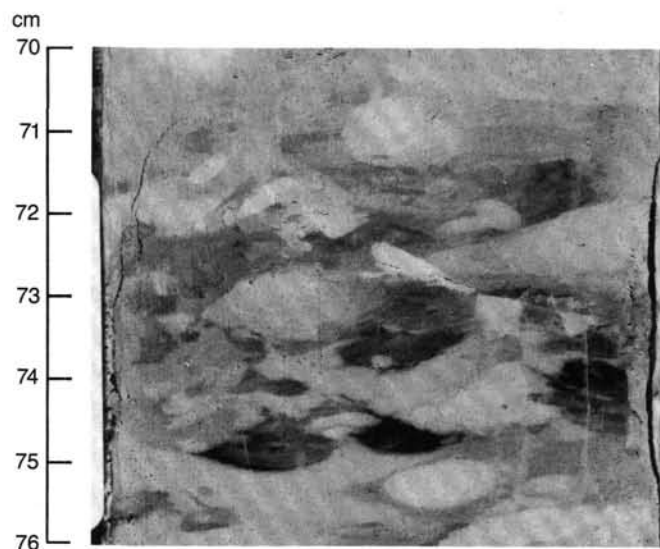


Figure 10. Strongly bioturbated, altered volcanic-ash-bearing layer, lower Paleocene (113-689B-23X-4, 70–76 cm).

gray (5Y 6/1) foraminiferal nannofossil chalk, and foraminifer-bearing nannofossil chalk.

As a minor lithology, fragmented cherts were recovered from all cores of this sequence (Fig. 11). The cherts vary in color from light gray (5Y 7/1) and light olive gray (5Y 6/2) to greenish gray (5GY 5/1, 6/1). Due to the sharp decrease in sediment recovery and slow rate of drilling this sequence, it is assumed that the chalk contains several thin chert layers.

Bioturbation is moderate to strong in sediments from Unit III, which contains well-preserved burrows of the same types as in Subunit IIIA.

Clay Mineralogy

The purpose of this study is to recognize the major variations that occurred in the paleoenvironments as expressed by the changing nature and abundance of clay minerals, using a sampling interval of one per core to one per three cores. Twenty-four samples were analyzed.

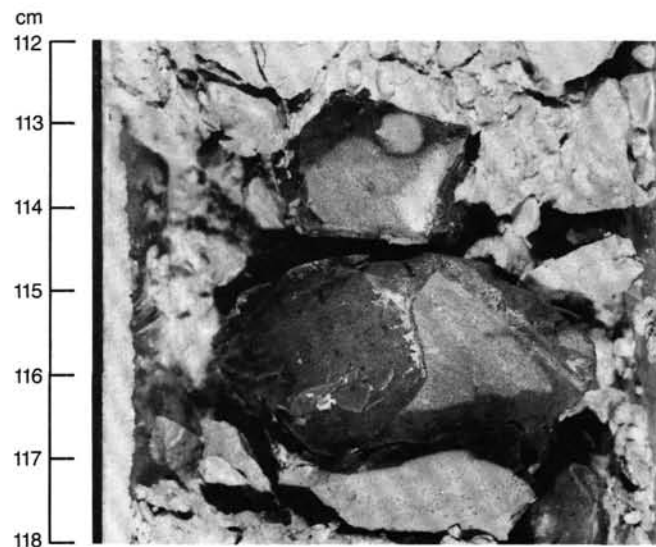


Figure 11. Nodular chert showing preserved diagenetic contact with chalk (113-689B-29X-2, 112–118 cm).

Results

Clay minerals identified in the analyses include chlorite, illite, kaolinite, and smectite. Based on the abundances of the minerals, three units of clay associations were determined for Site 689. These are designated Units C1 through C3, Unit C3 being further divided into two subunits (Fig. 12).

Unit C1, which extends from the seafloor to 62.5 mbsf, has a clay association of abundant to very abundant smectite and common to abundant illite, occasionally accompanied by common chlorite and kaolinite. Some samples are exclusively smectite. Poor clay content in some samples results from the greater dilution of the detrital supply by the biosiliceous components. The stratigraphic range of this unit is from lower Miocene to Pliocene.

Unit C2 extends from 62.5 to 139.4 mbsf and consists of abundant illite and smectite, generally associated with rare to common chlorite and kaolinite. Illite may also occur exclusively in Cores 113-689B-14H and 113-689B-15H, but only a more rigorous analysis can confirm the occurrence. The stratigraphic range of this unit is from the upper Eocene to lower Miocene.

Unit C3 extends from 139.4 mbsf to the bottom of Hole 689B at 297.3 mbsf. This unit is divided into two subunits, and the clay fraction consists predominantly of smectite.

Subunit C3a extends from 139.4 to 207.2 mbsf (upper Eocene to upper Paleocene) and consists exclusively of smectite.

Subunit C3b extends from 207.2 to 297.3 mbsf (upper Paleocene to upper Campanian/lower Maestrichtian). The clay association consists of very abundant smectite and rare illite.

Paleoenvironmental History

Very abundant and exclusive smectite found in Unit C3 (upper Campanian/lower Maestrichtian to upper Eocene) suggests that warm climatic conditions with alternating periods of humidity and aridity prevailed in source areas mainly characterized by low relief, as in most North Atlantic regions (Chamley, 1979) and in the southern part of the South Atlantic (Robert, 1987). This climatic pattern is similar to that found at present in most tropical and subtropical regions (Pedro, 1984). In Subunit C3b, the rare illite could have been derived from erosion in areas of rugged relief in a distant source area, or from a weak local tectonic event. Similar occurrences of illite off South Africa at DSDP Site 361 near the K/T boundary and during the Campanian (Robert, 1987) support the first hypothesis.

In Unit C2 (upper Eocene to lower Miocene), there is a significant increase in illite while at the same time a corresponding decrease in smectite. This suggests that hydrolysis strongly decreased, due to a major cooling event and/or a gradual increase in arid conditions. Similar increases of the illite content were observed on the Falkland Plateau at DSDP Sites 329 and 511 where the illite increased progressively from the upper Eocene to the lower Oligocene (Robert and Maillot, 1983), but showed relatively lower abundances than at Site 689. The weaker occurrences at the Falkland Plateau are probably due to a major input of detrital components derived from warmer continental areas adjacent to the South Atlantic. In the Ross Sea at DSDP Site 274, a similar increase of the illite content occurred later, during the lower Miocene (Robert et al., in press).

Unit C1 (lower Miocene to Pliocene) shows a decrease in the illite content, in association with a slight increase of smectite and principally fluctuations in the abundances of these minerals. This clay association is not representative of present climatic conditions on Antarctica where pedogenesis in deglaciated areas leads to the formation of chlorite and illite (Ugolini and Jackson, 1982). Modern marine sediments off ice-free Antarctic regions (Antarctic Peninsula, Adelie Coast) are also characterized by chlorite and illite (Michel, 1964; Chamley, 1965).

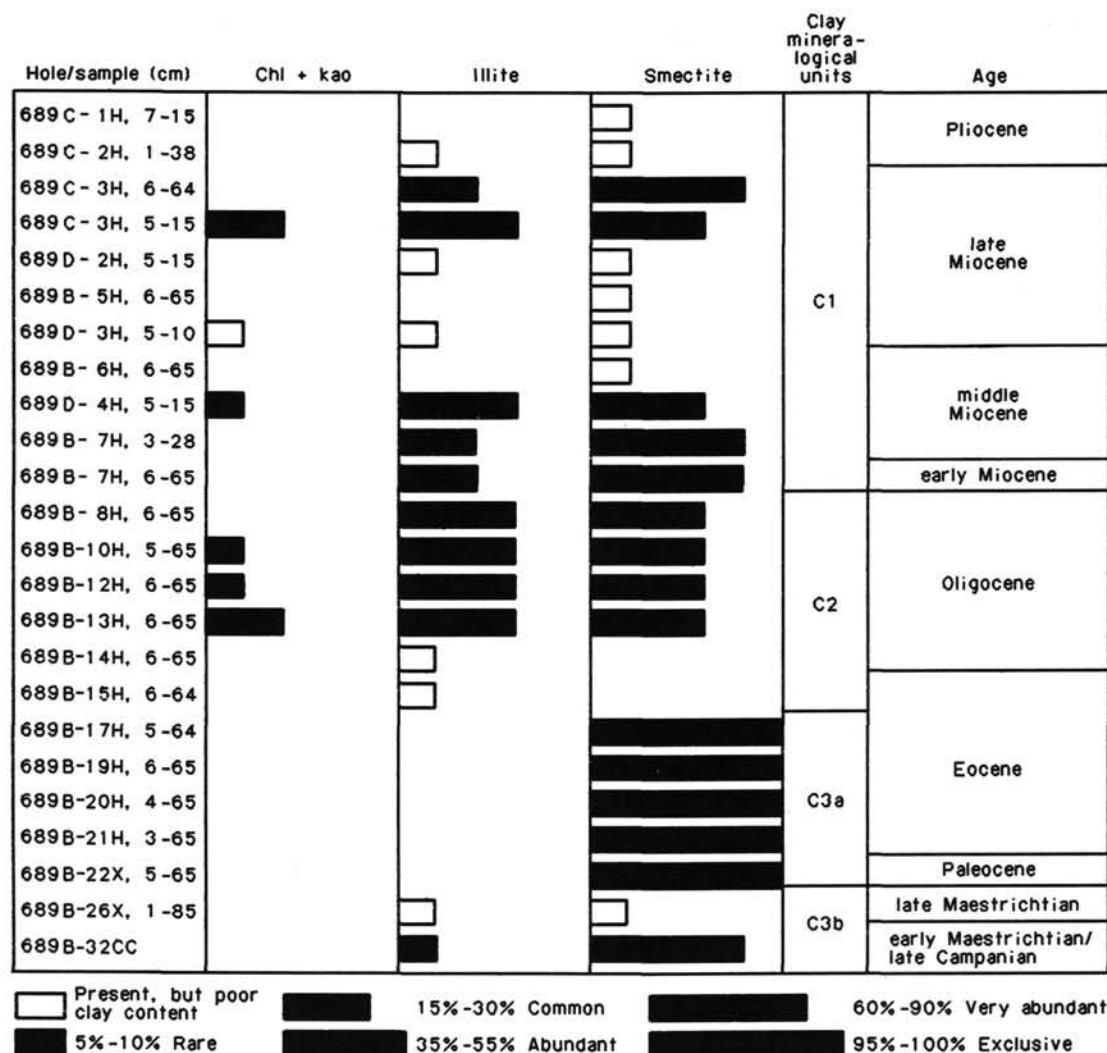


Figure 12. Clay mineralogy, Site 689; Chl = chlorite, Kao = kaolinite.

Abundant smectite occurrences have been recorded in the deepest waters of the southwest Atlantic Ocean at DSDP Sites 355, 358, 513, and 514 (Robert and Maillot, 1983) where they are associated with Antarctic Bottom Water, but lower smectite content prevails in intermediate or surface water regions, at DSDP Sites 356 and 357 in the southwest Atlantic, and also in the southeast Atlantic (Robert, 1982). In Subantarctic regions, abundant smectite occurs in both deep (DSDP Site 328) and intermediate (DSDP Sites 329, 511, and 512) waters (Robert and Maillot, 1983). In Antarctic regions, upper Pleistocene sediments off the ice shelf near Kapp Norvegia contain smectite (Grobe, 1986), as in other regions of the Southern Ocean (Jacobs, 1974). Thus, all Antarctic water masses seem to carry a detrital supply of smectite. Smectite may be derived by erosion of ancient (Mesozoic or early Cenozoic) smectite-rich sediments cropping out on or around Antarctica (Robert and Maillot, 1983). A similar evolution of the clay association was also observed in the Ross Sea at DSDP Site 274, where it occurred from the upper middle Miocene to the Pleistocene (Robert et al., in press).

Ice-rafted Dropstones

Nine ice-rafted dropstones were examined in hand specimen and in thin section from the top 20 m of Hole 689B and from the top 30 m of Hole 689D. The sediments from which these dropstones were collected range in age from late Pliocene to early

Miocene. The rocks are a representative suite selected from 14 dropstones recovered at Site 689.

In hand specimen, the dropstones range in size from 0.5 to 2.5 cm, are polished, and subrounded to angular. Oxidation (red-brown color) on the outside of one diabase pebble (Sample 113-689D-1H-2, 55-59 cm) from the Pliocene/Miocene boundary at 20.14 mbsf indicates a limited amount of chemical weathering. On the whole, however, chemical weathering is negligible. Metamorphic texture where present is well preserved, both amphibole and biotite grains being fresh.

Lithologic division of the dropstones is as follows: (1) basic plutonic, (2) felsic plutonic, and (3) metamorphic. Petrogenetically the basic igneous rocks are gabbro and diabase, the one felsic plutonic rock is granite, and the metamorphic rocks are hornblende-biotite gneiss and garnet-bearing quartzite.

Detailed descriptions of each specimen are presented in Table 2, and the location, age, and surrounding lithology in Figure 13.

The gabbros are characterized by equigranular texture and the diabase by glomeroporphyritic texture. They consist of plagioclase, augitic pyroxene, and some olivine. Hydrothermal alteration is evident from the wide range in anorthite content in the plagioclase; An_{10-50} (determined by the Michele-Levi method), and from clinozoisite aggregates within plagioclase grains. Blue-green amphibole rims the pyroxene, and there is a

Table 2. Petrographic description of dropstones from Leg 113, Site 689.^a

Rock number: 113-689B-2H-2; 44–45 cm
Name: hornblende-biotite gneiss
Size: 1.5 × 1.5 cm
Depth: 7.24 m
Shape: subrounded
Weathering: none

Major minerals	%	Accessory minerals	Comments
Plagioclase	45	Epidote	The rock has an apparent lineation; green hornblende poikilitically encloses quartz and plagioclase grains. Light minerals and dark minerals segregate into bands. Both hornblende and biotite are fresh and unaltered. Minor sericitization of plagioclase. Myrmekite is present, and quartz shows undulose extinction.
Hornblende	35	Microcline	
Quartz	10	Carbonate	
Biotite	8	Sphene	
		Corundum	
		Sericite	
		Magnetite	
		Pentlandite	

Rock number: 113-689C-3H-3; 93–94 cm
Name: quartzite (garnet-bearing)
Size: 2.0 × 1.5 cm
Depth: 22.0 m
Shape: subrounded, polished
Weathering: none

Major minerals	%	Accessory minerals	Comments
Quartz	60	Sericite	Equigranular feldspathic rock. Interlocking quartz-feldspar grains have irregular, embayed grain boundaries. Garnet porphyroblasts occasionally enclose quartz grains. Minor sericitic alteration of feldspars and some chlorite in garnet fractures.
Plagioclase	25	Apatite	
Garnet	13	Chlorite	
Biotite	2	Sphene	

Rock number: 113-689D-1H-2; 55–59 cm
Name: gabbro/diabase
Size: 1.0 × 0.5 cm
Depth: 20.15 m
Shape: elongate, slightly rounded, polished
Weathering: none

Major minerals	%	Accessory minerals	Comments
Plagioclase	50	Epidote	Partly gabbroic, partly diabasic texture. Hydrothermal alteration is evident; plagioclase shows a patchy alteration pattern, ranging in composition from albite to labradorite. Clinopyroxene is unaltered and is breaking down to chlorite. Spinel has graphic texture.
Clinopyroxene	37	Amphibole	
Magnetite	2–3	Sericite	
		Chlorite	

Rock number: 113-689D-1H-1; 35–36 cm
Name: diabase
Size: 1.0 × 0.5 cm
Depth: 18.45 m
Shape: subrounded, polished
Weathering: slightly oxidized (apparent only in thin section)

Major minerals	%	Accessory minerals	Comments
Plagioclase	43	Epidote	Extensively saussuritized rock; albitized plagioclase is not representative of original feldspar composition. There is some alteration of spinel to hematite(?).
Clinopyroxene	40	Chlorite	
Magnetite	10	Hematite	

Table 2 (continued).

Rock number: 113-689D-1H-2; 55–59 cm
Name: diabase
Size: 3.0 × 2.0 cm
Depth: 20.15 m
Shape: subrounded
Weathering: slight oxidation on surface

Major minerals	%	Accessory minerals	Comments
Plagioclase	55	Epidote	A glomeroporphyritic rock. Extensive saussurization altered the plagioclase composition to An ₁₀₋₄₅ . Olivine is often rimmed by clinopyroxene, and some olivine grains are enclosed by pyroxene grains. Iron-stain is the result of the breakdown of spinel.
Clinopyroxene	35	Sphene	
Olivine	7		
Spinel	1–2		

Rock number: 113-689D-1H-2; 55–59 cm
Name: granite
Size: 2.0 × 1.5 cm
Depth: 20.15 m
Shape: angular
Weathering: none

Major minerals	%	Accessory minerals	Comments
Microcline	40	Sericite	Equigranular rock with minor alteration. Feldspars are sericitized, but amphibole and biotite are fresh.
Orthoclase	30	Amphibole	
Quartz	28	Biotite	

Rock number: 113-689D-1H-3; 24–25 cm
Name: pink orthoclase feldspar
Size: 1.5 × 1.0 cm
Depth: 27.6 m
Shape: slightly rounded
Weathering: none

Hand specimen observations only

Rock number: 113-689D-1H-1; 130–131 cm
Name: diabase
Size: 0.5 × 1.0 cm
Depth: 19.4 m
Weathering: none
Mineralogy: plagioclase, amphibole

Rock number: 113-689D-1H-3; 24–25 cm
Name: diabase
Size: 0.4 × 0.4 cm
Depth: 21.3 m
Shape: angular
Weathering: none
Mineralogy: plagioclase, amphibole

^a When the major minerals do not equal 100%, the remaining percentage is distributed among the accessory minerals.

limited breakdown of amphibole to chlorite. The granite is coarse grained and contains turbid feldspars. The turbidity is caused by finely disseminated sericite within individual grains. Minor amphibole and biotite are relatively fresh and do not show evidence of secondary alteration.

In the amphibole-biotite gneiss the parallel alignment of blue-green hornblende is typical. Light and dark minerals are segregated into separate bands. Sphene, minor carbonate, corundum, opaques, and rutile are accessory minerals. Quartz shows undulose extinction, indicating high strain.

The garnet-bearing quartzite is equigranular and relatively free of secondary alteration. The matrix consists of interlocking quartz and feldspar grains with irregular, sutured grain boundaries. Subhedral-euhedral garnet and lath-shaped biotite make up

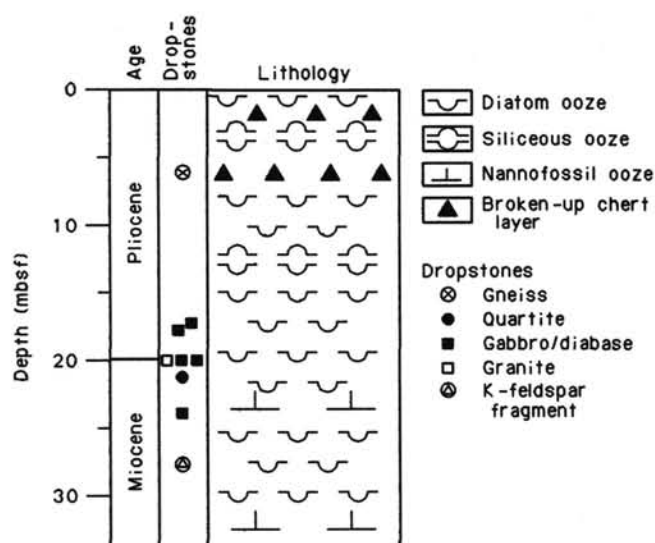


Figure 13. Stratigraphic location and surrounding lithology of ice-rafted dropstones, Site 689. Descriptions of the dropstones are given in Table 2.

the dark minerals of the rock. Small amounts of chlorite in a few garnet fractures indicate some retrograde metamorphism, but, on the whole, garnet and biotite are remarkably fresh and unaltered.

Petrographic observations indicate that the gneiss and the quartzite have been metamorphosed to the epidote/amphibolite facies (green amphibole, biotite, garnet); the granite shows only evidence of weak hydrothermal alteration (minor sericite); and mineralogy of the gabbro/diabase (epidote, blue-green amphibole-chlorite) is indicative of greenschist-epidote facies metamorphism.

The suite of dropstones recovered from Site 689 is representative of the geology of East Antarctica. The gneiss, quartzite, granite, and the gabbro/diabase could have been derived from Queen Maud Land (east of the Kirwan escarpment) where the gneissic basement is intruded by plutonic rocks of granitic to gabbroic composition (Dalziel and Elliot, 1973). A recent study on the petrology of Weddell Sea glacial sediments (Andrews, 1984) indicates that metamorphic rocks are common in the eastern part of the Weddell Sea, whereas sedimentary and volcanic rocks are characteristically found in the southwestern parts.

PHYSICAL PROPERTIES

Introduction

The objectives of the physical properties program at Site 689 were to help characterize the physical properties of high-latitude marine sediments and provide a link between geophysical and geological data. The physical properties program consisted of obtaining the following measurements: (1) index properties—bulk density, porosity, water content, and grain density; (2) vane shear strength—a relative measure of the resistance of the sediment to loads and a measure of its cohesiveness; (3) compressional wave velocity—the speed of sound in the sediments; and (4) thermal conductivity—the ability of the sediment to transport heat (see "Explanatory Notes" chapter, this volume).

Three lithostratigraphic units containing four subunits were reported in earlier sections of this report. They are as follows: Unit I ranges from 0 to 31.0 mbsf and is classified as upper Miocene to Quaternary radiolarian-diatom ooze; Subunit IIA ranges from 31.0 to 72.1 mbsf; Subunit IIB ranges from 72.1 to 149.1 mbsf. This unit contains upper Eocene to upper Miocene diatom-nannofossil ooze. Subunit IIIA, from 149.1 to 236.3 mbsf,

contains an upper Maestrichtian to upper Eocene nannofossil ooze; Subunit IIIB, 236.3 to 297.3 mbsf, is an upper Campanian(?)–lower Maestrichtian to upper Maestrichtian indurated nannofossil ooze/nannofossil chalk.

Index Properties

Two methods of determining the bulk densities and porosities of the sediments were used for Site 689. Bulk density, porosity, and water content were determined at discrete points within the cores by gravimetric determination. In addition, all core sections from Site 689 were logged on the GRAPE (gamma ray attenuation porosity evaluation) unit, from which bulk density and porosities are automatically computed assuming a grain density of 2.75 g/cm³. In view of the low grain densities encountered in Site 689, this introduced a systematic error into the bulk density data.

Index properties measured on samples from approximately every other section in each core are listed in Table 3. Profiles of bulk density, water content (wet basis), and grain density from Hole 689B are illustrated in Figure 14. A profile of porosity also from Hole 689B is shown in Figure 15. These figures illustrate the large variations in bulk density, water content, and porosity in the upper 100 m of Hole 689B. Bulk densities ranged from a low of 1.22 g/cm³ at 8.5 mbsf to a high of 2.35 g/cm³ at 260.6 mbsf. Water content mirrors bulk density and ranges from a high of 359% at 15 mbsf to a low of 26% at 291.5 mbsf. Grain density ranged from a high of 3.19 g/cm³ at 81.25 mbsf to a low of 1.55 g/cm³ at 15 mbsf. In Hole 690C a grain density of 3.32 g/cm³ was measured at 4.7 mbsf. The grain density at this site is unusual in that it is inversely related to water content and porosity (in upper 70 m) and directly related to bulk density. In most marine sediments the grain density is unrelated to either of these measures, essentially being a constant with a value between 2.65 and 2.75 g/cm³. These odd relationships reflect the influence of the presence of diatoms and the low density (specific gravity) of biogenic silica (2.02 g/cm³). The presence of radiolarian and diatom ooze accounts for the large variations in the index properties because of their very low bulk density and ability to form a strong fabric.

Silica content was not determined for Hole 689B sediments, but the percent calcium carbonate was measured (Table 4). Figure 16 is a profile of calcium carbonate percentages. The calcium carbonate content reflects the amount of silica present if the sediment contains only siliceous and calcareous components. In the upper 30.2 m of Hole 689B the CaCO₃ content is less than 2.9% and averaged 0.9%; at 30.9 and 31.3 mbsf it is 50.2% and 62.2%, respectively. The decreases in CaCO₃ in the upper 32 mbsf is reflected in the index properties, bulk density, water content, grain density, and porosity (Figs. 14 and 15). Below 32 mbsf the CaCO₃ content is almost always higher than 75%. As the CaCO₃ content stabilizes downhole, a steady decrease, with only minor perturbations, of porosity and water content and a steady increase in bulk density are observed. These variations are attributed to diagenetic alterations in the form of compaction (consolidation) and possible cementation. At 210 mbsf large increases in bulk density and decreases in porosity are associated with the occurrence of nannofossil ooze and semilithified ooze and chalk.

Compressional Wave Velocity

Sonic velocities (V_p) in sediment were measured using two methods. A continuous measurement of V_p was made through the whole core using a P -wave logger (PWL) installed next to the GRAPE source and detector. The Hamilton Frame Velocimeter was utilized for the laboratory determination of V_p on individual samples removed from the core using procedures outlined by Boyce (1976). V_p was measured in only one direction, as the

Table 3. Index properties measured on samples from Site 689.

Core, section interval (cm)	Depth (mbsf)	Water content (%)	Porosity (%)	Bulk density (g/cm ³)	Grain density (g/cm ³)
113-689A-					
1H-1, 101	1.0	266.34	87.71	1.24	2.12
1H-2, 99	2.5	198.09	83.77	1.29	2.47
1H-6, 145	7.5	168.62	76.73	1.25	1.92
113-689B-					
1H-3, 101	4.0	271.51	91.08	1.28	2.26
2H-1, 23	5.5	268.60	91.83	1.29	2.24
2H-3, 20	8.5	238.60	84.05	1.22	1.99
3H-1, 20	15.0	359.57	97.65	1.28	1.55
3H-3, 20	18.0	158.60	82.07	1.37	2.52
3H-5, 21	21.0	195.48	87.27	1.35	2.73
4H-1, 63	24.9	199.03	87.41	1.35	2.87
4H-3, 63	27.9	213.77	83.29	1.25	2.00
4H-5, 63	30.9	114.60	75.56	1.45	2.46
4H-5, 92	31.2	83.12	71.01	1.60	2.67
4H-6, 90	32.7	67.72	66.69	1.69	2.77
5H-2, 90	36.2	78.33	67.86	1.58	2.62
5H-4, 90	39.2	58.35	62.20	1.73	2.84
5H-6, 90	42.2	59.43	61.99	1.70	2.76
6H-2, 90	45.7	111.73	69.63	1.35	2.09
6H-4, 67	48.5	180.75	81.15	1.29	2.12
6H-6, 90	51.7	219.76	84.65	1.26	2.24
7H-2, 90	55.3	72.29	62.65	1.53	2.33
7H-4, 90	58.3	97.90	68.47	1.42	2.16
7H-6, 90	61.3	99.00	68.73	1.42	2.24
8H-3, 90	66.4	69.68	63.13	1.57	2.50
8H-5, 90	69.4	49.93	53.45	1.64	2.37
9H-2, 90	74.5	56.78	61.11	1.73	2.76
9H-4, 90	77.5	50.94	58.68	1.78	2.79
9H-6, 8	79.7	54.20	59.29	1.73	2.72
10H-2, 90	84.1	63.40	63.93	1.69	2.72
10H-4, 90	87.1	62.36	63.34	1.69	2.72
10H-6, 90	90.1	60.01	62.69	1.71	2.81
12H-1, 63	101.6	55.82	62.22	1.78	2.84
12H-3, 62	104.6	61.12	64.81	1.75	2.77
12H-5, 64	107.6	53.06	63.83	1.89	2.87
13H-1, 63	111.2	81.25	74.40	1.70	3.19
13H-3, 63	114.2	54.57	60.42	1.75	2.70
13H-5, 63	117.2	52.52	59.39	1.77	2.80
14H-1, 62	120.8	58.96	65.05	1.80	3.09
14H-3, 63	123.8	61.84	65.37	1.75	2.94
14H-5, 61	126.8	61.52	62.93	1.69	2.57
15H-1, 64	130.6	56.59	66.08	1.87	3.06
15H-3, 64	133.6	64.82	64.97	1.69	2.70
15H-5, 64	136.6	48.92	59.52	1.86	2.92
16H-1, 62	140.0	46.97	58.60	1.88	2.91
16H-3, 62	143.0	58.72	67.06	1.86	3.03
16H-5, 63	146.0	49.45	60.06	1.86	2.87
17H-1, 59	149.7	50.10	58.30	1.79	2.68
17H-3, 58	152.7	43.56	58.42	1.97	2.96
17H-5, 58	155.7	44.59	57.72	1.92	2.92
18H-2, 90	161.2	46.11	57.41	1.86	2.87
18H-4, 90	164.2	47.72	57.53	1.82	2.83
18H-6, 90	167.2	49.88	57.16	1.76	2.68
19H-2, 90	170.9	47.84	56.99	1.80	2.64
19H-4, 90	173.9	46.60	57.38	1.85	2.83
19H-6, 90	176.5	43.76	54.31	1.83	2.67
20H-2, 90	180.5	38.19	51.06	1.89	2.87
20H-4, 90	183.5	45.13	55.70	1.84	2.73
21H-1, 90	188.7	49.25	57.29	1.78	2.68
21H-3, 90	191.7	46.26	55.99	1.81	2.67
22X-5, 51	204.1	26.81	43.46	2.11	2.77
23X-1, 413	207.6	52.71	60.37	1.79	2.83
23X-2, 136	210.1	56.94	63.61	1.80	2.26
23X-3, 107	211.3	34.65	48.77	1.94	2.69
24X-7, 7	212.4	26.81	43.09	2.09	2.72
26X-7, 8	228.1			2.24	
27X-1, 65	246.7			2.18	
27X-2, 62	248.1			2.18	
28X-1, 44	256.1			2.19	
28X-4, 43	260.6			2.35	
29X-1, 140	266.6	39.30	55.09	2.00	2.99
29X-2, 136	268.1	33.50	50.66	2.07	2.85
30X-1, 135	276.3	35.72	53.13	2.07	2.93
32X-7, 23	291.5	26.02	42.21	2.09	2.58

Table 3 (continued).

Core, section interval (cm)	Depth (mbsf)	Water content (%)	Porosity (%)	Bulk density (g/cm ³)	Grain density (g/cm ³)
1H-1, 15	0.2	211.89	85.11	1.28	2.52
1H-2, 15	1.7	361.28	90.02	1.18	2.07
1H-3, 15	3.2	384.72	90.78	1.17	1.84
1H-4, 15	4.7	236.50	89.46	1.30	3.32
1H-5, 15	6.2	327.06	88.63	1.19	1.89
1H-6, 15	7.7	200.08	85.27	1.31	2.34
1H-7, 15	8.8	224.66	86.31	1.28	2.32
2H-1, 41	9.0	248.78	84.48	1.21	1.97
3H-1, 90	19.0	209.24	87.95	1.33	2.04
3H-2, 90	20.5	226.12	83.43	1.23	2.16
3H-3, 90	22.0	160.19	80.60	1.34	2.28
3H-4, 90	23.5	111.86	75.86	1.47	2.45
3H-5, 90	25.0	190.45	85.18	1.33	2.42
3H-6, 90	26.5	198.57	81.63	1.26	2.10
3H-7, 42	27.5	240.62	83.52	1.21	1.98
1H-1, 90	19.0	135.37	81.10	1.44	2.63
1H-3, 90	22.0	234.59	86.33	1.26	2.31
1H-4, 90	23.5	117.52	74.38	1.41	2.30
1H-5, 90	25.0	222.00	85.27	1.27	2.52
1H-6, 90	26.5	244.18	85.80	1.24	1.97
2H-1, 90	28.6	166.65	78.82	1.29	2.20
2H-2, 90	30.1	168.06	80.16	1.31	2.21
2H-3, 90	31.6	68.89	66.33	1.67	2.76
2H-4, 90	33.1	65.21	64.72	1.68	2.77
2H-5, 90	34.6	68.46	65.70	1.66	2.75
2H-6, 90	36.1	56.84	60.17	1.70	2.64
3H-1, 90	38.2	66.47	65.56	1.68	2.59
3H-2, 90	39.7	70.80	67.39	1.67	2.80
3H-3, 90	41.2	65.63	63.86	1.65	2.58
3H-5, 90	44.2	124.77	76.46	1.41	2.53
3H-6, 90	45.7	143.67	76.66	1.33	2.15
4H-1, 123	49.1	126.53	75.93	1.39	2.34
4H-2, 90	50.3	110.53	62.00	1.21	2.52
4H-3, 90	51.8	168.76	66.89	1.09	2.08
4H-4, 90	53.3	178.84	81.45	1.30	2.41
4H-5, 90	54.8	102.06	71.10	1.44	2.46
4H-6, 90	56.3	151.73	81.43	1.38	2.21

sediments in Hole 689B are bioturbated and acoustic anisotropy was at a minimum. Measurements on competent "biscuits" of core were made on sediments obtained by the XCB.

Figure 17 shows the V_p profile obtained by the Hamilton Frame Velocimeter for Hole 689B sediments. Table 5 lists the V_p determinations. Figure 18 shows the V_p values as obtained by the PWL. In most cases the agreement between the two methods of measurements is very good.

The V_p velocity in the radiolarian-diatom ooze of lithostratigraphic Unit I (0–31.0 mbsf) is relatively high for such low-density/high-porosity sediments. In this unit the density of the sediment appears to be the major factor that governs acoustic velocity. Within the silicious ooze the V_p velocity increases with increasing bulk density, attesting to the strong sediment fabric created by the diatoms. Between 31.2 and 45.7 mbsf the V_p decreases while the bulk density increases as much as 32%. This dependence of velocity on density is seldom observed, although it is quite common in most high-water-content clays. Figure 19 is a density profile created from GRAPE data from Section 113-689B-4H-5. Note the increase of density between 50 and 110 cm (30.8–31.4 mbsf) and compare this increase in density with a corresponding decrease in V_p at 30 mbsf (Fig. 18). This change in velocity marks the lower boundary of lithostratigraphic Unit I.

Figure 18 shows the V_p profile of PWL data and illustrates the increase in velocity at 50 mbsf due to a decrease in bulk density in Core 113-689B-6H. The velocity in the interval between 31 and 100 mbsf exhibits a decreasing gradient of 1.19 m/s/m. In the interval between 100 and 137 mbsf the velocity gradient is zero. From 137 to 180 mbsf an increasing velocity gradient of 1.16 m/s/m is observed.

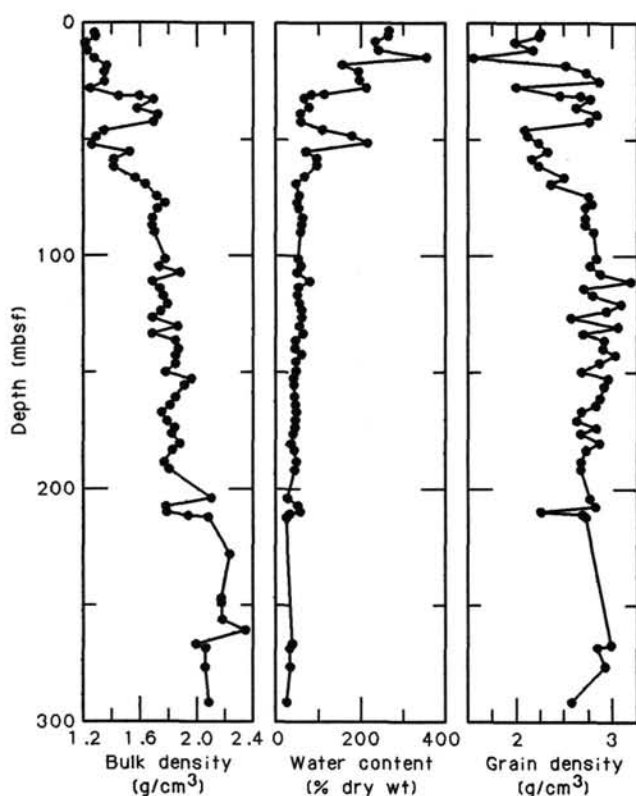


Figure 14. Profile of bulk density, water content, and grain density for Hole 689B.

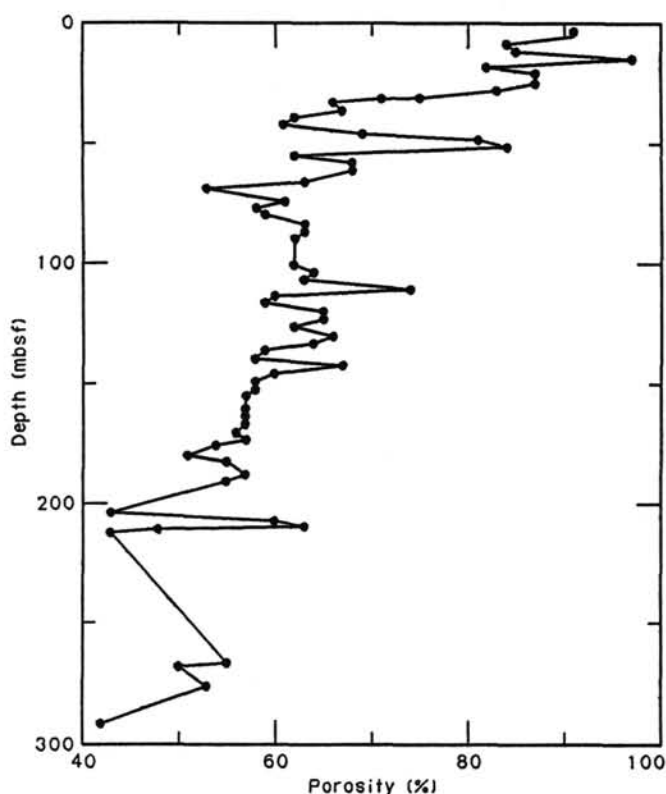


Figure 15. Profile of porosity for Hole 689B.

Table 4. Calcium carbonate percentages for sediments from Site 689.

Core, section interval (cm)	Depth (mbsf)	CaCO ₃ (%)	Core, section interval (cm)	Depth (mbsf)	CaCO ₃ (%)
113-689A-			113-689B-		
1H-1, 101	1.01	0.0	14H-5, 61	126.8	87.1
1H-2, 99	2.50	0.0	15H-1, 64	130.6	87.5
1H-3, 101	4.0	0.0	15H-3, 64	133.6	89.2
1H-3, 145	4.5	0.03	15H-4, 112	135.9	87.9
1H-6, 145	9.0	0.03	15H-5, 64	136.6	88.8
113-689B-			16H-1, 62	140.0	95.8
2H-1, 23	5.5	0.6	16H-3, 62	143.0	90.1
2H-3, 20	8.5	2.9	16H-5, 63	146.0	94.5
2H-4, 145	11.2	0.3	17H-1, 59	149.7	95.1
2H-5, 20	11.5	1.2	17H-3, 58	152.9	90.3
3H-1, 20	15.0	0.3	17H-5, 58	155.5	94.1
3H-3, 20	18.0	0.2	18H-2, 90	161.2	94.0
3H-4, 120	20.5	0.3	18H-4, 90	164.4	82.5
3H-5, 21	21.0	1.0	18H-4, 112	164.7	71.5
4H-1, 63	24.9	3.9	18H-6, 90	167.2	87.0
4H-3, 63	27.9	0.5	19H-2, 90	170.9	85.1
4H-4, 145	30.2	0.2	19H-4, 90	173.9	98.1
4H-5, 63	30.9	50.7	19H-6, 52	176.4	90.7
4H-5, 92	31.2	62.1	20H-2, 90	180.5	93.0
4H-6, 90	32.9	81.3	20H-4, 90	183.5	89.5
5H-2, 90	36.2	81.3	21H-1, 90	188.7	93.3
5H-4, 90	39.2	91.3	21H-3, 90	191.7	94.4
5H-4, 145	29.7	89.0	22X-1, 81	198.6	85.1
5H-6, 90	42.2	90.0	22X-3, 78	201.6	89.6
6H-2, 90	45.7	7.8	22X-4, 112	203.4	91.0
6H-4, 67	48.5	1.2	22X-5, 51	204.1	95.1
6H-4, 120	49.0	0.8	23X-1, 41	207.6	81.7
6H-6, 90	51.7	36.8	23X-2, 136	210.1	89.5
7H-2, 90	55.3	54.6	23X-3, 107	211.3	93.3
7H-4, 90	58.3	37.7	24X-CC, 10	212.7	89.6
7H-6, 90	61.3	0.2	25X-4, 112	218.4	92.3
8H-1, 90	63.4	51.2	28X-3, 112	260.1	91.5
8H-3, 90	66.4	63.1	29X-1, 140	266.6	90.8
8H-5, 90	69.4	68.4	29X-2, 136	268.1	84.0
9H-2, 90	74.5	89.6	30X-1, 135	276.3	84.0
9H-4, 90	77.5	85.1	32X-CC, 23	291.5	90.0
9H-4, 117	77.7	89.2	113-689C-		
9H-6, 8	79.7	75.5	1H-1, 15	0.2	5.1
10H-2, 90	84.1	98.5	1H-2, 15	1.7	0.3
10H-4, 90	87.1	84.1	1H-3, 15	3.2	0.3
10H-6, 90	90.1	76.9	1H-4, 15	4.7	0.2
11H-1, 90	92.2	83.1	1H-5, 15	6.2	0.3
11H-3, 90	95.2	79.1	1H-6, 15	7.7	0.3
11H-5, 90	98.2	84.9	1H-7, 15	8.8	0.3
12H-1, 63	101.6	61.8	2H-1, 41	9.0	0.2
12H-3, 62	104.6	85.1	3H-1, 90	19.0	7.6
12H-4, 112	105.1	86.0	3H-2, 90	20.5	0.5
12H-5, 64	107.6	83.0	3H-3, 90	22.0	0.3
13H-1, 63	111.2	63.9	3H-4, 90	23.5	37.5
13H-3, 63	114.2	90.0	3H-5, 90	25.0	6.2
13H-5, 63	117.2	92.6	3H-6, 90	26.5	0.3
14H-1, 62	120.8	85.1	3H-7, 42	27.5	2.8
14H-3, 63	123.8	87.4			

Vane Shear Strength

The undrained shear strength of the sediment was determined using the ODP motorized miniature vane shear device. Its operation and calculations follow procedures outlined by Boyce (1976). The shear strengths determined for Hole 689B sediments may be in error because the instrument drift over the period used was $\sim 25\%$. It was not known at what stage in the investigation the drift occurred. After recalibration all measurements were multiplied by a factor of 1.25. No attempts were made to measure the residual strength as outlined in the procedure handbook. The residual strength of noncohesive sediment such as diatom or nannofossil ooze was considered unmeasurable with the existing equipment.

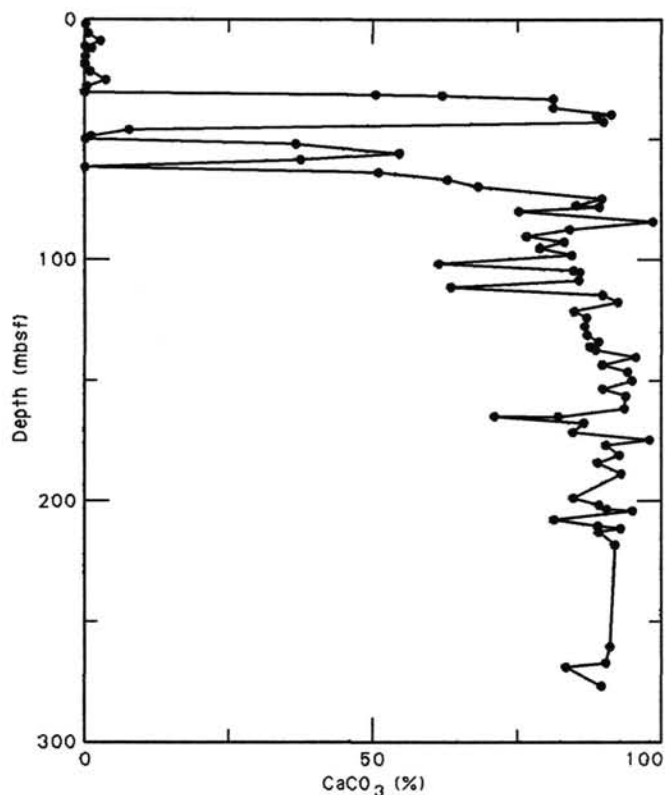


Figure 16. Profile of calcium carbonate percentages for Hole 689B (data given in Table 4).

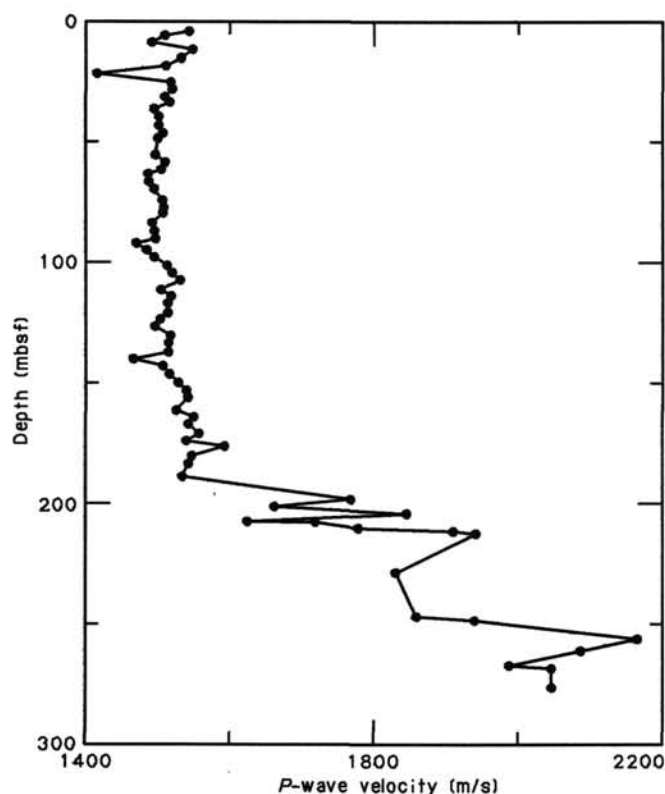


Figure 17. Compressional wave velocity (Hamilton Frame) profile for Hole 689B.

Table 5. Compressional wave velocities (Hamilton Frame) measured on samples from Hole 689B.

Core, section top (cm)	Depth (mbsf)	Velocity (m/s)	Core, section top (cm)	Depth (mbsf)	Velocity (m/s)
113-689B-			113-689B-		
1H-3, 101	4.0	1545	14H-1, 62	120.8	1516
2H-1, 23	5.5	1515	14H-3, 63	123.8	1506
2H-3, 20	8.5	1493	14H-5, 61	126.8	1497
2H-5, 20	11.5	1550	15H-1, 64	130.6	1520
3H-1, 20	15.0	1534	15H-3, 64	133.6	1518
3H-3, 20	18.0	1512	15H-5, 64	136.6	1517
3H-5, 21	21.0	1416	16H-1, 62	140.0	1470
4H-1, 63	24.9	1518	16H-3, 62	143.0	1508
4H-3, 63	27.9	1521	16H-5, 63	146.0	1518
4H-5, 63	30.9	1517	17H-1, 59	149.7	1531
4H-5, 92	31.2	1512	17H-3, 58	152.7	1543
4H-6, 90	32.7	1517	17H-5, 58	155.7	1545
5H-2, 90	36.2	1496	18H-2, 90	161.2	1528
5H-4, 90	39.2	1496	18H-4, 90	164.2	1554
5H-6, 90	42.2	1503	18H-6, 90	167.2	1546
6H-2, 90	45.7	1508	19H-2, 90	170.9	1560
6H-4, 67	48.5	1503	19H-4, 90	173.9	1543
7H-2, 90	55.3	1498	19H-6, 50	176.1	1596
7H-4, 90	58.3	1511	20H-2, 90	180.5	1551
7H-6, 90	61.3	1506	20H-4, 90	183.5	1546
8H-1, 90	63.4	1488	21H-1, 90	188.7	1537
8H-3, 90	66.4	1489	22X-1, 81	198.3	1772
8H-5, 90	69.4	1496	22X-3, 78	201.3	1665
9H-2, 90	74.5	1508	22X-5, 51	204.1	1849
9H-4, 90	77.5	1510	23X-1, 41	207.6	1628
9H-6, 8	79.7	1508	23X-1, 42	207.6	1722
10H-2, 90	84.1	1494	23X-2, 136	210.1	1781
10H-4, 90	87.1	1497	23X-3, 107	211.3	1914
10H-6, 90	90.1	1498	24X-7, 7	212.4	1944
11H-1, 90	92.2	1473	26X-7, 8	228.1	1834
11H-3, 90	95.2	1486	27X-1, 65	246.7	1864
11H-5, 90	98.2	1496	27X-2, 62	248.1	1942
12H-1, 63	101.6	1515	28X-1, 44	256.1	2165
12H-3, 62	104.6	1522	28X-4, 43	260.6	2088
12H-5, 64	107.6	1533	29X-1, 140	266.6	1992
13H-1, 63	111.2	1506	29X-2, 136	268.1	2049
13H-3, 63	114.2	1520	30X-1, 135	276.3	2050
13H-5, 63	117.2	1516			

Figure 20 shows a profile of undrained vane shear strength. The most striking feature of this profile is the large scatter of shear strength values down the profile. One unusual feature of the strength of the sediments at this site is that the highest strength values were found in the upper 100 m of the section. The *in-situ* shear strength of the chalk found below 200 mbsf would have values highly in excess of those measured. There is an indication that the high values of strength in the upper 75 m of the section reflect the mixing of silicious ooze with nannofossil ooze. Mixtures such as this can form a very strong fabric, one that resists a shearing stress and yet does not have sufficient rigidity to possess a high acoustic velocity. Another interesting feature is the association of porosity and shear strength in the upper 50 m of the section. The shear strength follows the porosity. The obvious explanation for this unusual association is in the amount of siliceous ooze present. We see again that the presence of silicious material is the factor that overrides the more conventional associations.

Thermal Conductivity

The thermal conductivity of the sediment samples in Hole 689B was measured following the methods of Von Herzen and Maxwell (1959) using the needle-probe technique. The needle probe was inserted through a drilled hole in the core liner so that the probes were oriented perpendicular to the core axis.

The thermal conductivity of the sediment samples in Hole 689B was measured to the depth of 94.6 mbsf. Thermal conduc-

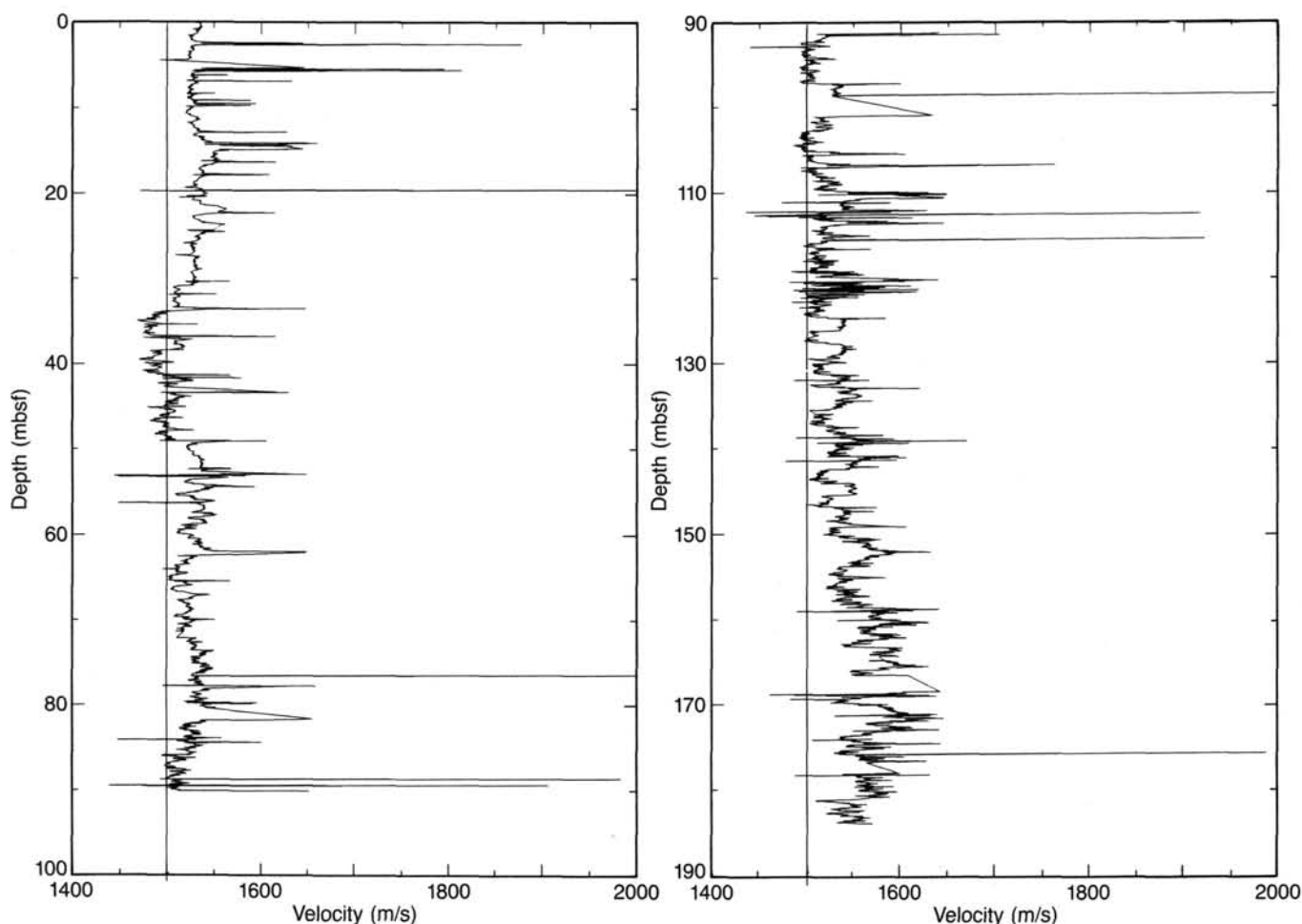


Figure 18. Compressional wave velocity profile (PWL) for Hole 689B.

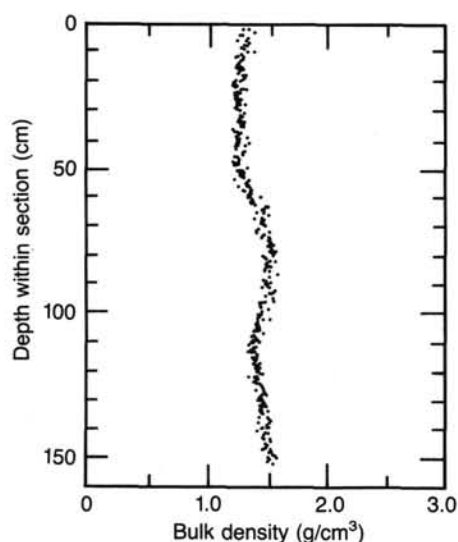


Figure 19. Bulk density profile of Section 113-689B-4H-5 from GRAPE data.

tivity ranged from a low of 0.689 W/m-K to a high of 1.468 W/m-K. Table 6 lists the values of thermal conductivity, and Figure 21 is a profile generated from those values. Thermal conductivity is directly related to bulk density and inversely related

to water content. The thermal gradient for the section measured at Hole 689B is 0.008 W/m-K/m.

Summary

The results of physical property measurements at Site 689 demonstrate the effect that density, in this case low-density biogenic silica and high-density calcium carbonate ooze, can have on the index properties, as well as compressional wave velocities. It was also demonstrated that physical properties can delineate geotechnical boundaries which in most cases can be associated with lithostratigraphic boundaries and seismic horizons. Figure 22 shows the association of units within Hole 689B as determined by lithostratigraphic, seismic, and geotechnical methods.

The geotechnical zones designated in Figure 22 are based on the following characteristics. Unit G-I (0–31.2 mbsf) contains a low-bulk-density, high-velocity, high-porosity sediment that corresponds to the siliceous ooze of lithostratigraphic Unit I. Units G-II (31.2–45.7 mbsf) and G-IV (51.5–74 mbsf) contain a high-density and low-velocity calcium carbonate sediment that corresponds to the diatom-nannofossil ooze of lithostratigraphic subunit IIA. Unit G-III (45.7–51.7 mbsf) is a low-density, high-velocity, low calcium carbonate sediment that has no lithostratigraphic counterpart. Unit G-V (74–150 mbsf) corresponds to lithostratigraphic Subunit IIB, a nannofossil ooze. It consists of sediment with almost constant physical and acoustical properties and has a high calcium carbonate content. Unit G-VI (150–190 mbsf) is based on an increase in velocity, almost constant

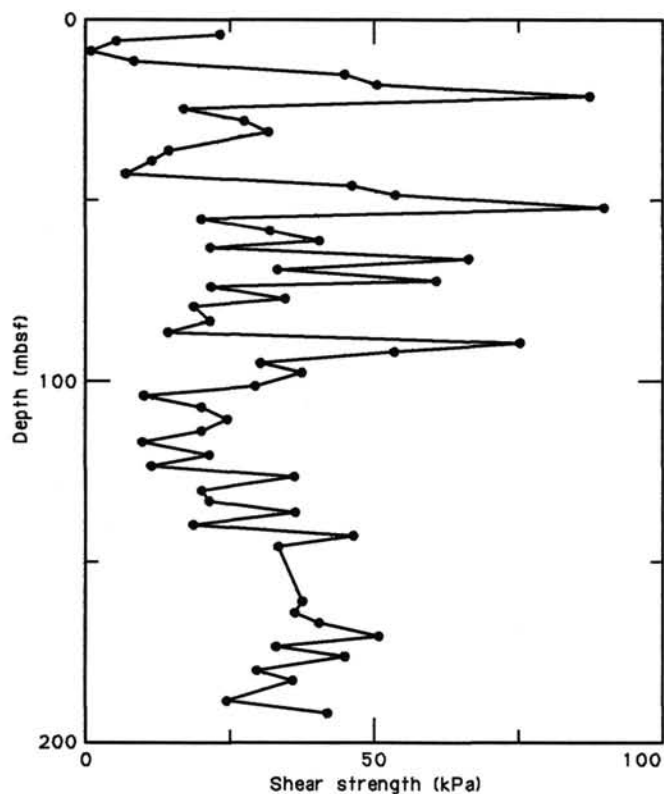


Figure 20. Undrained shear strength profile of Hole 689B.

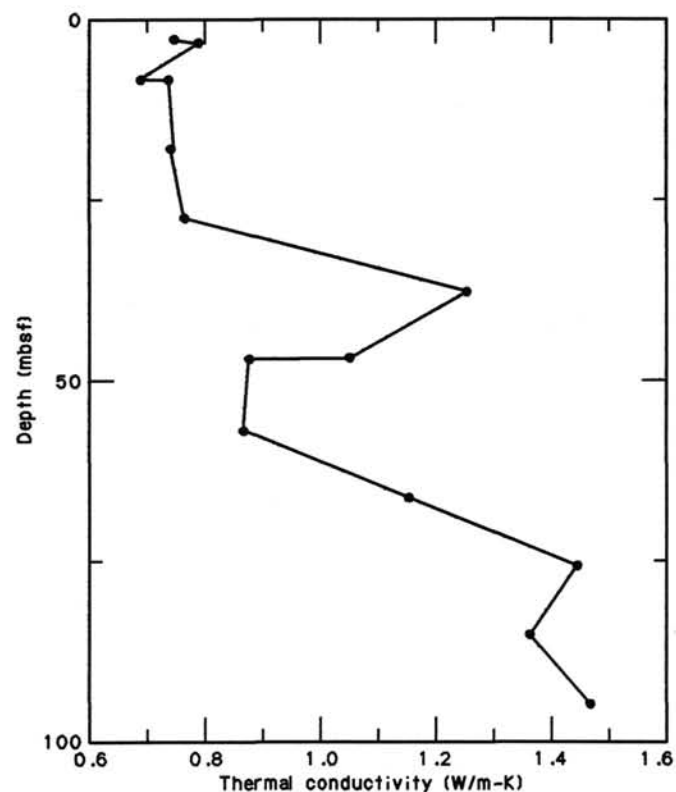


Figure 21. Thermal conductivity profile of Hole 689B.

Table 6. Thermal conductivity values measured on samples from Hole 689B.

Core, section top (cm)	Depth (mbsf)	(W/m-K)
113-689B-		
1H-3, 20	3.2	0.748
1H-3, 30	3.3	0.788
2H-3, 20	8.5	0.689
2H-3, 30	8.6	0.738
3H-3, 20	18.0	0.748
3H-3, 30	18.1	0.743
4H-3, 20	27.5	0.762
4H-3, 30	27.6	0.766
5H-3, 60	37.4	1.254
5H-3, 70	37.5	1.252
6H-3, 25	46.6	1.052
6H-3, 60	46.9	0.877
6H-3, 70	47.0	0.875
7H-3, 83	56.7	0.864
8H-3, 25	65.8	1.152
9H-3, 25	75.4	1.446
10H-3, 25	85.0	1.364
11H-3, 25	94.6	1.468

porosity, and increasing calcium carbonate content and bulk density. This zone does not have a corresponding lithostratigraphic unit and is contained within Subunit IIIA. Unit G-VII (190–297.3 mbsf) is based on large increasing changes in index properties, shear strength, and velocity. The top of this unit may represent a hiatus or the boundary between a semilithified ooze and nannofossil chalk. This unit can be further subdivided at 254 mbsf where a large increase in velocity takes place. Physical property data for Holes 689A, 689C, and 689D are listed in Ta-

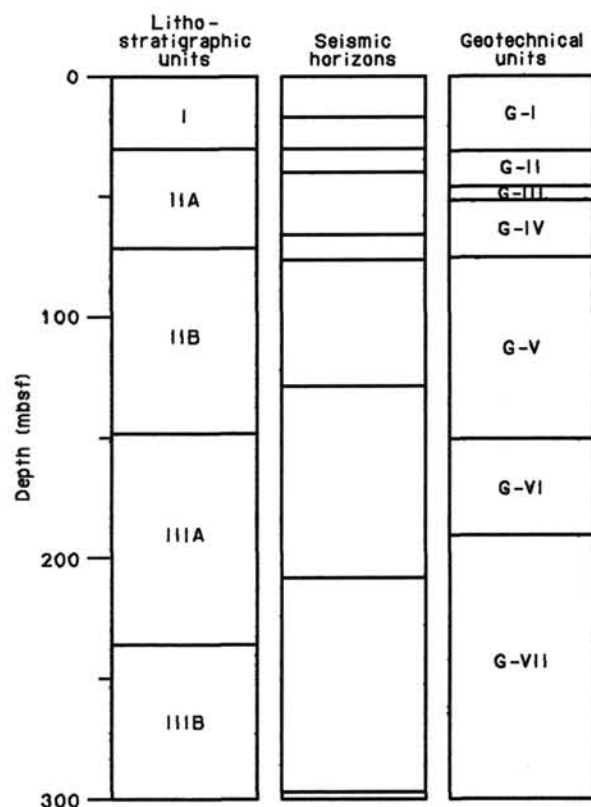


Figure 22. Boundaries and horizons determined by lithostratigraphic, seismic, and geotechnical methods. Line in "Geotechnical units" column designates boundary based on change of single property.

ble 3. The thermal conductivity of sediments from Hole 689B ranged from 0.689 W/m-K to 1.468 W/m-K.

SEISMIC STRATIGRAPHY

Site 689 was chosen originally as shotpoint (SP) 1000 on multichannel seismic line UB Maud-3 (Univ. of Bergen Seismological Observatory, Norway). UB Maud-3 (Fig. 3) was shot 12-fold, at a 50-m shot spacing and using one 600-in.³ Bolt air gun. A 3.5-kHz profile (Fig. 4) was run along the same line. Also in the vicinity is profile BGR 86-32 (Bundesanstalt für Geowissenschaft und Rohstoffe, Hannover, FRG), on which the alternative site W2B was located. Our approach to and departure from Site 689 chose different tracks from these, since the drilling target was broad and the region sparsely surveyed (see track chart, Fig. 2). *JOIDES Resolution's* profiler used one or two 80-in.³ water guns, a single-channel streamer, and digital recording; the system was in use while approaching and leaving the site. On the approach, the guns were not firing regularly because of icing.

The time resolution and penetration of these profiles vary considerably. Line UB Maud-3 penetrates to likely volcanic basement at 400 milliseconds (ms) two-way traveltime (tw) sub-bottom, and shows possible primary reflections beneath basement, but the dominant frequency is 50 Hz and the wavetrain of individual reflections is as long as 40 ms. This limits its capacity for resolving detail. The 3.5-kHz record is complementary, having a primary pulse length of 2 ms or less, and here a remarkably high 250-ms penetration. *JOIDES Resolution's* water-gun records have adequate penetration for this site, and stratigraphic resolution as much as four times that of UB Maud-3.

No holes at Site 689 were logged, so that the relation between time down the seismic record and depth down the hole could be derived only from shipboard velocity determinations on the cores, using the PWL and Hamilton Frame apparatus. The values obtained using these two methods are in approximate agreement (see "Physical Properties" section, this chapter), although there is commonly a small unexplained "core section" effect on PWL measurements. Either method will suffice to relate the cored section to the profiles. The physical properties measurements have also revealed an interesting relation between velocity, density, and carbonate/silica content near the top of the section, which should lead eventually to a more complete explanation for the nature of some of the shallow reflections.

Figure 23 shows velocities extracted from PWL records from Hole 689B cores, together with a simplified velocity/depth model based upon them. It compares well with Figure 17 (Hamilton Frame values). For the depth range sampled by APC, down to about 200 mbsf, Hamilton Frame and PWL values agree; the velocity/depth model is biased slightly high to take account of likely differences between *in-situ* and laboratory conditions. Below 200 mbsf, XCB-cored, the model velocities are intermediate between (lower) PWL values and (higher) Hamilton Frame values, on the assumption that, with lower recovery and core biscuiting, the harder, denser, and therefore probably faster lithologies will have been recovered and measured preferentially.

The several reflection profiles available do not all show similar reflectors at the same depths. This is an inevitable consequence of the differences in seismic source characteristics. In Figure 24, *JOIDES Resolution's* site approach profile is compared with the velocity/depth model, and the major reflectors are listed in Table 7. A very weak seafloor reflection is followed by three reflections in the uppermost 100 ms which result from density changes related to sharp silica/carbonate alternations in the top 70 mbsf (Pliocene-Pleistocene to lower Miocene-upper Oligocene). Individual reflections in the next 160 ms (to the upper Paleocene) are weaker, probably because of the more uniform carbonate lithology downhole, but they can be traced along

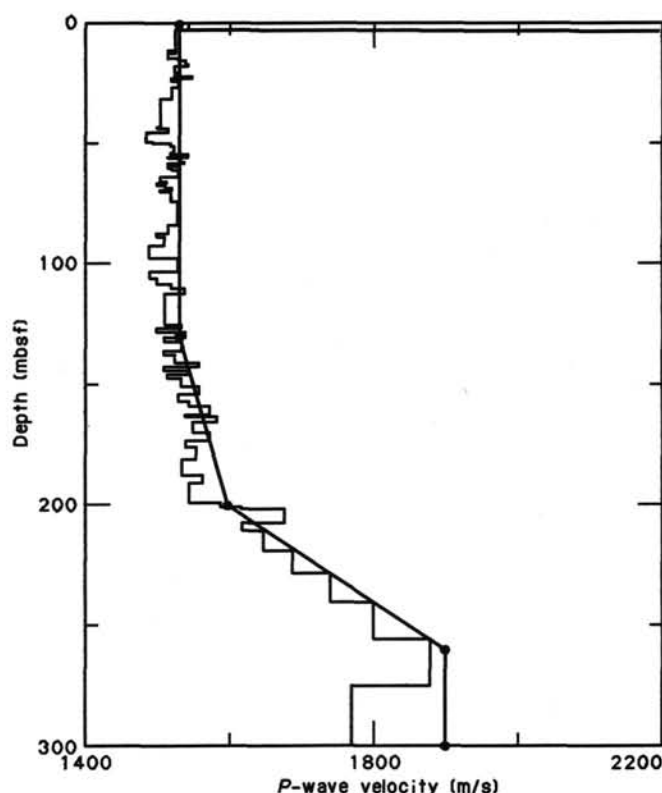


Figure 23. Velocities extracted from PWL records of Hole 689B cores, with velocity model used to relate downhole depth to two-way traveltime on seismic records.

the seismic record away from the site. A series of weak reflectors beginning at 245 ms is associated with the progressive formation of chalk and chert, and thus may not be time-planes away from the site. The base of Hole 689B at 297.3 mbsf lies about 365 ms below seafloor, perhaps only 25–45 m above volcanic basement, taken to be the strong irregular reflector at 345 ms on the seismic records.

Site 689 is located in a basement depression, seemingly open only to the north. From the site survey data available, this sheltered location appeared to offer the best possibility on the crest of Maud Rise of finding a continuous sedimentary succession. This remains the case, and in general the sediments thin away from the site. In particular, sediments of early and middle Miocene age (at 40–70 mbsf) pinch out to the north, suggesting a period of stronger bottom current flow. Preliminary bio- and magnetostratigraphic studies have identified a hiatus at 68 mbsf. Even more prominently, reflectors representing upper Eocene to upper Oligocene sediments (98–145 mbsf at the site) are truncated away from the site by the overlying sediments. This is best interpreted as a period of stronger current action during the late Oligocene and corresponds to a hiatus or period of low deposition. None of the other hiatuses or intervals of reduced deposition tentatively identified at the site (upper Pliocene and Quaternary, upper Oligocene to Miocene, uppermost Paleocene to upper lower Eocene, Danian) have any expression in the seismic records.

Older sediments remain largely conformable away from the site, except in their relation to basement. Reflectors below about 225 mbsf at the site (of Maestrichtian-Campanian age) lap onto basement, suggesting at least the possibility that part of Maud Rise near Site 689 was subaerial until the latest Cretaceous.

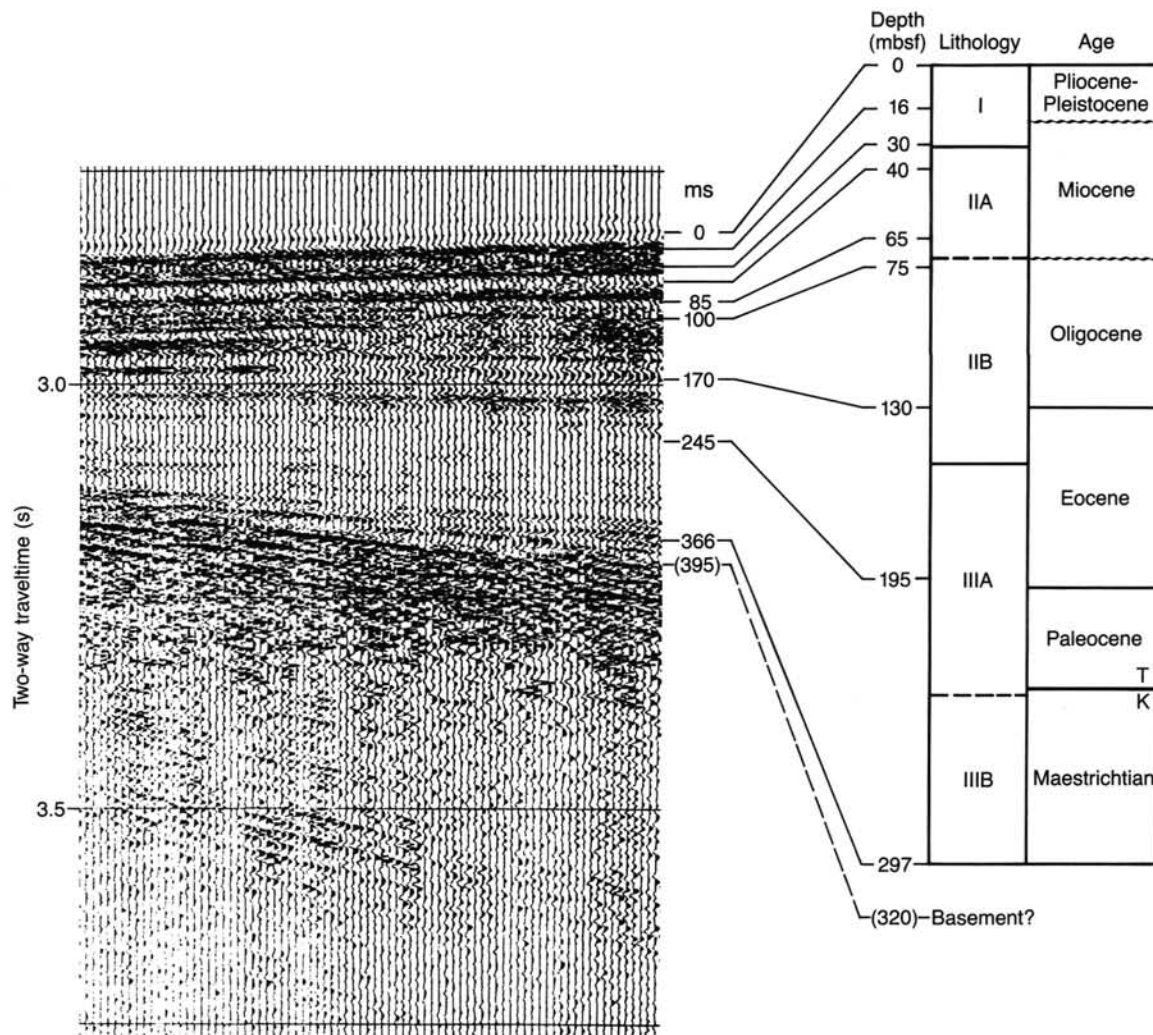


Figure 24. Section of profile acquired on *JOIDES Resolution's* approach to Site 689, compared with drilled section in Hole 689B.

Table 7. Main seismic reflectors at Site 689.

Two-way traveltime below seafloor (m/s)	Depth (mbsf)	Sediment age	Comments
21	about 16	Pliocene (Gilbert)	Silicoflagellate zone in siliceous ooze—small increase in bulk density.
42	about 30	middle-late Miocene	Top of diatom nannofossil ooze: density increase, water content drop.
60	about 40	late middle Miocene	Top of a diatom ooze: density decrease. Polarity inverted.
85–100	65–75	early-middle Miocene/late Oligocene (hiatus?)	Nannofossil ooze beneath siliceous ooze: density increase over 10–20 m.
170	about 130	Eocene/Oligocene boundary	Base of weak reflector set, small but variable silica content, in lower Oligocene.
245	195	early Eocene	Top of weak reflector set caused as chalk forms from ooze.
about 366	297	late Campanian?/early Maestrichtian	Base of Hole 689B in stronger reflectors: cherts?
395	320	?	Basement?

BIOSTRATIGRAPHY

Site 689 was drilled in 2080 m of water near the crest of Maud Rise to obtain a predominantly carbonate and in part biosiliceous-rich Cenozoic and older section beneath the present-day Antarctic water mass. This was the first of a two-site transect to study the vertical water-mass history of the rise. The mission at this site was accomplished through the penetration of 297.3 m of Quaternary to Campanian(?) sediment in Hole 689B, with an average core recovery of 77%. Beneath a topmost 1-cm-thick Quaternary foraminiferal ooze lay some 30 m of middle Pliocene-upper Miocene biosiliceous ooze with minor amounts of carbonate. The remainder of the Miocene (down to 66 mbsf) consisted of varying proportions of nannofossil and biosiliceous oozes, whereas the Oligocene through Cretaceous strata were composed of nannofossil ooze and chalk. The hole sampled a possibly complete K/T boundary section. The upper 133.8 m of section was recovered using the APC in Holes 689C and 689D in order to bridge coring gaps down to the Eocene.

All depths referred to are depths below seafloor, and samples are from core-catcher (CC) material unless specified otherwise. On the summary biostratigraphic correlation chart (Fig. 25), unless samples within a core were studied, the age and biostratigraphic zone assigned to a core-catcher sample are extrapolated to the midpoint of the overlying and underlying core. The section is described from the top down.

Planktonic Foraminifers

Planktonic foraminifers were examined from all core catchers in Hole 689B. Additional samples were also examined from each core in order to document species ranges and to identify chronostratigraphic boundaries within cores. Preservation of planktonic foraminifers varied considerably through the section. In general, Eocene through Cretaceous planktonic foraminifers are well preserved. The Oligocene is marked by a number of changes in preservational quality, ranging from poor to excellent. Where present, Miocene-Pliocene planktonic foraminifers exhibit moderate to good preservation. Preservation of Quaternary planktonic foraminifers is excellent.

Quaternary planktonic foraminifers are very abundant at the top of Core 113-689B-1H. Abundances drop dramatically to rare to common in the Pliocene to lower Miocene and upper Oligocene, and increase noticeably toward the base of the Oligocene. Planktonic foraminifers become very abundant across the Eocene/Oligocene boundary. Abundances continue to be high in the Eocene through Upper Cretaceous.

Quaternary

A thin veneer of Quaternary planktonic foraminiferal ooze at the top of Core 113-689B-1H is composed entirely of Antarctic forms of sinistrally coiled *Neogloboquadrina pachyderma*.

Neogene

The Pliocene to upper Miocene is marked by essentially monospecific assemblages typical of modern polar assemblages but quite different from Subantarctic assemblages where biostratigraphic zonations exist. Therefore, no zonal scheme could be applied. Nonetheless, the Pliocene and Miocene can be differentiated tentatively on the basis of changes in species dominance. In the Pliocene sinistrally coiled *N. pachyderma* is the dominant form, with rare occurrences of *Globigerina quinqueloba* and *Globigerina bulloides*. The upper and middle Miocene is dominated by *G. bulloides* with fewer numbers of *Globorotalia scitula* and *Globigerinita glutinata*. The incursion of *N. pachyderma* into the Antarctic water mass appears to have been during the latest Miocene, corresponding approximately to Core 113-689B-5H. The lower Miocene samples examined contain rare occurrences of *Catapsydrax dissimilis* in Core 113-689B-7H.

Paleogene

The boundary between the Miocene and the Oligocene cannot be determined on the basis of planktonic foraminiferal evidence. Several species of late Oligocene affinity, however, do occur in Cores 113-689B-9H through -11H. These include *Globigerina labiacrassata*, *Globigerina juvenilis*, and *Tenuitella munda*. The late Oligocene appears to have been a transitional interval between the Neogene with the truly "polar" assemblages and the earlier Paleogene with more diverse faunas.

The last appearances of *Subbotina angiporoides* and *Chiloguembelina cubensis* within Core 113-689B-12H are used to delineate the boundary between the upper and lower Oligocene. Lower Oligocene faunas composed of abundant *Subbotina angiporoides* and *C. cubensis* together with rare to few *T. munda*, *Tenuitella gemma*, and *Globorotaloides suteri* occur in Section 113-689B-12H, CC, through Sample 113-689B-14H-5, 110-114 cm. The last appearance of *Globigerinathea index* was observed in Section 113-689B-14H, CC, and is used to mark the boundary between the Oligocene and Eocene. The boundary between the Oligocene and the Eocene is in a zone of CaCO_3 dissolution. This dissolution zone was observed in Section 113-689B-12H-2 in which planktonic foraminifers are rare and the siliceous components show a great deal of breakage. Below this, in Section 113-689B-12H-4, foraminifers, including *G. index*, are abundant and well preserved. In Section 113-689B-12H-1, above the dissolution zone, lower Oligocene planktonic foraminifers are common and well preserved, but the sediments are predominantly siliceous.

The upper Eocene assemblages observed in Cores 113-689B-15H to 113-689B-18H are similar to middle-latitude faunas described from the Falkland Plateau (Krasheninnikov and Basov, 1983) and Southwestern Pacific deep-sea sites (Jenkins, 1975; Jenkins and Srinivasan, 1985). *Globigerinathea index* is the dominant species together with the larger globigerinids, including *Subbotina linaperta* and *S. angiporoides*. *Chiloguembelina cubensis* is a conspicuous component in the smaller size fraction. Other species present discontinuously through this interval include *Pseudohastigerina micra*, *Globorotaloides suteri*, and *Catapsydrax* spp.

The upper/middle Eocene boundary is approximated between Samples 113-689B-17H-5, 35-37 cm, and 113-689B-18H-5, 36-38 cm, marked by the last appearance of *Acarinina* species. The latter sample contains abundant *Acarinina coalingsensis* (*Acarinina primitiva* of some authors), *Acarinina pseudotopilensis*, *Acarinina collactea*, as well as abundant *Subbotina eocaenica/patagonica*. Except for possibly *A. coalingsensis* and *A. collactea*, the ranges of these latter species do not extend to the top of the middle Eocene and it appears therefore that the uppermost middle Eocene is condensed between these two samples. This is also supported by nannofossil evidence (see "Calcareous Nannofossils" discussion below).

The boundary between the middle and lower Eocene is difficult to determine on planktonic foraminiferal evidence. Section 113-689B-21H, CC, however, contains rare to common *Acarinina pentacamerata*, a relatively short-ranging species that spans the lower/middle Eocene boundary from approximately Zones P9 to P11. This species occurs with abundant *Subbotina eocaenica/patagonica*, *A. coalingsensis*, *A. collactea*, *Acarinina bullbrooki*, and a number of less-abundant forms, including *Planorotalites planoconica*. Although exact biostratigraphic placement is difficult, the presence of *A. pentacamerata* appears to restrict the maximum age of Core 113-689B-21H to the latest early Eocene, and the middle/lower Eocene boundary is tentatively placed within this core. This is important because Sample 113-689B-22X-4, 35-39 cm, contains a distinct upper Paleocene fauna that includes *Acarinina nitida*, *Acarinina soldadoensis*, *Acarinina esnaensis*, *A. coalingsensis*, and *Planorotalites australiformis*. Fur-

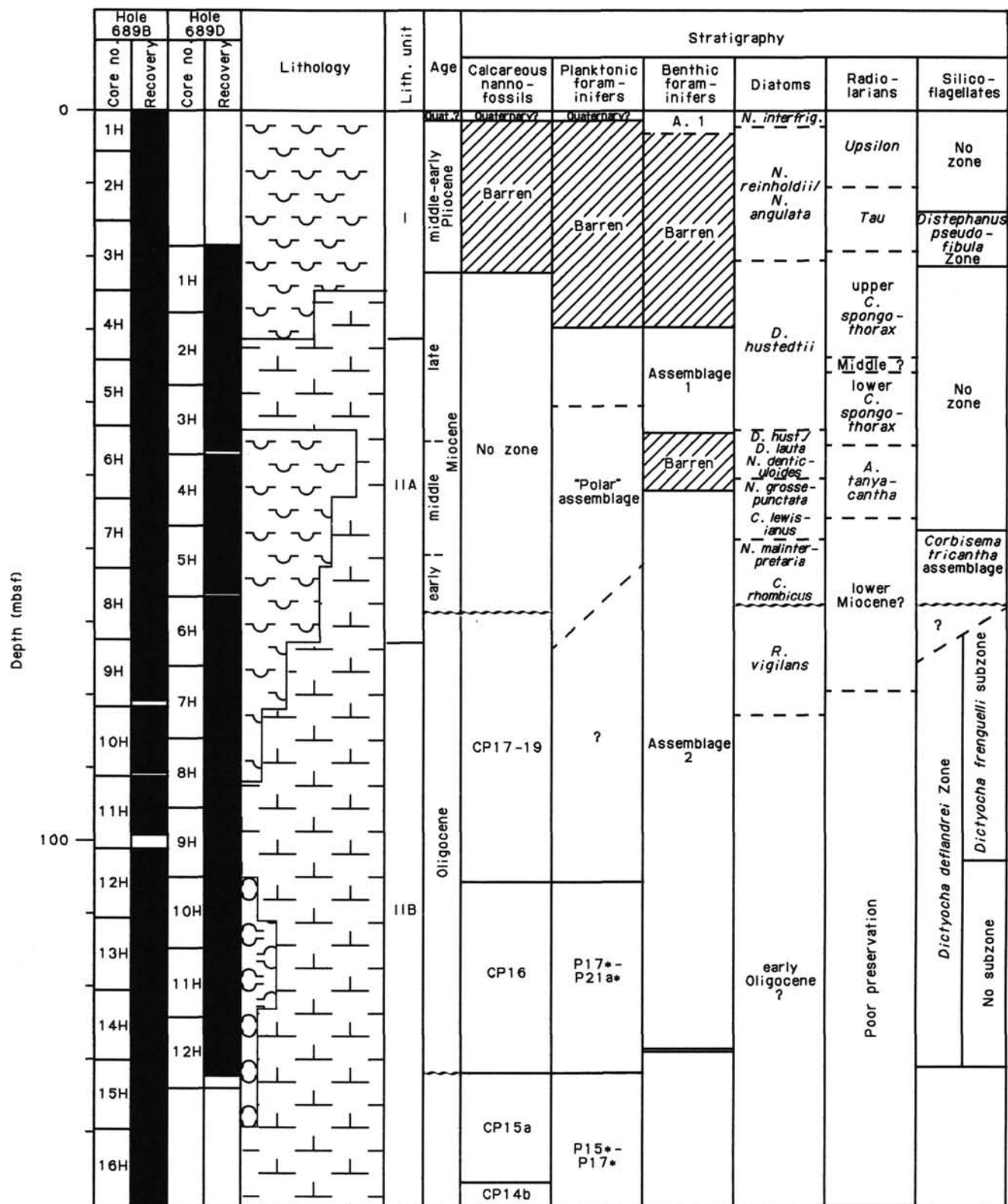


Figure 25. Biostratigraphic correlation chart, Site 689; * designates zonal equivalence.

ther sampling between Samples 113-689B-22X-4, 35-39 cm, and 113-689B-21H-1, 110-114 cm, should help to constrain the boundary between the Eocene and Paleocene. Cores 113-689B-23X and 113-689B-24X contain a similar fauna to that of Core 113-689B-22X with the addition of *Acarinina mckannai*, *Moro-*

zovella convexa, *Morozovella djanensis*, and *Subbotina varianta*. Both *M. convexa* and *M. djanensis* have restricted ranges within the upper Paleocene and help to constrain the maximum age of these sediments to approximately the equivalent of upper Zone P3 to Zone P4. Below this an apparent hiatus occurs within the

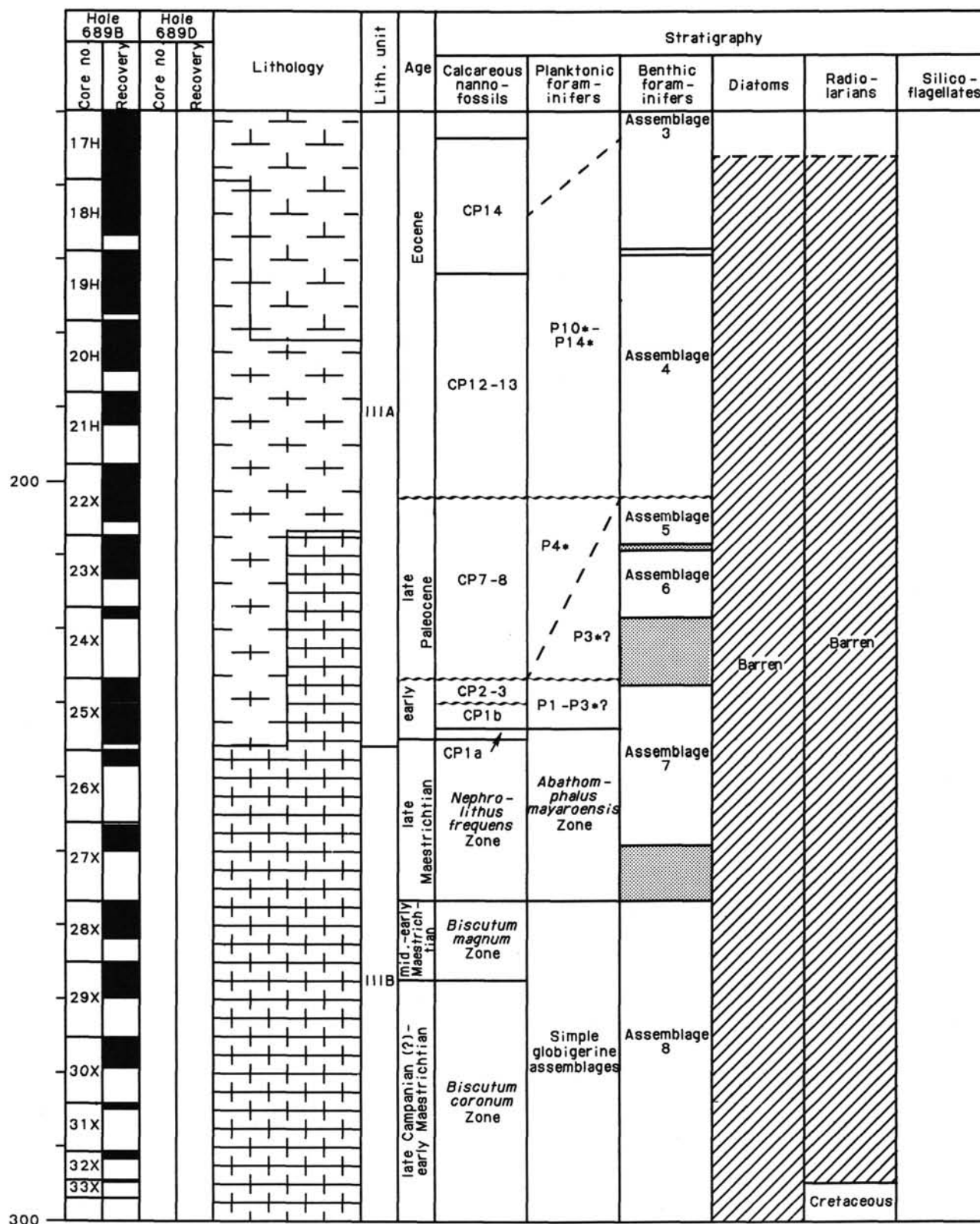


Figure 25 (continued).

top of Core 113-689B-25X. Sample 113-689B-25X-5, 48-50 cm, contains common *Planorotalites eugubina* and *Hedbergella monmouthensis*. The apparent absence of *Subbotina pseudobulloides* and *Chiloguembelina* spp. suggests that this sample is in the lowermost Paleocene *P. eugubina* Zone. The extent of the hiatus

separating the upper Paleocene in Core 113-689B-24X and the lowermost Paleocene in Sample 113-689B-25X-5, 48-50 cm, is, at present, estimated only on calcareous nannofossil evidence, which indicates that the equivalent of lower Zone P3-Zone P1 is condensed within Sections 1-5 of Core 113-689B-25X.

The boundary between the Cretaceous and Tertiary is observed between Samples 113-689B-25X-5, 48–50 cm, and 113-689B-25X-5, 91–94 cm, across a distinct bioturbated “green” horizon (Fig. 26; see “Lithostratigraphy” section, this chapter). Below the bioturbated zone, Sample 113-689B-25X-5, 91–94 cm, contains abundant upper Maestrichtian species including common *Abathomphalus mayaroensis*, the zonal index species for the uppermost Maestrichtian. Although detailed samples have not yet been analyzed across the boundary, it does appear that the K/T boundary is complete, albeit smeared by bioturbation (see “Calcareous Nannofossils” discussion below).

Abundant specimens of the upper Maestrichtian zonal marker *Abathomphalus mayaroensis* occur from Sample 113-689B-28X-1,

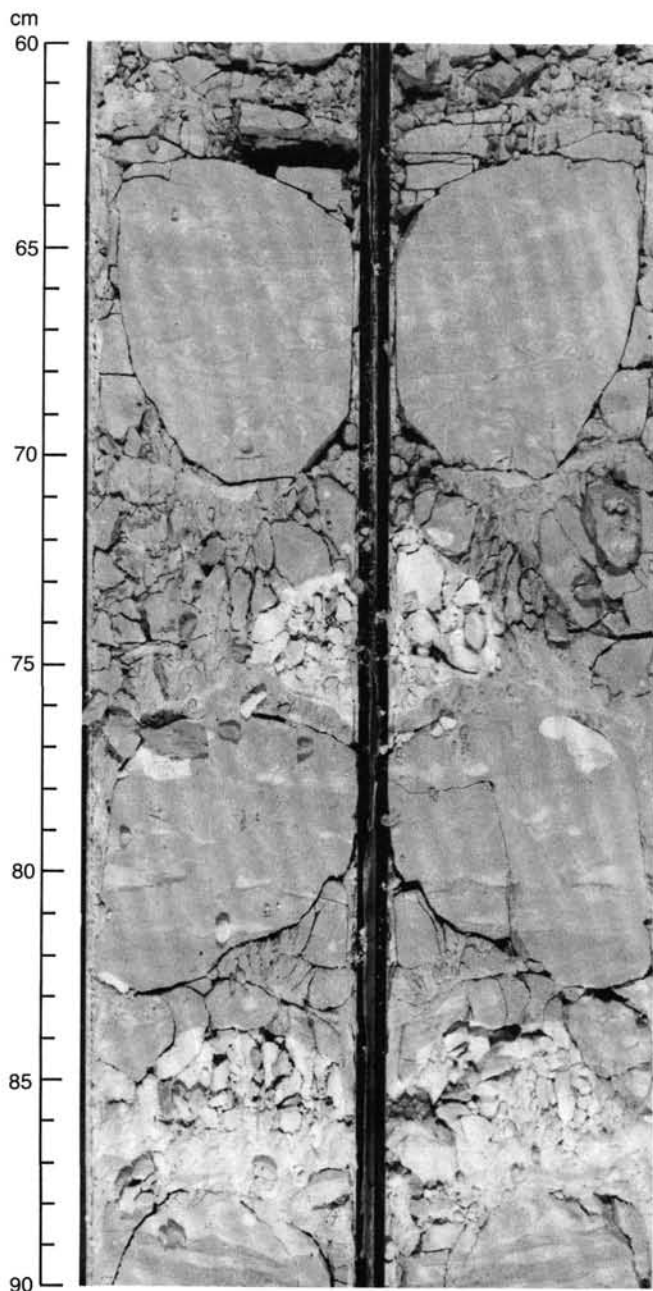


Figure 26. K/T boundary in Hole 689B. Contact at approximately 113-689B-25X-5, 84–85 cm.

76–80 cm, through Section 113-689B-25X, CC (B. Huber, written comm., 1987). This range parallels the distribution in Hole 689B of the calcareous nannoplankton species *Nephrolithus frequens*, in Hole 689B, which is also an upper Maestrichtian index species. Several other keeled planktonic taxa occur within this interval, including *Abathomphalus intermedius*, *Rugotruncana circumnodifer*, and *Globotruncana arca*. The presence of *A. intermedius* without *A. mayaroensis* in Sample 113-689B-28X-2, 80–84 cm, indicates a late middle Maestrichtian age. No zonal marker species and few keeled specimens occur below Section 113-689B-28X-2. This lower interval is dominated by simple globigerine morphotypes such as *Heterohelix* spp., *Globigerinelloides multispinatus*, *Hedbergella monmouthensis*, and an undescribed species tentatively placed in *Rugoglobigerina*. A very unusual planktonic taxon, similar in appearance to strongly spinose forms of the Tertiary genus *Acarinina*, occurs in most of the Maestrichtian samples. These low trochospiral, globular morphotypes strongly differ from previously described Cretaceous planktonic foraminiferal genera.

Benthic Foraminifers

Benthic foraminifers were studied in a mud-line sample, all core-catcher samples from Hole 689B, and additional samples from intervals where benthic assemblages show major changes. Core-catcher and additional samples from Cores 113-689B-1H through -3H are barren of benthic foraminifers, as were samples from Samples 113-689B-6H-1, 40–43 cm, through 113-689B-6H-6, 40–43 cm. Section 113-689B-7H, CC, contained only 82 specimens (not sufficient for study). All other samples contain at least 200 specimens of benthic foraminifers; benthic foraminifers are rare compared to planktonic microfossils in most samples (exceptions are Section 113-689B-25X, CC, and Sample 113-689B-25X-4, 105–107 cm). Preservation is moderate to good when benthic foraminifers are present; most samples from Cores 113-689B-22H through -25X show evidence of reworking (presence of many broken specimens, rare Cretaceous planktonic and benthic foraminifers). Relative abundances of species were determined for all samples (see “Explanatory Notes” chapter, this volume, for methods). The benthic foraminiferal fauna in all samples studied is predominantly calcareous with only few species and few specimens of agglutinated forms.

Benthic foraminiferal faunas at Site 689 were subdivided into eight assemblages: (1) the mud-line sample (Quaternary) and Sections 113-689B-4H, CC, and -5H, CC (middle to upper Miocene; all samples above 45 mbsf that contain benthic foraminifers); (2) Section 113-689B-6H, CC, through Sample 113-689B-15H-1, 40–43 cm (lower Miocene through uppermost Eocene; 52.99–130.31 mbsf); (3) Samples 113-689B-15H-2, 40–43 cm, through 113-689B-19H-1, 40–43 cm (upper through middle Eocene; 131.31–168.91 mbsf); (4) Samples 113-689B-19H-2, 40–43 cm, through 113-689B-22X-4, 40–43 cm (middle Eocene; 170.41–202.41 mbsf); (5) Samples 113-689B-22X-5, 40–43 cm, through 113-689B-23X-1, 40–43 cm (lower Eocene?; 203.91–207.61 mbsf); (6) Sample 113-689B-23X-2, 40–43 cm, through Section 113-689B-24X, CC (upper Paleocene; 209.11–226.6 mbsf); (7) Sample 113-689B-25X-1, 100–103 cm, through Section 113-689B-27X, CC (lower Paleocene to upper Maestrichtian; 227.61–255.6 mbsf); and (8) Sample 113-689B-28X-2, 40–43 cm, through Section 113-689B-33X, CC (lower Maestrichtian; 257.5–297.3 mbsf).

Depth estimates using Paleogene and older faunas are tenuous, but comparison of Site 689 faunas with faunas from the South Atlantic (Tjalsma and Lohmann, 1983; Dailey, 1983; Van Morkhoven et al., 1986) leads to an estimate of lower bathyal depths (1500–2000 m) for assemblages 1 through 5. Assemblages 6 and 7 may have lived at middle bathyal depths (1000–1500 m),

whereas assemblage 8 probably indicates an upper bathyal depth (500–1000 m).

Study of the benthic foraminiferal faunas at the low resolution discussed here shows clearly that higher resolution studies are necessary for an understanding of the evolution of benthic foraminiferal faunas through the Cenozoic.

Assemblage 1 (Quaternary to upper middle Miocene)

The mud-line sample contains a mostly calcareous fauna, without a strongly dominant component. The diversity (31 species at 200 specimens) is low compared to deep-sea faunas from other areas (see, e.g., Douglas and Woodruff, 1981). Common species are *Epistominella exigua* (6%), *Globocassidulina subglobosa* (7%), *Melonis sphaeroides* (18%), *Cibicidoides* spp. (15%), and *Eggerella bradyi* (14%). Similar faunas have been described by Anderson (1975) from the Weddell Sea. Benthic foraminifera are very rare in Sections 113-689B-4H, CC, and 113-689B-5H, CC (middle-upper Miocene). These samples contain a fauna of relatively low diversity (less than 30 species per 200 specimens counted), as compared to an average of about 60 species in the equatorial Pacific (Thomas, 1985), and 50–60 species in the northeast Atlantic Ocean (Thomas, 1987). The assemblage is characterized by strong dominance of a few taxa, but the dominant taxon differs between samples: *Nuttallides umbonifera* (55%) in Section 113-689B-4H, CC, and *Gyroidinoides* spp. (25%) and *Bolivina decussata* (26%) in Section 113-689B-5H, CC. The samples are grouped together because they have few *Stilostomella* (<5%), in contrast with lower samples. There is a barren interval between the samples containing faunas of assemblage 1 and those containing assemblage 2 (43.71–51.21 mbsf).

Assemblage 2 (lower Miocene to upper Eocene)

Section 113-689B-6H, CC, through Sample 113-689B-15H-1, 4–43 cm, contain variable faunas, characterized by a high relative abundance of *Stilostomella* spp. (12%–40%), and a relatively low diversity (28–38 species, average 31). *Nuttallides umbonifera* becomes gradually more abundant upsection, from 9% in Section 113-689B-14H, CC, to 63% in Section 113-689B-8H, CC, but is less common (4%) in -6H, CC, and -7H, CC. *Gyroidinoides* spp., *Oridorsalis* spp., and *Pullenia* spp. are common accessory species. *Cibicidoides mundulus* (12%–22%) and *Globocassidulina subglobosa* (1%–10%) are common in Sections 113-689B-11H, CC, through 113-689B-14H, CC. *Bolivina decussata* (23%) and *Reussella tortuosa* (19%) are abundant in Section 113-689B-6H, CC, *Uvigerina peregrina* (25%) in Section 113-689B-7H, CC. *Astronion pusillum* is common (11%) in Sections 113-689B-8H, CC, and 113-689B-9H, CC; the latter sections also contain common *Uvigerina peregrina* (10%). *Turritina alsatica* (an Oligocene species) occurs from Section 113-689B-8H, CC, down, and is common (>5%) between 110.60 and 123.62 mbsf (in Cores 113-689B-13H and the upper part of 113-689B-14H). These species are all common deep-sea faunal components, but the faunas reflect a unique abundance pattern. The high relative abundance of *N. umbonifera* might indicate the presence of a water mass highly corrosive to CaCO_3 , with high CO_2 content (Bremer and Lohmann, 1982; Miller, 1983). The lower boundary was chosen above the last appearance (l.a.) of *Bulimina elongata*.

Assemblage 3 (upper to middle Eocene)

Assemblage 3 resembles assemblage 2 because all samples have a high relative abundance of *Stilostomella* spp. (22%–52%). *Bulimina elongata* is present in all samples (2%–28%). Diversity is higher in assemblage 3 (32–40 species, 37 average). *Cibicidoides* spp. vary from 1% to 21% (mainly *C. praemundulus* and *C. dayi*). Species belonging to *Gyroidinoides*, *Pullenia*, and

Oridorsalis, and *G. subglobosa* are common accessory species. *Nuttallides umbonifera* is rare (0.5%–5%). *Nuttallides truempyi* has its l.a. in Section 113-689B-17H, CC (5%) and is common (28.8%) in Section 113-689B-18H, CC. The l.a. of *N. truempyi* occurs considerably lower than the l.a. of *Globigerinatheka index* (in Section 113-689B-14H, CC), in contrast with its range in many sites in the Pacific and Atlantic (Corliss, 1981; Tjalsma and Lohmann, 1983; Thomas, 1985); this may be a result of the relatively shallow depth (1500–2000 m). The lower boundary is taken above the l.a. of *Bulimina semicostata*; it is a gradual boundary, because *B. semicostata* is very rare just below its l.a.

Assemblage 4 (middle Eocene)

Assemblage 4 contains abundant *Stilostomella* (14%–40%), and diversity is higher than in assemblage 3 (37–44 species, average 40). *Pullenia* spp., *Oridorsalis* spp., and *Gyroidinoides* spp. are common accessory species. *Cibicidoides praemundulus* is common (15%) in Section 113-689B-20H, CC, and has its first appearance (f.a.) in Section 113-689B-21H, CC (5%). *Nuttallides umbonifera* and *N. truempyi* are rare (<5%). *Bulimina semicostata* (5%–10%) and *Siphogenerinoides eleganta* (4%–7%) occur only in assemblage 4. *Bulimina simplex* is common (5%–14%). Assemblage 4 and all lower assemblages at Site 689 contain 2%–6% *Lenticulina* spp., which are rare or absent in the upper part of the section. The lower boundary is at the f.a. of *Bulimina semicostata*; this is an abrupt boundary, probably as a result of a hiatus in Section 113-689-22X-4.

Assemblage 5 (uppermost Paleocene? to lower Eocene)

This assemblage was found in a short interval in the lower part of Core 113-689B-22X and the upper part of Core 113-689B-23X. The diversity is low (27 species). The assemblage is characterized by high relative abundances of *Bulimina simplex* (39.5%) and *Bulimina trinitatensis* (12.5%), with common *Aragonia semireticulata* (9.4%) and *Tappanina selmensis* (9%). *Nuttallides truempyi* is common (5%). *Siphogenerinoides brevispinosa* is rare (<2%). Species of *Gyroidinoides*, *Oridorsalis*, and *Pullenia* are rare; *Stilostomella* spp. are only 1.5% of the assemblage. Notable is the absence of *Stensioina* spp. and *Cibicidoides* spp. The lower assemblage boundary is taken at the l.a. of *Stensioina beccariiiformis*; there appears to be considerable reworking, and there may be a hiatus or interval of slow sedimentation rates in Core 113-689B-23X. The faunal changes between Assemblage 5 and Assemblage 6 are the most important changes observed in the section at Site 689. The dating of this faunal event is difficult at Site 689 because of the possible presence of a hiatus and problems in calcareous nannofossil and planktonic foraminiferal biostratigraphy at high latitudes, but comparison with as yet unpublished oxygen and carbon isotopic data suggests that this important benthic faunal event occurred near (but below) the Paleocene/Eocene boundary.

Assemblage 6 (lower Paleocene)

Assemblage 6 is characterized by the high relative abundance of *Stensioina* spp. (mainly *S. beccariiiformis*; 25%–30%), the presence of *Bulimina thanetensis* (2%–33%), and *Bulimina midwayensis* (1%–3%). *Nuttallides truempyi* and *Stilostomella* spp. have low relative abundances (2%–8%). *Osangularia navarroana* and *Coryphostoma midwayensis* have their l.a. in Sample 113-689B-23X-2, 40–43 cm. Diversity is higher than in Assemblage 5 (32–42 species, average 37). Similar faunas have been described from Cretaceous and Paleocene sediments deposited at middle bathyal to shallow lower bathyal water depths (e.g., Dailey, 1983; Tjalsma and Lohmann, 1983); the fauna at Site 689 is similar to that described by Dailey (1983) from the Rio Grande Rise. The presence of *S. beccariiiformis* indicates a Paleocene age for Sample 113-689B-23X-2, 40–42 cm. The lower boundary was taken at the f.a. of *B. thanetensis*.

Assemblage 7 (lower Paleocene to upper Maestrichtian)

This assemblage is characterized by the presence of *S. beccariiiformis* together with common (12%–17%) *Osangularia navarroana*, in the absence of *B. thanetensis*. The K/T boundary is present between Section 113-689B-25X, CC, and Sample 113-689B-25X-4, 105–107 cm. *Stensioina beccariiiformis* is less common (6%–7%) around the K/T boundary (Section 113-689B-26X, CC, through Sample 113-689B-25X-4, 105–107 cm), more common higher in the section (assemblage 6, 25%–30%) and lower in the section (Section 113-689B-27X, CC: 16.5%, and assemblage 8, see below). *Neoeponides hillebrandti* and *Eouviagerina gracilis* occur in Sample 113-689B-25-4, 105–107 cm (just above the K/T boundary), and in no other samples at Site 689 (but in more samples at Site 690, see “Site 690” chapter, this volume). *Nuttallides truempyi* is common (2%–7%), but abundant (31.3%) in Sample 113-689B-25X-4, 105–107 cm; *Pullenia coryelli* is also abundant (20%) in this sample (4%–9% in other samples). *Gyroidinoides* spp. (especially *G. quadratus*) are abundant below the K/T boundary in Sections 113-689B-25X, CC, and 113-689B-26X, CC (15%–20% vs. 5%–9% in other samples). The diversity is relatively high (35–50 species, average 45), with the lowest value in Section 113-689B-25X, CC (below the K/T boundary). The lower boundary is taken at the f.a. of *Osangularia navarroana*.

Assemblage 8 (lower Maestrichtian)

The diversity in the lowermost assemblage of Hole 689B is lower (32–52 species, average 41); the faunas are dominated by *S. beccariiiformis* (25%–50%). Other species have strongly fluctuating relative abundances, e.g., *Coryphostoma* spp. (0%–38%), *Præbulimina reussi* (0%–22%, i.a. in Section 113-689B-28X, CC), and *Neoeponides hillebrandti* (0%–22%). In some samples there are rare *Lenticulina spissicostata*, a large, heavily calcified species typical for upper bathyal or shallower depths. The strong dominance of *S. beccariiiformis* and the presence of *L. spissicostata* suggest an upper bathyal depth of deposition. The ranges of deep-sea benthic foraminifers in Maestrichtian and Campanian are not well defined, but comparison of the fauna at Site 689 with that at Site 516 (South Atlantic, Dailey, 1983) suggests that the oldest sediment at Site 689 is lowermost Maestrichtian. For a comparison of the faunas at Site 689 with those at Site 690 (also located on Maud Rise) and a preliminary discussion of faunal changes in benthic foraminifers during the Cenozoic, see “Site 690” chapter, this volume. Taxonomy and a more thorough discussion was given by Thomas (pers. comm., 1988).

Calcareous Nannofossils

Calcareous nannofossils are rare in the foraminiferal ooze at the top of the section (Hole 689B), absent in the subjacent middle-lower Pliocene diatom and silicoflagellate oozes, and common to abundant at most levels in the Miocene, especially below 30 mbsf. Preservation in the Miocene ranges from good to moderate with etching but no overgrowths. Throughout the remainder of the hole, nannofossils are abundant, but preservation is generally moderate with etching in the upper Oligocene and strong etching and overgrowth below that level. Preservation of the Paleocene nannofossil oozes is better than that of the Eocene nannofossil oozes and the Cretaceous chalks. The Cretaceous material is sufficiently lithified to require soaking in calgon to disperse the coccoliths.

Holes 689A, 689B, and 698C

Neogene

Foraminiferal ooze at the top of the section (top of Cores 113-689B-1H and 113-689C-1H) contains rare calcareous nan-

nofossils. Sample 113-689B-1H, top, yielded a single well-preserved specimen of *Pseudoemiliania lacunosa*, which ranges from middle Pliocene to upper Pleistocene (0.44 Ma). Coccoliths are absent in the subjacent Pliocene diatom/silicoflagellate ooze, which extends down through Core 113-689B-2H. This latter core is equivalent to Core 113-689A-1H and the base of Core 113-689C-1H.

Miocene nannofossils are few in Core 113-689B-3H (the equivalent of Core 113-689C-3H) where they consist essentially of two taxa, abundant *Coccolithus pelagicus* and common *Reticulofenestra perplexa* (= *Dictyococcites antarcticus* Haq). The latter species, however, is strongly dominant in the nannofossil ooze of Cores 113-689B-4H and -5H, where it represents 99% of the assemblage. Below that, down through the Miocene section, *Coccolithus pelagicus* and the one or two species of *Reticulofenestra* present exhibit extreme fluctuations in assemblage dominance over meter to dekameter intervals. Haq (1980) attributes these sharp fluctuations to climate-induced, latitudinal migrations of Antarctic or warmer water assemblages across the South Atlantic during the Miocene. Floras dominated by *Reticulofenestra perplexa* represent the coldest water and southernmost assemblage, whereas *C. pelagicus*-dominated assemblages denote a somewhat warmer association to the north.

The low diversity of the Miocene nannofossil assemblages precludes their zonation. Reworking of Oligocene nannofossil and diatom taxa into the Miocene at this site is negligible, in contrast to sites to the north which lie in the path of the circumpolar current (e.g., DSDP Site 329 on the Falkland Plateau; Barker et al., 1977). This circumstance will allow better calibration of nannofossil paleoecological events against the more finely zoned diatom biostratigraphy.

Paleogene

The nannofossil Miocene/Oligocene boundary is placed at the top of Section 113-689B-8H-4, which contains the uppermost occurrences of *Chiasmolithus altus* (very abundant) and *Reticulofenestra bisecta* (common). The latter may be reworked and a hiatus is suspected at this level because these two forms should disappear sequentially rather than together. An erosional disconformity is further implied by the presence of rare chiasmoliths, *Reticulofenestra hillae*, and *Isthmolithus recurvus* in Miocene Section 113-689B-7H, CC. The latter two taxa are lower Oligocene or older.

Sample 113-689B-12H-5, 25 cm, contains common *Reticulofenestra umbilica/hillae*, which is indicative of the lower Oligocene. Rare specimens occur in Cores 113-689B-11H and -10H; these are considered to be reworked. The last occurrence of *Isthmolithus recurvus* in Sample 113-689B-13H-2, 130 cm, denotes the lowermost Oligocene *Blackites spinosus* Zone (Wise, 1983). *Reticulofenestra oamaruensis* occurs consistently within the upper five sections of Core 113-689B-14H. The other members of this moderately preserved nannofossil assemblage include rare *Zygrhablithus bijugatus* and *Markalius inversus*, common *Isthmolithus recurvus* and *Chiasmolithus oamaruensis*, abundant *Chiasmolithus altus*, *Reticulofenestra bisecta*, and *R. umbilica*, and very abundant *Coccolithus pelagicus*.

Discoasters are absent throughout the Oligocene and middle to upper Eocene, thus there is no reliable way to pick the Oligocene/Eocene boundary at this site using calcareous nannofossils. This boundary is placed on the basis of planktonic foraminifers between Sections 113-689-15H-1 and -2, which suggests that the uppermost Eocene *Isthmolithus recurvus* Subzone (CP15b) is missing.

Isthmolithus recurvus is indeed absent in Sample 113-689B-15H-2, 131 cm, which on the other hand does contain the Eocene index species *Reticulofenestra reticulata* (W. Wei, written comm., 1987) and is assigned to the upper Eocene *Chiasmo-*

lithus oamaruensis Subzone (CP15a). The base of that subzone is placed between Sections 6 and 7 of Core 113-689B-16H based on the first appearance datum (FAD) of *Chiasmolithus oamaruensis*. Core 113-689B-18H contains abundant *Chiasmolithus expansus*, *C. solitus*, *Coccolithus pelagicus*, and rare *Reticulofenestra umbilica*, an assemblage characteristic of the *Discoaster bifax* Subzone (CP14a). The assemblage in Sample 113-689B-19H-3, 30 cm, lacks *R. umbilica*, and therefore should belong to the *Nannotetrina quadrata* Zone (CP13), although the generally rare zonal marker has not yet been observed in our section. Other taxa include rare *Cepekella lumina*, few *Neococcolithes dubius*, and abundant *Zygrhablithus bijugatus*. No significant changes in this basic assemblage were noted down through the middle of Core 113-689B-22X, and this interval cannot be further divided at present due to the general lack of discoasters and other warmer water marker species traditionally used for correlation. The absence of the lowest Eocene index species, however, implies a hiatus within Core 113-689B-22X.

Section 113-689B-22X, CC, does contain discoasters, including *Discoaster multiradiatus* and related forms assignable to the *Discoaster multiradiatus* Zone (CP8). *Fasciculolithus involutus* is abundant, and the overall assemblage closely approximates that described from time-equivalent strata at Site 327 on the Falkland Plateau (Wise and Wind, 1977). Preservation is still moderate but improved in Core 113-689B-23X, which extends to the base of Zone CP8. Preservation changes to good in Core 113-689B-24X, which contains common *Helicolithus universus*. Several members of the *Helicolithus* plexus may be present, including *H. riedelii*, which marks the base of Zone CP7, in Sample 113-689B-25H-1, 5 cm. This sample immediately overlies a color and lithologic change at 10–11 cm in the same section, which represents a major disconformity. The interval not represented in the sediments due to the hiatus comprises Zones CP6–CP4, which span the upper/lower Paleocene boundary.

The FAD of *Cruciplacolithus edwardsii* is placed at Sample 113-689B-25X-3, 149 cm, which marks the base of a combined CP2–CP3 Zone. It may be possible to use the FAD of *C. primus* to delineate the base of Subzone CP1b of the *Zygodiscus sigmoides* Zone, but this has not been done with any certainty at this writing due to the complications discussed in the next section.

Cretaceous/Tertiary (K/T) Boundary

The K/T boundary was captured in Section 113-689B-25X-5 approximately at the interval where the color changes downward from green to white (Fig. 26). The greenish color over a 40-cm section is apparently due to the presence of altered volcanic clay and vitric ash at the boundary (see "Lithostratigraphy" section, this chapter). Smear slides were made at several intervals in Section 113-689B-25X-5 between 70 and 106 cm in an effort to pinpoint the position of the K/T contact.

Approximately 80% of the specimens from the darkest green sample examined (113-689B-25X-5, 70 cm) are Danian taxa; the other 20% are reworked Cretaceous forms. *Zygodiscus sigmoides* is common in this interval. The sample taken from Section 5 at 106 cm is an upper Maestrichtian pure semilithified ooze characterized by *Nephrolithus frequens* (J. Pospichal, written comm., 1987). Preservation is poor to moderate, in contrast to the Danian sample, in which preservation is moderate to good.

The apparent contact between the predominantly white Maestrichtian and predominantly greenish Danian material occurs between 84 and 85 cm. Above that lie white clastlike pods inset within the greenish ooze. White pods at 74.5 and 77 cm yielded assemblages that are 99% Maestrichtian in composition. The surrounding greenish matrix contains varying percentages of Danian coccoliths of Subzone CP1b. For instance, the matrix at 78.5 cm immediately below the angular white clastlike pod con-

sists of about 60% Danian forms. Maybe the intensity and hue of the greenish color throughout this interval can serve as a means to estimate the percentage of Tertiary coccoliths present.

A major complication in delineating this K/T boundary is that the interval has been intensely bioturbated by Zoophycos and other infauna. Greenish burrows are distinct down to 115 cm in Section 5, and are detectable as low as 130 cm. On the other hand, distinct whitish blebs (burrow fills) occur as high as 55.5 cm within the green Danian matrix. This bioturbation plus fracturing due to drilling have tended to expand the boundary interval. Possibly the original boundary occurred at about 73 cm (top of the highest large clastlike pod of Maestrichtian sediment), but the apparent contact has since been lowered over 10 cm by the strong bioturbation.

To prove that sedimentation was continuous across this K/T boundary, it will first be necessary to establish the presence of an interval between the extinction of the Cretaceous taxa and the first occurrence of the *Cruciplacolithus* plexus. This interval should occupy the lower portion of Subzone CP1a, and would probably be characterized in this region by abundant *Zygodiscus sigmoides* and *Markalius inversus*. Few other species would be discernible under transmitted light in a microscope aboard ship. It is possible that such a "gap zone" was originally present in this sequence, but that it is now undetectable due to the bioturbation. Bioturbation could have closed the gap by post-depositional mixing of *Cruciplacolithus* species down to and below the original K/T contact. On the other hand, sediments deposited immediately after the K/T crisis event may have subsequently been eroded away. A case for an erosional disconformity would be supported if it can be determined that the white clasts in green matrix at 77 and 77.5 cm are rip-up clasts indicative of high-energy scouring. Further detailed work will be necessary to determine the exact nature of this boundary and whether sedimentation was continuous across it.

Upper Cretaceous

The high-latitude zonation applied at this site for the Upper Cretaceous is derived from Wind and Wise (1983) and Wise (1983) based on previous work in the area by Wise and Wind (1977) and Wind (1979a, b). The zonal scheme is outlined in the "Explanatory Notes" chapter (this volume) and consists of three high-latitude zones: the *Nephrolithus frequens*, *Biscutum magnum*, and *Biscutum coronum* Zones. Wind and Wise (1983) also found the Maestrichtian zonation of Sissingh (1977) to be of use when applied to their sequence on the Falkland Plateau. For shipboard work at the present site, however, where the preservation of the Maestrichtian floras is not ideal, the high-latitude zonation proved to be more applicable.

The interval from the K/T boundary in Section 113-689B-25X-5 down through Core 113-689B-27X is assigned to the *Nephrolithus frequens* Zone. The presence of *Nephrolithus frequens* was established by shore-based scanning electron microscopy (SEM) performed by J. Pospichal (written comm., 1987). Long-ranging Upper Cretaceous taxa in the assemblage include abundant *Prediscosphaera cretacea*, *Arkhangelskiella cymbiformis*, and *Kamptnerius magnificus* and common *Eiffellithus turrisseifeli*, *Cretarhabdus conicus*, and *Ahmuelierella octoradiata*. Preservation is moderate in Core 113-689B-25X, but deteriorates toward the bottom of the zone where it is poor.

Core 113-689B-28X is dominated by *Biscutum magnum* and is assigned to the nominate zone, which extends downhole to Sample 113-389B-29X-2, 28 cm. Shore-based SEM study shows that this interval contains *Nephrolithus corystus*, which is present down to the base of the hole (J. Pospichal, written comm., 1987). *Nephrolithus frequens* appears to be essentially confined to the upper Maestrichtian.

Diversity increases in the *Biscutum coronum* Zone. In addition to the nominate species and those mentioned previously,

Biscutum dissimilis, *B. notaculum*, *Reinhardtites levis*, and species of *Monomarginatus* and *Misceomarginatus* can be distinguished. Preservation is poor in Cores 113-689B-30X through -33X, but *Biscutum magnum* is still present and little change can be noted in the assemblages. The base of the hole probably lies near the Maestrichtian/Campanian boundary.

Summary and Conclusions

1. The successful drilling of a long, predominantly carbonated Miocene to Campanian(?) section at Site 689 means that Maud Rise will now displace the Falkland Plateau as the southern anchor of north-south biostratigraphic or biogeographic nanofossil study through the Atlantic basins. The strong fluctuations in the compositions of the Miocene nanofossil assemblages indicate that the sequence will be amenable to detailed biogeographic and paleoclimatic studies such as those by Haq (1980).

2. Diversity in these high-latitude nanofossil assemblages is limited as expected. Nevertheless, the Maestrichtian-Paleocene assemblages exhibit a diversity similar to those of equivalent age from the Falkland Plateau if diagenesis is taken into account (diagenesis is more severe at the present site because the carbonate content is higher). Compared with the simple diversity curves for the Falkland Plateau by Wise et al. (1985, Fig. 7 and App. 2), nanofossil diversity at Site 689 is lower for the Eocene and Oligocene sections owing to the virtual absence of discoasters throughout the section and diminished preservation. Diversity in the Miocene appears comparable between these two regions.

From the above, one can postulate that during the Maestrichtian through Paleocene interval, Site 689 lay under a relatively warm water mass that extended from Maud Rise at least to the region of the Falkland Plateau to the north. Farther to the north on the Rio Grande Rise, however, a different, warmer Paleogene nanofossil assemblage flourished (Haq et al., 1977). At some point by about middle Eocene time a colder water mass developed over Maud Rise. Sediments accumulating were essentially devoid of discoasters and appreciable numbers of sphenoliths. This situation persisted through the remainder of the Eocene, obviating our present attempt to determine the Eocene/Oligocene boundary at Site 689 by nanofossils, and suggesting that Maud Rise lay under a distinctly cooler water mass relative to the Falkland Plateau. This water mass apparently expanded and extended over the Falkland Plateau during the early Oligocene, at which point discoasters disappeared from the section there until a slight warming event, represented in the top of the drilled section at Site 511 (compare Wise et al., 1985, Fig. 6; Wise, 1983, Table 1A). Thereafter, nanofossil diversity declined due to successive extinctions until very low diversity assemblages pervaded the water masses throughout the region during the Miocene. There is little evidence that nanofossils inhabited these waters during the Pliocene.

3. The nanofossil record suggests hiatuses across the lower/upper Paleocene boundary (Zones CP4-CP6 are missing), Paleocene/Eocene boundary (Zones CP9-CP11 are missing), and in combination with planktonic foraminiferal stratigraphy, across the Eocene/Oligocene boundary (Zone CP15b missing). A disconformity is suspected near the nanofossil Oligocene/Miocene boundary.

4. Significant gaps in the previously known nanofossil biostratigraphic record for the South Atlantic sector of the Southern Ocean have been filled by the acquisition of the middle-upper Maestrichtian/Danian section on Maud Rise. Of prime importance will be the correlation of the high-latitude nanofossil zonations for the Maestrichtian/Paleocene with those of other microfossil groups and magnetostratigraphy.

Diatoms

Hole 689A

Section 113-689A-1H, CC, contains abundant lower Pliocene diatoms. The co-occurrence of *Nitzschia angulata* and *Nitzschia praeinterfrigidaria* indicates an interval in the middle part of the lower Pliocene. The presence of chert in the top of the core made it difficult to identify the sediment/water interface. However, samples from around the chert yielded middle Pliocene diatoms with some admixture of younger forms. Thus, we apparently did not sample the sediment/water interface, but middle Pliocene sediment occurs near the core top with, possibly, a slight overburden of younger material.

Hole 689B

The interval in Cores 113-689B-1H through -8H contains common to abundant diatoms. The diatom ooze in the upper part of the section is occasionally diluted by clay (as much as 3%-5%) while within an interval from Section 113-689B-4H-6 to Section 113-689B-6H-1 and below Section 113-689B-7H-1 the abundance is affected by the presence of biogenic calcareous ooze (largely coccoliths). Below Core 113-689B-8H, the calcareous component becomes overwhelming and diatoms are present only in trace fragments. Exceptions to this are found in Cores 113-689B-12H through the upper part of -15H where diatoms again become common.

Examination of the top of Core 113-689B-1H indicates the presence of a mixed assemblage of Quaternary and lower-upper Pliocene species. The lower part of Cores 113-689B-1H and -2H are lower Pliocene, the principal diagnostic taxa being *Nitzschia praeinterfrigidaria*, *Nitzschia angulata*, *Rhizosolenia barboi*, *Coscinodiscus intersectus*, and *Nitzschia tunicata*. Interestingly, we observed a marked increase of *Ethmodiscus rex* fragments in the interval from Sample 113-689B-1H-3, 28-29 cm, to Sample 113-689B-2H-2, 28-29 cm. A reasonably complete lower Pliocene section seems to be present in this hole since Core 113-689B-3H bottoms in the uppermost Miocene. The most diagnostic form in this core is *Denticulopsis hustedtii*, which has its last consistent appearance in Section 113-689B-3H-4. Other upper Miocene species, however, such as *Nitzschia claviceps*, *N. efferans*, and *Coscinodiscus deformans* are also present.

Cores 113-689B-4H and -5H were assigned to the upper Miocene. Although this interval is in the *Denticulopsis hustedtii* Zone, the dominant taxon is *Denticulopsis dimorpha*, a species which peaks in abundance between Sections 113-689B-4H-6 and 113-689B-6H-1. This peak is tentatively dated as late middle to early late Miocene. Besides containing various species of the genus *Denticulopsis*, the sample also contains *Nitzschia claviceps*, *N. januaria*, and *Coscinodiscus endoi*.

The interval in Sections 113-689B-5H-7 through 113-689B-6H-5 contains lower upper to middle Miocene sediments, representing the *Denticulopsis hustedtii*/*D. lauta* and the *Nitzschia denticuloides* Zones. Besides the nominate taxa, diagnostic species include *D. dimorpha*, *D. praedimorpha*, *Nitzschia efferans*, and members of the *Actinocyclus ingens* group.

Sections 113-689B-6H-6 through 113-689B-7H-4 were placed in the middle Miocene *Nitzschia grossepunctata* and *Coscinodiscus lewisianus* Zones. In this interval we found *N. grossepunctata*, *N. efferans*, and *Denticulopsis maccollumii*. We did not encounter the nominate species *C. lewisianus*, but we noted the last appearance of *Rhaphidodiscus marylandicus* in Sample 113-689B-7H-4, 28-29 cm; this last appearance was placed in the lower portion of the *C. lewisianus* Zone by Weaver and Gombos (1981).

The interval in Sections 113-689B-7H-5 through 113-689B-8H-3 belongs to the lower Miocene *Nitzschia malinterpretaria* and *Coscinodiscus rhombicus* Zones. We noted *Thalassiosira spinosa*, *T. spinosa* var. *aspinosa*, *Synedra jouseana*, *Nitzschia evanescens*, *N. pusilla* and members of the *Actinocyclus ingens* group, and rare *Rocella gelida*. The last appearance of *C. rhombicus* was found in Sample 113-689B-7H-6, 28–29 cm.

The Miocene/Oligocene boundary can be placed in Section 113-689B-8H-4 between samples at 28–29 cm and 74–76 cm. The species *Bogorovia veniamini*, an indicator for the lowermost Miocene and uppermost Oligocene, was not found. Sample 113-689B-8H-4, 74–76 cm, contains *Lisitzina ornata*, *Coscinodiscus rhombicus*, *Rocella gelida*, *R. schraderi*, and *R. vigilans*. *Rocella* species peak in abundance in the uppermost Oligocene. Section 113-689B-8H-5, 74–76 cm, shows common *Rocella vigilans*. Based on the diatoms in Core 113-689B-8H we assume an unconformity near the Oligocene/Miocene boundary spanning uppermost Oligocene to the lowermost Miocene.

Sections 113-689B-8H, CC, to 113-689B-11H, CC, contain only rare, poorly preserved diatoms. Identifiable taxa include *Synedra jouseana* and *Pyxilla reticulata*. Fragments of other *Pyxilla* species, however, as well as *Hemiaulus*, are also present. In contrast, Sections 113-689B-12H, CC, to 113-689B-14H, CC, contain common diatoms with moderate preservation. The diatom assemblages are diversified and indicative for the lower Oligocene. Although species such as *Asterolampra insignis*, *Hemiaulus incisus*, *Coscinodiscus superbus*, and *Melosira architecturalis* are present, it was not possible to attribute the diatom associations to established zones (Fenner, 1984) based on the core-catcher samples. Important zonal marker species such as *Rhizosolenia gravida* and *R. antarctica* were not found. Various species of *Hemiaulus* are present (e.g., *H. polycystinorum*, *H. polymorphus*) as well as *Pyxilla reticulata*, *Rouxia granda*, and *Asterolampra gradiata*. Section 113-689B-14H, CC, marks the lowest level with good preservation. Below this, diatoms are either not present or are so rare or poorly preserved that identification and age designation are not possible. Accompanying the disappearance of diatoms below Core 113-689B-15H is an increase in abundance of zeolites (clinoptilolite). Their presence suggests that biogenic silica in the sediments was dissolved and reprecipitated.

Hole 689C

Hole 689C is similar to the upper three cores of Hole 689B. Sections 113-689C-1H, CC, and 113-689C-2H, CC, are lower Pliocene. Diagnostic species include *Nitzschia angulata*, *N. praerigidaria*, and *Rhizosolenia barboi*. Section 113-689C-3H, CC, contains *Denticulopsis hustedtii* and, therefore, very likely falls near the Miocene/Pliocene boundary. Other taxa include *Rhizosolenia barboi* and members of the *Actinocyclus ingens* group. As in Holes 689A and 689B, much of the Pleistocene and upper Pliocene is missing.

Hole 689D

Hole 689D did not begin at the sediment/water interface but was washed down to 27.6 mbsf. Section 113-689D-1H, CC, is lowermost Miocene and placed in the *Denticulopsis hustedtii* Zone. Besides the nominate taxon, the sample also contained *Nitzschia donahuensis*, *Coscinodiscus deformans*, and the *Actinocyclus ingens* group. Section 113-689D-2H, CC, is placed in the *Denticulopsis hustedtii* Zone. Other diagnostic taxa include *Nitzschia claviceps* and *Denticulopsis dimorpha*. The presence of these species and the absence of *Denticulopsis praedimorpha* indicate that this sample is likely middle to uppermost upper Miocene.

Section 113-689D-3H, CC, can be placed in the lower upper and middle Miocene *Denticulopsis hustedtii*/*D. lauta* and the

Nitzschia denticuloides Zones. The sample contains *Denticulopsis lauta*, *Azpeitia tabularis*, and the *Actinocyclus ingens* group. Section 113-689B-4H, CC, belongs to the middle Miocene *Nitzschia grossepunctata* Zone and contains *Denticulopsis maccollumii* and *Mediaria splendida*. Section 113-689D-5H, CC, belongs in the lower Miocene *Nitzschia malinterpretaria* Zone and, besides this taxon, also contains *Thalassiosira spinosa* and *Synedra jouseana*.

As in Hole 689B on this site, we encountered moderately preserved lower Oligocene and possibly upper Eocene diatom assemblages (Sections 113-689D-6H, CC, through 113-689D-11H, CC). Although there were sufficient diatoms to identify the lower Oligocene, preservation was not good enough for even preliminary zonal designations.

Summary

At Site 689, we recovered a well-preserved diatom record ranging through the Neogene and upper Oligocene to possibly the upper Eocene. No undisturbed Quaternary sequence was found due to drilling disturbance possibly linked to the presence of a middle to upper Pliocene chert layer. Oligocene diatoms are rare to few and poorly preserved. The occurrence of zeolites in Eocene sediments suggest that biogenic silica, formerly present in the sediments, has been dissolved and reprecipitated. The Neogene diatom record is assigned to the diatom zonation of Weaver and Gombos (1981), and the upper Oligocene to upper Eocene (?) diatom assemblages could not be readily attributed to established high-latitude zonations (Fenner, 1984). We note an unconformity near the Oligocene/Miocene boundary. Because of both surface and deep-water dynamics, Southern Ocean sediments are generally characterized by extensive reworking, sometimes to the point where such sediments cannot be used for stratigraphic or paleoenvironmental analysis. Strikingly, there is a marked lack of sediment mixing at Site 689, except for the topmost part of the section, at and just below the sediment/water interface.

See additional comments on diatom stratigraphic problems in the "Biostratigraphy" section ("Site 697" chapter, this volume).

Taxonomic Note

The nominate taxon for the lower Pliocene *N. angulata* Zone is not conspecific with the extant *Nitzschia angulata* (O'Meara) Hasle (1972), nor is it comparable to the species figured as *N. angulata* by Barron (1985, Fig. 14.14). We did not encounter *N. angulata* (O'Meara) Hasle in lower Pliocene sediments during Leg 113 nor was it reported by Schrader (1976) in DSDP sites in the Pacific sector of the Southern Ocean. The *Nitzschia* species which occur common to abundant in the lower Pliocene in the present material have more affinities to species identified as *Nitzschia porteri* and *Nitzschia* sp. 14 by Schrader (1976). Unfortunately, Weaver and Gombos (1981), who first described the *Nitzschia angulata* Zone, did not photographically document and nominate the taxon. Because this evident taxonomic uncertainty cannot be cleared up, we will continue to use the name *Nitzschia angulata* for this species for Leg 113 material and for the diatom zone until shore-based revision. *Eucampia antarctica* and *E. balaustium* are used interchangeably in this volume and refer to the same species.

Radiolarians

The radiolarian record recovered at Site 689 can be divided into several intervals based on preservation. Middle Miocene to middle Pliocene radiolarians are well preserved and abundant. Upper Oligocene and lower Miocene radiolarian assemblages are poorly preserved and consist predominantly of robust, dissolution-resistant forms and orosphaerid spines. Lowermost Oligocene and uppermost Eocene radiolarian assemblages are by con-

trast very well preserved. Middle Eocene through Maestrichtian sediments are barren of radiolarians. Sediments recovered from the base of the section and dated on the basis of other microfossil groups as upper Campanian(?) / lower Maestrichtian (Core 113-689B-33X) contain a moderately well-preserved assemblage of radiolarians.

Reworking and downhole contamination of radiolarian assemblages were virtually absent in the samples examined. The single exception to this occurred in Sample 113-689D-5H, CC, where few reworked lower Oligocene to upper Eocene radiolarians were found in a lower Miocene assemblage. The stratigraphic indicators found in each hole follow.

Hole 689A

In Hole 689A we recovered a single core. The core-catcher sample is dated as upper Pliocene (Phi Zone), based on the occurrence of *Antarctissa strelkovi*, *Antarctissa ewingi*, *Pterocanium charybdeum trilobum*, *Eucyrtidium calvertense*, and *Clathrocyclas bicornis*, and on the absence of lower Pliocene indicators *Desmospyris spongiosa* and *Helotholus vema*.

Hole 689B

At Hole 689B we recovered 33 cores ranging from Quaternary to approximately uppermost Campanian(?) / lower Maestrichtian.

Section 113-689B-1H, CC, is dated as lower Upsilon Zone (middle Pliocene), based on the occurrence of *H. vema*, *D. spongiosa*, *E. calvertense*, *A. ewingi*, and *P. titan*. Section 113-689B-2H, CC, is basal Pliocene (lower Tau Zone) based on the occurrence of abundant *Lychnocanium grande*, and on the presence of *Eucyrtidium pseudoinflatum*, *E. calvertense*, and *Dendrospyris haysi*.

Cores 113-689B-3H through -5H are assigned to the *Cycladophora spongothorax* Zone, based on the occurrence of the nominate species and several other typical upper Miocene forms. *Actinomma tanyacantha* occurs in Section 113-689B-5H, CC, indicating that the base of Core 113-689B-5H lies in the lower *C. spongothorax* Zone. *A. tanyacantha*, *Amphistylus angelinus*, *Dendrospyris megalcephalis*, *Cycladophora golli*, *Cycladophora golli regipileus*, *Cyrtocapsella isopera*, and *Sethoconus* sp. Chen (1975) are seen in Section 113-689B-6H, CC. This assemblage is assigned to the basal part of the *A. tanyacantha* Zone (middle Miocene), although the ranges of *A. tanyacantha* and *C. isopera* do not overlap in Chen's (1975) zonal scheme. The core-catcher material from Core 113-689B-7H was not examined. From Core 113-689B-8H down, poor preservation makes accurate age assignment difficult. Core 113-689B-8H is tentatively assigned to the lower Miocene, based on the presence of *A. angelinus*, *C. g. golli*, *C. isopera*, and *Sethoconus* sp. Chen (1975).

Core 113-689B-9H is tentatively assigned to the Oligocene, based on the occurrence of *C. isopera*, and a single (broken) specimen of *Calocyclus semipolita*. Core 113-689B-10H contains *C. isopera*, *Sethoconus* sp. Chen (1975), *Cyclampterium* sp. cf. *milowi*, and *Lithomelissa challengerai*, and is assigned to the Oligocene based on the reported ages of the latter two species in Leg 28 sediments (Chen, 1975). Section 113-689B-11H, CC, was essentially barren of radiolarians, containing only orosphaerid spines. Section 113-689B-12H, CC, contains a very well-preserved Oligocene radiolarian assemblage. Many species reported by Chen (1975) from the Oligocene were seen, including *C. semipolita*, *Cyclampterium* sp. cf. *milowi*, *Eucyrtidium* sp. Chen (1975), and *L. challengerai*. Section 113-689B-13, CC, was not examined. Sections 113-689B-14H, CC, through -16H, CC, are lower Oligocene or upper Eocene, based on the occurrence of *Periphaena decora*, and in Section 113-689B-14H, CC, of *Lychnocanoma amphitrite*. The range of *Periphaena decora* is from 55

Ma to 36 Ma, and the range of *L. amphitrite* from 41 Ma to 36 Ma at low latitudes (Sanfilippo and Riedel, 1973; Berggren et al., 1985). All three samples contain common *Cyclampterium* sp. cf. *milowi*, and Section 113-689B-14H, CC, also contains *Sethoconus* sp. Chen (1975), *Calocyclus semipolita*, and *Spongodiscus* sp. cf. *cruciferus*. Sections 113-689B-17H, CC, through -32X, CC, are barren of radiolarians. Section 113-689B-33X, CC, contained a moderately preserved assemblage of Cretaceous radiolarians, including common *Amphipyndax* sp. and hagiastroid species.

Hole 689C

At Hole 689C we recovered three cores. Sections 113-689C-1H, CC, and -2H, CC, are middle Pliocene in age (lower Upsilon Zone), based on the presence of *H. vema*, *D. spongiosa*, *E. calvertense*, *P. c. trilobum*, *Clathrocyclas bicornis*, *P. titan*, *A. ewingi*, *A. strelkovi*, and *A. denticulata*. Section 113-689C-3H, CC, is uppermost Miocene (upper *C. spongothorax* Zone), based on the occurrence of *C. spongothorax*, *S. universus*, and *E. pseudoinflatum*.

Hole 689D

At Hole 689D we recovered 12 cores, with the top of the upper core at approximately 18 mbsf. Hole 689D core numbers are thus about two less than coeval sediments with the same numbers in Hole 689B. Section 113-689D-1H, CC, is uppermost Miocene (upper *C. spongothorax* Zone). Species encountered include *C. spongothorax*, *D. haysi*, *E. pseudoinflatum*, *S. universus*, *Triceraspyris coronata* (?), and *P. titan*. Section 113-689D-2H, CC, is lower *C. spongothorax* Zone. Species include *C. spongothorax*, *A. tanyacantha*, *A. conradae*, *Sethoconus* sp. Chen (1975), *P. haysi*, and forms transitional between *S. universus* and *A. angelinus*. The middle *C. spongothorax* Subzone is inferred to occur within Core 113-689D-2H. Section 113-689D-3H, CC, is middle Miocene (*A. tanyacantha* Zone), based on the presence of *A. tanyacantha* and the absence of *C. spongothorax*. Section 113-689D-4H, CC, contains a lower or lower middle Miocene assemblage of species, including *C. g. golli*, *C. g. regipileus*, *A. angelinus*, *Lithatractus timmsi*, *C. isopera*, *C. tetrapera*, *Sethoconus* sp. Chen (1975), and *Eucyrtidium punctatum*. Section 113-689D-5H, CC, contains common *A. angelinus* and *P. haysi*, and less abundant individuals of *C. g. golli*, *E. cienkowski*, *Sethoconus* sp. Chen (1975), *A. antedenticulata*, and *C. isopera*, and is tentatively assigned to the lower Miocene. Rare reworked Oligocene or upper Eocene specimens were seen in this sample, including *Cyclampterium* sp. cf. *milowi* and *P. decora*. Section 113-689D-6H, CC, has a poorly preserved radiolarian assemblage. A tentative age of early Miocene was assigned due to the presence of *E. cienkowski*, *A. conradae*, and *P. haysi*. The latter species is morphologically atypical and may represent an early transitional form.

Radiolarians from Sections 113-689D-7H, CC, and -8H, CC, are poorly preserved. A tentative age of Oligocene is assigned based on the presence of rare, commonly broken specimens of *L. challengerai*. The radiolarian assemblage in Section 113-689D-9H, CC, is very poorly preserved and contains no stratigraphically useful radiolarians. Sections 113-689D-10H, CC, through -12H, CC, contain poorly preserved radiolarian assemblages with *Cyclampterium* sp. cf. *milowi*, *C. semipolita*, *Periphaena decora*, and (in -12H, CC, only) *Lychnocanoma amphitrite*. These samples were assigned to the lower Oligocene to upper Eocene.

Discussion

At Site 689 we recovered a generally well preserved and relatively complete radiolarian sequence from the middle Miocene to the middle Pliocene. Little or no reworking was observed in the sequence, which will permit construction of a relatively de-

tailed biostratigraphy. Chen's (1975) zones for the middle and late Miocene are recognized at this site, confirming Weaver's (1983) finding that Chen's (1975) zonation can be used to correlate Neogene sediments throughout the Antarctic. The presence of *Periphaena decora* and other cosmopolitan taxa in the Paleogene suggest that a widely applicable Paleogene zonation can be developed, although considerable taxonomic work will be needed for this time interval.

Silicoflagellates

Silicoflagellates are well represented in the Pliocene and lower Oligocene at Site 689, but are less common in the Miocene except at selected intervals. Sections 113-689B-1H-4 to -2H-5 contain large numbers of specimens which, at selected intervals, comprise veritable silicoflagellate oozes. These are strongly dominated by *Distephanus speculum* down to Section 113-689-2H-2 and by *D. boliviensis* below that. Sections 113-689B-2H-6 to -3H-5 are dominated by members of the *D. pseudofibula* plexus, including both symmetric and asymmetric varieties of *D. pseudofibula* and forms often referred to as *D. speculum varians*. These cores belong to the *D. pseudofibula* Zone, which Shaw and Ciesielski (1983) place in the middle Gilbert. The Miocene is not zoned here, although it may be possible to recognize the extinction of *Corbisema triacantha* in Section 113-689B-7H-5 based on a very small number of specimens.

Sections 113-689B-8H-5 to 14H-5 are characterized by *Mesocena apiculata*, *Distephanus crux*, and *Dictyocha frenquelli* in the upper part. Much of the interval can be assigned to the *Dictyocha deflandrei* Zone of Bukry (1975). The *Dictyocha frenquelli* Subzone extends downhole to Section 113-689B-12H-2 based on the first occurrence of the nominative species. The boundary between the lower two subzones of the *D. deflandrei* Zone, however, cannot be drawn because *Mesocena apiculata* continues downhole to the disconformity at the base of the Oligocene sections. There is a sharp abundance peak (acme) of *Naviculopsis trispinosa* in Section 113-689B-13H-2, however, which may coincide with the extinction of this taxon. Slightly lower in the section in Hole 689D, Core 113-689D-10H yielded a diverse assemblage, which includes *Distephanus crux*, *Mesocena apiculata*, and *M. oamaruensis*. The upper Eocene Section 113-689D-12H, CC, contains well-preserved *Dictyocha quadria*.

Palynology

Smear slides reveal that most of the sections of Site 689 lack organic matter. The few core-catcher samples from Hole 689B which were processed (Cores 113-689B-3H, -28X, -29X, -32X, -33X) were all barren of palynomorphs.

In the upper Miocene siliceous oozes (Cores 113-689B-4H and -5H), a cyclic(?) sedimentation was observed, with alternating lighter and darker layers. The latter contain land-derived, organic material. Coal pieces as large as 1 mm in diameter contained woody remains with preserved internal structures, vitrinite particles, and amorphous organic matter. This kerogen seems to be mature or at least transitional between brown coal and lignite, which indicates a heating temperature of over 100°C or an approximate burial depth in excess of 3000 m. The processed samples (113-689D-4H-1, 130-132 cm, and 113-689D-4H-2, 93-94 cm) contain no palynomorphs, so the age of the coal is unknown. It is suggested that these coaly particles were ice-rafted from Antarctica.

Smear slides of white and darker greenish intervals from the K/T boundary transition zone (Sample 113-689B-25X-5, 65 cm) are almost completely devoid of kerogen. Thus, the greenish gray color is probably not caused by the presence of kerogens.

Summary

At Site 689 we sampled a 297.3-m sequence from the Quaternary to the lower Maestrichtian/upper Campanian(?) boundary.

This sequence consists of nearly pure siliceous and calcareous oozes and chalk with negligible admixtures of terrigenous or ice-rafted components. Core recovery was excellent, sedimentation rates relatively uniform (except for hiatuses at the Oligocene/Miocene boundary, the Eocene/Oligocene boundary, the Paleocene/Eocene boundary, and the lower Paleocene/upper Paleocene boundary). Drilling disturbance was minimal except at the top and base of the section where thin porcelanitic cherts were encountered. The quality of this double APC/XCB section and the high carbonate content from the upper Miocene down should establish it as a premier Southern Ocean reference section for paleontologic and isotopic studies. Its ideal geographic location near the continental margin of East Antarctica positions it as the southernmost anchor for pan-Atlantic biostratigraphic, biogeographic, and isotopic studies using siliceous and calcareous microfossils.

Neogene

The foraminiferal ooze at the top of the section yielded rare nannofossils, low-diversity calcareous benthic foraminifers, and a monospecific, possibly Quaternary, Antarctic planktonic foraminiferal assemblage (*Neogloboquadrina pachyderma*). Other than that, lithostratigraphic Unit I was dominated by diatoms and silicoflagellates (middle-lower Pliocene to upper Miocene); some intervals contain no carbonate. The siliceous microfossils are well preserved and the existing radiolarian and diatom zonations can be used to subdivide the majority of the section. A hiatus at about 20 mbsf is suggested by paleomagnetic stratigraphy (see "Paleomagnetism" section, this chapter), but this is as yet unconfirmed by the preliminary biostratigraphic results.

Preservation of siliceous microfossils remains good down through the Miocene of lithostratigraphic Unit IIA despite the strong dilution by nannofossil ooze at various levels. Planktonic foraminifers consist of essentially monospecific assemblages characteristic of modern polar water masses. An important event is the incursion of *Neogloboquadrina pachyderma* into the Antarctic water mass during the middle to late Miocene (Core 113-689B-5H). Calcareous benthic foraminifers have a low diversity in Cores 113-689B-4H through the top of -6H, with somewhat higher diversity lower in lithostratigraphic Unit IIA; faunas indicate depths of about 2000 m. Calcareous nannofossils consist of less than a half dozen species, two or three of which alternate dominance over meter or dekameter intervals, presumably in response to climate-induced migrations of polar and subpolar water masses over the site (Haq, 1980). Quantitative biogeographic studies of the diatom, radiolarian, nannofossil, and planktonic foraminiferal assemblages keyed to the excellent time control provided by the siliceous zonations and paleomagnetic stratigraphy should elucidate in some detail the nature and timing of these glacially related climatic events.

The low diversity of the planktonic foraminifers and of the highly calcareous nannofossils prevents the application of existing calcareous zonal schemes in the Miocene. Zonation of Unit IIA is dependent on the biosiliceous zonations. The Miocene at this site does not exhibit the pervasive reworking of siliceous and calcareous microfossils that characterizes sequences to the north which lie in the path of the circumpolar current (e.g., Site 329 on the Maurice Ewing Bank). This circumstance should aid in the further refinement and calibration via paleomagnetic stratigraphy of the Miocene siliceous biostratigraphies of Antarctic waters.

Although most of the section is barren of palynomorphs, the upper Miocene oozes of lithostratigraphic Unit IIA exhibit a cyclic(?) alternation of light and dark layers. The latter contain land-derived organic matter, with pieces of ice-rafted coal in Cores 113-689D-4H and -5H. The woody remains display well-preserved internal structures, and the kerogen appears to be mature (at least transitional between brown coal and lignite).

Paleogene

The upper Oligocene-upper Eocene lithostratigraphic Unit IIB is dominated by nannofossil oozes with appreciable admixtures of biosiliceous material in the upper and lower portions of the Oligocene (especially in Cores 113-689B-8H and -12H), which are separated by an interval of poor preservation and low abundance. Radiolarians and diatoms are particularly diverse and well preserved in Core 113-689B-12H, but nannofossils begin to show strong overgrowths at that level. The Oligocene planktonic foraminiferal faunas are more varied than the succession of truly "polar," monospecific assemblages of the Miocene, and as such, represent a transition to the more diverse faunas of the lower Paleogene. Nevertheless, the diversity is never sufficient to allow the existing temperate zonations to be applied anywhere in the Cenozoic section at this site.

The presence of several reworked nannofossil species in Core 113-689B-7H and an abrupt change in the diatom and nannofossil assemblages between Sections 113-689B-7H-3 and 113-689B-8H-4 suggest a disconformity at the Miocene/Oligocene boundary. The Oligocene/Eocene contact could be determined only via planktonic foraminifers (LAD of *Globigerinatheka index*) due to the absence of discoasters, which are missing essentially throughout the Oligocene-middle Eocene. This boundary is characterized by CaCO_3 dissolution, thus planktonic and benthic foraminifers are rare (Cores 113-689B-14H and -15H); there is probably a hiatus across the boundary (no nannofossil Zone CP15b).

Benthic foraminifers show increased diversity downhole, with increasing importance of buliminid species down from the Eocene/Oligocene boundary.

The upper Eocene planktonic foraminiferal faunas range down to Core 113-689B-18H where the LAD of *Acarinina coalensis* marks the top of the middle Eocene. The upper and middle Eocene assemblages generally show a close similarity to the cool temperate faunas described from New Zealand (Jenkins, 1971). The nannofossils appear more restricted than those of New Zealand (Edwards, 1971) or of the Falkland Plateau (Wise, 1983). This difference is accentuated somewhat by the diminished preservation of the Maud Rise floras, which are etched and overgrown in this carbonate-rich section. Core 113-689B-14H marks the lowest level of well-preserved and identifiable diatoms. They disappear completely from the section below Core 113-689B-15H, where an increase in the abundance of zeolites (clinoptilolite) suggests their conversion to secondary forms of silica. Radiolarians disappear below Core 113-689B-16H, but reappear briefly at the base of the hole.

A downhole increase in the abundance of planktonic foraminifers near the upper/middle Eocene boundary marks the division between lithologic Units II and III. Few nannofossil and planktonic foraminiferal datums could be distinguished in the middle Eocene, and no unequivocal lower Eocene assemblages were recognized. Only one specimen of *Discoaster* was noted.

Benthic foraminifers increase in diversity downhole in the uppermost middle Eocene (Core 113-689B-19H); buliminid species become more abundant. In view of the apparent absence of lowest Eocene strata, a disconformity or highly condensed sequence is postulated between the Eocene and the Paleocene, in Sample 113-689B-22X-4, 58 cm, at a marked break in lithology. Section 113-689B-22X, CC, is assigned to nannofossil *Discoaster multiradiatus* Zone (CP8). The coccolith assemblage closely approximates that described from time-equivalent strata at Site 327 on the Falkland Plateau. Core 113-689B-24X belongs to the *Heliolithus riedelii* Zone (CP7). Preservation of nannofossils improves downward from moderate to good through this zone. A hiatus is present across the upper/lower Paleocene boundary in the topmost part of Core 113-689B-25X; calcareous nannofossil Zones CP4-CP6 are not represented.

Upper Paleocene planktonic foraminiferal assemblages lack the *Morozovella* species used to delineate the low- to middle-latitude zonations, an observation which supports Boersma and Premoli-Silva's (1983) suggestion that this group is biogeographically limited to lower latitudes.

A short interval in Core 113-689B-22X (below the hiatus) and the top of Core 113-689B-23X contains a low diversity benthic foraminiferal fauna with abundant *T. selmensis* and *Aragonia semireticulata*. Benthic assemblages change dramatically to typical *Stensioina* faunas with much higher diversity in Core 113-689B-23X, with the LAD of *Stensioina beccariiiformis* in Section 113-689B-23X-2. This LAD marks the most important benthic foraminiferal faunal change of the Cenozoic. *S. beccariiiformis* faunas are common in Upper Cretaceous and Paleocene sediments described elsewhere, such as at Site 516 on the Rio Grande Rise, where they denote middle bathyal to shallow lower bathyal water depths (1000-1500 m; Dailey, 1983; Van Morkhoven et al., 1986). This change in water depth reflects the subsidence experienced by Maud Rise following its formation during the Late Cretaceous. *Stensioina* faunas continue down through the remainder of the section, with changes in species composition.

Cretaceous/Tertiary (K/T) Boundary

The K/T boundary was captured in Section 113-689B-25X-5. The upper Danian nannofossil Zones CP4, CP5, and CP6 are missing near the top of Core 113-689B-25X due to a disconformity, but the lowermost Danian zones are present. The K/T boundary apparently lies between about 84 and 85 cm in Section 5. Greenish Danian ooze above this boundary is assigned to the nannofossil *Cruciplacolithus tenuis* Subzone (CP1b) based on common *Cruciplacolithus edwardsii*. The foraminiferal assemblage contains abundant *Planorbulites eugubina* but no *Subbotina pseudobulloides*. A nearly pure white semilithified chalk below contains abundant *Nephrolithus frequens* among the nanoflora and a diverse upper Maestrichtian planktonic foraminiferal fauna, including *Globotruncana* cf. *G. plummerae* and *Hedbergella* spp. A few 1- to 3-cm clastlike pods of Cretaceous chalk lie scattered in the greenish Danian matrix as far as 10 cm above the boundary. These could indicate some erosional disturbance of the boundary itself. On the other hand, these pods could be accounted for by strong bioturbation, which has all but obliterated the boundary contact. The bioturbation has also mixed Danian and Cretaceous nannofossils across the boundary, thereby making it difficult to confirm the presence or absence of a complete boundary section. The presence of a *P. eugubina* Zone foraminiferal assemblage, however, suggests that the boundary sequence is relatively complete. Benthic foraminiferal faunas show changes in relative abundances but minor extinctions. The faunal changes start below the nannofossil K/T boundary.

An unusual observation is the detection of altered volcanogenic clay and vitric glass in the 40-cm greenish clay interval in the vicinity of the K/T boundary (see "Lithostratigraphy" section, this chapter). This material, derived from volcanic sources, seems to be associated with the lowermost Danian sediments of the *P. eugubina* Zone and Zone CP1, and corresponds roughly in its position to the "boundary clays" recorded at DSDP Sites 516 and 524 in the South Atlantic (Barker et al., 1983; Hsu et al., 1984). This engenders speculation as to whether these clays and the one at the present site, which today are separated as far as 4630 km, could have recorded the same volcanic event or related volcanic events. This speculation will be evaluated during our subsequent shore-based research in light of recent articles which suggest excessive volcanism as the ultimate cause of the Cretaceous extinction event(s). One such paper (Officer et al., 1987) cites the initiation of volcanic activity at the Reunion hot-

spot (Indian Ocean) and a peak in explosive volcanism on the Walvis Ridge, both of which are important volcanic sources in this part of the world at the approximate time of the K/T event.

Cretaceous

The Cretaceous can be subdivided using the high-latitude nanofossil zones of Wind and Wise (1983). The interval from the K/T contact down through Core 113-689B-27X contains a moderately preserved assemblage assigned to the *Nephrolithus frequens* Zone, which corresponds roughly to the upper Maestrichtian and spans the same interval here as the planktonic foraminiferal *Abathomphalus mayaroensis* Zone. As with the Danian section above, these strata have not previously been observed at DSDP/ODP sites in the South Atlantic sector of the Southern Ocean.

Preservation of nanofossils deteriorates noticeably downhole by Core 113-689B-27X, which marks the beginning of lithostratigraphic Unit IIIB. This unit encompasses the indurated, lithified calcareous sequence, and consists of a series of cherts with interbedded minor cherts. Core 113-689B-28X belongs to the nanofossil *Biscutum magnum* Zone, which is roughly middle to earliest Maestrichtian in age. The diversity of benthic foraminifers drops at the *Nephrolithus frequens* Zone/*Biscutum magnum* Zone boundary. Depositional depths for the lower part of the section are estimated at 500–1000 m.

The sequence below Sample 113-689B-29X-2, 28 cm, is assigned to the *Biscutum coronum* Zone, the top of which marks the extinction of several members of a more diverse nanofossil assemblage that extends from the lowest Maestrichtian to about the lower/middle Campanian boundary. Because middle Campanian carbonate has never been recovered in the Southern Ocean, it has not been possible to subdivide reliably the middle to upper Campanian interval in order to further restrict the lower limit of the *Biscutum coronum* Zone. Nevertheless, it appears that the bottom of this hole is near the Campanian/Maestrichtian boundary.

Preservation of calcareous microfossils is poor at the bottom of the hole, and Core 113-689B-33X contains a low-diversity benthic foraminiferal assemblage (assemblage 8), which provides little information about the environment of deposition. This core does contain, however, moderately preserved radiolarians, a microfossil group which had not been observed in the section since Core 113-689B-17H (Eocene). Their former presence in the sediments of Cores 113-689B-31X and -32X is probably indicated by the porcelanitic cherts. Similar cherts eventually forced the abandonment of this site.

PALEOMAGNETISM

The pelagic sedimentary sequence draping Maud Rise offers an excellent opportunity to determine for the first time a Cenozoic magnetostratigraphy for a high-latitude Southern Ocean site.

Micropaleontological age determinations of the core-catcher samples from the uppermost cores of Hole 689B suggest that the average sedimentation rate approximates 0.5 cm/1000 yr. Therefore, already in an early stage of the sampling we reduced the paleomagnetic sampling interval to 25 cm. This ensured that a resolution of at least 50,000 yr would be achieved, which is necessary for the unequivocal identification of polarity intervals of the same duration.

Although a measurement of all samples was not possible during the shipboard investigation, we measured the natural remanent magnetization (NRM) of at least two samples per section with the MOLSPIN magnetometer. This seemed to be a good compromise between the time limitations imposed by the sampling/measuring process and our aim to develop a satisfactory magnetostratigraphy. Thus about 255 samples were measured

for Hole 689B. Figure 27 shows the inclination and the intensity of the NRM vector of the measured samples plotted as a function of depth below seafloor. The mean intensity was higher than originally expected for the dominantly biogenic sediments encountered at this site. With a few exceptions all samples could be satisfactorily measured on the long spin setting of the magnetometer. The intensities range from 0.06 to 11.8 mA/m and seem to be correlated in some parts to lithologic changes.

The distribution of inclination values (Fig. 28) shows a notable but not serious bias towards negative values that can be attributed to a partial overprint by the present geomagnetic field. The distribution appears nearly bimodal, with two maxima in the interval from -60° to -75° and 0° to -15° , although there is also a broad variation of positive inclination values. The vector addition of the recent field vector and the primary magnetization component leads often to shallower positive inclination values or even negative values for the reversed polarity samples. Nonetheless, the downhole inclination record shows a few intervals associated with steep positive inclinations. Notable amongst these reversed magnetozones are those in Cores 113-689B-2H and -13H. Shore-based alternating field demagnetization will undoubtedly reveal others. It should generally improve the fidelity of the polarity reversal record obtained for Site 689 for those short magnetozones based on only one sample and/or shallow inclination values.

For our preliminary interpretation of the inclination record, the polarity is not obtained directly by the sign of the inclination value, but by separating the bimodal distribution at approximately -30° due to the assumed normal overprint. All values below this limit are assumed to be normally magnetized; shallower inclinations and high positive inclination values are assigned to a reversed polarity. By adopting this procedure about 62% of all values appear to be normal and 38% reversed. The resultant downhole polarity pattern for Hole 689B is shown in comparison to the geomagnetic polarity time scale for the Neogene through the lower Paleogene (Fig. 29). The proposed assignment is not unambiguous and not in total agreement with the biostratigraphic results from micropaleontological studies of core-catcher samples. However, the presented age-depth relationship is an optimum in the sense that it requires a minimum number of hiatuses and maintains fairly constant sedimentation rates over longer time periods. The questionable assignment of approximately 12% of the samples to normal polarity above the 50:50 ratio expected has to be kept in mind and emphasizes the necessity of the denser sampling intervals and of detailed shore-based demagnetization.

According to our age-depth correlation, three major hiatuses are recognized in the upper Miocene (5.9–8.9 Ma), the middle to lower Miocene (15–19 Ma), and the lower Miocene to lower Oligocene (22–33 Ma). The inferred sedimentation rate otherwise remains fairly constant at 7–9 m/m.y. down to a depth of 145 mbsf, then changes to 4 m/m.y. for middle to late Eocene time. The uncertainty in assignments for the oldest part of the Cenozoic record we sampled prevents us from estimating the sedimentation rate for that interval.

SEDIMENTATION RATES

Biostratigraphic and Magnetostratigraphic Data

The sedimentation rate curve for Site 689 (Fig. 30) is constructed from two data sources. Magnetic polarity data were matched to a best-fitting correlation with the geomagnetic polarity reversal time scale of Berggren et al. (1985) ("Paleomagnetism" section, this chapter). This correlation was constructed without recourse to biostratigraphic data (Fig. 29).

Biostratigraphic ages derived from planktonic and benthic foraminifers, diatoms, radiolarians, and calcareous nanofos-

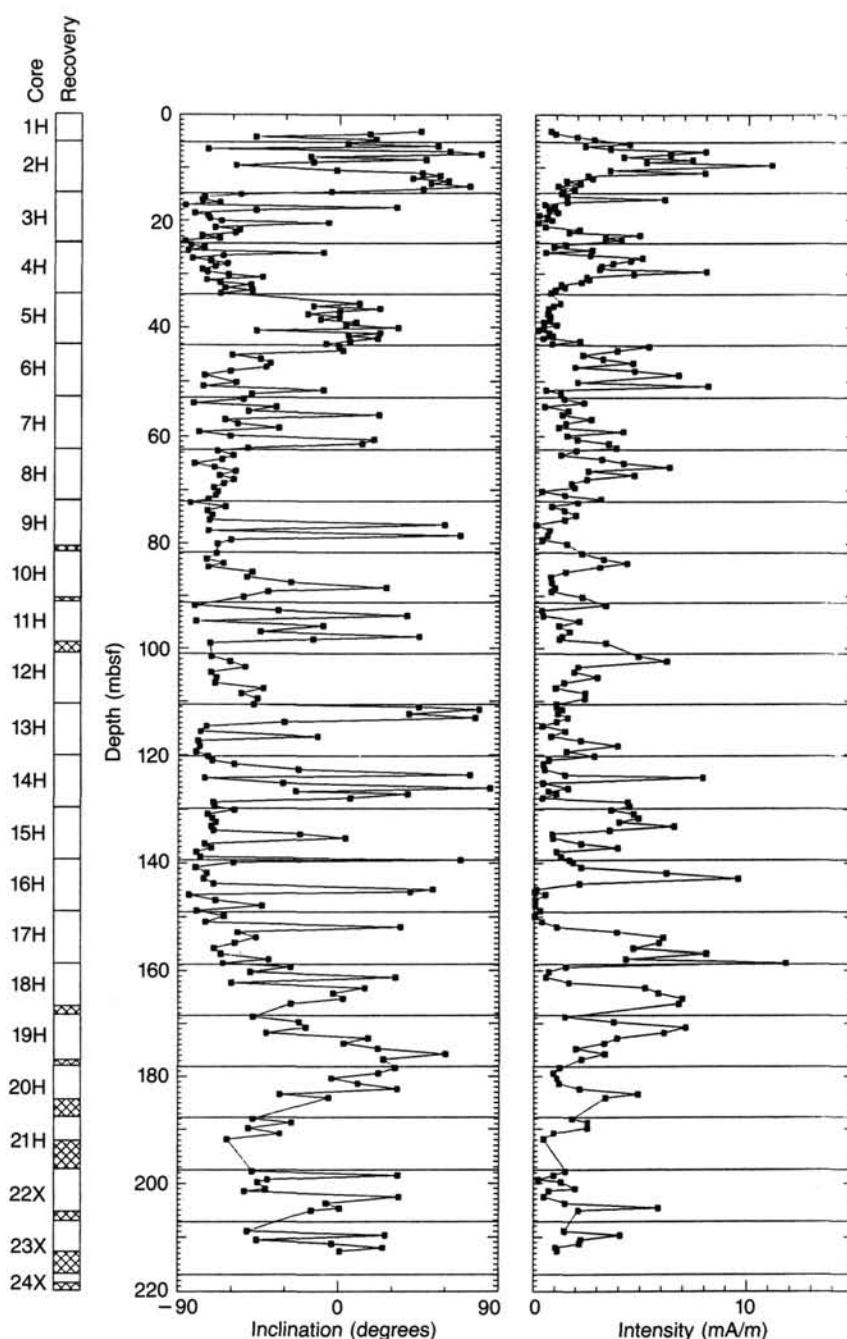


Figure 27. Downhole variation in NRM inclination and intensity for Hole 689B. Pattern indicates no recovery.

sils provided the other source of age information. Biostratigraphic data used to construct the age-depth relationship (Table 8) consist of selected datum levels and zonal assignments that have been correlated to the chronostratigraphic scale. The accuracy of the calibration between biostratigraphy and chronostratigraphy varies considerably for different fossil groups and time intervals. In particular, the pre-Pliocene diatom and radiolarian stratigraphies are not well calibrated chronostratigraphically.

Magnetostratigraphic ages are determined by the comparison of the inferred downhole polarity pattern to a geomagnetic polarity time scale. Due to an average time span between the measured samples of approximately 100,000 yr, a number of short

polarity intervals are naturally overlooked, and thus the potential high frequency information cannot be used for an unequivocal identification of polarity patterns. The preliminary interpretation is based on a relatively small number of polarity reversals which are fitted to the polarity time scale under the assumption of fairly constant sedimentation and a minimum number of hiatuses. Two apparent long normal magnetozones from 20 to 35 mbsf and from 62 to 77 mbsf together with a normal polarity overprint on about 20% of the samples make the interpretation more difficult and open for later reinterpretation. Shore-based study, including magnetic cleaning by stepwise demagnetization, is required to obtain a more complete polarity record.

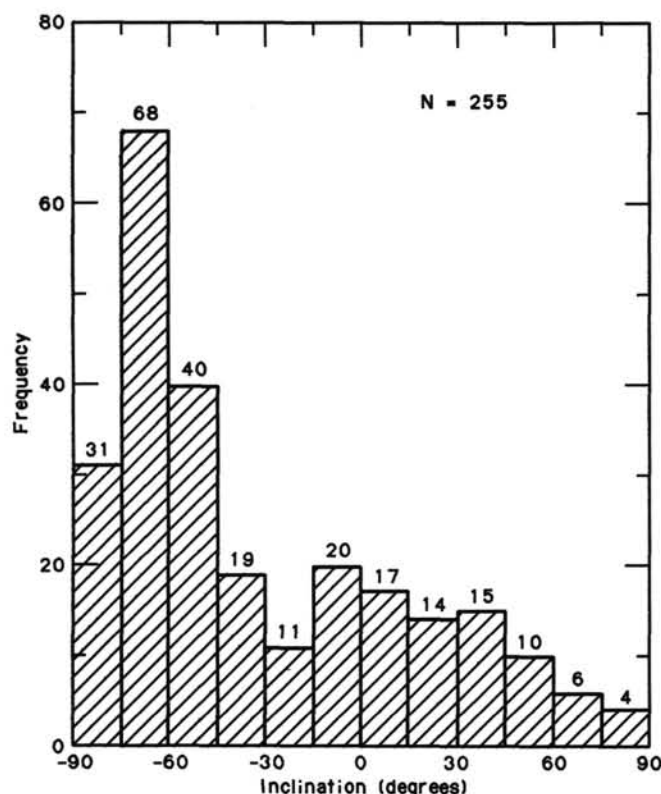


Figure 28. Frequency distribution of NRM inclination values for Hole 689B.

Age-Depth Curve, Site 689

An age-depth curve for Site 689 is shown in Figure 30, together with the biostratigraphic and magnetostratigraphic data used to produce the line of correlation. The figure was constructed as follows: the solid line connecting unlabeled datum points is based on paleomagnetic data; the labeled data points with identifying numbers (Table 8) show the independently determined stratigraphic information. The age-depth curve is shown as a solid line with more tentative intervals as dashed lines and hiatuses as wavy lines. Magnetostratigraphic data error boxes represent in depth the distance between the two samples of different polarities assigned to different magnetozones. From the preceding and the following magnetozone boundary a sedimentation rate, and from this, a corresponding error in the age determination is calculated. This age error is represented by the horizontal box size. Biostratigraphic data are of three types. First and last occurrences of species are known only to occur within a finite depth interval, although the age of the datum is generally reported without any associated error estimate. These data thus plot as vertical lines. Age ranges for individual samples by contrast have a finite age range but do not have any depth uncertainty, and plot as horizontal lines. Finally, a few first appearance datums (FAD's) and last appearance datums (LAD's) for which uncertainty estimates are available are plotted as boxes. Many samples have more than one age range estimate from different fossil groups. To make the overlap between multiple dates clear, small solid circles are used to mark the end of each datum which plots as a line. FAD's and LAD's only represent oldest and youngest possible ages, respectively, for a depth interval. Arrows on these datum types are used to indicate this on the figure. The vertical columns on the left of each figure give core numbers and recovery (cross-hatched = no recovery), and the magnetic polarity data. The agreement between the two

data sets is relatively good below 110 m and above 50 m, and a single age-depth curve can be chosen which reasonably fits both types of information. Discrepancies between the biostratigraphic and magnetostratigraphic ages are seen in the interval between those depths.

Biostratigraphic data suggest that the 56–67 mbsf interval is lower Miocene, whereas the magnetostratigraphic age estimate is less (middle Miocene). Given the uncertain calibration of the siliceous biostratigraphies in this time interval, we have chosen to use the magnetostratigraphic data to construct this portion of the age-depth curve.

An even larger discrepancy between the magnetostratigraphic and biostratigraphic ages occurs between approximately 67 and 106 mbsf. Biostratigraphic data assign this interval an Oligocene age, whereas the magnetostratigraphic age estimate (data points connected by a solid line, see "Paleomagnetism" section, this chapter) is early Miocene. Precise magnetostratigraphic interpretation of this interval is difficult due to apparently overprinted normal polarity zones. The biostratigraphic data for the Oligocene, on the other hand, are derived from several different microfossil groups, and the calcareous microfossil stratigraphies are, at least in comparison to the Miocene biosiliceous data, relatively well calibrated to the chronostratigraphic scale. The biostratigraphic data were thus used to construct the age-depth curve in this interval. An alternative interpretation of the magnetostratigraphic data which corresponds more closely to the biostratigraphic data for this interval is shown by the solid boxes connected by a dashed line. Note that there should be a hiatus over the complete lower Miocene if the first magnetostratigraphic correlation is correct; this is in strong contradiction with biostratigraphic data on all microfossil groups. Biostratigraphic tie-points are needed for the assignment of such a short, apparently incomplete, overprinted polarity pattern to the geomagnetic polarity time scale. This alternative interpretation suggests a constant but lower sedimentation rate than suggested by the original interpretation of the magnetostratigraphic data (4 m/m.y.).

Hiatuses

Hiatuses or severely condensed sections are probably present at several levels within Site 689 (Fig. 30, Table 8). Such an interval occurs at the top of the section, although more data are needed to determine the nature of sedimentation during this interval (upper Pliocene to Quaternary).

A hiatus at approximately 21 mbsf (Core 113-689B-3H) is inferred from paleomagnetic data, separating lower Pliocene sediments from lower upper Miocene sediments. Biostratigraphic ranges in this depth interval are not known well enough at the present time to confirm this.

A hiatus appears to be present within Core 113-689B-8H at 67.5 mbsf, separating lower Miocene and upper Oligocene sediments. Magnetostratigraphic data in this depth interval are inconclusive, and the existence of this hiatus is based on biostratigraphic data; the duration has not been established.

Biostratigraphic data suggest the presence of a hiatus in Core 113-689B-15H (~131 mbsf; calcareous nannofossil Zone CP15b not represented). No confirmation can be found in the magnetostratigraphic data; the duration of the hiatus should be at least 1.1 m.y. (duration of Zone CP15b).

Biostratigraphic data on calcareous nannofossils and planktonic and benthic foraminifers ("Biostratigraphy" section, this chapter) clearly show a hiatus in Sample 113-689B-22H-4, 58 cm (~203 mbsf), which separates middle Eocene from upper Paleocene sediments. Calcareous nannofossil Zones CP9 through CP11 are not represented, suggesting a duration of at least 5 m.y. There is an evident level of color change at the hiatus with reworked clasts above the color boundary.

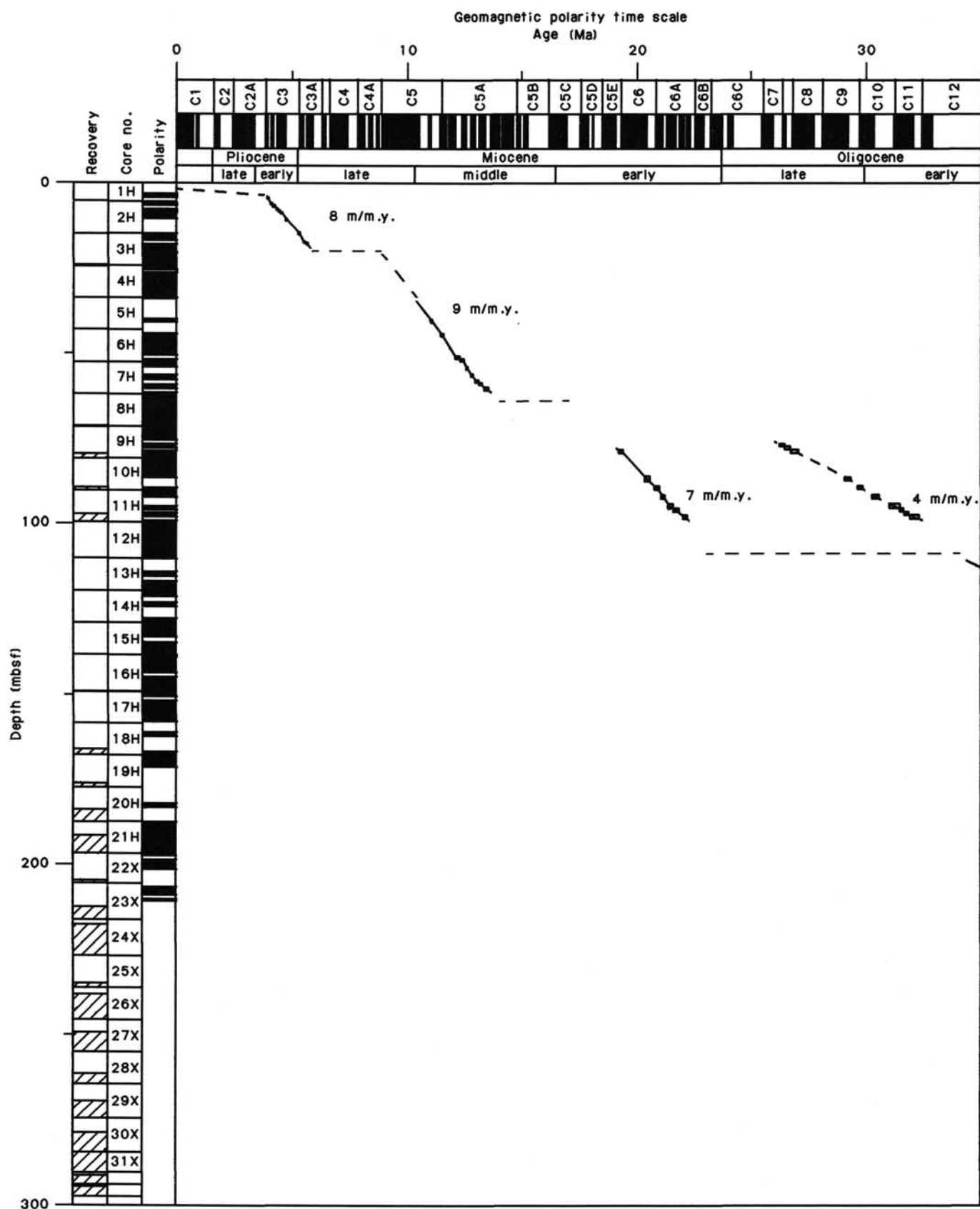


Figure 29. Assignment of the inferred magnetostratigraphy for Hole 689B to the established geomagnetic polarity time scale resulting in estimates of sedimentation rates. Alternative interpretations are given for the interval 80–100 mbsf.

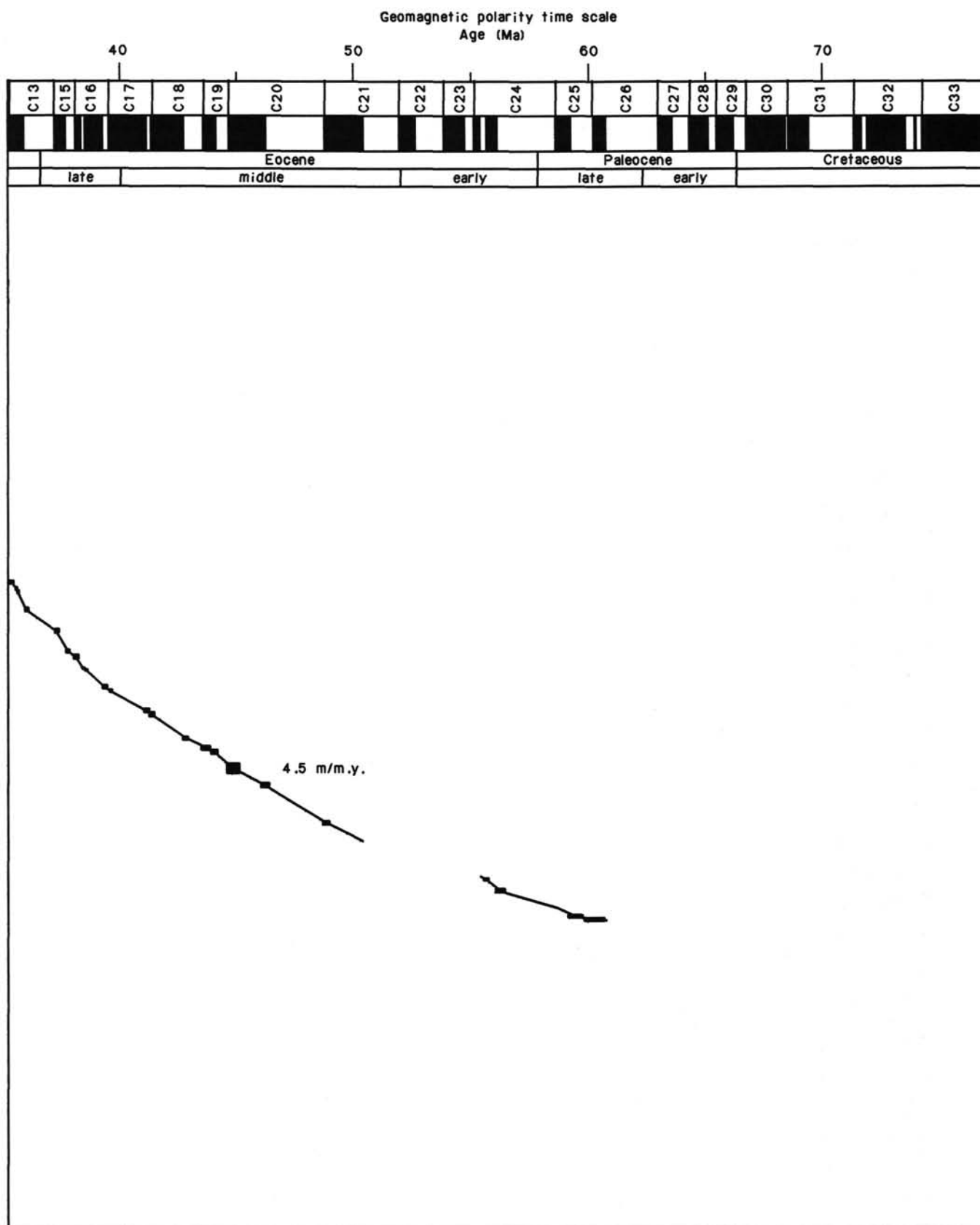


Figure 29 (continued).

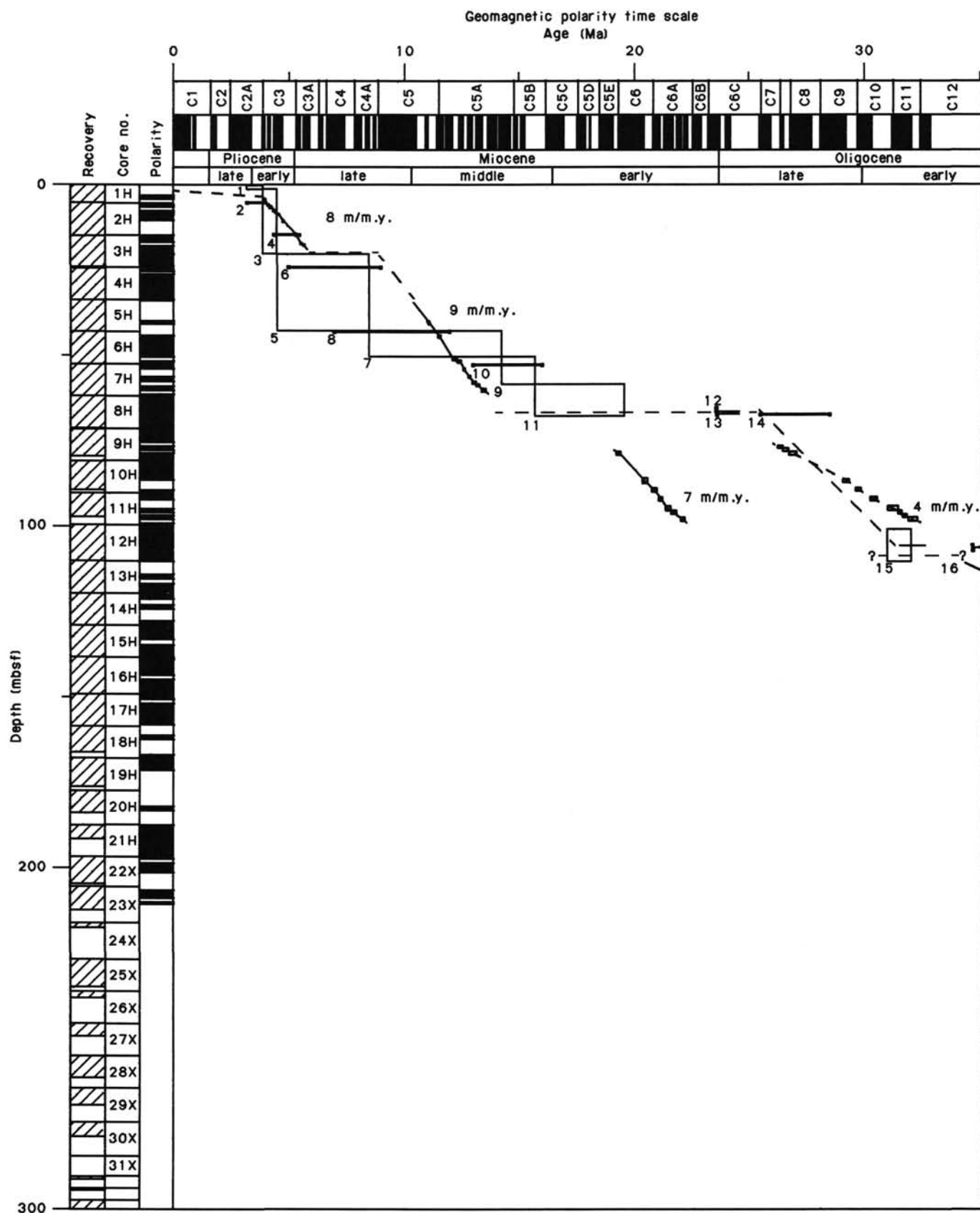


Figure 30. Age-depth interpretation of Site 689. See text for explanation.

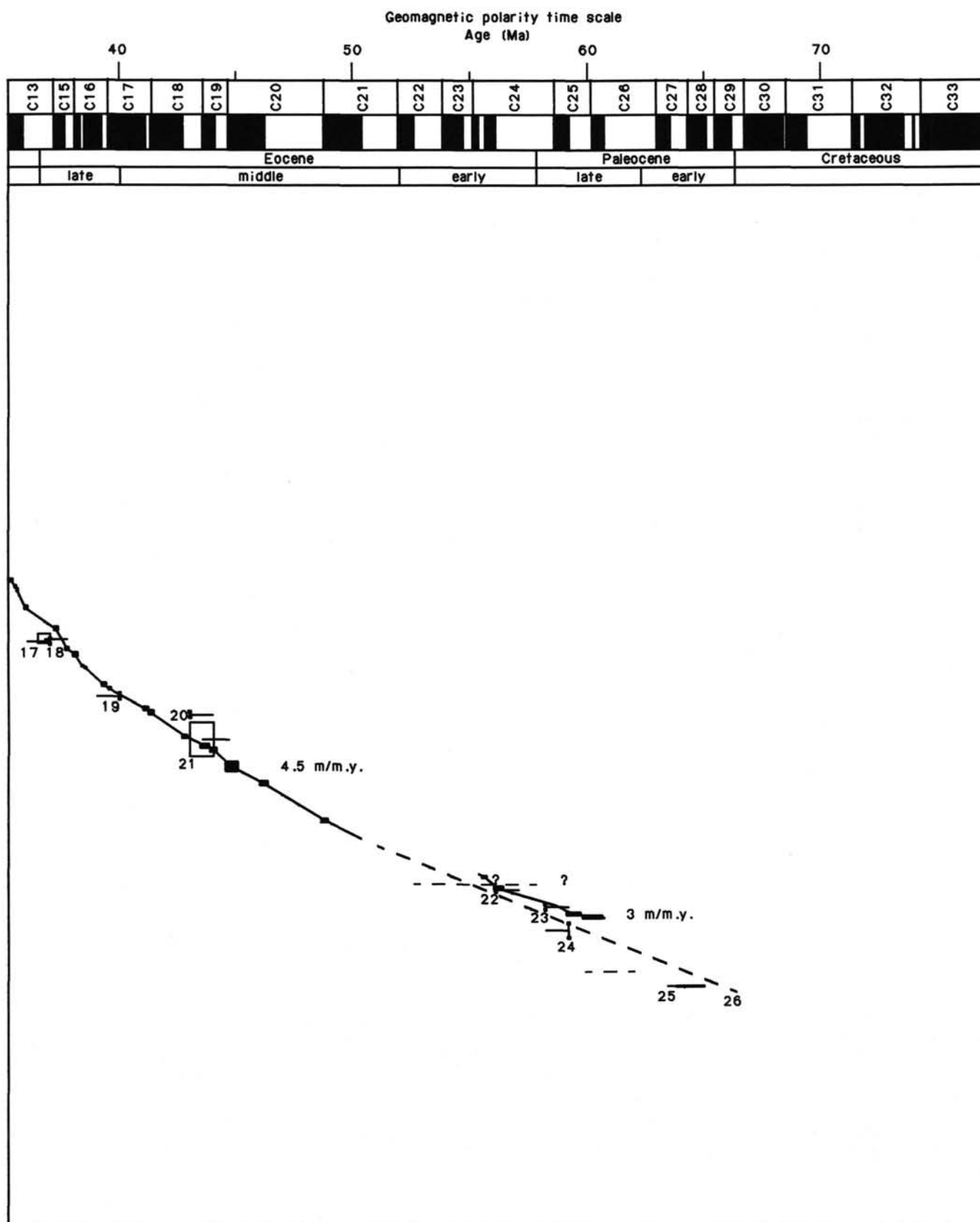


Figure 30 (continued).

Table 8. Biostratigraphic data used to construct sedimentation rate in Figure 31.

	Datum	Depth range (m)	Age range (m.y.)
1	<i>N. interfrigidaria</i> Zone - D	0.0-1.2	3.2-3.9
2	lower Upsilon Zone - R	5.3	3.2-4.0
3	<i>N. angulata-N. reinholdii</i> Zone - D	1.2-20.3	3.9-4.52
4	lower middle Tau Zone - R	14.8	4.4-5.5
5	<i>D. hustedii</i> Zone - D	20.3-43.0	4.52-8.5
6	upper <i>C. spongothorax</i> Zone - R	24.3	5.0-9.0
7	<i>D. hustedii-D. lauta-N. denticuloides</i> Zone - D	43.0-50.5	8.5-14.25
8	lower <i>C. spongothorax</i> Zone - R	43.3	7.0-12.0
9	<i>N. grossepunctata-C. lewisianus</i> Zone - D	50.5-58.5	14.25-15.7
10	lower <i>A. tanyacantha</i> Zone - R	52.9	13.0-16.0
	* hiatus (Oligocene/Miocene boundary) - D, N	± 67.5	?
11	<i>N. malinterpretaria-C. rhombicus</i> Zone - D	58.5-67.8	15.7-19.6
12	LAD <i>C. altus</i> - N	65.8-67.3	23.6
13	Miocene/Oligocene boundary (hiatus) - D	66.2-67.7	23.6
14	upper <i>R. vigilans</i> Zone - D	67.7	25.5-28.5
15	LAD <i>S. angiporoides</i> - PF	101.0-110.6	32.0
16	LAD <i>R. umbilica</i> - N	105.8-107.3	34.7
	* hiatus (Zone CP15b missing) - N	± 131.0	36.7-37.8
17	LAD <i>G. index</i> - PF	129.9-132.5	36.5-37.0
18	FAD <i>I. recurvus</i> - N	131.2-132.8	37.0
19	FAD <i>C. oamurensis</i> - N	147.2-148.7	40.0
20	LAD <i>C. solitus</i> - N	152.3-153.8	43.0
21	LAD <i>Acarinina</i> spp. - PF	155.5-165.2	42.0-43.0
	* hiatus (Zones CP9-CP11 missing) - N, PF	± 203	52.6-57.8
22	LAD <i>T. selmensis</i> - BF	202.4-203.9	56.1
23	LAD <i>S. beccariiiformis</i> - BF	207.6-209.1	58.2
24	FAD <i>D. multiradiatus</i> - N	212.9-217.2	59.2
	* hiatus (Zones CP4-CP6 missing) - N	226.5	59.8-62.0
25	FAD <i>C. edwardsii</i> - N	231.4	63.8-65.0
26	K/T boundary - N	233.4-233.5	66.4

Note: Depth ranges of first and last appearance datums (FAD and LAD) and zones. A single value in the depth range column indicates a sample with a zonal or assemblage age assignment. Age range given for zones, and in some instances for uncertainty in age calibration of FAD or LAD. Letters following each name refer to the fossil group. D = diatoms; R = radiolarians; N = calcareous nannofossils; PF = planktonic foraminifers; BF = benthic foraminifers. * = duration of hiatuses is given as the minimum value, i.e., the duration of the biostratigraphic zone not represented in the sediment.

Another hiatus is suggested by the calcareous nannofossils and planktonic foraminiferal data from the topmost part of Core 113-689B-25X (~227 mbsf); Zones CP4 through CP6 are not represented, suggesting a duration of the hiatus of at least 2 m.y.

Sedimentation Rates

The age-depth relationship of Figure 30 can be used to calculate sedimentation rates for specific depth intervals, although one premise of the preliminary interpretation of the magnetostratigraphic data was to retain sedimentation rates as constant as possible. An average sedimentation rate of 8-9 m/m.y. is estimated for the Neogene, not including the hiatus at 20 mbsf.

An average rate of 7 m/m.y. is estimated for the upper Oligocene based on the magnetostratigraphic data, but the combination of biostratigraphic and paleomagnetic data suggests a rate of 4 m/m.y. Age determinations from biostratigraphic and magnetostratigraphic shipboard studies are in close agreement for the middle and upper Eocene and indicate an average sedimentation rate of 4.5 m/m.y. In the Paleocene and lower Eocene some inconsistencies seem to exist between paleomagnetic and biostratigraphic data and even between different fossil groups and thus the sedimentation rate estimated for this interval (3 m/m.y.) is only tentative.

INORGANIC GEOCHEMISTRY

Introduction and Operation

Data on the chemical composition of interstitial water are from Hole 689B on Maud Rise. Ten whole-round squeezed sedi-

ment samples (4-5 cm and 6-10 cm thickness) were analyzed. The three deepest whole-round samples are from XCB cores, the others from APC cores. In addition, three samples were taken in the interval 2.85-7.46 mbsf (for studies of a chert layer see below). These were sampled after splitting the core with a wire, and 50-60 mL of sediment was cut from the working half. The chemical data are summarized in Table 9.

Evaluation of Data

For overall evaluation of the data a charge balance was carried out. In routine work, a charge excess or deficiency of more than 2% is intolerable. The data do not include sodium. However, within experimental limits, in pelagic sediments from areas with moderate heat flow which are not underlain by evaporites, sodium/chloride ratios do not differ from those in seawater. Sodium is calculated by multiplying the Na/Cl ratio of seawater by the measured chloride concentration. Figure 31A shows the charge imbalance vs. depth. In all samples there is a slight excess positive charge, but nowhere greater than 2%. The increasing imbalance toward the bottom of the hole may indicate that the assumption of a constant Na/Cl ratio is not valid. It is possible that sodium is involved in the same type of reactions that affect calcium and magnesium (see below). On the other hand, a systematic error in one of the methods would create a similar anomaly. There are no anions that occur at millimole per liter levels other than those considered. Since the bacterial activity is very low (see below), the charge balance calculations are not invalidated by the lack of data on ammonia. The data set from 135.5 mbsf (Section 113-689B-15H-4) is not included in this analysis because of the reported chloride analysis (Table 9), which is probably an artifact.

Chlorinity and Salinity

Chloride data are presented in Figure 31B. The average concentration of chloride is the same as in seawater (556 mmol/L). The result from 135.5 mbsf is an artifact and is not included in the graph. The slightly lower chlorinity level at the very top is within experimental uncertainties. The salinity data (Table 9) show considerable scatter and do not correlate with the chlorinity.

pH

The pH (Fig. 31C and Table 9) shows small variations with the highest readings in the upper core (pH = 7.82). In most diagenetic reactions, pH is a master variable and its accurate determination is important. Interpretation of laboratory results, however, and extrapolation to downhole conditions are complicated. The major potential problem is degassing of the sample during retrieval. Sayles (1980) showed that in deep-sea surficial sediments, the concentration of dissolved calcium is controlled by the solubility of calcite.

For kinetic reasons degassing of the samples and rising pH do not cause instantaneous precipitation of calcite. Thus, the measured concentration of dissolved calcium and the alkalinity may be utilized to calculate the *in-situ* pH, on the assumption of calcite saturation. This method has been used successfully to calculate the pH of waters buried to more than 4000 mbsf (P. Egeberg, unpubl. data).

Due to low bacterial activity (see below) and therefore low carbon dioxide pressure (little degassing), the carbonate-rich sediments of Site 689 are well suited for testing this hypothesis. For the calculations, we used the pressure-dependent apparent solubility product for calcite determined by Sayles (1980), the thermodynamic second dissociation constant for carbonic acid, and the total activity coefficients for carbonate and bicarbonate ions, provided by Stumm and Morgan (1981). Calculations were carried out at 5°C and 230 atmospheres (the average hole conditions).

Table 9. Summary of shipboard interstitial water data for Hole 689.

Core, section interval (cm)	Depth (mbsf)	pH	Alk. (mmol/L)	Sal. (g/kg)	Cl ⁻ (mmol/L)	SO ₄ ²⁻ (mmol/L)	Ca ²⁺ (mmol/L)	Mg ²⁺ (mmol/L)	K ⁺ (mmol/L)	SiO ₂ (μmol/L)	PO ₄ ³⁻ (mmol/L)
113-689B-											
1H-2, 135-142	2.85			35.7	554.3	29.49	11.39	53.71	12.3	994	5.8
1H-3, 78-85	3.78			36.0	551.9	29.19	11.54	53.72	12.0	1062	6.3
1H-3, 145-150	4.45	7.82	2.91	35.9	547.5	29.49	11.58	52.79	11.6	815	5.8
2H-2, 66-70	7.46			35.0	551.3	28.90	11.35	53.81	11.4	1196	11.0
3H-4, 120-15	20.50	7.65	3.19	35.0	556.7	28.02	11.92	52.78	11.1	819	5.5
6H-4, 120-125	49.00	7.66	3.15	35.3	560.1	28.30	12.67	51.71	12.5	796	2.8
9H-4, 120-125	77.80	7.31	2.90	35.3	559.1	26.68	13.49	50.97	11.4	808	2.1
12H-4, 115-125	106.65	7.66	3.10	35.7	558.2	26.68	14.77	49.56	10.2	787	2.1
15H-4, 115-125	135.55	7.78	3.06	35.5	581.0	28.02	16.11	50.35	10.5	774	2.3
18H-4, 115-125	164.45	7.81	3.10	35.0	558.0	25.66	16.58	48.11	10.7	608	1.7
22X-4, 115-125	203.15	7.48	2.43	37.7	559.1	25.95	17.97	47.21	9.9	606	1.6
25X-4, 115-125	232.25	7.54	2.35	35.7	558.2	26.84	18.67	46.67	10.2	580	1.4
28X-3, 115-125	259.75	7.57	2.06	35.7	560.9	26.25	20.86	45.33	9.0	570	1.5

A comparison of calculated and measured pH is given in Figure 31C. The generally good agreement indicates that degassing may have affected the measured pH in only three samples.

Alkalinity, Sulfate, and Phosphate

Sulfate data are shown in Figure 31D. The concentration of sulfate decreases from seawater values (29.5 mmol/L) at the surface to about 26 mmol/L at 260 mbsf. The sulfate profile may be fitted with an exponential model, indicating that very little sulfate reduction takes place at depth. This is consistent with the very low concentration of organic matter and its refractive nature (as seen from its pyrolytic behavior; see "Organic Geochemistry" section, this chapter). Comparatively low rates of deposition and inferred high oxygen levels in the bottom water allowed most of the organic matter to be oxidized before burial.

The alkalinity profile also reflects the low bacterial activity. Only slightly elevated levels (as compared to seawater) are observed (Fig. 31E). In fact, below 180 mbsf alkalinity decreases slightly. The pH calculations suggest that alkalinity is removed by precipitation of calcium as authigenic calcite. Calcite overgrowths on nanofossils were observed below the upper Oligocene.

The distribution of orthophosphate (Fig. 31F) confirms the interpretation of the sulfate and alkalinity profiles. The concentration of orthophosphate decreases exponentially from about 6 mmol/L at the surface to 2 mmol/L at depth. The primary source for dissolved phosphate is organic matter.

Calcium and Magnesium

Calcium and magnesium data are presented in Figures 31G and 31H, respectively. The concentration of calcium increases linearly from seawater levels at the top of the hole. In contrast the content of dissolved magnesium decreases linearly from seawater concentration in the upper sections. Sayles and Manheim (1975) interpreted similar profiles as resulting from dolomitization. Dolomitization of calcium carbonate would give rise to this distribution of the alkaline earths, but, even if the slope of Ca vs. Mg is close to -1 (-0.9, $r = -0.88$, $n = 13$) the interstitial water is undersaturated with respect to dolomite. The linear profiles are typical diffusion features and indicate the presence of a reaction zone below where calcium is produced and magnesium consumed. Similar alkaline earth profiles have been described from DSDP Legs 8 and 15 (Lawrence et al., 1975), and in a number of holes drilled later by DSDP and ODP. Usually, however, the profiles are not linear through the entire sequence. At Site 689, the bacterially-mediated reactions are so suppressed by the lack of organic matter that they do not obscure the picture created by the inorganic reactions, making mass balance calculations comparatively reliable. Probably the reactions taking place at the sediment/crust boundary resemble a

kind of reversed weathering of altered volcanics as suggested by Wollast (1974) and Perry et al. (1975). The generally decreasing levels of dissolved silica (Fig. 31I) in the lower part of the hole may be significant in this connection. At Site 690 (also on Maud Rise), strongly altered basalt (see "Site 690" chapter, this volume) was cored. At both sites volcanic glass, clay minerals, and zeolites were abundant in the deeper sections.

Potassium

The concentration of potassium decreases from 12.3 mmol/L in the uppermost section to 9.0 mmol/L at the bottom of the hole (Fig. 31J). Repeated analysis revealed that the potassium high at 49 mbsf is not an analytical error. The possibility that the sample may have been contaminated cannot be ruled out, but there are not many sources for potassium contamination. The decreasing concentration of potassium with increasing depth may be related to reactions between oceanic crust and seawater (see above).

Dissolved Silica

In the first core in Hole 689A a chert layer was observed. It was decided to sample closely for pore water extraction if the same layer should turn up in Hole 689B. In Hole 689B a similar layer was observed at 2.55 mbsf. Samples for dissolved silica analysis were taken to study the mechanisms of formation. Fragmented chert layers were observed in the upper section of several deeper cores, and these were suspected to have fallen down the hole from the water/sediment interface.

On the larger chert fragments one of the flat sides usually showed botryoidal structures as if having been exposed to water. The silica data (Fig. 31I) indicate that the downcore transport of chert to 2.55 mbsf has seriously disturbed this section, making any interpretation of the mechanism impossible. It is significant that on the scale of resolution offered by these data, the concentration of silica decreases from top to bottom, thus any diffusive transport would be downward. Probably the upper section contains a subsurface maximum not observed here.

All samples are supersaturated with respect to quartz and undersaturated with respect to amorphous silica. The abrupt shift in concentration at about 150 mbsf coincides with the disappearance of diatoms in the upper Eocene.

ORGANIC GEOCHEMISTRY

Headspace Analyses for Low-Molecular-Weight Hydrocarbons

Following ODP practice, 13 samples, principally of the uppermost 50 m of the section, were analyzed by a headspace method (Table 10). Extremely low levels of methane, less than

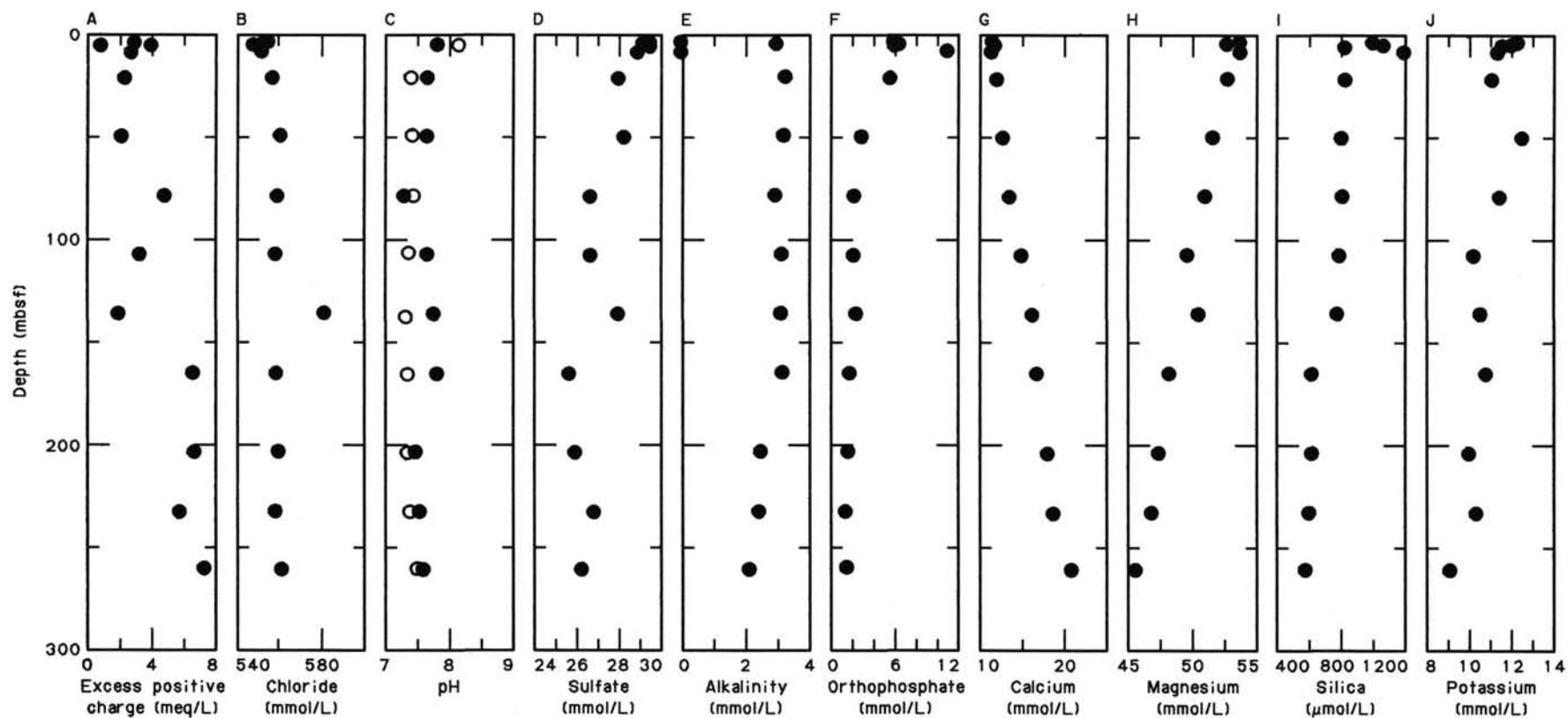


Figure 31. Concentrations vs. depth for Hole 698B. A. Charge imbalance. B. Chloride. C. pH; circles = calculated values; dots = measured values. D. Sulfate. E. Alkalinity. F. Orthophosphate. G. Calcium. H. Magnesium. I. Dissolved silica. J. Potassium.

Table 10. Low-molecular-weight hydrocarbon determinations by headspace analysis, Hole 689B.

Core, section interval (cm)	Depth (mbsf)	Methane ^a (μL/L)	Ethane (μL/L)	Propane (μL/L)	Ratio methane/ethane	Age
113-689B-						
1H-3, 145-150	4.5	7.1	0.04	0.34	178	Pliocene
2H-4, 145-150	11.3	—	0.49	—	—	Pliocene
3H-4, 120-125	20.6	7.1	—	0.19	—	Pliocene
4H-4, 146-150	30.3	0.0	4.9	1.0	—	late Miocene
5H-4, 145-150	39.8	3.4	3.0	6.4	1.1	middle/lower Miocene
6H-4, 117-120	48.0	1.9	3.6	13.5	0.5	middle Miocene
9H-4, 111-120	77.8	20.4	—	—	—	Oligocene
12H-4, 117-120	106.7	18.3	—	—	—	Oligocene
15H-4, 112-115	135.6	11.5	2.1	—	5.5	Eocene
18H-4, 112-115	164.5	9.5	—	—	—	Eocene
22X-4, 112-115	203.2	9.6	—	—	—	Paleocene
25X-4, 112-115	232.3	11.9	4.0	0.03	2.7	Paleocene
28X-3, 112-115	259.8	2.5	3.2	0.06	0.8	Maestrichtian

^a Corrected for 2.9 ppm methane in laboratory air.

20.4 μL/L of sediment in all instances, were encountered, accompanied by trace levels of ethane and propane.

Cylindrical samples 1.2 cm in diameter, of 7.6–10 mL volume, were collected as the core was divided into 1.5-m sections, immediately sealed in 22-mL vials, and heated to 70°C for a period of 1 hr, minimally. A headspace sample of 0.25 mL was injected into the Hewlett Packard 5890 gas chromatograph and analyzed by the associated Natural Gas Analyser. Evaluation of this apparatus revealed that it possesses a “memory” for C₆₊ material from standards which it releases at the trace levels of the samples, or alternatively, C₆₊ material is present in the atmosphere. The latter is occasionally the case, as petroleum-based solvents are used in the laboratory area. The instrument also shows a surprising variation in response to standard quantities of methane, as appraised by the HP 3392A integrator. This integrator, in the experience of the writer, is unsuited to the quantitation of trace levels of material. Quantitation was carried out using the HP 1000 laboratory automation system.

Values of the ratio methane/ethane in the samples were frequently infinite due to the absence of detectable ethane. Below the first sample at 4.5 mbsf where the ratio value was 178, ratio values averaged 2.1. Although ODP advises substantial caution in further coring if the ratio is lower than 1000, this limit must be interpreted with due regard to the volumes of gas recovered. The trace levels at Hole 689B are not accompanied by butane or heavier compounds suggestive of petroleum. Furthermore, the highly oxidized nature of the sediments, indicated by their white to tan color, low total organic carbon (TOC), and the refractory nature of the kerogen, as shown below, fails to indicate significant activity of methanogenic bacteria. Such bacterial activity is responsible for the larger fraction of shallow methane occurrences elsewhere. In the circumstances, low methane/ethane ratios found at Hole 689B are not suggestive of any hazard.

The hypothesis that methanogenic bacteria were relatively inactive during sedimentation at this site can be further evaluated in the light of the interstitial water analyses. Methanogens are obligate anaerobes which are inhibited by sulfate ion. Sulfate levels show a slight exponential decrease from seawater concentration, 29.5 mmol/L, near the sediment surface to 26 mmol/L at 260 mbsf (see “Inorganic Geochemistry” section, this chapter). Therefore, levels of sulfate have nowhere been significantly lowered by sulfate-reducing bacteria, and the generation of methane has been substantially precluded.

Rock-Eval Analyses

The samples employed for headspace analysis were also analyzed by Rock-Eval II, which provides TOC data in addition to kerogen evaluation (Table 11). Total carbon was also determined by coulometric means because the Rock-Eval TOC values appeared to be anomalously low on the basis of analyses of standards.

S₂, the yield of pyrolytic hydrocarbons, was below the detection limit in 7 of 13 cases. In 5 of the remaining cases T_{max} was extremely high (>499°C). Both observations are indicative of the presence of inert kerogen of a high maturity level, probably recycled. Substantial S₃ values indicate a highly oxidized state.

The formation of pelagic oozes is potentially accompanied by the preservation of the lipids of the contributing organisms as Type II kerogen, if aerobic bacterial activity is sufficiently inhibited. At this site, however, conditions have been consistently oxic, promoting the activity of aerobes. For the Neogene and Oligocene sections at least, this is in keeping with the expectable high level of oxygenation of the water column at high southerly latitudes.

Organic-Rich Layers

Core 113-689B-3H (Pliocene), comprising diatomaceous ooze, was distinguished by the occurrence of scattered diffuse layers of black particulate, possibly coaly material. Material from Sample 113-689B-3H-6, 103–104 cm, was used for Rock-Eval analysis. However, Type III kerogen was not indicated by the analysis probably because of the low level of organic carbon.

DOWNHOLE MEASUREMENTS

Downhole Temperature Measurement

Two temperature measurements, in Cores 113-689D-3H and 113-689D-6H, with the APC tool at Site 689, used the Von Herzen temperature recording device #5. Reliable data, however, were taken only from Core 113-689D-3H. Data from Core 113-689D-6H could not be recovered due to a mechanical pin connection problem, and we can show only one temperature datum at 47.0 mbsf, Core 113-689D-3H. Figure 32 shows the temperature record obtained with the APC tool for Core 113-689D-3H. The temperature reached 8.695°C just after the penetration due

Table 11. Rock-Eval analyses of sediments, Site 689.^a

Core, section	Depth (mbsf)	S1 mg(HC)/g(rock)	S2 mg(HC)/g(rock)	S3 mg(CO ₂)/g(rock)	TOC (%)	%C ^b	HI mg(HC)/g(C)	OI mg(HC)/g(C)	T _{max} (°C)	PI	S2/S3
1H-3	4.5	0.26	^c 1.12	0.11	0.11	0.06	^c 1010	100	499	0.19	10.18
2H-4	11.3	0.23	^c 1.05	0.01	0.10	0.09	^c 1050	10	561	0.18	105.0
^d 3H-3		0.10	0.64	0.10	0.06		^c 1066	166	568	0.22	6.40
3H-4	20.6	0.15	^c 1.43	0.42	0.13	0.06	^c 1100	323	579	0.09	3.40
^e 3H-6		0.20	1.18	0.03	0.11		^c 1072	27	550	0.14	39.33
4H-4	30.3	0.12	^c 0.51	0.13	0.05	0.05	^c 1020	260	558	0.19	3.92
5H-4	39.8	0.02	0.00	1.23	0.00	0.06	0	0	—	1.00	0.0
6H-4	48.0	0.15	^c 0.96	0.29	0.09	0.03	^c 1066	322	587	0.14	3.31
9H-4	77.8	0.03	0.00	1.33	0.00	—	0	0	—	1.00	0.0
12H-4	106.7	0.01	0.00	1.45	0.00	—	0	0	—	—	0.0
15H-4	135.6	0.02	0.00	1.35	0.00	—	0	0	—	—	0.0
18H-4	164.5	0.02	0.00	1.12	0.00	—	0	0	—	—	0.0
22H-4	203.2	0.02	0.00	0.66	0.00	—	0	0	—	—	0.0
25H-4	232.3	0.04	0.00	0.80	0.00	—	0	0	—	—	0.0
28H-3	259.8	0.01	0.01	0.78	0.00	0.62	0	0	259	—	0.1

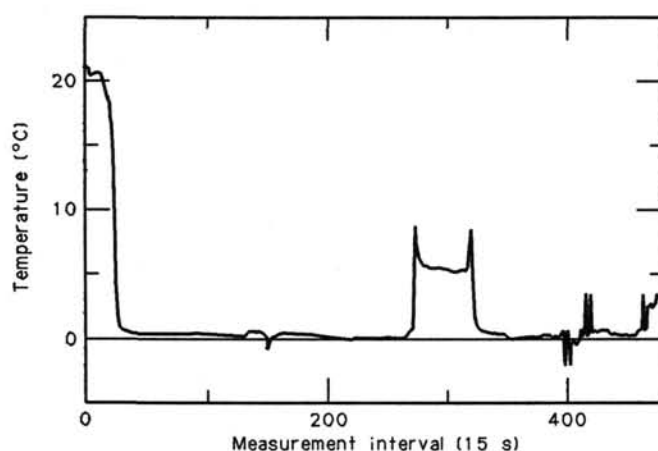
^a Hole 113-689B unless otherwise indicated.^b Coulometric data, total carbon minus carbonate carbon.^c Chart exhibits rising baseline without peaks. Others linear, no peaks.^d Hole 113-689C.^e Hole 113-689D.

Figure 32. Temperature measurement of Core 113-689D-3H with Von Herzen APC tool #5.

to the effect of frictional heat production, and was 5.233°C just before pulling out. The temperature gradually approximated the true formation temperature.

The temperature data obtained by the APC tool can be extrapolated to equilibrium following Horai and Von Herzen (1985). The *JOIDES Resolution* has two computer programs for extrapolation of the APC tool temperature records to equilibrium. Program "DECAY3" produces a theoretical decay curve of the temperature rise by frictional heating due to penetration. Program "FITTING3" calculates the equilibrium temperature by fitting the temperature data to the theoretical decay curve. These two programs were revised during Leg 112. There seem to be problems in "DECAY3"; the theoretical decay curves computed for the first several minutes after penetration are very different from those tabulated by Horai (unpublished paper). There might be an error in the integration of the Bessel function, but it is possible that the table of Horai is wrong. "FITTING3" works properly. We used both programs to evaluate the temperature data the first 2 min after penetration. The equilibrium temperature is estimated to be 4.5°C at 47.0 mbsf.

SUMMARY AND CONCLUSIONS

Site 689 lies near the crest of Maud Rise at 64°31.009'S, 3°5.996'E and 3°6.026'E at a water depth of 2080 m. Maud Rise is an ovoid aseismic ridge, elongated along 30°–210°, standing 2000 m above its surroundings, 700 km north of and topographically isolated from East Antarctica. Thus Site 689 is isolated from influences of terrigenous sediment transport from the East Antarctic continent except for wind-blown and ice-raftered components. This site was selected to obtain a high-quality (APC-XCB), continuously-cored biogenic sequence through the uppermost Mesozoic and Cenozoic below the present-day Antarctic water mass. It is the shallowest of two sites on Maud Rise which form part of a depth transect for studies of the vertical water-mass structure during the late Phanerozoic around the Antarctic. The seismic profile exhibits a relatively simple, thin (0.4 s TWT) sequence of draped and mounded, mainly weakly reflective sediments inferred to be pelagic oozes, above a distinct reflector considered to represent basaltic basement.

Four holes were drilled at Site 689: Hole 689A consists of a single APC core from 2.3 to 11.8 mbsf, providing 98% recovery; Hole 689B consists of 21 APC cores from 0 to 197.5 mbsf and 12 XCB cores from 197.5 to 297.3 mbsf, providing 77% recovery; Hole 689C consists of 3 APC cores from 0 to 27.6 mbsf with 76% recovery, and Hole 689D consists of 12 APC cores from 18.1 to 133.8 mbsf with 100% recovery. The quality of the cores is generally excellent with marked disturbance only in the uppermost cores of each hole. Hole 689B was abandoned at an estimated 25–45 m above basement, when progress in drilling cherty layers became too slow.

The sedimentary sequence is exclusively pelagic, biogenic in origin, and ranges from upper Campanian(?) / lower Maestrichtian (~75 Ma) to Quaternary. The APC part of the section extends from the lower middle Eocene (~49 Ma) to the Quaternary. The preliminary biostratigraphy and magnetostratigraphy indicate the presence of sedimentary hiatuses or highly condensed sequences throughout the section. These occur across the upper to lower Paleocene boundary (missing nannofossil Zones CP4–CP6, about 2 m.y.), the Paleocene-Eocene boundary (missing nannofossil Zones CP9–CP11, about 5 m.y.), the Eocene to Oligocene boundary? (missing nannofossil Zone CP15b, about 1.1 m.y.), Oligocene/Miocene boundary, possibly within the up-

per Miocene, and upper Pliocene to Quaternary. The seismic stratigraphy shows reflectors pinching out and truncating, which suggest that the most prominent effects of bottom-current activity on sediments away from the site were produced in the early to middle Miocene and late Oligocene. A paleomagnetic polarity stratigraphy has been identified for the upper Neogene, with excellent prospects for all Cenozoic sediments recovered. Site 689 provides a fine biostratigraphic sequence that, in conjunction with Site 690, will form the southernmost anchor for Atlantic biostratigraphy, biogeography, and isotopic stratigraphy. This is the first sequence to be cored in the Antarctic that provides an uppermost Mesozoic and Cenozoic calcareous nannofossil and planktonic foraminiferal biostratigraphy. Site 689 also contains a high-quality Neogene record of siliceous microfossils. The upper Maestrichtian and lower Paleocene in Site 689 represent the first such recovery in the Southern Ocean. Except for the topmost part of the Site 689 sequence, there is a marked lack of sediment mixing and microfossil mixing by bottom currents. This is unusual for the Southern Ocean, where diatoms and other microfossils are often reworked and mixed by active bottom currents. Mixed assemblages of siliceous and calcareous microfossils from the upper Eocene through the Neogene have allowed the first biostratigraphic calibration to be carried out between these groups in the Antarctic region. It has also been possible for the first time to calibrate chronologically the early Neogene biosiliceous record using magnetostratigraphy. The sedimentation across the K/T boundary was probably continuous at Site 689; the boundary is associated with a 40-cm interval of vitric ash and clay of apparent volcanic origin. The K/T boundary appears to lie between the predominantly white chalk and greenish volcanic sediments, occurring between 84 and 85 cm in Section 113-689B-25X-5.

At Site 689 we sampled 297 m of almost pure siliceous and calcareous oozes to chalk, with chert layers at the top and bottom of the sequence (Fig. 5). The upper part of the sequence (upper Miocene to Quaternary) consists entirely of biosiliceous oozes, above a middle part (upper Eocene through upper Miocene) of interbedded siliceous and calcareous oozes, in turn overlying a lower interval (Upper Cretaceous through upper Eocene) of calcareous ooze and chalk without biosiliceous sediments. The siliceous intervals are dominated by diatoms, although radiolarians and silicoflagellates are important elements at a number of levels. The carbonate sediments are dominated by calcareous nannofossils, with planktonic foraminifers abundant in the lower part of the sequence (Upper Cretaceous through upper Eocene).

The sediment becomes more indurated with depth; calcareous sediments above 190 mbsf (middle Eocene) consist of ooze. Sediments between 190 and 236 mbsf (middle Eocene to uppermost Cretaceous) consist of semilithified ooze to chalk, with increasing chalk toward the base. Chalk without ooze occurs below the K/T boundary, at 233 mbsf.

The sequence contains only traces of nonbiogenic components; a few volcanic ash-bearing layers (4–35 cm thick) occur in the Paleocene. Ice-rafted dropstones are very rare throughout the Neogene and occur in only one upper Oligocene core (113-689B-10H). The organic content is very low. Sediments are light-colored and lack pyrite or other evidence of sediment reduction. All data suggest deposition in a highly oxidizing environment, probably resulting from the high level of oxygenation of waters expected at high latitudes, and the moderate to low rates of sedimentation.

The sequence at Site 689 has been divided into three units (Fig. 5) based upon compositional differences (Fig. 6) and diagenetic maturity.

Unit I extends from the seafloor to 31 mbsf and is upper Miocene to Quaternary. The sediment is dominated by diatom ooze

with varying amounts of other biosiliceous components. A thin chert layer (<10 cm) is at the top of the sequence.

Unit II extends from about 31 m to 149.1 mbsf and consists of a mixture of biosiliceous and calcareous oozes ranging from upper Eocene to upper Miocene. The calcareous component is dominated by calcareous nannofossils; foraminifers are relatively unimportant. The upper part of Unit II (Subunit IIA), upper Oligocene to upper Miocene, consists of alternating biosiliceous and calcareous ooze. The lower part of Unit II (Subunit IIB) is dominated by calcareous nannofossil ooze and contains diatomaceous horizons. Foraminifers become an additional, but still minor, component.

Unit III extends from 149.1 mbsf to the bottom of the hole (297.3 mbsf) and consists of nannofossil ooze and chalk with varying amounts of foraminifers. Subunit IIIA, of latest Maestrichtian to upper Eocene, is a semilithified calcareous ooze to chalk sequence. Subunit IIIB, of uppermost Campanian(?) / lower Maestrichtian to upper Maestrichtian is entirely chalk, except for several thin chert layers.

The dominant microfossil components change through the sequence as follows: Upper Cretaceous to upper Eocene—calcareous nannofossils and planktonic foraminifers; Oligocene—calcareous nannofossils and diatoms; Miocene—diatoms and calcareous nannofossils; upper Miocene and Pliocene—diatoms and silicoflagellates.

Planktonic foraminifers are abundant from the Upper Cretaceous to the lower Oligocene, common in the Oligocene, and rare to common in the lower Miocene and Pliocene. They are well preserved throughout, except in one upper Eocene interval. Calcareous benthic foraminifers are moderately common through lithostratigraphic Unit IIA and all lower units. Calcareous nannofossils exhibit good to moderate preservation in the Miocene and Pliocene, where calcareous sediments are less important, while in all deeper levels preservation is of lower quality. Radiolarians are effectively absent below the late Oligocene except for short intervals in the upper Campanian? / lower Maestrichtian and the uppermost Eocene and lowermost Oligocene. From the upper Oligocene to the lower Miocene, they are poorly preserved and consist of dissolution-resistant forms. From the middle Miocene to the Pliocene they are abundant and well preserved. Diatoms occur only as rare trace fragments below the Neogene, having undergone diagenetic change in the carbonate sediments, except in the silica-rich uppermost Eocene-lowermost Oligocene. The group is well preserved in the upper Miocene and Pliocene where carbonate is absent.

Paleoenvironmental History of Site 689

Upper Cretaceous and Cenozoic sediments at Site 689, near the crest of Maud Rise, were laid down in a pelagic, open-ocean environment at lower to middle bathyal depths, sinking from 500–1000 m to the present depth of ~2000 m over the last 65 m.y., during which time the Rise has lain at the same distance (700 km) from Antarctica. Calcareous and siliceous oozes were deposited in a relatively uncomplicated environment at these shallow depths, and with virtually no terrigenous sedimentary influences other than very rare ice-rafted dropstones during the late Oligocene and Neogene, traces of fine eolian sediments, and volcanic ash and its alteration products in the earliest Cenozoic.

Sediments and microfossil diversity and assemblages clearly reflect a sequential cooling of the Antarctic water mass, inferred to be related to Antarctic glacial development. The siliceous biogenic facies progressively replaced the carbonate facies during the Cenozoic, with initial siliceous sedimentation in the late Eocene, a major increase in siliceous sedimentation beginning near the base of the Neogene, and exclusively siliceous sedimentation from the late Miocene. The rate of sediment accumulation was always low for biogenic sediments, compared with many other

oceanic areas, and apparently quite uniform over long intervals of time. During the Paleocene through Oligocene, sedimentation rates were about 4 m/m.y. For the Neogene, sedimentation rates between hiatuses are double (7–9 m/m.y.). Site 689, located just south of the Antarctic Divergence, has always lain well to the south of the high-productivity biogenic belt of the Polar Front. During the Cenozoic, this has been an oceanic backwater.

During the Late Cretaceous, and continuing through the late Eocene, nannofossil ooze rich in planktonic foraminifers was laid down. Siliceous biogenic productivity is inferred to have been low during this interval, and post-Campanian siliceous material has since been diagenetically altered to zeolite or chert. Benthic foraminiferal assemblages suggest deposition in upper lower bathyal to middle bathyal depths during the Late Cretaceous to Paleocene, somewhat shallower than in the younger intervals. Diversities in the calcareous nannofossils and planktonic foraminiferal assemblages are low compared with low-latitude areas, but nevertheless high enough to imply temperate climatic conditions.

The terminal Cretaceous event is marked here, as elsewhere, by the sudden extinction of almost all species of planktonic foraminifers and calcareous nannofossils, leaving residual, extremely low diversity assemblages in the earliest Paleocene. The biotic crisis apparently coincided with the beginning of an episode of volcanic activity that laid down about 40 cm of volcanogenic sediments at Site 689 in the earliest Cenozoic. Planktonic foraminifers associated with these sediments are small, morphologically simple, and of very low diversity. The benthonic foraminiferal assemblages exhibit some change but no major extinctions over the K/T boundary interval.

During the earliest Paleocene, the diversity of the planktonic assemblages increased as a result of evolution. A hiatus of about 2 m.y. interrupted the record during the middle part of the Paleocene. Surface waters during the Paleocene seem to have been relatively warm (temperate to transitional) based on high planktonic diversities and the presence of discoasters. The similarity of calcareous microfossil assemblages at Maud Rise and at the Falkland Plateau suggests minimal surface-water environmental gradients. Farther north on the Rio Grande Rise, different, warmer assemblages flourished. For instance, the morozovellids (planktonic foraminifers) were absent at Site 689 during the late Paleocene, yet were important elements at lower latitudes. A hiatus of about 5 m.y. interrupted the record during the late Paleocene and early Eocene. A considerable change in the benthic foraminiferal assemblages just below this hiatus (in planktonic foraminiferal Zone P6) reflects widespread faunal change at the end of the Paleocene (Tjalsma and Lohmann, 1983).

Water depths at Site 689 approached those of the present day (lower bathyal; 2000 m) by the early Eocene. During the Eocene, deposition of calcareous nannofossil ooze continued. By the middle Eocene, surface waters had cooled over Maud Rise. Sediments accumulating were essentially devoid of discoasters or appreciable numbers of sphecoliths, both warmth-loving groups. In contrast with the Paleocene, a biogeographic discontinuity and inferred surface-water temperature gradient had developed between Maud Rise and the Falkland Plateau. Eocene calcareous nannofossil assemblages on the Falkland Plateau contain both discoasters and sphecoliths (Wise et al., 1985), and hence are more diverse than on Maud Rise. Nevertheless, the diversity of the Eocene calcareous planktonic assemblages on Maud Rise remained high enough to suggest temperate conditions. Radiolarian assemblages were generally similar to those of lower latitudes.

Further changes in water masses occurred near the end of the Eocene, as reflected by the first appearance of diatomaceous sediments in the sequence, and changes in benthic foraminiferal

assemblages, notably a decrease in diversity and a loss of buliminid species. Calcareous nannofossils remained dominant, while planktonic foraminifers were reduced in importance. A distinct interval of carbonate dissolution occurred in close association with the hiatus across the Eocene/Oligocene boundary. The theory that surface waters cooled near the beginning of the Oligocene is supported by a decrease in the diversity of planktonic foraminifers and calcareous nannofossils. Decrease in diversity of benthic foraminifers indicates cooling of deep waters, and a decrease in buliminid species suggests concomitant better oxygenation. At this time, the discoasters essentially disappeared from the Falkland Plateau sequence (Wise et al., 1985) reflecting an expansion of cool waters to the north. Planktonic foraminiferal assemblages during the Oligocene appear to have a subpolar rather than a polar aspect. The middle Oligocene is marked by a further decrease in planktonic foraminiferal diversity, such as has been recognized in the Subantarctic South Pacific (DSDP Site 277). By the late Oligocene, a noticeable increase had occurred in the dissolution of benthic and planktonic foraminifers, as intermediate waters became more corrosive.

The first dominantly siliceous sediments were deposited in the latest Oligocene, reflecting a further major development of the Antarctic water mass. Diatom and calcareous nannofossil oozes were deposited alternately until the middle late Miocene, in a transitional interval between the dominantly calcareous Paleogene and the dominantly siliceous interval leading up to the present day. The development of the biosiliceous facies near the beginning of the Neogene coincided with the appearance of polar calcareous planktonic assemblages. Planktonic foraminiferal assemblages became monospecific, and there was a drastic reduction in calcareous nannofossil diversity (from about six to two species) and benthic foraminiferal diversity. Faunal and floral diversities also became similar between Maud Rise and the Falkland Plateau. The Neogene radiolarian fauna became endemic to the Antarctic.

Beginning in the middle late Miocene, only biosiliceous sediments were deposited on Maud Rise. These were dominated by diatom oozes, but included silicoflagellate oozes at times. The latest Miocene may have been a time of increased bottom water activity, creating a hiatus.

The early and middle Pliocene is well represented by biosiliceous oozes, but much of the late Pliocene and Quaternary is represented by yet another hiatus, of 3 m.y. duration. Two thin layers of chert were formed at the top of the siliceous section, probably beneath a thin calcareous ooze which is widespread on Maud Rise (R. Gersonde, pers. comm., 1987), but was not sampled at Site 689. The genesis of this unusually young chert requires study, but may be related to the presence of the overlying calcareous ooze.

REFERENCES

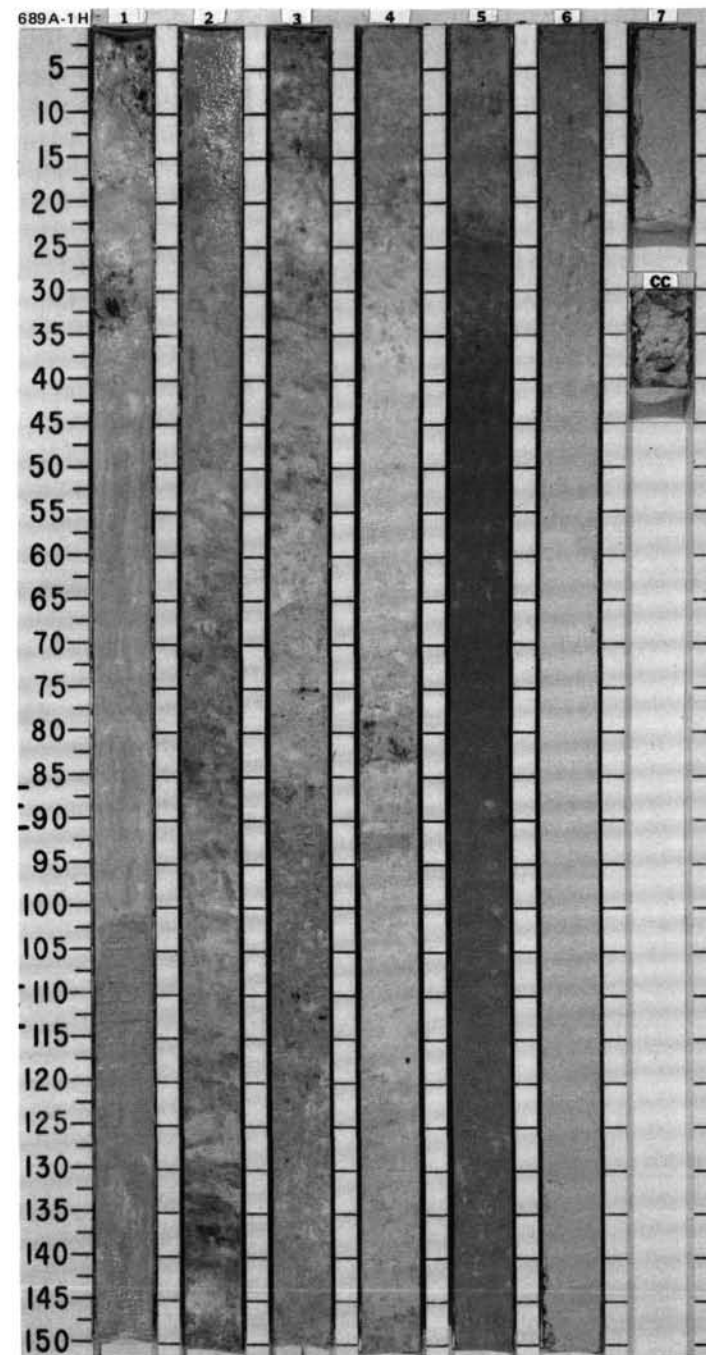
- Anderson, J. B., 1975. Ecology and distribution of foraminifera in the Weddell Sea of Antarctica. *Micropaleontology*, 21:69–9.
- Andrews, B. A., 1984. Petrology of Weddell Sea glacial sediments: Implications for provenance and glacial history. *Antarctic J. U.S.*, 18: 94–94.
- Barker, P. F., Dalziel, I.W.D., et al., 1977. *Init. Repts. DSDP*, 36: Washington (U.S. Govt. Printing Office).
- Barker, P. F., Carlson, R. L., Johnson, D. A., et al., 1983. *Init. Repts. DSDP*, 72: Washington (U.S. Govt. Printing Office).
- Barron, J. A., 1985. Miocene to Holocene planktonic diatoms. In Bolli, H. M., Saunders, J. B., and Perch-Nielsen, K. (Eds.), *Plankton Stratigraphy*: Cambridge (Cambridge Univ. Press), 763–809.
- Berggren, W. A., Kent, D. V., Flynn, J. J., and Van Couvering, J. A., 1985. Cenozoic geochronology. *Geol. Soc. Am. Bull.*, 96:1407–1418.
- Boersma, A., and Premoli-Silva, I., 1983. Paleocene planktonic foraminiferal biogeography and the paleoceanography of the Atlantic Ocean. *Micropaleontology*, 29:355–381.

- Boyce, R. E., 1976. Definitions and laboratory techniques of compressional sound velocity parameters and water content, wet-bulk density, and porosity parameters by gravimetric and gamma ray attenuation techniques. In Schlanger, S. O., Jackson, E. D., et al., *Init. Repts. DSDP*, 33: Washington (U.S. Govt. Printing Office), 931-935.
- Bremer, M. L., and Lohmann, G. P., 1982. Evidence for primary control of the distribution of certain Atlantic Ocean benthonic foraminifera by degree of carbonate saturation. *Deep-Sea Res.*, 19:987-988.
- Bukry, D., 1975. Silicoflagellate and coccolith stratigraphy, Deep Sea Drilling Project, Leg 29. In Kennett, J. P., Houtz, R. E., et al., *Init. Repts. DSDP*, 29: Washington (U.S. Govt. Printing Office), 845-872.
- Carter, D.J.T., 1980. *Echo-sounding correction tables (NP139)*. Taunton, U.K. (Br. Ministry Defense, Hydrogr. Dept.).
- Chamley, H., 1965. Observations sur quelques sédiments marins prélevés près des côtes de Terre Adélie (Antarctique). *Rec. Trav. St. Mar. d'Endoume*, 36:215-228.
- , 1979. North Atlantic clay sedimentation and paleoenvironment since the Late Jurassic. In Talwani, M., Hay, W., and Ryan, W.B.F., (Eds), *Deep Drilling Results in the Atlantic Ocean: Continental Margins and Paleoenvironment*: Washington, D.C. (Am. Geophys. Union), 342-360.
- Chen, P. H., 1975. Antarctic radiolaria. In Hayes, D. E., Frakes, L. A., et al., *Init. Repts. DSDP*, 28: Washington (U.S. Govt. Printing Office), 407-474.
- Corliss, B. H., 1981. Deep-sea benthonic foraminiferal faunal turnover near the Eocene/Oligocene boundary. *Mar. Micropaleontol.*, 6:374-384.
- Dailey, D. H., 1983. Late Cretaceous and Paleocene benthic foraminifera from Deep Sea Drilling Project Site 516, Rio Grande Rise, western South Atlantic Ocean. In Barker, P. F., Carlson, R. L., and Johnson, D. A., et al., *Init. Repts. DSDP*, 72: Washington (U.S. Govt. Printing Office), 757-782.
- Dalziel, I.W.D. and Elliot, D. H., 1973. The Scotia Arc and Antarctic Margin. In Nairn, A.E.M., and Stehli, F. G. (Eds.), *The Ocean Basins and Margins: The South Atlantic* (Vol. 1): New York (Plenum Press).
- Deacon, G.E.R., 1937. The hydrology of the Southern Ocean. *Discovery Repts.*, 15:1-124.
- De Felice, D. R., and Wise, S. W., 1981. Surface lithofacies, biofacies and diatom diversity patterns as models for delineation of climatic change in the Southeast Atlantic Ocean. *Mar. Micropaleontol.*, 6: 29-70.
- Douglas, R. G., and Woodruff, F., 1981. Deep-sea benthic foraminifera. In C. Emiliani, (Ed.), *The Sea* (Vol. 7): New York (Wiley-Interscience), 1233-1327.
- Edwards, A. R., 1971. Calcareous nannoplankton zonation of the New Zealand Paleogene. In Farinacci, A. (Ed.), *Proc. 2nd Planktonic Conf.*: Rome (Ed. Tecnoscienza), 381-519.
- Fenner, J., 1984. Eocene-Oligocene planktonic diatom biostratigraphy in high and low latitudes. *Micropaleontology*, 30:319-342.
- Gordon, A. L., Martinson, D. G., and Taylor, H. W., 1981. The wind-driven circulation in the Weddell-Enderby Basin. *Deep-Sea Res.*, 28A: 151-163.
- Grobe, H., 1986. Sedimentation processes on the Antarctic continental margin at Kapp Norvegia during the Late Pleistocene. *Geol. Rundsch.*, 75:97-104.
- Haq, B. U., 1980. Biogeographic history of Miocene calcareous nannoplankton and paleoceanography of the Atlantic Ocean. *Micropaleontol.*, 26:414-443.
- Haq, B. U., Lohmann, G. P., and Wise, S. W., 1977. Calcareous nannoplankton biogeography and its paleoclimatic implications: Cenozoic of the Falkland Plateau (DSDP Leg 36) and Miocene of the Atlantic Ocean. In Barker, P. F., Dalziel, I. W. D., et al., *Init. Repts. DSDP*, 36: Washington (U.S. Govt. Printing Office), 745-759.
- Hasle, R. G., 1972. *Fragilariopsis* Hustedt as a section of the genus *Nitzschia* Hassal. *Nova Hedwigia*, 39:111-119.
- Horai, K., and Von Herzen, R. P., 1985. Measurement of heat flow on Leg 86 of the Deep Sea Drilling Project. In Heath, G. R., Burckle, L. H., et al., *Init. Repts. DSDP*, 86: Washington (U.S. Govt. Printing Office), 759-777.
- Hsü, K. J., La Brecque, J. L., et al., 1984. *Init. Repts. DSDP*, 73: Washington (U.S. Govt. Printing Office).
- Jacobs, M. B., 1974. Clay mineral changes in Antarctic deep-sea sediments and Cenozoic climatic events. *J. Sediment. Petrol.*, 44:1079-1086.
- Jenkins, D. G., 1971. New Zealand Cenozoic planktonic foraminifera. *N.Z. Geol. Surv. Paleontol. Bull.*, 42.
- , 1975. Cenozoic planktonic foraminiferal biostratigraphy of the Southwestern Pacific and Tasman Sea, DSDP Leg 29. In Kennett, J. P., and Houtz, R. E., et al., *Init. Repts. DSDP*, 29: Washington (U.S. Govt. Printing Office), 449-467.
- Jenkins, D. G., and Srinivasan, M. S., 1985. Cenozoic planktonic foraminifera of the southwest Pacific. In Kennett, J. P., and von der Borch, C. C., et al., *Init. Repts. DSDP*, 90: Washington (U.S. Govt. Printing Office), 795-834.
- Krashennikov, V. A., and Basov, I. A., 1983. Cenozoic planktonic foraminifera of the Falkland Plateau and Argentine Basin, Deep Sea Drilling Project Leg 71. In Ludwig, W. J., Krashennikov, V. A., et al., *Init. Repts. DSDP*, 71: Washington (U.S. Govt. Printing Office), 821-858.
- Lawrence, J. R., Gieskes, J. M., and Broecker, W. S., 1975. Oxygen isotope and cation composition of DSDP pore water and the alteration of layer II basalts. *Earth Planet. Sci. Lett.*, 27:1-10.
- Martinson, D. G., Killworth, P. D. and Gordon, A. L., 1981. A convective model for the Weddell Polynya. *J. Phys. Oceanogr.*, 11:466-488.
- Michel, J. P., 1964. *Contribution à l'étude sédimentologique de l'Antarctique*: Paris (Com. Nat. Fr. Rech. Antarct.), 5.
- Miller, K. G., 1983. Eocene-Oligocene paleoceanography of the deep Bay of Biscay: benthic foraminiferal evidence. *Mar. Micropaleontol.*, 6:269-295.
- Officer, C. B., Hallam, A., Drake, C. L., and Devine, J. D., 1987. Late Cretaceous and paroxysmal Cretaceous/Tertiary extinctions. *Nature*, 326:143-149.
- Pedro, G., 1984. Distribution des principaux types d'altération chimique à la surface du globe. *Sci. Géol. Bull.*, 37:333-347.
- Perry, E. A., Jr., Gieskes, J. M., and Lawrence, J. R., 1975. Mg, Ca and O^{18}/O^{16} exchange in the sediment-pore water system, Hole 149, DSDP. *Geochim. Cosmochim. Acta.*, 10:413-423.
- Robert, C., 1982. Modalité de la sédimentation argileuse en relation avec l'histoire géologique de l'Atlantique Sud [Thesis]. Univ. Aix-Marseille.
- , 1987. Clay mineral associations and structural evolution of the South Atlantic: Jurassic to Eocene. *Palaeogeogr. Palaeoclimatol., Palaeoecol.*, 58:87-108.
- Robert, C. and Maillot, H., 1983. Paleoenvironmental significance of clay mineralogical and geochemical data, Southwest Atlantic, DSDP Legs 36 and 71. In Ludwig, W.J., Krashennikov, V., et al., *Init. Repts. DSDP*, 71:317-343.
- Robert, C., Caulet, J. P., and Maillot, H., in press. Evolution climatique et hydrologique en mer de Ross (Site DSDP 274) au Néogène, d'après les associations de Radiolaires, la minéralogie des argiles et la géochimie minérale. *C. R. Acad. Sci. Ser. 2*.
- Sanfilippo, A., and Riedel, W. R., 1973. Cenozoic radiolaria (exclusive of theopirids, artostrobilids and amphipyndacids) from the Gulf of Mexico, Deep Sea Drilling Project Leg 10. In Worzel, J. L., Bryant, W., et al., *Init. Repts. DSDP*, 11: Washington (U.S. Govt. Printing Office), 475-611.
- Sayles, F. L., 1980. The solubility of $CaCO_3$ in seawater at 2°C based upon *in situ* sampled pore water composition. *Mar. Chem.* 9:223-235.
- Sayles, F. L., and Manheim, F. T., 1975. Interstitial solutions and diagenesis in deeply buried marine sediments: results from the Deep Sea Drilling Project. *Geochim. Cosmochim. Acta.*, 39:103-128.
- Schrader, H. J., 1976. Cenozoic planktonic diatom biostratigraphy of the Southern Pacific Ocean. In Hollister, C. D., Craddock, C., et al., *Init. Repts. DSDP*, 35: Washington (U.S. Govt. Printing Office), 605-672.
- Shackleton, N. J., and Kennett, J. P., 1975. Paleotemperature history of the Cenozoic and the initiation of Antarctic glaciation: oxygen and carbon isotope analyses in DSDP Sites 277, 279, 281. In Kennett, J. P., Houtz, R. E., et al., *Init. Repts. DSDP*, 29: Washington (U.S. Govt. Printing Office), 743-755.
- Shaw, C. A., and Ciesielski, P. F., 1983. Silicoflagellate biostratigraphy of middle Eocene to Holocene subantarctic sediments recovered by Deep Sea Drilling Project Leg 71. In Ludwig, W. J., Krashennikov, V. A., et al., *Init. Repts. DSDP*, 71: Washington (U.S. Govt. Printing Office), 687-737.

- Sissingh, W., 1977. Biostratigraphy of Cretaceous calcareous nannoplankton. *Geol. Mijnbouw*, 56:37-65.
- Stumm, W., and Morgan, J. J., 1981. *Aquatic Chemistry*, (2nd ed.): New York (Wiley).
- Tectonic Map of the Scotia Arc, 1985. 1:3,000,000 BAS (Misc) 3, Cambridge, British Antarctic Survey.
- Thomas, E., 1985. Late Eocene to Recent deep-sea benthic foraminifers from the central equatorial Pacific Ocean. In Mayer, L., Theyer, F., Thomas, E., et al., *Init. Repts. DSDP*, 85: Washington (U.S. Govt. Printing Office), 655-694.
- , 1987. Oligocene to Recent deep-sea benthic foraminifers from the northeast Atlantic Ocean (DSDP Sites 608 and 610). In Ruddiman, W. F., Kidd, R. B., Thomas, E., et al., *Initial Reports DSDP*, 94: Washington (U.S. Govt. Printing Office), 997-1032.
- Tjalsma, R. C., and Lohmann, G. P., 1983. Paleocene-Eocene bathyal and abyssal benthic foraminifera from the Atlantic Ocean. *Microplaeontology, Spec. Publ.*, 4:1-90.
- Ugolini, F.C., and Jackson, M.L., 1982. Weathering and mineral synthesis in Antarctic soils. In Craddock, C. (Ed), *Antarc. Geosci., I.U.G.S., Series B*, 4:1101-1108.
- Von Herzen, R. P., and Maxwell, A. E., 1959. The measurements of thermal conductivity of deep-sea sediments by a needle probe method. *J. Geophys. Res.*, 1535-1541.
- Weaver, F. M., 1983. Cenozoic radiolarians from the southwest Atlantic, Falkland Plateau region, Deep Sea Drilling Project Leg 21. In Ludwig, W. J., Krasheninnikov, V. A., et al., *Init. Repts., DSDP*, 71: Washington (U.S. Govt. Printing Office), 667-686.
- Weaver, F. M., and Gombos, A. M., 1981. Southern high-latitude diatom biostratigraphy. *Soc. Econ. Paleontol. Mineral. Spec. Publ.*, 32: 445-470.
- Wind, F. H., 1979a. Late Campanian and Maestrichtian calcareous nannoplankton biogeography and high-latitude biostratigraphy [Dissert.]. Florida State Univ., Tallahassee.
- , 1979b. Maestrichtian-Campanian nannofloral provinces of southern Atlantic and Indian Oceans. In Talwani, M., Hay, W., and Ryan, W.B.F. (Eds.), *Deep Drilling Results in the Atlantic Ocean: Continental Margins and Paleoenvironment*. Am Geophys. Union, Maurice Ewing Ser., 3:1-57.
- Wind, F. H., and Wise, S. W., 1983. Correlation of Upper Campanian-Lower Maestrichtian calcareous nannofossil assemblages in drill and piston cores from the Falkland Plateau, Southwest Atlantic Ocean. In Ludwig, W. J., Krasheninnikov, V. A., et al., *Init. Repts. DSDP*, 71: Washington (U.S. Govt. Printing Office), 481-550.
- Wise, S. W., 1983. Mesozoic and Cenozoic calcareous nannofossils recovered by Deep Sea Drilling Project Leg 71 in the Falkland Plateau region, southwest Atlantic Ocean. In Ludwig, W. J., Krasheninnikov, V. A., et al., *Init. Repts. DSDP*, 71: Washington (U.S. Govt. Printing Office), 481-550.
- Wise, S. W., Gombos, A. M., and Muza, J. P., 1985. Cenozoic evolution of polar water masses, southwest Atlantic Ocean. In Hsü, K. J., Weissert, H. J., (Eds.), *South Atlantic Paleooceanography*: Cambridge (Cambridge Univ. Press), 283-324.
- Wise, S. W., and Wind, F. H., 1977. Mesozoic and Cenozoic calcareous nannofossils recovered by DSDP Leg 36 drilling on the Falkland Plateau, Southwest Atlantic sector of the Southern Ocean. In Barker, P. F., Dalziel, I.W.D., et al., *Init. Repts. DSDP*, 36: Washington (U.S. Govt. Printing Office), 269-492.
- Wollast, R., 1974. The silica problem. In Goldberg, E. D. (Ed.), *The Sea*: New York (Wiley), 359-353.

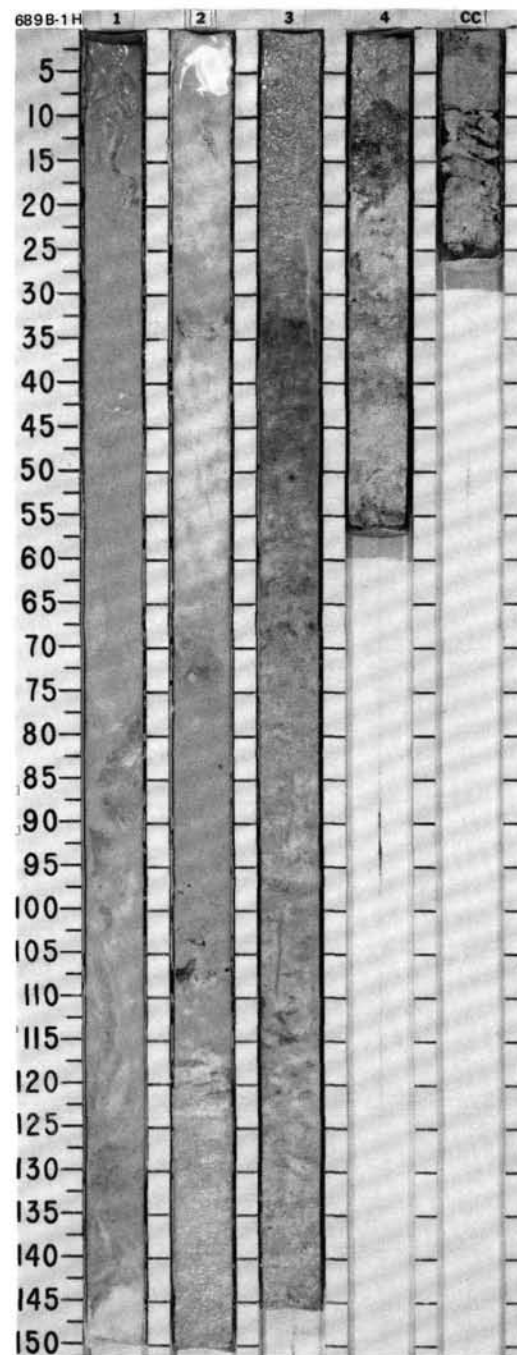
Ms 113A-106

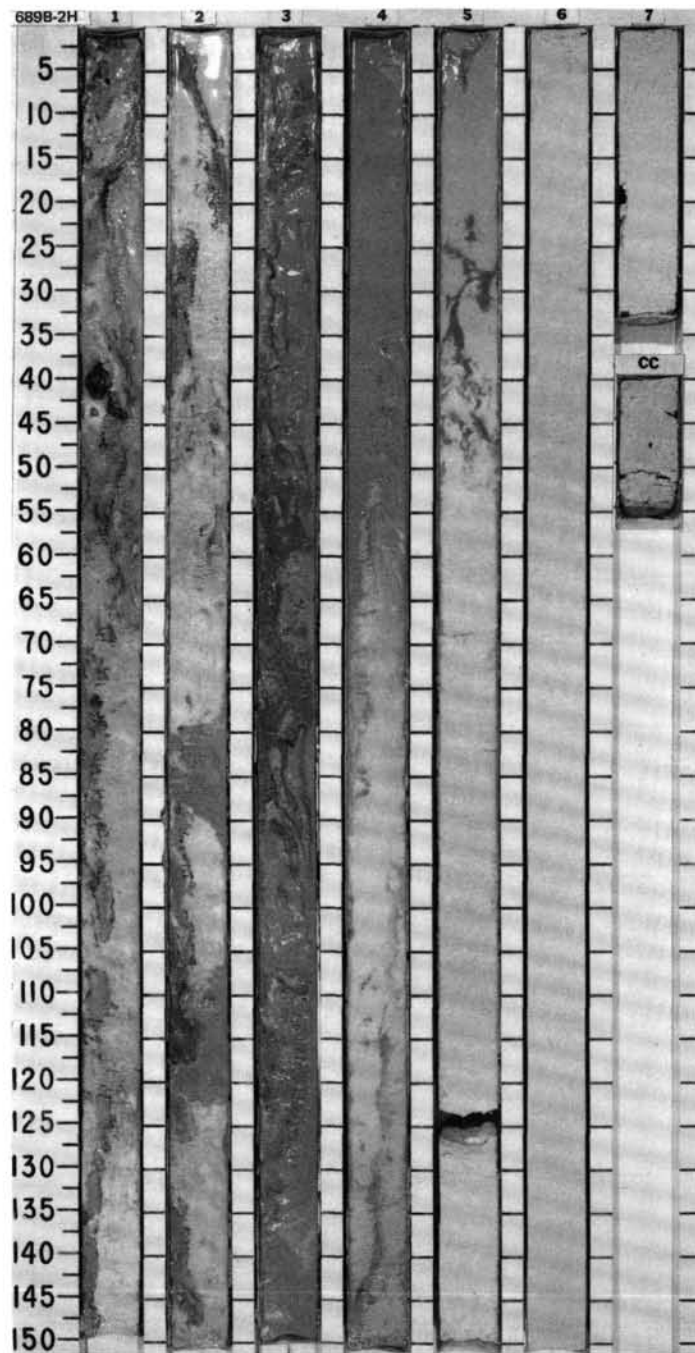
TIME-ROCK UNIT	BIOSTRAT. ZONE/ FOSSIL CHARACTER				CHEMISTRY	SECTION	METERS	GRAPHIC LITHOLOGY	DRILLING DISTURB.	SED. STRUCTURES	SAMPLES	LITHOLOGIC DESCRIPTION
	FORAMINIFERS	NANNOFOSSILS	RADIOLARIANS	DIATOMS								
PLIOCENE												
R.G												* *



SITE 689 HOLE B CORE 1H CORED INTERVAL 2080.2-2085.2 mbsl; 0-5.3 mbsf

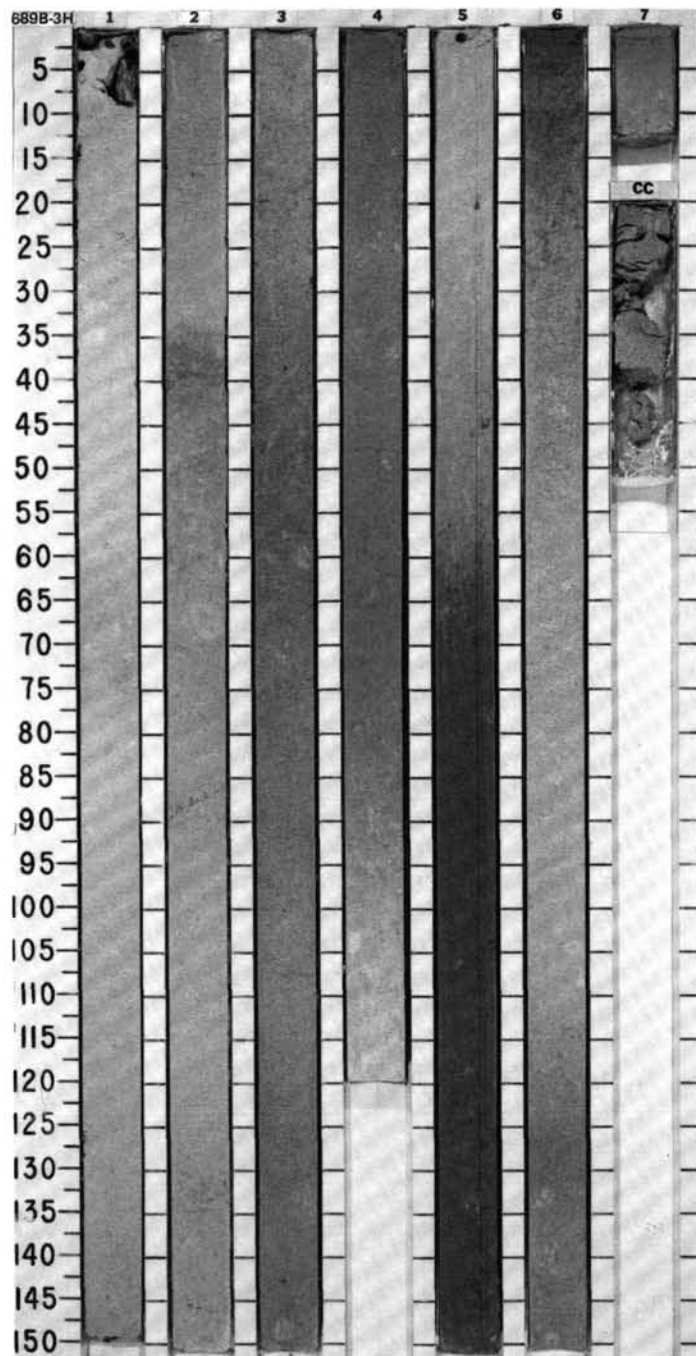
TIME-ROCK UNIT	BIOSTRAT. ZONE/ FOSSIL CHARACTER		SECTION	METERS	GRAPHIC LITHOLOGY	DRILLING DISTURB.	SED. STRUCTURES	SAMPLES	LITHOLOGIC DESCRIPTION																																																						
	FORAMINIFERS NANNOFOSSILS	RADIOLARIANS DIATOMS																																																													
LOWER PLIOCENE / QUATERNARY	A.G	QUATERNARY Lower Upsilon <i>N. angulata - N. reinholdii</i>	1	0.5 1.0				*	RADIOLARIAN-DIATOM OOZE and RADIOLARIAN-BEARING DIATOM OOZE Major lithologies: Radiolarian-diatom ooze and radiolarian-bearing diatom ooze, white (2.5Y 8/2, 10YR 8/2), and light gray (2.5Y 7/2) in Sections 1 and 2. Percentage of radiolarians decreases irregularly downcore. Darker colored layers contain a trace to 2% of clay. Silicoflagellates form about 2%. Minor lithology: Chert occurs as fragments in Section 2, 98-108 cm. Bioturbation is strong in Sections 3 and 4; colors including grayish brown (2.5Y 5/2), pale yellow (2.5Y 7/4, 8/4), light yellowish brown (2.5Y 6/4), and light olive brown (2.5Y 5/4) are mixed on a scale ranging from individual burrows to intervals 30 cm thick. Burrows are circular or oval to irregular in shape, 5-10 cm across. Vertical burrows 4 mm wide and up to 10 cm long occur in Section 3. SMEAR SLIDE SUMMARY (%): <table><thead><tr><th></th><th>1, 101 D</th><th>2, 15 D</th><th>2, 126 M</th><th>3, 33 D</th><th>3, 126 D</th></tr></thead><tbody><tr><td>Quartz</td><td>Tr</td><td>—</td><td>Tr</td><td>Tr</td><td>—</td></tr><tr><td>Clay</td><td>Tr</td><td>Tr</td><td>—</td><td>2</td><td>1</td></tr><tr><td>Foraminifers</td><td>Tr</td><td>—</td><td>—</td><td>—</td><td>—</td></tr><tr><td>Nannofossils</td><td>—</td><td>Tr</td><td>—</td><td>—</td><td>—</td></tr><tr><td>Diatoms</td><td>73</td><td>70</td><td>84</td><td>76</td><td>92</td></tr><tr><td>Radiolarians</td><td>25</td><td>27</td><td>15</td><td>20</td><td>5</td></tr><tr><td>Sponge spicules</td><td>Tr</td><td>—</td><td>—</td><td>—</td><td>—</td></tr><tr><td>Silicoflagellates</td><td>2</td><td>3</td><td>Tr</td><td>2</td><td>2</td></tr></tbody></table>		1, 101 D	2, 15 D	2, 126 M	3, 33 D	3, 126 D	Quartz	Tr	—	Tr	Tr	—	Clay	Tr	Tr	—	2	1	Foraminifers	Tr	—	—	—	—	Nannofossils	—	Tr	—	—	—	Diatoms	73	70	84	76	92	Radiolarians	25	27	15	20	5	Sponge spicules	Tr	—	—	—	—	Silicoflagellates	2	3	Tr	2	2
										1, 101 D	2, 15 D	2, 126 M	3, 33 D	3, 126 D																																																	
	Quartz									Tr	—	Tr	Tr	—																																																	
	Clay									Tr	Tr	—	2	1																																																	
	Foraminifers									Tr	—	—	—	—																																																	
Nannofossils	—	Tr	—	—	—																																																										
Diatoms	73	70	84	76	92																																																										
Radiolarians	25	27	15	20	5																																																										
Sponge spicules	Tr	—	—	—	—																																																										
Silicoflagellates	2	3	Tr	2	2																																																										
B																																																															
A.G																																																															
A.G																																																															
B																																																															



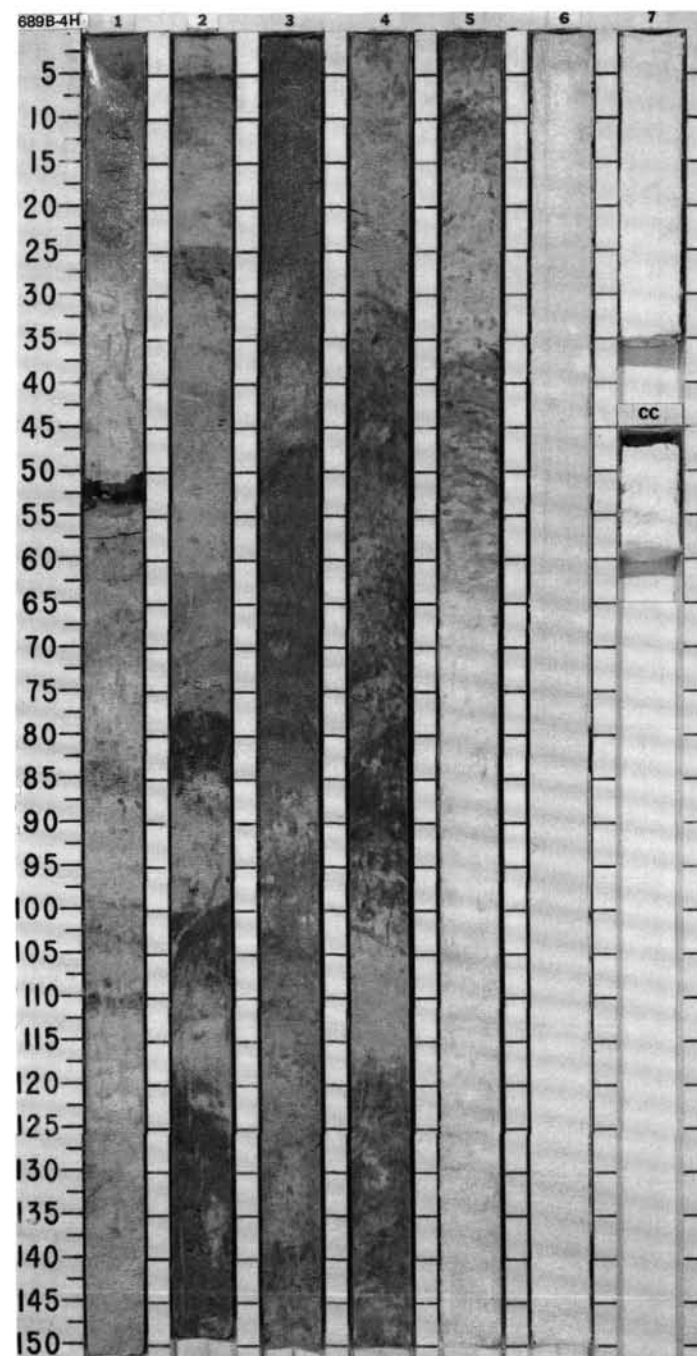
SITE 689

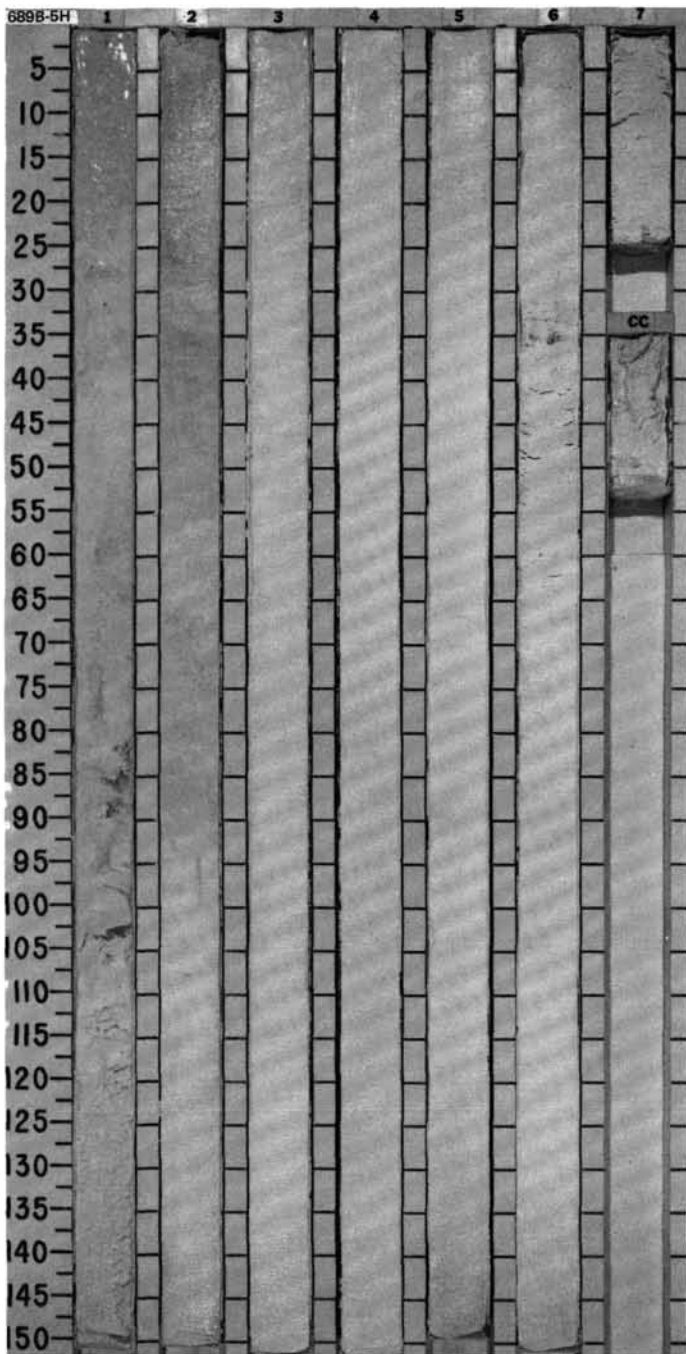
SITE 689 HOLE B CORE 3H CORED INTERVAL 2095.0-2104.5 mbsl; 14.8-24.3 mbsf

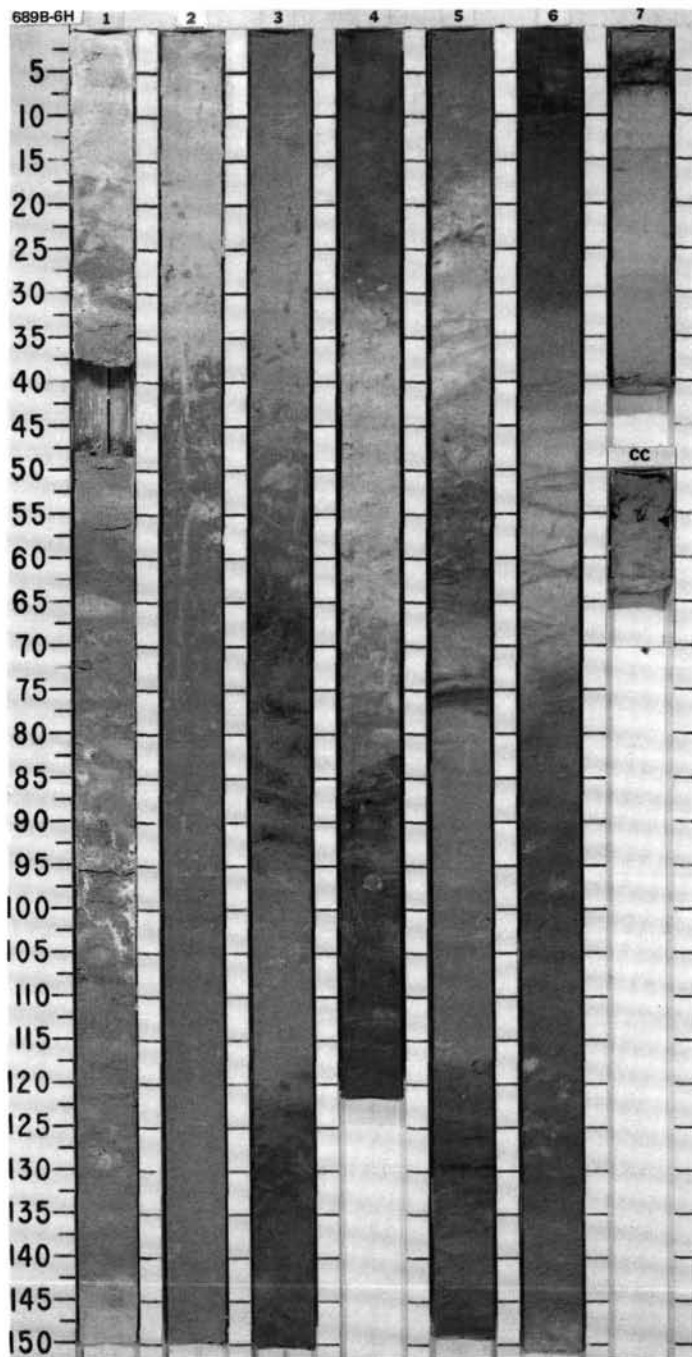
TIME-ROCK UNIT	BIOSTRAT. ZONE/ FOSSIL CHARACTER	PHYS. PROPERTIES	CHEMISTRY	SECTION	METERS	GRAPHIC LITHOLOGY	DRILLING DISTURB.	SED. STRUCTURES	SAMPLES	LITHOLOGIC DESCRIPTION
UPPER MIOCENE	FORAMINIFERS NANNOFOSSILS RADIOLARIANS DIATOMS PALYNOFORMS	PHYS. PROPERTIES	CHEMISTRY	SECTION	METERS	GRAPHIC LITHOLOGY	DRILLING DISTURB.	SED. STRUCTURES	SAMPLES	LITHOLOGIC DESCRIPTION
F.G	no Zone	0.3% ●	0.3% ●	1	0.5				*	SILICOFLAGELLATE-DIATOM OOZE, RADIOLARIAN- AND SILICOFLAGELLATE-BEARING DIATOM OOZE, SILICOFLAGELLATE- AND RADIOLARIAN-BEARING DIATOM OOZE, and DIATOM-NANNOFOSSIL OOZE
F.M	Upper <i>C. spongothorax</i>	0.2% ●	0.2% ●	2	1.0				*	Major lithologies: Silicoflagellate-diatom ooze, white (10YR 8/2), pale yellow (5Y 7/3, 8/3), and light gray (2.5Y 7/2; 5Y 7/1, 7/2). Radiolarian- and silicoflagellate-bearing diatom ooze, light brownish gray (2.5Y 6/2), white (5Y 8/1, 2.5Y 8/2), and grayish brown (2.5Y 5/2). Silicoflagellate- and radiolarian- bearing diatom ooze, light brownish gray (2.5Y 6/2), white (5Y 8/1, 2.5Y 8/2), and grayish brown (2.5Y 5/2). Diatom-nannofossil ooze, light gray (10YR 7/2) and pale brown (10YR 6/3). Chert fragments are present in top 5 cm, and probably fell downhole.
A.G	<i>N. reinholdii</i> - <i>N. angularata</i>	0.3% ●	0.3% ●	3					*	SMEAR SLIDE SUMMARY (%):
A.G	<i>Denticulopsis hustedtii</i>	1.0% ●	1.0% ●	4					*	COMPOSITION:
B				5					*	1, 75 D 2, 75 D 3, 50 D 4, 50 D 5, 20 D 5, 120 D 6, 75 D
				6					*	Quartz Tr 1 Tr — Tr 5 Tr
				7					*	Clay 1 Tr 1 Tr — 1 Tr
				CC					*	Foraminifers — — Tr — — — 2
									*	Nannofossils — Tr — Tr — — 2 51
									*	Diatoms 70 60 65 75 75 81 40
									*	Radiolarians 4 4 7 15 15 10 5
									*	Silicoflagellates 25 35 27 10 10 1 2



TIME-ROCK UNIT	BIOSTRAT. ZONE/ FOSSIL CHARACTER				PALEOMAGNETICS	PHYS. PROPERTIES	CHEMISTRY	SECTION	METERS	GRAPHIC LITHOLOGY	DRILLING DISTURB.	SED. STRUCTURES	SAMPLES	LITHOLOGIC DESCRIPTION																																																																								
	FORAMINIFERS	NANNOFOSSILS	RADIOLARIANS	DIATOMS																																																																																		
UPPER MIOCENE	C.G													RADIOLARIAN-BEARING DIATOM OOZE, DIATOM OOZE, NANNOFOSSIL-DIATOM OOZE, and DIATOM-NANNOFOSSIL OOZE Major lithologies: Radiolarian-bearing diatom ooze, light gray (2.5Y 6/2) and light brownish gray (2.5Y 5/2), colors alternate on a scale of 10-40 cm. Radiolarians decrease downcore. Light to moderate bioturbation. Long vertical burrows in Section 2. Diatom ooze, light gray (2.5Y 7/2), yellowish brown (10YR 5/4), and pale brown (10YR 6/3). Moderate to strong bioturbation. Colors alternate on a scale of 20-40 cm. Nannofossil-diatom ooze occurs as a transition lithology in Section 5. Diatom-nannofossil ooze, pure white (10YR 8/0), faint, minor bioturbation near top. SMEAR SLIDE SUMMARY (%): <table><tr><td></td><td>1, 75 D</td><td>2, 120 D</td><td>3, 65 D</td><td>4, 64 D</td><td>5, 30 D</td><td>5, 120 D</td><td>6, 75 D</td></tr><tr><td>COMPOSITION:</td><td></td><td></td><td></td><td></td><td></td><td></td><td></td></tr><tr><td>Quartz</td><td>Tr</td><td>—</td><td>—</td><td>—</td><td>—</td><td>—</td><td>—</td></tr><tr><td>Clay</td><td>2</td><td>—</td><td>Tr</td><td>—</td><td>—</td><td>—</td><td>—</td></tr><tr><td>Nannofossils</td><td>Tr</td><td>—</td><td>—</td><td>—</td><td>2</td><td>40</td><td>80</td></tr><tr><td>Diatoms</td><td>80</td><td>90</td><td>92</td><td>95</td><td>95</td><td>60</td><td>10</td></tr><tr><td>Radiolarians</td><td>13</td><td>8</td><td>5</td><td>3</td><td>3</td><td>Tr</td><td>—</td></tr><tr><td>Sponge spicules</td><td>—</td><td>2</td><td>Tr</td><td>Tr</td><td>Tr</td><td>—</td><td>—</td></tr><tr><td>Silicoflagellates</td><td>5</td><td>Tr</td><td>3</td><td>2</td><td>Tr</td><td>Tr</td><td>Tr</td></tr></table>		1, 75 D	2, 120 D	3, 65 D	4, 64 D	5, 30 D	5, 120 D	6, 75 D	COMPOSITION:								Quartz	Tr	—	—	—	—	—	—	Clay	2	—	Tr	—	—	—	—	Nannofossils	Tr	—	—	—	2	40	80	Diatoms	80	90	92	95	95	60	10	Radiolarians	13	8	5	3	3	Tr	—	Sponge spicules	—	2	Tr	Tr	Tr	—	—	Silicoflagellates	5	Tr	3	2	Tr	Tr	Tr
		1, 75 D	2, 120 D	3, 65 D	4, 64 D	5, 30 D	5, 120 D	6, 75 D																																																																														
	COMPOSITION:																																																																																					
	Quartz	Tr	—	—	—	—	—	—																																																																														
	Clay	2	—	Tr	—	—	—	—																																																																														
Nannofossils	Tr	—	—	—	2	40	80																																																																															
Diatoms	80	90	92	95	95	60	10																																																																															
Radiolarians	13	8	5	3	3	Tr	—																																																																															
Sponge spicules	—	2	Tr	Tr	Tr	—	—																																																																															
Silicoflagellates	5	Tr	3	2	Tr	Tr	Tr																																																																															
A.G	no Zone																																																																																					
A.G	C. spongothorax																																																																																					
C.M	D. hustedtii																																																																																					
B																																																																																						



[illegible]

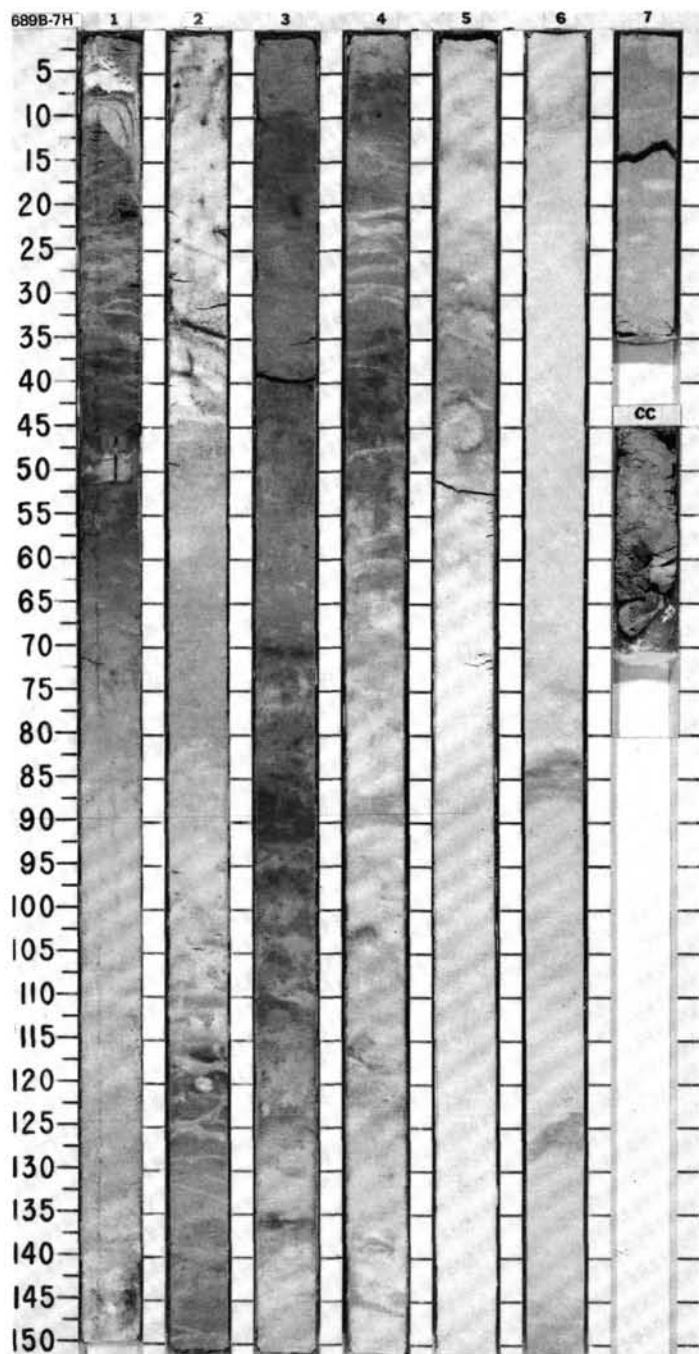
[illegible]

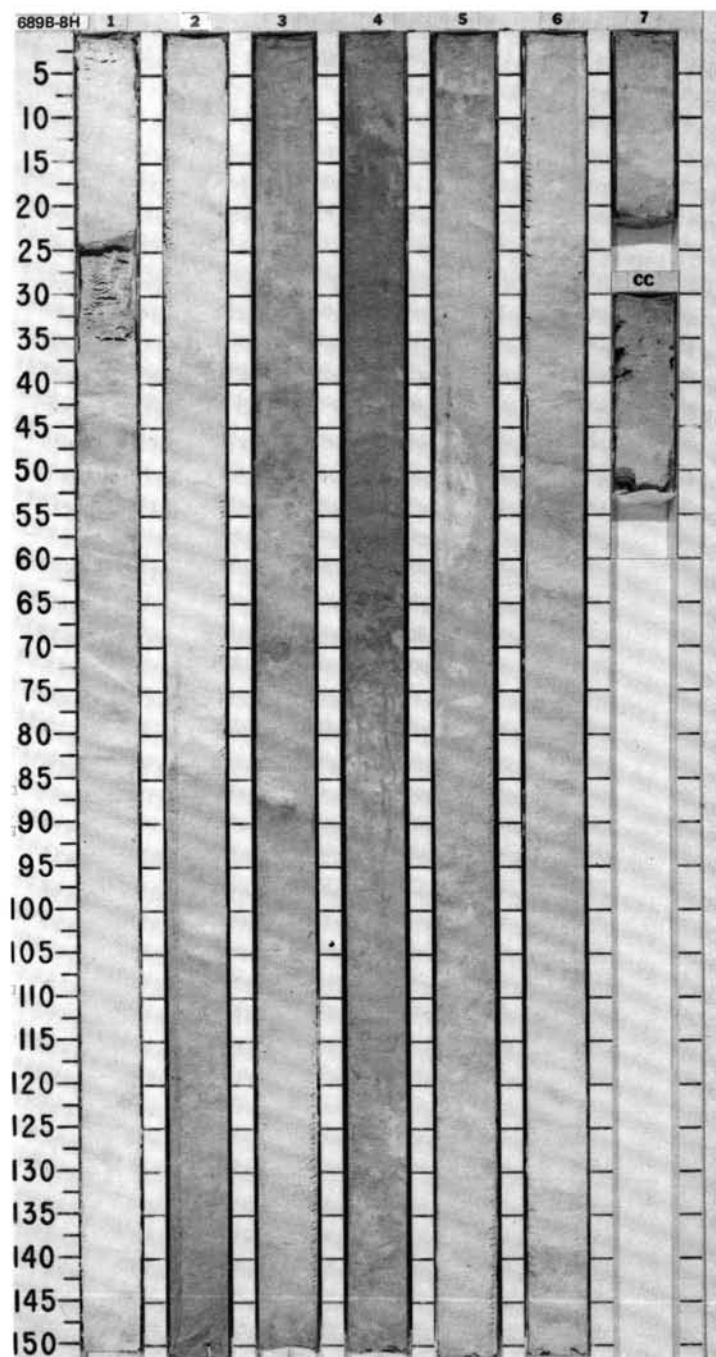
SITE689HOLEB

COREINTERVAL

2133.1-2142.7 mbsl; 52.9-62.5 mbsf

TIME-ROCK UNIT	BIOSTRAT. ZONE/ FOSSIL CHARACTER	PHYS. PROPERTIES	CHEMISTRY	SECTION	METERS	GRAPHIC LITHOLOGY	DRILLING DISTURB.	SED. STRUCTURES	SAMPLES	LITHOLOGIC DESCRIPTION
FORAMINIFERS	NANNOFOSSILS	RADIOLARIANS	DIATOMS	PALYMONORPHS						
F.M	F.M									
C.M	C. rhombicus - N. maleinterpretaria									
B										

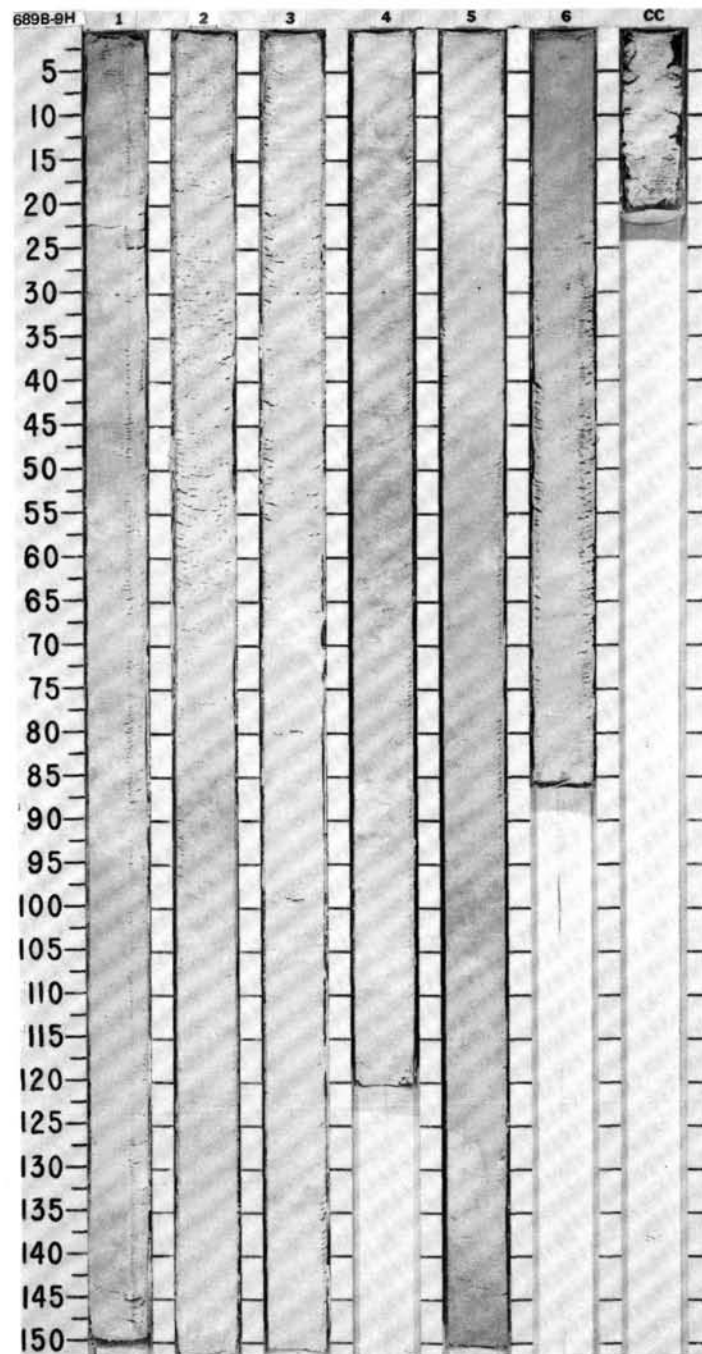


[illegible]

SITE689HOLEB

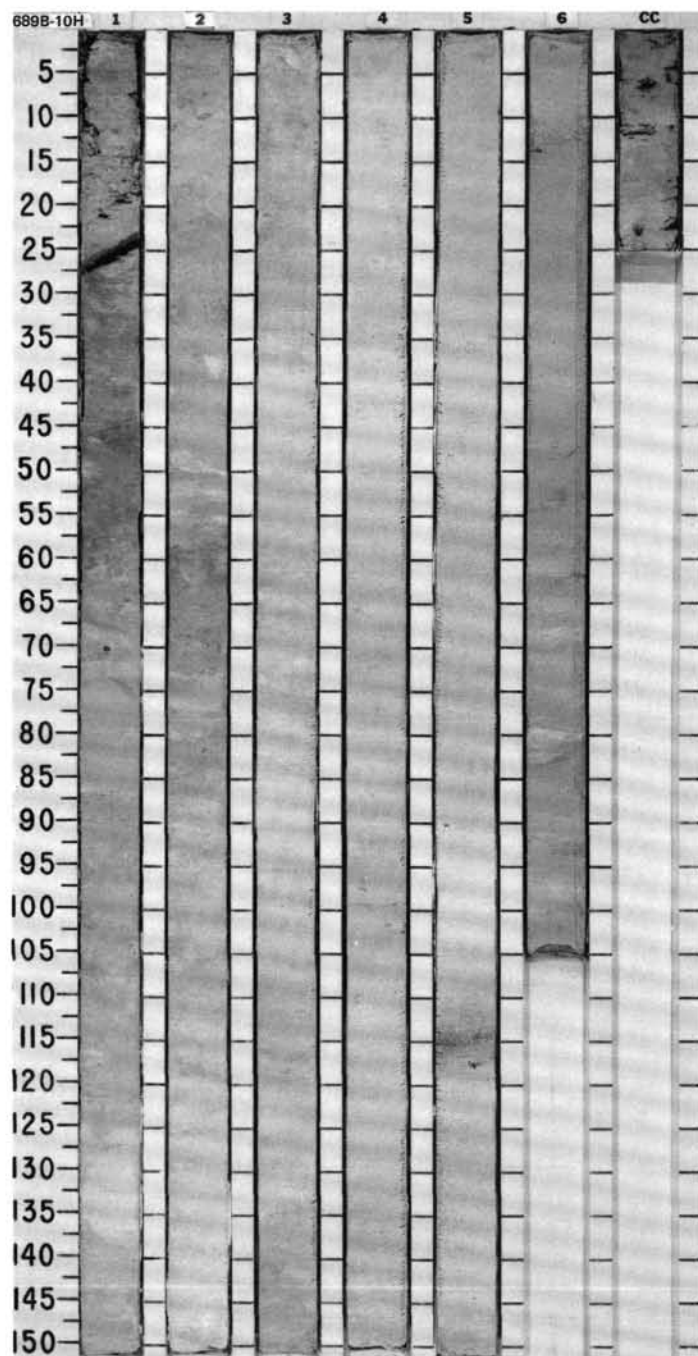
CORED INTERVAL2152.3-2161.9 mbsl; 72.1-81.7 mbsf

TIME-ROCK UNIT	BIOSTRAT. ZONE/ FOSSIL CHARACTER				PHYS. PROPERTIES	CHEMISTRY	SECTION	METERS	GRAPHIC LITHOLOGY	DRILLING DISTURB.	SED. STRUCTURES	SAMPLES	LITHOLOGIC DESCRIPTION
	FORAMINIFERS	NANNOFOSSILS	RADIOLARIANS	DIATOMS	PALYNOFORMPHES	PALEOMAGNETICS							
UPPER OLIGOCENE													DIATOM-NANNOFOSSIL OOZE, DIATOM-BEARING NANNOFOSSIL OOZE, and FORAMINIFER- AND SILICEOUS-BEARING NANNOFOSSIL OOZE
?								0.5				*	Major lithologies: Diatom-nannofossil ooze, white (10YR 8/1) and light gray (10YR 7/1). Diatom-bearing nannofossil ooze, white (10YR 8/1) and light gray (10YR 7/1). Foraminifer- and siliceous-bearing nannofossil ooze, white (10YR 8/1) and light gray (10YR 7/1).
CP19-CP17								1.0				*	Color changes in core are small and gradational. Bioturbation is minor to moderate throughout the core and consists of halo burrows, vertical burrows, and Planolites.
OLIGOCENE ?								2				*	SMEAR SLIDE SUMMARY (%):
?								3				*	COMPOSITION:
								4				*	1, 35 2, 35 3, 35 4, 35 5, 35 6, 35
								5				*	D M D D D D
								6				*	Foraminifera 15 9 5 9 5
								7				*	Nannofossils 75 70 76 75 66 70
								8				*	Diatoms 25 10 9 20 20 25
								9				*	Radiolarians — 5 6 — 5 —
								10				*	
								11				*	
								12				*	
								13				*	
								14				*	
								15				*	
								16				*	
								17				*	
								18				*	
								19				*	
								20				*	
								21				*	
								22				*	
								23				*	
								24				*	
								25				*	
								26				*	
								27				*	
								28				*	
								29				*	
								30				*	



SITE 689 HOLE B CORE 10H CORED INTERVAL 2161.9-2171.5 mbsl; 81.7-91.3 mbsf

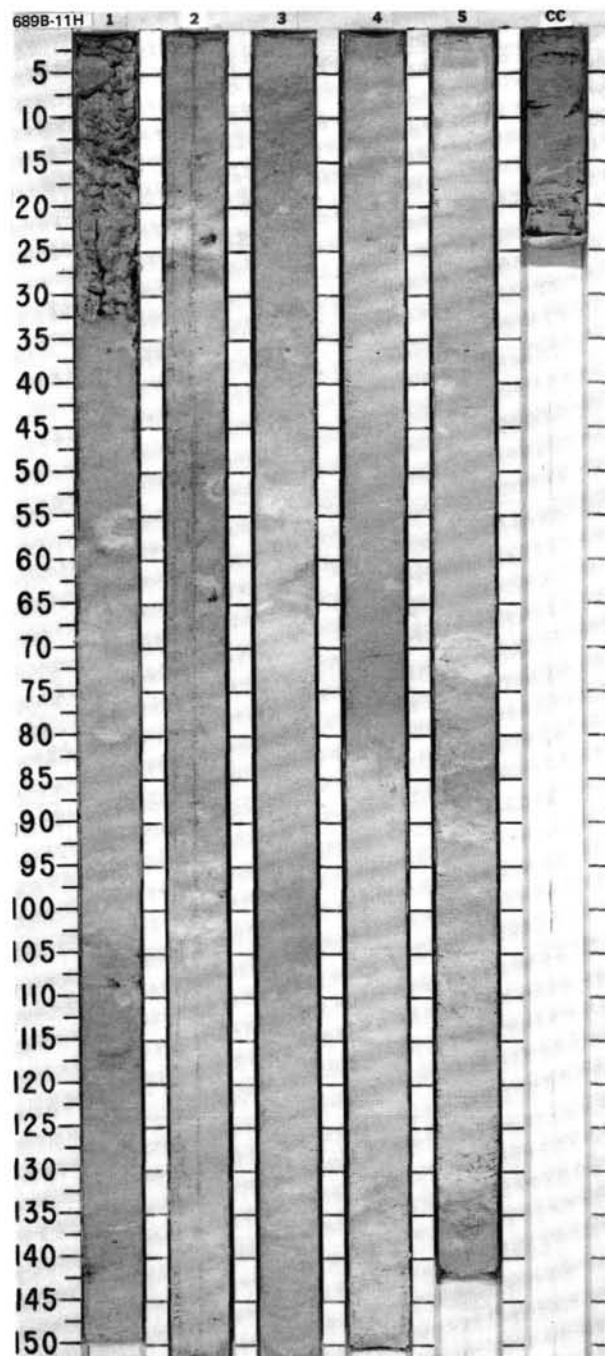
TIME-ROCK UNIT	BIOSTRAT. ZONE/ FOSSIL CHARACTER				PHYS. PROPERTIES	CHEMISTRY	SECTION	METERS	GRAPHIC LITHOLOGY	DRILLING DISTURB.	SED. STRUCTURES	SAMPLES	LITHOLOGIC DESCRIPTION
	FORAMINIFERS	NANNOFOSSILS	RADIOLARIANS	DIATOMS									
UPPER OLIGOCENE													
UPPER OLIGOCENE													
CP19-CP17													
OLIGOCENE													
OLIGOCENE													



SITE 689

SITE 689 HOLE B CORE 11H CORED INTERVAL 2171.5-2181.2 mbsl; 91.3-101.0 mbsf

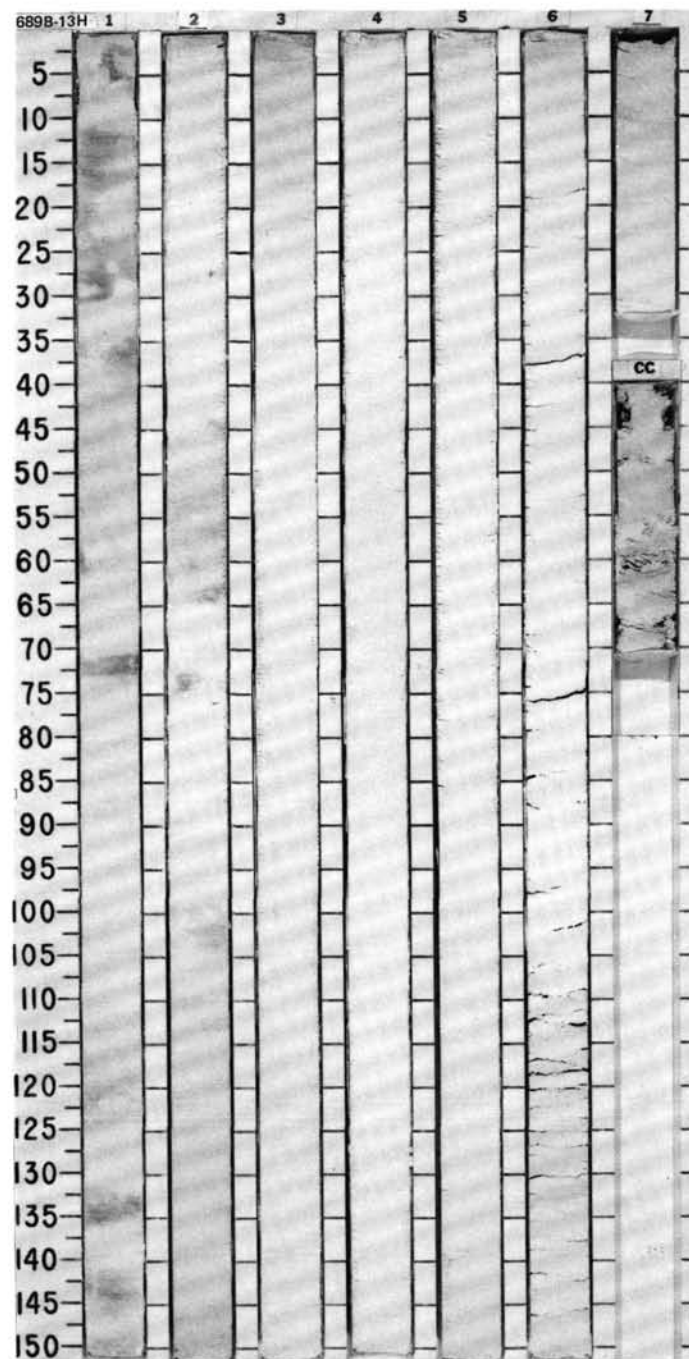
TIME-ROCK UNIT	BIOSTRAT. ZONE/ FOSSIL CHARACTER					SECTION	METERS	GRAPHIC LITHOLOGY	DRILLING DISTURB.	SED. STRUCTURES	SAMPLES	LITHOLOGIC DESCRIPTION	
	FORAMINIFERS	NANNOFOSSILS	RADIOLARIANS	DIATOMS	PALYNOMORPHS								
													PALEOMAGNETICS
OLIGOCENE UPPER OLIGOCENE CP19-CP17	C.G					● V-1494	● 83.1%				*	NANNOFOSSIL OOZE Major lithology: Nannofossil ooze, light gray (2.5Y 7/2, 7/1, 6-5/2). Minor bioturbation includes halo burrows, <i>Zoophycos</i> in Sections 2, 3, and 5; <i>Planolites</i> in Sections 3 and 5, and a vertical burrow in Section 3. A 6-cm-long, angular chert fragment occurs in Section 1, 20-28 cm. It has probably fallen in from a near-surface chert layer. A 3-mm-long dropstone occurs in Section 1, 140 cm. SMEAR SLIDE SUMMARY (%): COMPOSITION: Quartz Accessory minerals: Heavy minerals Foraminifers Nannofossils Diatoms Radiolarians Sponge spicules	
	A.M					● V-1497	● 79.2%			*			
	R.VP										*		
	R.P										*		
	B						● V-1498	● 84.9%			*		
									</				

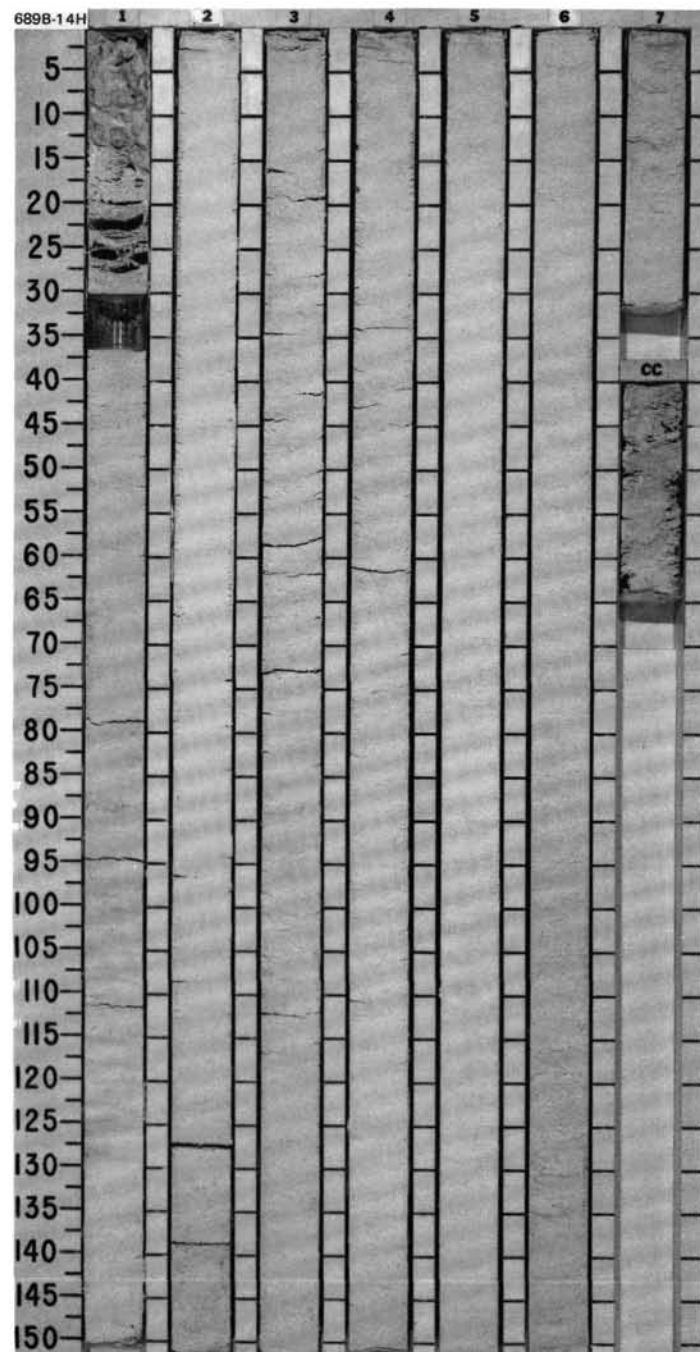


TIME-ROCK UNIT		BIOSTRAT. ZONE/ FOSSIL CHARACTER				PALEOMAGNETICS	PHYS. PROPERTIES	CHEMISTRY	SECTION	METERS	GRAPHIC LITHOLOGY	DRILLING DISTURB.	SED. STRUCTURES	SAMPLES	LITHOLOGIC DESCRIPTION
FORAMINIFERS	NAUNFOSSILS	RADICLARIANS	DIATOMS	PALYNOMORPHS											
LOWER OLIGOCENE															
LOWER OLIGOCENE		CP19-CP17													
OLIGOCENE															
OLIGOCENE															
CP16															
C.M															
B															
A.G															
A.M															
A.G															
C.M															
B															
A.G															
A.M															
A.G															
C.M															
B															
A.G															
A.M															
A.G															
C.M															
B															
A.G															
A.M															
A.G															
C.M															
B															
A.G															
A.M															
A.G															
C.M															
B															
A.G															
A.M															
A.G															
C.M															
B															
A.G															
A.M															
A.G															
C.M															
B															
A.G															
A.M															
A.G															
C.M															
B															
A.G															
A.M															
A.G															
C.M															
B															
A.G															
A.M															
A.G															
C.M															
B															
A.G															
A.M															
A.G															
C.M															
B															
A.G															
A.M															
A.G															
C.M															
B															
A.G															
A.M															
A.G															
C.M															
B															
A.G															
A.M															
A.G															
C.M															
B															
A.G															
A.M															
A.G															
C.M															
B															
A.G															
A.M															
A.G															
C.M															
B															
A.G															
A.M															
A.G															
C.M															
B															
A.G															
A.M															
A.G															
C.M															
B															
A.G															
A.M															
A.G															
C.M															
B															
A.G															
A.M															
A.G															
C.M															
B															
A.G															
A.M															
A.G															
C.M															
B															
A.G															
A.M															
A.G															
C.M															
B															
A.G															
A.M															
A.G															
C.M															
B															
A.G															
A.M															
A.G															
C.M															
B															
A.G															
A.M															
A.G															
C.M															
B															
A.G															
A.M															
A.G															
C.M															
B															
A.G															
A.M															
A.G															
C.M															
B															
A.G															
A.M															
A.G															
C.M															
B															
A.G															
A.M															
A.G															
C.M															
B															
A.G															
A.M															
A.G															
C.M															
B															
A.G															
A.M															
A.G															
C.M															
B															
A.G															
A.M															
A.G															
C.M															
B															
A.G															
A.M															
A.G															
C.M															
B															
A.G															
A.M															
A.G															
C.M															
B															
A.G															
A.M															
A.G															
C.M															
B															
A.G															
A.M															
A.G															
C.M															
B															
A.G															
A.M															
A.G															
C.M															
B															
A.G															
A.M															
A.G															
C.M															
B															
A.G															
A.M															
A.G															



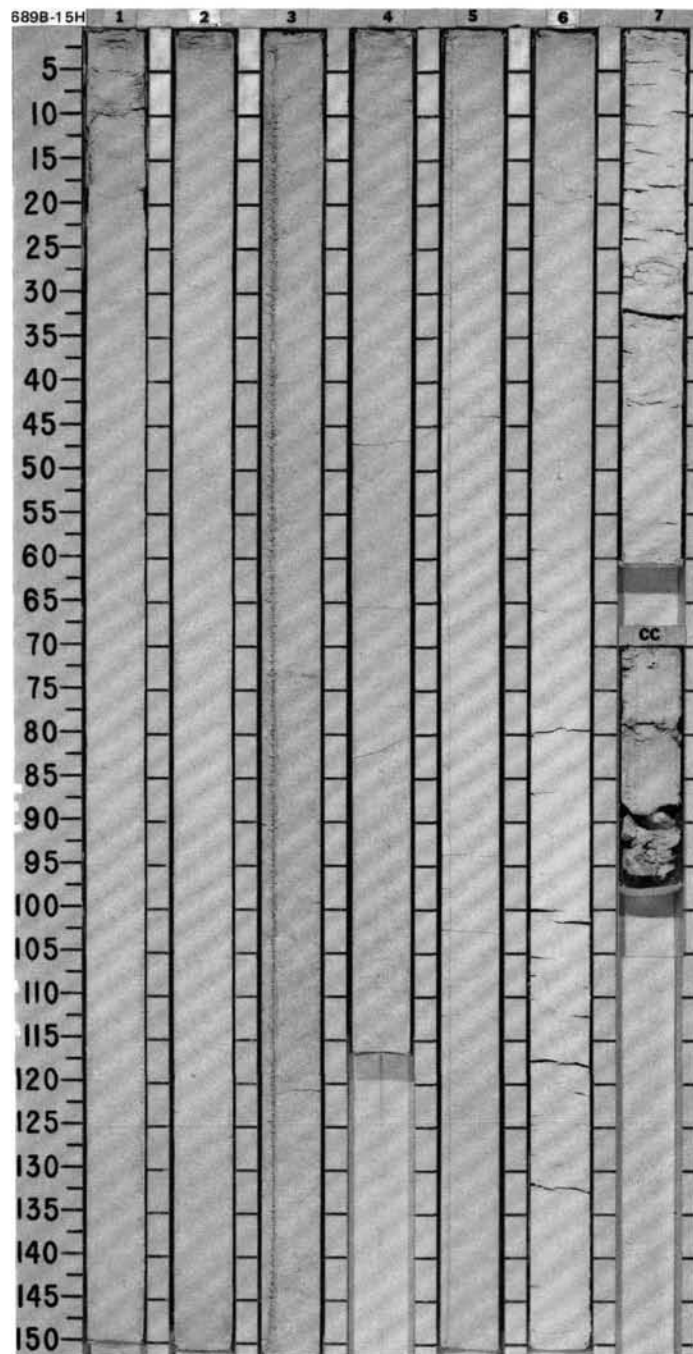
SITE	689	HOLE	B	CORE	13H	CORED INTERVAL	2190.8-2200.4 mbsl; 110.6-120.2 mbsf
------	-----	------	---	------	-----	----------------	--------------------------------------

[illegible]

[illegible]

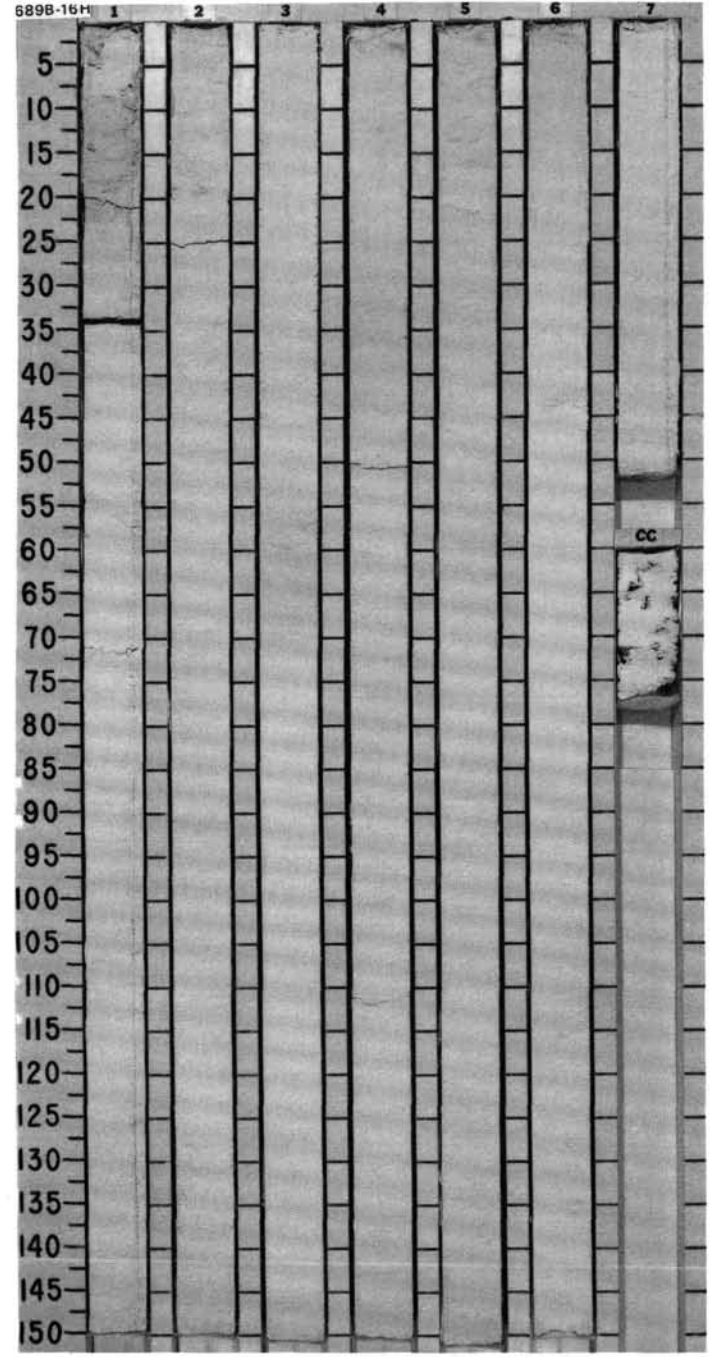
SITE 689 HOLE B CORE 15H CORED INTERVAL 2210.0 - 2219.6 mbsl; 129.9 - 139.4 mbsf

TIME-ROCK UNIT	BIOSTRAT. ZONE/ FOSSIL CHARACTER					PHYS. PROPERTIES	CHEMISTRY	SECTION	METERS	GRAPHIC LITHOLOGY	DRILLING DISTURB.	SED. STRUCTURES	SAMPLES	LITHOLOGIC DESCRIPTION							
	FORAMINIFERS	NANNOFOSSILS	RADIOLARIANS	DIATOMS	PALYNOFORS																
UPPER EOCENE - LOWER OLIGOCENE	A.M. A.M. A.P. R.P.	UPPER EOCENE	CP15a	UPPER EOCENE	LOWER OLIGOCENE to UPPER EOCENE	Q=59 V=1.85	V=1517 ● ● 88.8%	Q=65 V=1.69	V=1517 ● ● 89.2%	Q=71 V=1.87	V=1520 ● ● 87.5%	1	0.5 1.0	2	3	4	5	6	7	CG	
														DIATOM-BEARING NANNOFOSSIL OOZE							
														Major lithology: Diatom-bearing nannofossil ooze, white (10YR 8/0, 8/2); rare to moderate bioturbation. Sections 3, 4, and 5 contain a few scattered sand grains (volcanic glass?).							
														Minor lithology: Foraminifer-bearing nannofossil ooze in Section 7, white (10YR 8/2). Gradational boundary with diatom-bearing nannofossil ooze.							
														SMEAR SLIDE SUMMARY (%):							
														COMPOSITION:							
														1, 50 D	2, 50 D	3, 50 D	4, 50 D	5, 50 D	6, 50 D	7, 35 D	
														Quartz	—	Tr	3	—	Tr	—	—
														Volcanic glass	3	Tr	1	Tr	Tr	Tr	Tr
														Accessory minerals:							
														Heavy minerals	—	—	Tr	—	—	—	—
														Foraminifers	—	2	Tr	Tr	1	2	15
														Nannofossils	82	82	84	85	87	92	78
														Diatoms	15	15	10	10	10	5	5
														Radiolarians	1	Tr	5	2	2	1	1
														Sponge spicules	—	—	—	Tr	—	—	—
														Silicoflagellates	—	Tr	—	—	—	Tr	1



SITE 689 HOLE B CORE 16H CORED INTERVAL 2219.6-2229.3 mbsl; 139.4-149.1 mbsf

TIME-ROCK UNIT	BIOSTRAT. ZONE/ FOSSIL CHARACTER	PHYS. PROPERTIES	SECTION	METERS	GRAPHIC LITHOLOGY	DRILLING DISTURB.	SED. STRUCTURES	SAMPLES	LITHOLOGIC DESCRIPTION
UPPER EOCENE									
A.G									
A.M CP14b	CP15a								
C.P	LOWER OLILOCENE or UPPER EOCENE								
R.P									
B									
		7-1.87 • 95.8% 7-1.470	1	0.5 1.0				*	NANNOFOSSIL OOZE Major lithology: Nannofossil ooze, white (10YR 8/0, 8/1), although some subtle color variations are present that cannot be quantified with the colors on the Munsell Color Chart. SMEAR SLIDE SUMMARY (%): COMPOSITION: Quartz 1 Tr 1 Tr — — Volcanic glass Tr — — — — Accessory minerals: Heavy minerals — Tr — — — — Foraminifers 5 2 3 3 5 3 Nannofossils 89 96 89 95 90 92 Diatoms 5 2 5 1 5 5 Radiolarians Tr Tr 2 1 Tr Tr
		9-67 7-1.85 • 90.1% 9-1508	2					*	
		9-67 7-1.85 • 94.5% 9-1518	3					*	
			4					*	
			5					*	
			6					*	
			7					*	



SITE 689 HOLE B CORE 17H CORED INTERVAL 2229.3-2239.0 mbsl; 149.1-158.8 mbsf

TIME-ROCK UNIT	BIOSTRAT. ZONE/ FOSSIL CHARACTER	PHYS. PROPERTIES	CHEMISTRY	SECTION	METERS	GRAPHIC LITHOLOGY	DRILLING DISTURB.	SAMPLES	LITHOLOGIC DESCRIPTION
UPPER EOCENE	FORMINIFERS								
UPPER EOCENE	NANNOFOSSILS								
	RADIOLARIANS								
	DIAZONES								
	PALYMONOPHIS								
	PALYMONOPHIS								
		● V-1531	● 95.1%		0.5			*	
					1				
					1.0				
					2				
					3				
					4				
					5				
					6				
					7				
					CC				

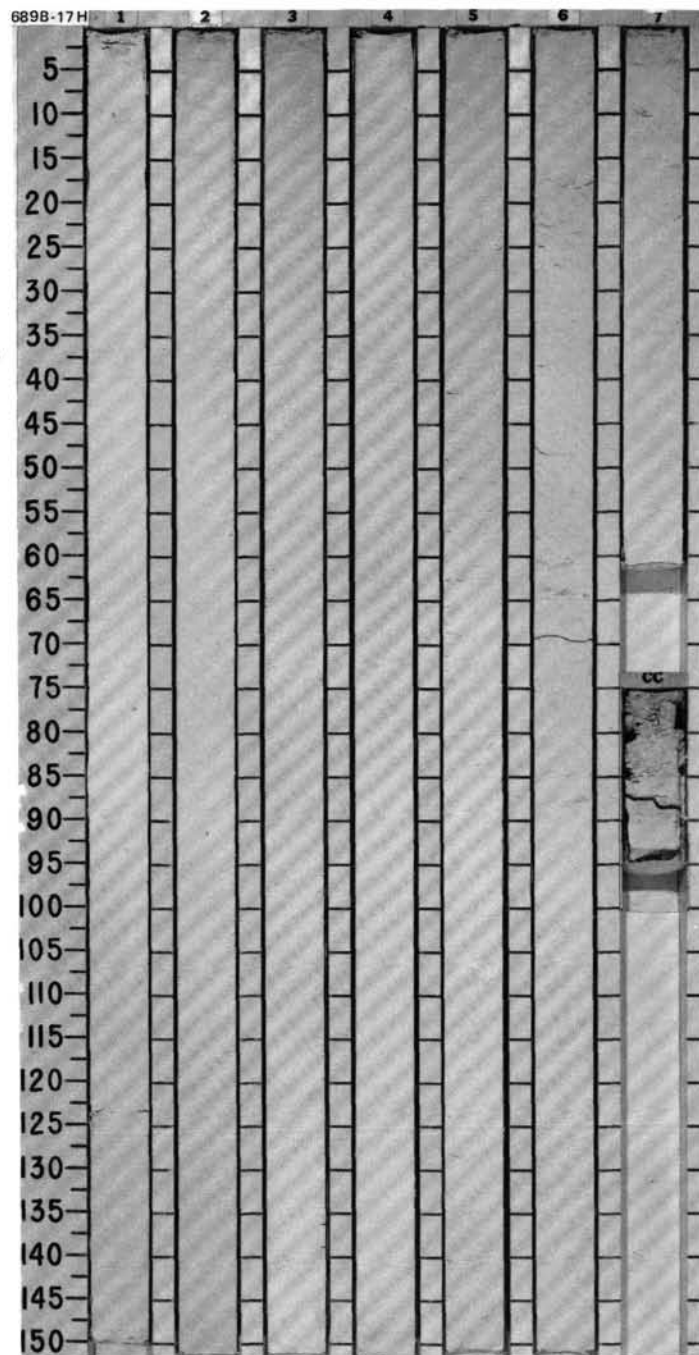
NANNOFOSSIL OOZE

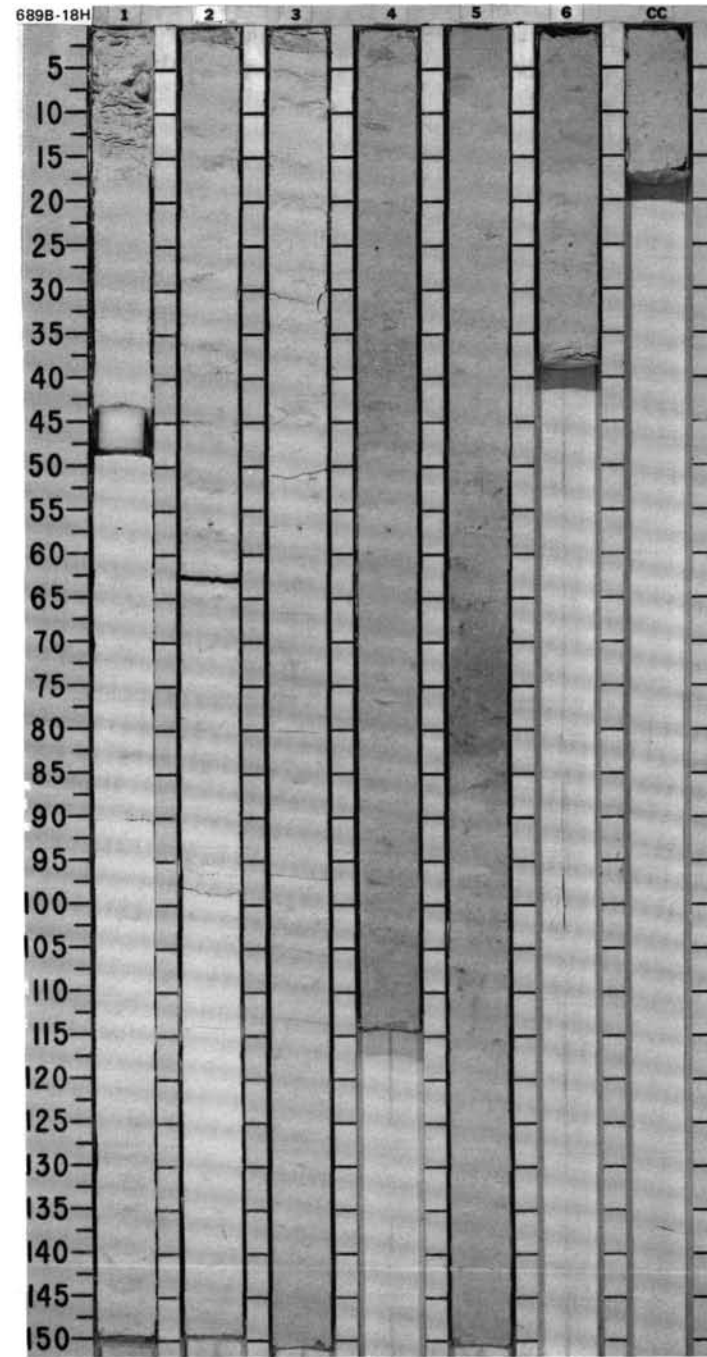
Major lithology: Nannofossil ooze, white (10YR 8/0, 8/1).

Local minor bioturbation, which includes a vertical burrow.

SMEAR SLIDE SUMMARY (%):

	1, 50 D	2, 50 D	3, 50 D	4, 50 D	5, 50 D	6, 50 D
COMPOSITION:						
Calcite/dolomite	—	—	Tr	—	—	—
Accessory minerals:						
Zeolites	1	1	Tr	2	Tr	—
Foraminifers	5	5	10	7	5	4
Nannofossils	94	94	90	91	95	95
Radiolarians	—	—	—	—	Tr	1
Silicoflagellates	—	—	—	—	—	Tr

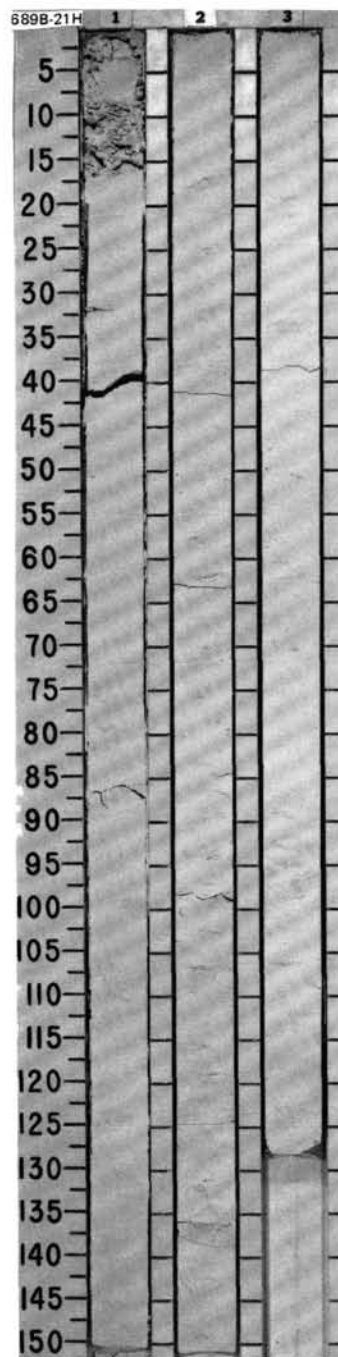


[illegible]

SITE 689 HOLE B CORE 20H CORED INTERVAL 2258.3-2268.0 mbsl; 178.1-187.8 mbsf

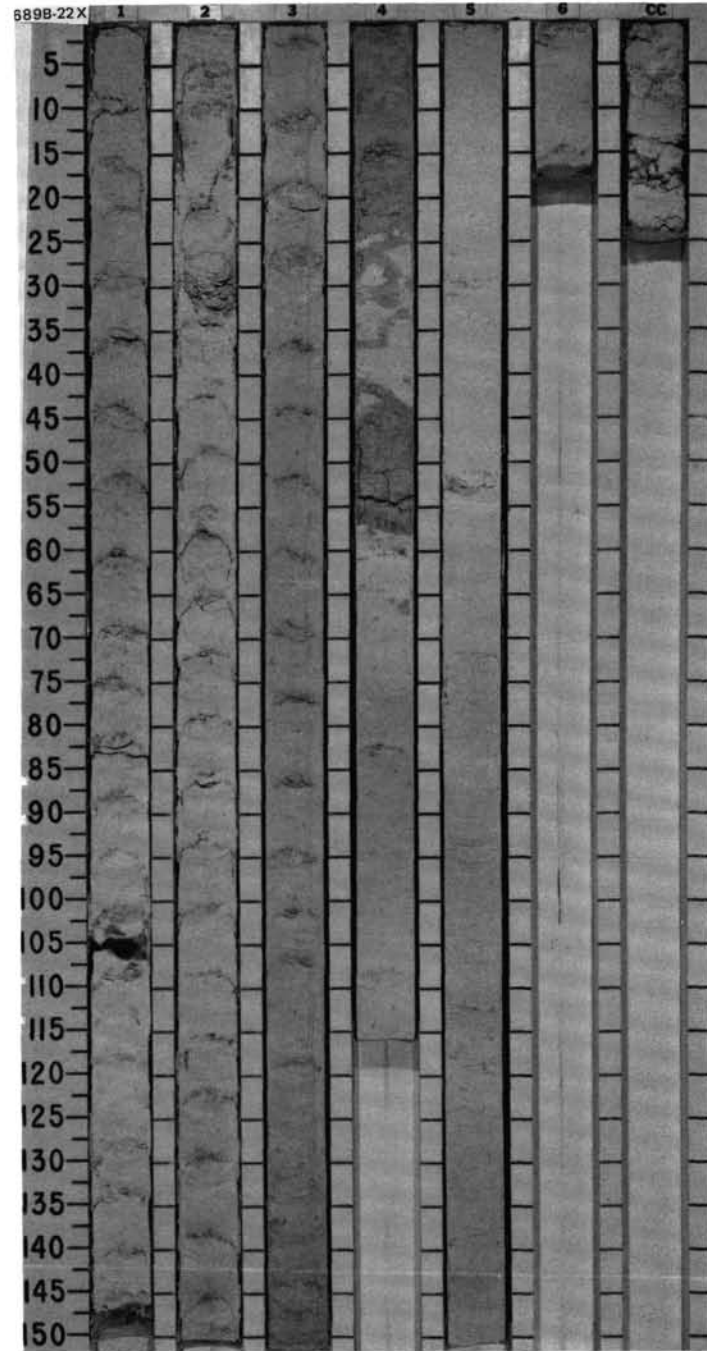
LOWER - MIDDLE EOCENE											LITHOLOGIC DESCRIPTION										
TIME-ROCK UNIT	BIOSTRAT. ZONE/ FOSSIL CHARACTER										SECTION METERS	GRAPHIC LITHOLOGY	DRILLING DISTURB.	SED. STRUCTURES	SAMPLES						
	FORAMINIFERS																				
	NANNOFOSSILS																				
	RADIOLARIANS																				
	DIATOMS																				
PALYNOFORMS																					
PALEOMAGNETICS																					
PHYS. PROPERTIES																					
CHEMISTRY																					
SECTION																					
METERS																					

SITE		689		HOLE		B		CORE		21H		CORE INTERVAL		2268.0-2277.7 mbsl; 187.8-197.5 mbsf									
TIME-ROCK UNIT		BIOSTRAT. ZONE/ FOSSIL CHARACTER				PHYS. PROPERTIES		CHEMISTRY		SECTION		METERS		GRAPHIC LITHOLOGY		DRILLING DISTURB.		SED. STRUCTURES		SAMPLES		LITHOLOGIC DESCRIPTION	
		FORAMINIFERS		NANNOFOSSILS		RADIOGLARIANS		DIATOMS		PALYNOFORMS		PALEOMAGNETICS											
LOWER - MIDDLE EOCENE		A.G		CP12-CP13																			
		A.P																					
		B																					
		R.P																					
		B																					
		94.5% ● 94.4%		94.3% ● 93.3%		94.3% ● 93.3%		94.3% ● 93.3%															



SITE 689 HOLE B CORE 22X CORED INTERVAL 2277.7-2287.4 mbsl; 197.5-207.2 mbsf

UPPER PALEOCENE - LOWER EOCENE															
TIME-ROCK UNIT	BIOSTRAT. ZONE/ FOSSIL CHARACTER					PHYS. PROPERTIES		CHEMISTRY	SECTION	METERS	GRAPHIC LITHOLOGY	DRILLING DISTURB.	SED. STRUCTURES	SAMPLES	LITHOLOGIC DESCRIPTION
FORAMINIFERS	NANNOFOSSILS	RADIOLARIANS	DIATOMS	PALYNOFORMS	PALEOMAGNETICS										
A.G	P4*														
A.MCP8	CP12-CP13														
B															
B															

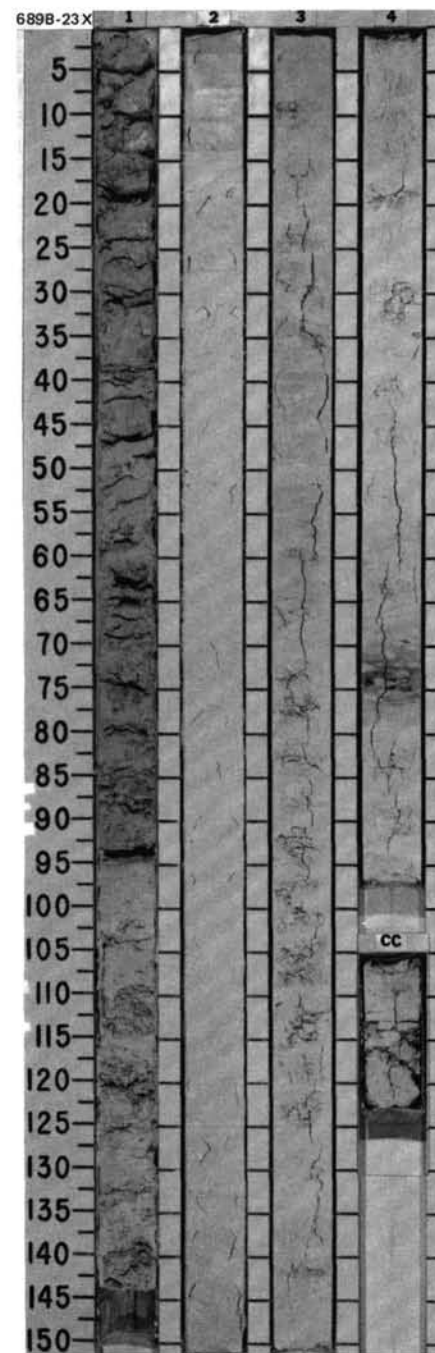


SITE 689 HOLE B CORE 23X CORED INTERVAL 2287.4-2297.1 mbsl; 207.2-216.9 mbsf

UPPER PALEOCENE											TIME-ROCK UNIT		
BIOSTRAT. ZONE/ FOSSIL CHARACTER				PALEOMAGNETICS	PHYS. PROPERTIES	CHEMISTRY	SECTION	METERS	GRAPHIC LITHOLOGY	DRILLING DISTURB. SED. STRUCTURES		SAMPLES	LITHOLOGIC DESCRIPTION
FORAMINIFERS	NANNOFOSSILS	RADIOLARIANS	DIATOMS										
A.G	P3* - P4*			● 43.3%	● 89.5%	● 81.7%	1	0.5 1.0			*	FORAMINIFER-NANNOFOSSIL OOZE/CHALK and FORAMINIFER-BEARING NANNOFOSSIL OOZE/CHALK Major lithologies: Foraminifer-nannofossil ooze/chalk and foraminifer-bearing nannofossil ooze/chalk, white (10YR 8/1); ooze/chalk transition difficult to monitor because of coring "biscuits" throughout Section 1 and present in Sections 2 and 3. Bioturbation is minor, consisting primarily of <i>Zoophycos</i> and <i>Planolites</i> . Minor lithology: Light gray layer (10YR 7/1) in Section 4, 70-80 cm; similar composition, strongly bioturbated. SMEAR SLIDE SUMMARY (%): COMPOSITION: Volcanic glass Tr — Tr — Accessory minerals: Pyrite Tr — Tr — Zeolite Tr — Tr — Foraminifers 25 20 25 15 Nannofossils 75 80 75 85	
A.M	CP8												
B													
B													
B													
CC													

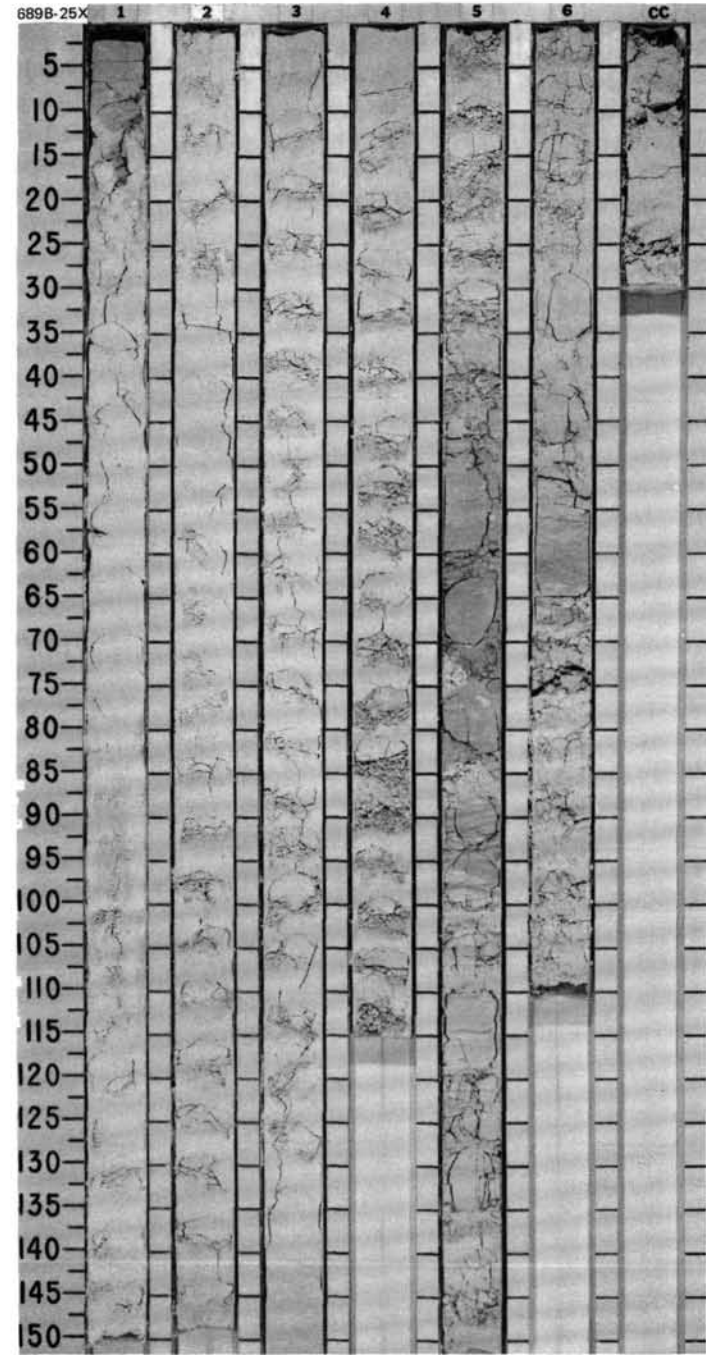
SITE 689 HOLE B CORE 24X CORED INTERVAL 2297.1-2306.8 mbsl; 216.9-226.6 mbsf

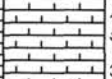

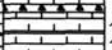
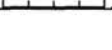
TIME- ROCK UNIT	BIOSTRAT. ZONE/ FOSSIL CHARACTER				CHEMISTRY	SECTION	METERS	GRAPHIC LITHOLOGY	DRILLING DISTURBS.	SED. STRUCTURES	SAMPLES	LITHOLOGIC DESCRIPTION															
	FORAMINIFERS	NANNOFOSSILS	RADIOLARIANS	DIATOMS																							
	PALEOMAGNETICS																										
	PHYS. PROPERTIES																										
	V-1944 ●																										
UPPER PALEOCENE	A.G	UPPER PALEOCENE			● 89.6%	1						FORAMINIFER-BEARING NANNOFOSSIL OOZE/CHALK Major lithology: Foraminifer-bearing nannofossil ooze/chalk, white (10YR 8/0). Chalk/ooze alternations (biscuits). Minor bioturbation in CC (<i>Zoophycos</i>). Minor lithology: Chert, light gray (5Y 7/2), angular, elliptical fragments up to 7 cm long, in Section 1, 8-30 cm. SMEAR SLIDE SUMMARY (%): <table><tr><td></td><td>1, 50</td><td>CC, 25</td></tr><tr><td></td><td>D</td><td>D</td></tr></table> COMPOSITION: <table><tr><td>Foraminifers</td><td>20</td><td>20</td></tr><tr><td>Nannofossils</td><td>65</td><td>80</td></tr><tr><td>Calcspheres</td><td>15</td><td>—</td></tr></table>		1, 50	CC, 25		D	D	Foraminifers	20	20	Nannofossils	65	80	Calcspheres	15	—
	1, 50	CC, 25																									
	D	D																									
Foraminifers	20	20																									
Nannofossils	65	80																									
Calcspheres	15	—																									
	A.M	CP7				CC																					
	B																										
	B																										
	B																										



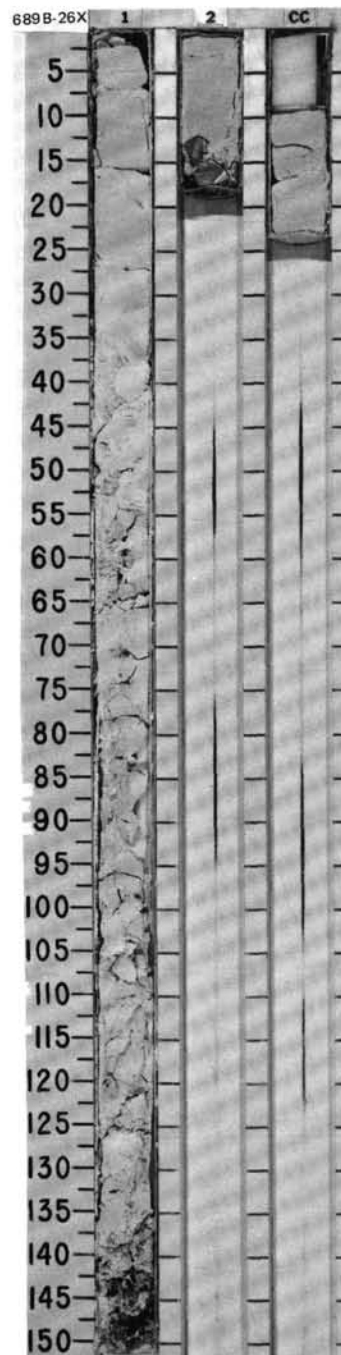
SITE 689 HOLE B CORE 25X CORED INTERVAL 2306.8-2316.5 mbsl; 226.6-236.3 mbsf

TIME-ROCK UNIT		BIOSTRAT. ZONE/ FOSSIL CHARACTER		SECTION	METERS	GRAPHIC LITHOLOGY	DRILLING DISTURB.	SED. STRUCTURES	SAMPLES	LITHOLOGIC DESCRIPTION
UPPER MAESTRICHTIAN	LOWER PALEOCENE	FORAMINIFERS	NANNOFOSSILS							
A.G. ↑	CG	Danian	CP1	1	0.5 1.0				*	FORAMINIFER-BEARING NANNOFOSSIL OOZE/CHALK Major lithology: Foraminifer-bearing nannofossil ooze/chalk, white (10YR 8/0). Ooze/chalk transition: coring "biscuits" in all sections. Minor bioturbation includes <i>Zoophycos</i> , <i>Chondrites</i> , and <i>Planolites</i> . Up to 10% calcispheres are present. Minor lithology: Slightly ashy foraminifer-bearing nannofossil ooze/chalk, white (5Y 8/1). Moderate bioturbation (mainly <i>Zoophycos</i>), in Section 5, 35-80 cm.
A.M. ↑	A.M.	CP3 - 4	CP7							
B				2					*	SMEAR SLIDE SUMMARY (%): COMPOSITION: Quartz — Tr — — — — — Calcite/dolomite — Tr — — — — — Accessory minerals 4 — — — — — 8 Tr Opal 5 Tr Tr Tr — — — Chlorite Tr — — — — — — Zeolite — Tr Tr — — — — Foraminifers 10 10 15 15 10 15 10 Nannofossils 81 80 75 75 80 72 85 Calcispheres — 10 10 10 10 5 5
B										
B				3					*	
B										
B				4					*	
B										
B				5					*	
B										
B				6					*	
B										
CC										

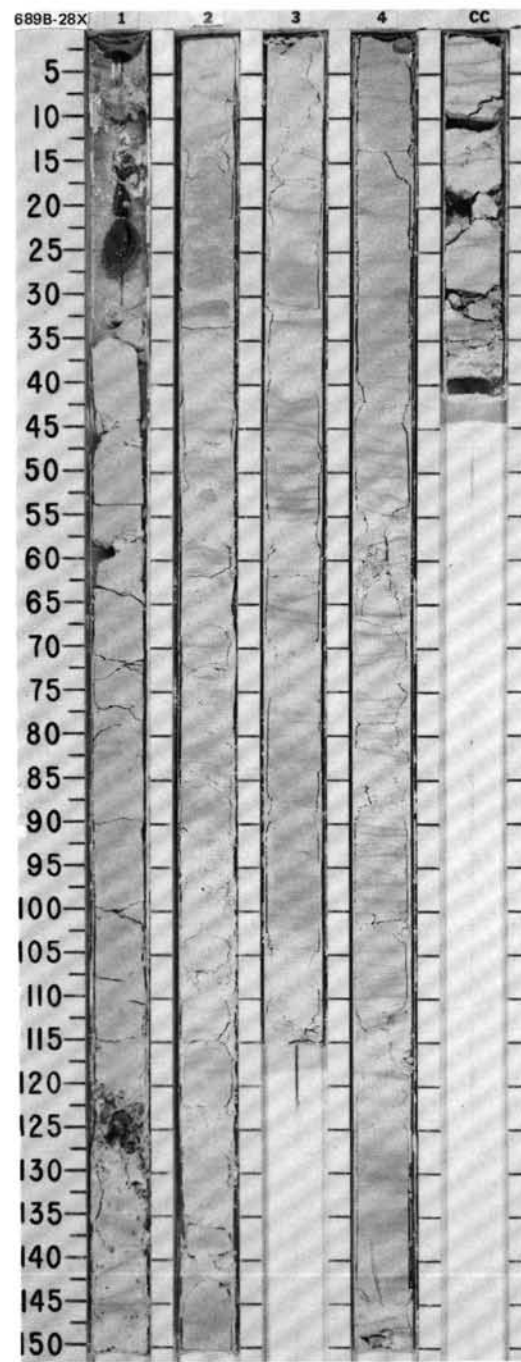


SITE		689		HOLE B		CORE 26X		CORED INTERVAL		236.5 - 2326.2 mbsl; 236.3 - 246.0 mbsl																
TIME-ROCK UNIT	BIOSTRAT. ZONE/ FOSSIL CHARACTER				PHYS. PROPERTIES	CHEMISTRY	SECTION	METERS	GRAPHIC LITHOLOGY	DRILLING DISTURB. SED. STRUCTURES	SAMPLES	LITHOLOGIC DESCRIPTION														
	FORAMINIFERS	NANNOFOSSILS	RADIOLARIANS	DIAZONIS																						
UPPER MAESTRICHTIAN	A.G	<i>Abathomphalus Mayaroensis</i> ZONE			V-1834 ●							<p>NANNOFOSSIL CHALK</p> <p>Major lithology: Nannofossil chalk, white (10YR 8/0), moderately bioturbated where core is not too disturbed (<i>Chondrites</i> and <i>Zoophycos</i>). Most nannofossils are recrystallized.</p> <p>Minor lithology: Chert as fragments 3-6 cm long, dark yellowish brown (10YR 3/4), and angular with conchoidal fractures at base of Section 1; and as fragments 1-3 cm long, angular, and light olive gray (5Y 6/2) at base of Section 2.</p> <p>SMEAR SLIDE SUMMARY (%):</p> <p style="text-align: right;">1, 50 D</p> <p>COMPOSITION:</p> <table><tr><td>Feldspar</td><td>Tr</td></tr><tr><td>Accessory minerals:</td><td></td></tr><tr><td>Zeolite</td><td>3</td></tr><tr><td>Recrystallized carbonate</td><td>50</td></tr><tr><td>Foraminifers</td><td>2</td></tr><tr><td>Nannofossils</td><td>40</td></tr><tr><td>Calcspheres</td><td>5</td></tr></table>	Feldspar	Tr	Accessory minerals:		Zeolite	3	Recrystallized carbonate	50	Foraminifers	2	Nannofossils	40	Calcspheres	5
	Feldspar	Tr																								
	Accessory minerals:																									
	Zeolite	3																								
	Recrystallized carbonate	50																								
Foraminifers	2																									
Nannofossils	40																									
Calcspheres	5																									
A.M	<i>Nephrolithus frequens</i> ZONE				1	0.5		*																		
B						1.0																				
B					2																					
B					CC																					

SITE		689	HOLE	B	CORE	27X	CORED INTERVAL		2326.2-2335.8 mbsl; 246.0-255.6 mbsf				
TIME-ROCK UNIT	BIOSTRAT. ZONE/ FOSSIL CHARACTER				PHYS. PROPERTIES	CHEMISTRY	SECTION	METERS	GRAPHIC LITHOLOGY	DRILLING DISTURB.	SED. STRUCTURES	SAMPLES	LITHOLOGIC DESCRIPTION
	FORAMINIFERS	NANNOFOSSILS	RADICULARIANS	DIATOMS									
	PALYNOFORMS												
UPPER MAESTRICHTIAN													
A.G	<i>Abathomphalus mayoreus</i> Zone				● V-1864		1	0.5				*	FORAMINIFER-BEARING NANNOFOSSIL CHALK Major lithology: Foraminifer-bearing nannofossil chalk, white (5Y 8/1). Minor to strong bioturbation, including <i>Zoophycos</i> and <i>Chondrites</i> . Nannofossils are recrystallized.
A.M	<i>Nephrolithus frequens</i> Zone							1.0					
B													
B					● V-1942		2				*	SMEAR SLIDE SUMMARY (%): COMPOSITION: Accessory minerals Tr — — Zeolite 2 2 — Foraminifers 15 20 25 Nannofossils 83 78 75 Diatoms — — Tr	
B													
B							3				*		

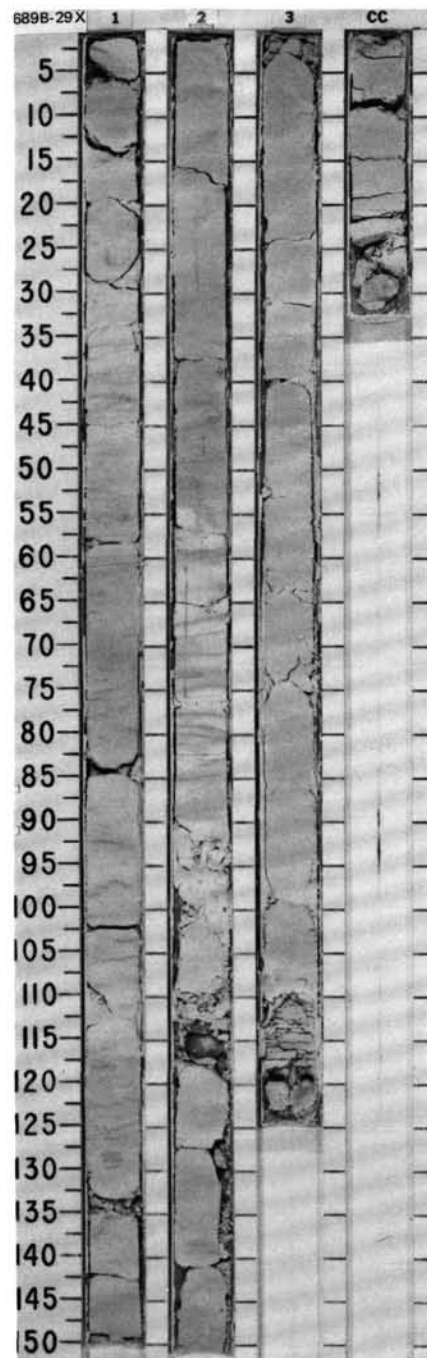


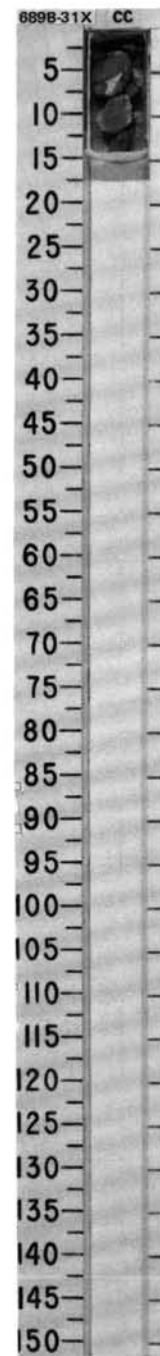
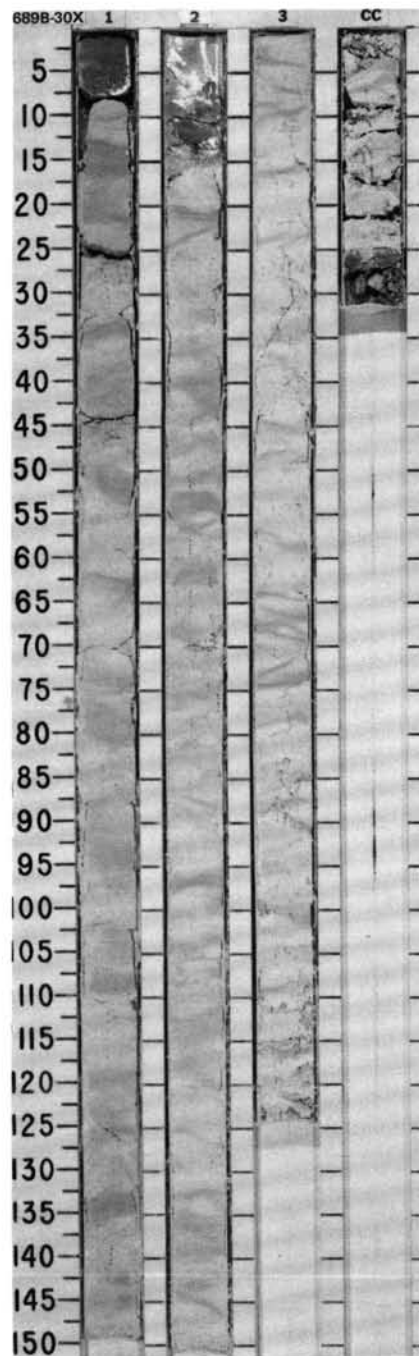
SITE 689 HOLE B CORE 28X CORED INTERVAL 2335.8-2345.4 mbsl; 255.6-265.2 mbsf																																														
TIME-ROCK UNIT	BIOSTRAT. ZONE/ FOSSIL CHARACTER				SECTION	METERS	GRAPHIC LITHOLOGY	DRILLING DISTURB.	SED. STRUCTURES	SAMPLES	LITHOLOGIC DESCRIPTION																																			
	FORAMINIFERS	NANNOFOSSILS	RADIOLARIANS	DIATOMS																																										
				PALYNOMORPHS																																										
				PALEOMAGNETICS																																										
				PHYS. PROPERTIES																																										
				CHEMISTRY																																										
LOWER to MIDDLE MAESTRICHTIAN																																														
A.G	Maestrichtian				1	0.5	VOID	X		*	FORAMINIFER-BEARING NANNOFOSSIL CHALK and FORAMINIFER-NANNOFOSSIL CHALK Major lithologies: Foraminifer-bearing and foraminifer-nannofossil chalk, white (5Y 8/1); bioturbation-induced mottles mix the white with light gray (5Y 7/1). Primarily strong bioturbation, mainly <i>Zoophycos</i> and <i>Chondrites</i> . Foraminifer content increases downcore. Minor lithologies: Chert, dark yellowish brown (10YR 3/4), Section 1, top and 121-130 cm. Altered volcanic ash(?) foraminifer-nannofossil chalk, greenish gray (5GY 6/1), occurs in laminae in Section 2, 50, 60, 70, 130, and 145 cm; Section 3, 50, 55, 65, 83, and 100 cm; and Section 4, 130-142 cm. SMEAR SLIDE SUMMARY (%): <table><tr><td></td><td>1, 50 D</td><td>2, 50 D</td><td>3, 55 M</td><td>4, 50 D</td></tr><tr><td>Quartz</td><td>Tr</td><td>Tr</td><td>3</td><td>1</td></tr><tr><td>Accessory minerals:</td><td></td><td></td><td></td><td></td></tr><tr><td> Epidote</td><td>—</td><td>Tr</td><td>Tr</td><td>—</td></tr><tr><td> Foraminifers</td><td>15</td><td>20</td><td>25</td><td>40</td></tr><tr><td> Nannofossils</td><td>85</td><td>80</td><td>72</td><td>59</td></tr><tr><td> Radiolarians</td><td>Tr</td><td>—</td><td>—</td><td>—</td></tr></table>		1, 50 D	2, 50 D	3, 55 M	4, 50 D	Quartz	Tr	Tr	3	1	Accessory minerals:					Epidote	—	Tr	Tr	—	Foraminifers	15	20	25	40	Nannofossils	85	80	72	59	Radiolarians	Tr	—	—	—
	1, 50 D	2, 50 D	3, 55 M	4, 50 D																																										
Quartz	Tr	Tr	3	1																																										
Accessory minerals:																																														
Epidote	—	Tr	Tr	—																																										
Foraminifers	15	20	25	40																																										
Nannofossils	85	80	72	59																																										
Radiolarians	Tr	—	—	—																																										
C.P	Biscutum magnum Zone				1.0		X																																							
B					2		X		*																																					
B							X																																							
B					3		X		*																																					
B							X																																							
					4		X		*																																					
							X																																							
					CC		X		*																																					
							X																																							

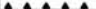


SITE 689 HOLE B CORE 29X CORED INTERVAL 2345.4-2355.1 mbsl; 265.2-274.9 mbsf

TIME-ROCK UNIT	BIOSTRAT. ZONE/ FOSSIL CHARACTER				SECTION	METERS	GRAPHIC LITHOLOGY	DRILLING DISTURB.	SED. STRUCTURES	SAMPLES	LITHOLOGIC DESCRIPTION
	FORAMINIFERS	NANNOFOSSILS	RADIOLARIANS	DIAZONES							
UPPER CAMPANIAN (?) TO LOWER MAESTRICHIAN	A, G	Maestrichtian									
	A, M	Biscutum magnum Zone									
	B										
	B										
	B										



[illegible]

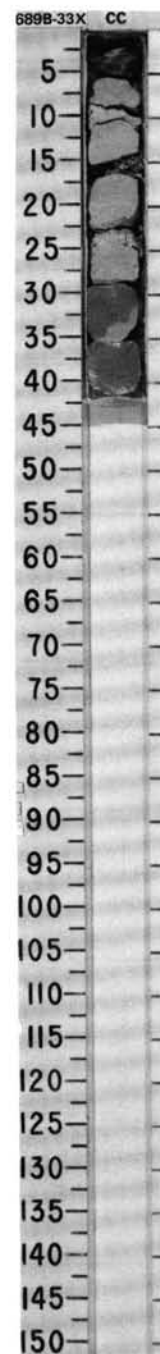
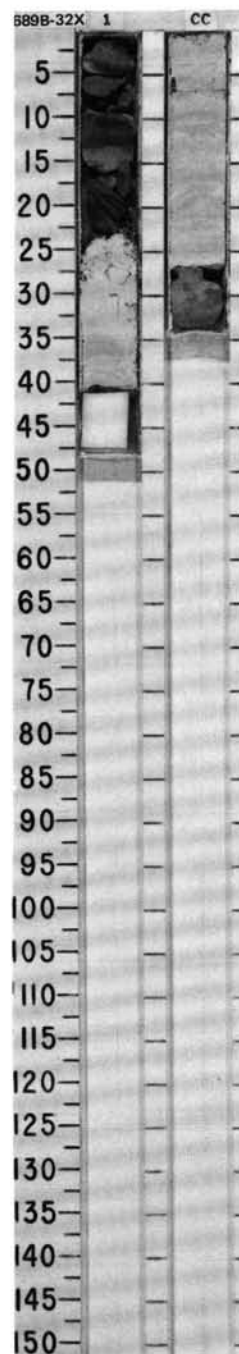
UPPER CAMPANIAN (?) to LOWER MAESTRICHTIAN	TIME-ROCK UNIT		BIOSTRAT. ZONE/ FOSSIL CHARACTER				GRAPHIC LITHOLOGY	DRILLING DISTURB. SED. STRUCTURES	SAMPLES	LITHOLOGIC DESCRIPTION
	FORAMINIFERS		NANNOFOSSILS		RADIOLARIANS	DIATOMS				
	PALYNOMORPHS									
	PHYS. PROPERTIES									
	CHEMISTRY		SECTION		METERS					
	A.G <i>Maestrichtian</i>		A.M <i>Biscutum caronum</i> Zone					X		CHERT Major lithology: Chert, gray (5Y 6/1), angular fragments. One piece has a small amount of chalk adhering to it.
	B		B							

SITE 689 HOLE B CORE 32X CORED INTERVAL 2371.0-2374.5 mbsl; 290.8-294.3 mbsf

TIME-ROCK UNIT	BIOSTRAT. ZONE/ FOSSIL CHARACTER				PHYS. PROPERTIES	CHEMISTRY	SECTION	METERS	GRAPHIC LITHOLOGY	DRILLING DISTURB. BED. STRUCTURES	SAMPLES	LITHOLOGIC DESCRIPTION
	FORAMINIFERS	NANNOFOSSILS	RADIOLARIANS	DIATOMS								
UPPER CAMPANIAN (?) to LOWER MAESTRICHTIAN	A, G				● 90.0%		1					NANNOFOSSIL CHALK Major lithology: Nannofossil chalk, white (2.5Y 8/0, 8/1) and light gray (5Y 7/1). Faint laminae, which may be due to drilling disturbance. Minor lithology: Chert, greenish gray (5GY 5/1, 6/1) and light greenish gray (5GY 7/1). Burrow-mottled, including <i>Zoophycos</i> ; diffuse, thinly bedded in Section 1. SMEAR SLIDE SUMMARY (%): COMPOSITION: Quartz Nannofossils
	<i>Maestrichtian</i>						0.5					
	<i>Biscutum coronum</i> Zone	A, M										
		B										
	B											
	B											

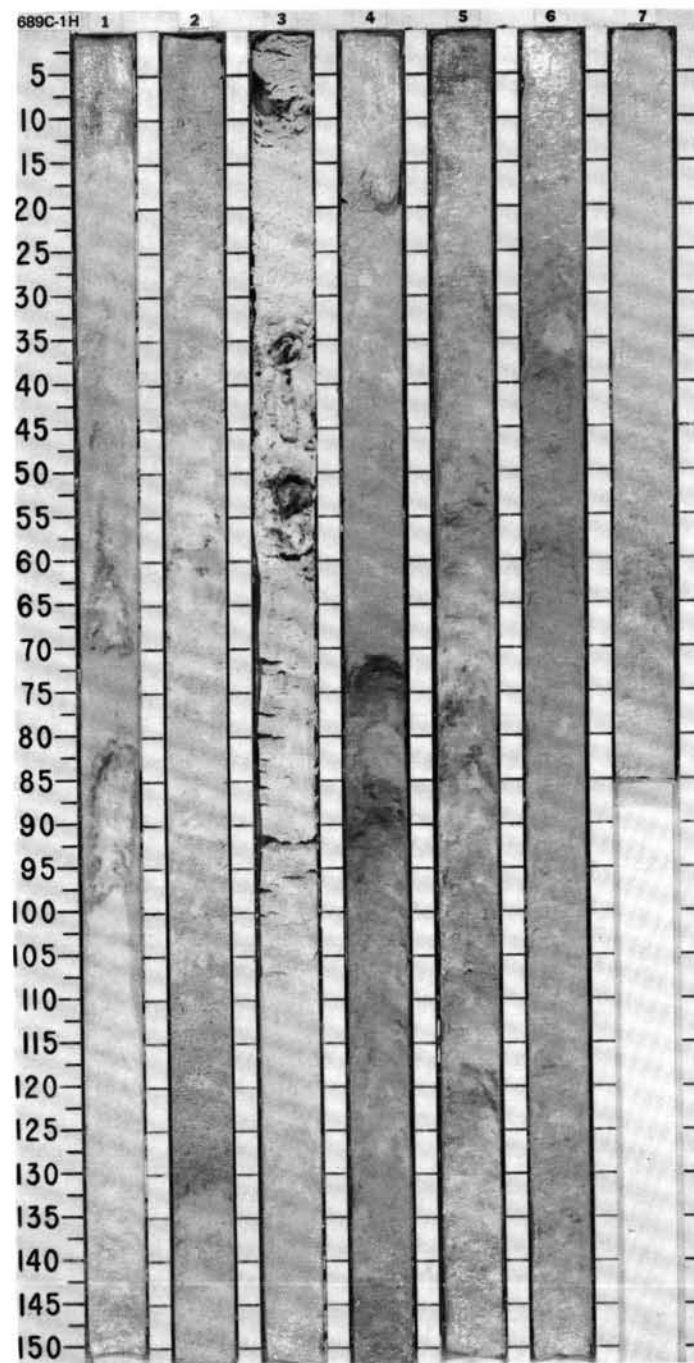
SITE 689 HOLE B CORE 33X CORED INTERVAL 2374.5-2377.5 mbsl; 294.3-297.3 mbsf

TIME-ROCK UNIT	BIOSTRAT. ZONE/ FOSSIL CHARACTER				PHYS. PROPERTIES	CHEMISTRY	SECTION	METERS	GRAPHIC LITHOLOGY	DRILLING DISTURB.	BED. STRUCTURES	SAMPLES	LITHOLOGIC DESCRIPTION
	FORAMINIFERS	NANNOFOSSILS	RADIOLARIANS	DIATOMS									
UPPER CAMPANIAN (?) to LOWER MAESTRICHTIAN	A, G						CC						<p>NANNOFOSSIL CHALK</p> <p>Major lithology: Nannofossil chalk, white (2.5Y 8/0, 8/1) and light gray (5Y 7/1).</p> <p>Minor lithology: Chert, greenish gray (5GY 5/1, 6/1) and light greenish gray (5GY 7/1).</p>
	<i>Maestrichtian</i>												
		A, M											
		A, M	B	B									

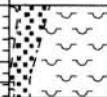


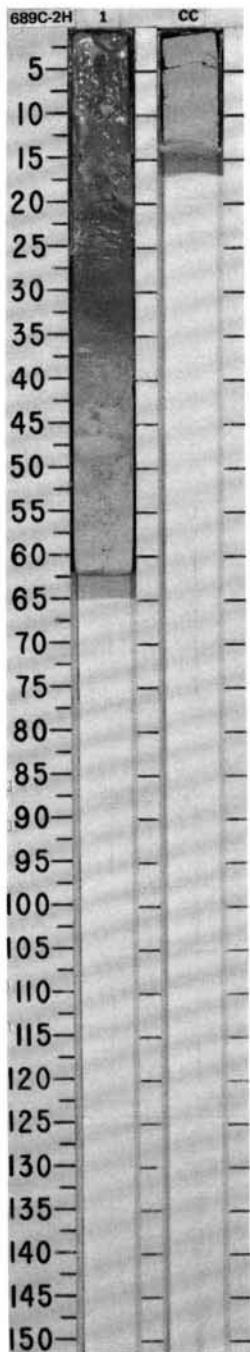
SITE 689 HOLE C CORE 1H CORED INTERVAL 2080.2-2088.8 mbsl; 0-8.6 mbsf

TIME-ROCK UNIT	BIOSTRAT. ZONE/ FOSSIL CHARACTER				SECTION METERS	GRAPHIC LITHOLOGY	DRILLING DISTURB.	SED. STRUCTURES	SAMPLES	LITHOLOGIC DESCRIPTION	
	FORAMINIFERS	NANNOFOSSILS	RADIOLARIANS	DIATOMS							PALYNOFOSPHS
PHYS. PROPERTIES											
LOWER PLIOCENE					5.1% ●						
					0.3% ●				*		
									*		
					0.3% ●						
					0.2% ●				*		
					0.3% ●				*		
					0.3% ●				*		
					0.3% ●				*		
					0.3% ●				*		
					0.3% ●				*		



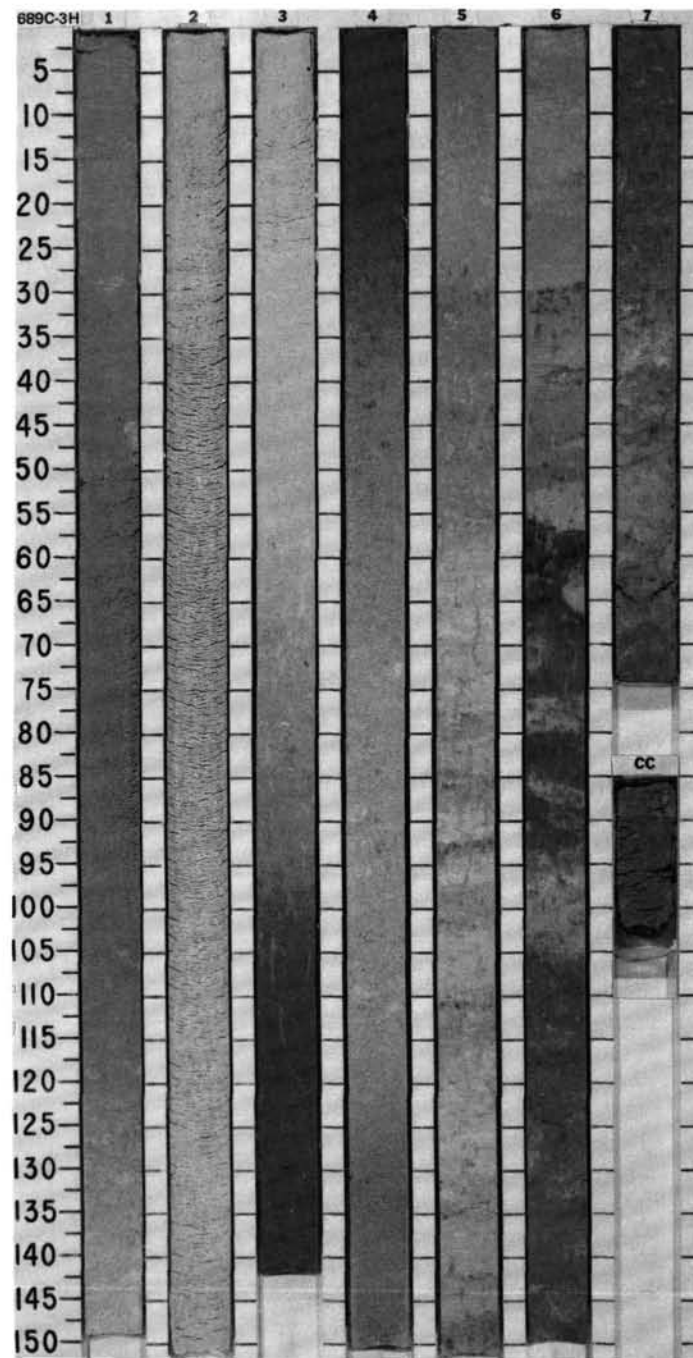
SITE 689 HOLE C CORE 2H CORED INTERVAL 2088.8-2098.3 mbsl; 8.6-18.1 mbsf

TIME- ROCK UNIT	BIOSTRAT. ZONE/ FOSSIL CHARACTER					GRAPHIC LITHOLOGY	DRILLING DISTURB.	SED. STRUCTURES	SAMPLES	LITHOLOGIC DESCRIPTION
	FORAMINIFERS									
	NANNOFOSSILS									
	RADIOLARIANS									
	DIATOMS									
LOWER PLIOCENE	PALYNOFORMS									RADIOLARIAN- AND SILICOFAGELLATE-BEARING DIATOM OOZE
	PALEOMAGNETICS									
	PHYS. PROPERTIES									
	CHEMISTRY									
	SECTION									
	METERS									
	● 0.2%									
	B								*	
	B								*	
	A.G								*	
	LOWER Upson								*	
	N. angulata - N. reinholdii								*	
	B								*	



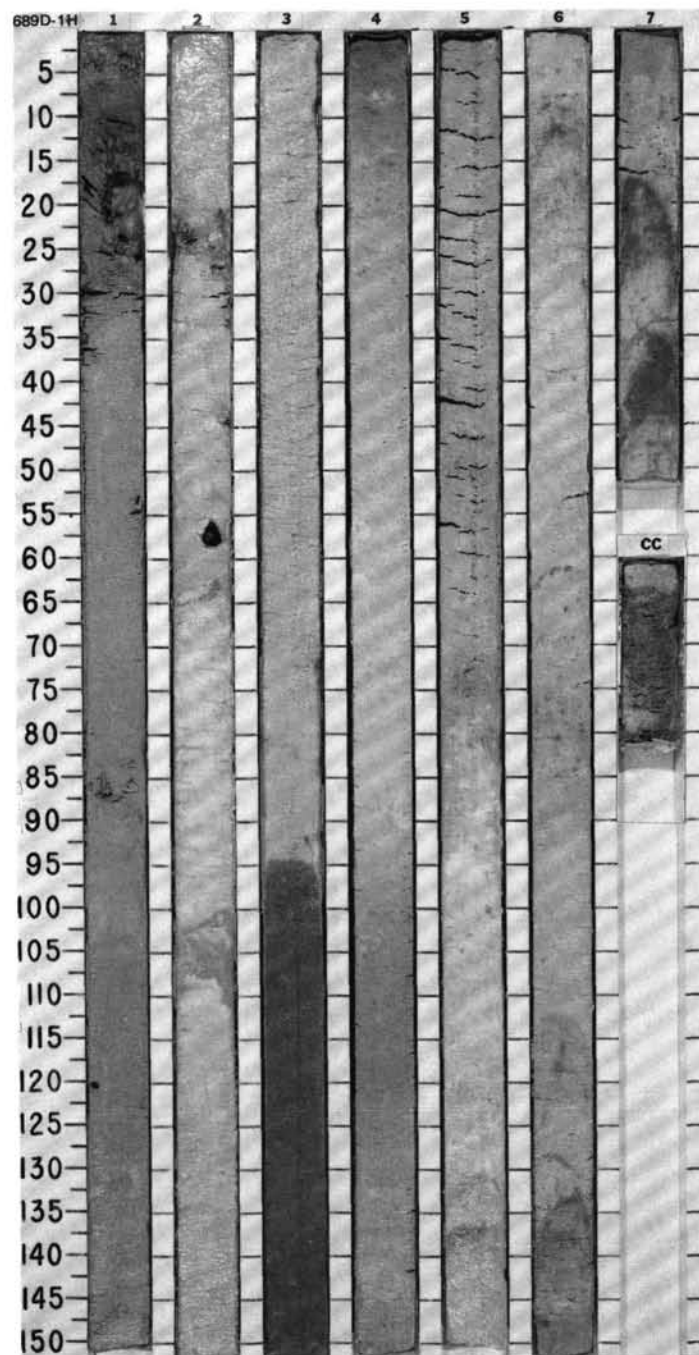
SITE 689 HOLE C CORE 3H CORED INTERVAL 2098.3-2107.8 mbsl; 18.1-27.1 mbsf

UPPER MIOCENE													
TIME-ROCK UNIT	BIOSTRAT. ZONE/ FOSSIL CHARACTER				PHYS. PROPERTIES	CHEMISTRY	SECTION	METERS	GRAPHIC LITHOLOGY	DRILLING DISTURB.	SED. STRUCTURES	SAMPLES	LITHOLOGIC DESCRIPTION
FORAMINIFERS	NANNOFOSSILS	RADIOLARIANS	DIATOMS	PALYNOMORPHS									
UPPER C. spongothorax													
D. hustedtii													



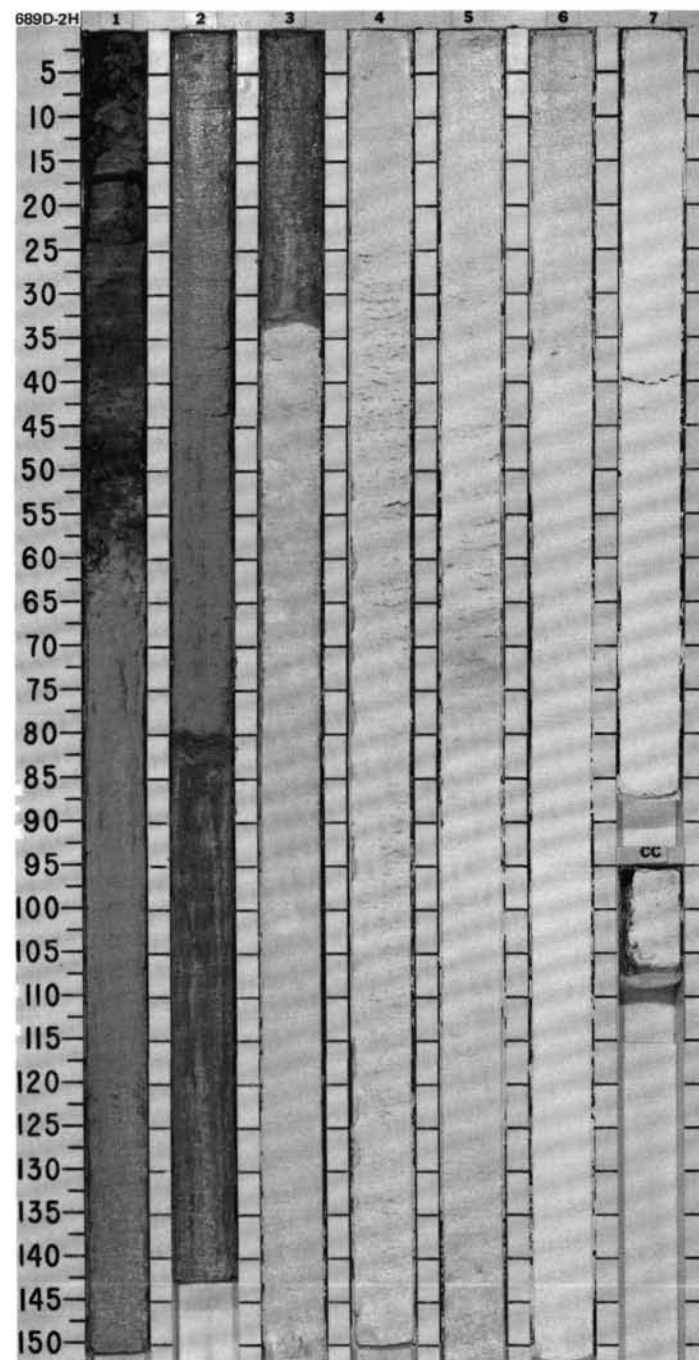
SITE 689 HOLE D CORE 1H CORED INTERVAL 2098.3-2107.8 mbsl; 18.1-27.6 mbsf

TIME-ROCK UNIT	BIOSTRAT. ZONE/ FOSSIL CHARACTER	SECTION	METERS	GRAPHIC LITHOLOGY	DRILLING DISTURB.	SAMPLES	LITHOLOGIC DESCRIPTION
UPPER MIOCENE							
	FORAMINIFERS						
	NANNOFOSSILS						
	RADIOLARIANS						
	DIATOMS						
	PALYNOMORPHS						
	PALEOMAGNETICS						
	PHYS. PROPERTIES						
	CHEMISTRY						
		1	0.5 1.0			*	DIATOM OOZE, NANNOFOSSIL-BEARING DIATOM OOZE, and DIATOM-NANNOFOSSIL OOZE Major lithologies: Diatom ooze, white (5Y 8/1) to pure white (10YR 8/0) in Section 2 grading to light olive brown (2.5Y 5/3) in Section 3, white (2.5Y 8/2) to white (10YR 8/0) in Section 5 grading to pale brown (10YR 6/3) in Section 6, with very white (10YR 8/0) intercalations. Nannofossil-bearing diatom ooze, light gray (10YR 7/1). Diatom-nannofossil ooze, white (10YR 8/2) grading to light gray (2.5Y 7/2). Minor lithology: Chert, as fragments, in Sections 1 and 2. Dropstones occur in Section 1, 120 cm, as a 9-mm-long granitic rock with lots of pink feldspar, and in Section 2, 58 cm, as a 3-cm-long stone. SMEAR SLIDE SUMMARY (%): COMPOSITION: Clay — — — — — Accessory minerals — — — — — Hornblende — — — — — Foraminifers — — — — — Nannofossils 20 2 2 55 5 2 2 Diatoms 73 85 86 39 90 94 93 Radiolarians 5 8 5 4 3 3 3 Sponge spicules 2 — — — — — Silicoflagellates — 5 2 1 2 — 2 Plant debris — — — — —
		2				*	
		3				*	
		4				*	
		5				*	
		6				*	
		7				*	
		CC					



TIME-ROCK UNIT	BIOSTRAT. ZONE/ FOSSIL CHARACTER				SECTION METERS	GRAPHIC LITHOLOGY	DRILLING DISTURB. SED. STRUCTURES SAMPLES	LITHOLOGIC DESCRIPTION				
	FORAMINIFERS	NANNOFOSSILS	RADIOLARIANS	DIATOMS								
PALEOMAGNETICS	PHYS. PROPERTIES	CHEMISTRY										

UPPER MIOCENE	A.G	no zone	1	0.5 1.0		*	DIATOM OOOZE, RADIOLARIAN-BEARING DIATOM OOOZE, and DIATOM-NANNOFOSSIL OOOZE Major lithologies: Diatom ooze, white (2.5Y 8/2). Radiolarian-bearing diatom ooze, pale brown (10YR 6/3) in Section 1, and white (2.5Y 8/2) to pale yellow (2.5Y 7/3) in Section 2. Diatom-nannofossil ooze, pure white (10YR 8/0). Minor lithology: Chert fragments in Section 1. Bioturbation is primarily absent, although in local occurrences it is moderate. <i>Planolites</i> is observed. Several sharp color changes occur and may be due to coring disturbance. SMEAR SLIDE SUMMARY (%): <table><tr><td></td><td>1, 100 D</td><td>2, 100 D</td><td>3, 50 D</td><td>4, 50 D</td><td>5, 50 D</td><td>6, 50 D</td><td>7, 50 D</td></tr><tr><td>COMPOSITION:</td><td></td><td></td><td></td><td></td><td></td><td></td><td></td></tr><tr><td>Accessory minerals</td><td>Tr</td><td>Tr</td><td>—</td><td>—</td><td>—</td><td>—</td><td>—</td></tr><tr><td>Nannofossils</td><td>—</td><td>—</td><td>65</td><td>60</td><td>60</td><td>70</td><td>54</td></tr><tr><td>Diatoms</td><td>95</td><td>85</td><td>35</td><td>40</td><td>40</td><td>30</td><td>40</td></tr><tr><td>Radiolarians</td><td>5</td><td>15</td><td>Tr</td><td>Tr</td><td>—</td><td>—</td><td>5</td></tr><tr><td>Silicoflagellates</td><td>—</td><td>—</td><td>—</td><td>—</td><td>—</td><td>—</td><td>1</td></tr></table>		1, 100 D	2, 100 D	3, 50 D	4, 50 D	5, 50 D	6, 50 D	7, 50 D	COMPOSITION:								Accessory minerals	Tr	Tr	—	—	—	—	—	Nannofossils	—	—	65	60	60	70	54	Diatoms	95	85	35	40	40	30	40	Radiolarians	5	15	Tr	Tr	—	—	5	Silicoflagellates	—	—	—	—	—	—	1
		1, 100 D	2, 100 D	3, 50 D				4, 50 D	5, 50 D	6, 50 D	7, 50 D																																																				
	COMPOSITION:																																																														
	Accessory minerals	Tr	Tr	—				—	—	—	—																																																				
	Nannofossils	—	—	65				60	60	70	54																																																				
	Diatoms	95	85	35				40	40	30	40																																																				
	Radiolarians	5	15	Tr				Tr	—	—	5																																																				
Silicoflagellates	—	—	—	—	—	—	1																																																								
A.G	LOWER C. <i>Spongothorax</i>	2																																																													
C.M	<i>D. hustedtii</i> <i>D. lauta</i> - <i>N. deulicoides</i>	3																																																													
B		4																																																													
		5																																																													
		6																																																													
		7																																																													

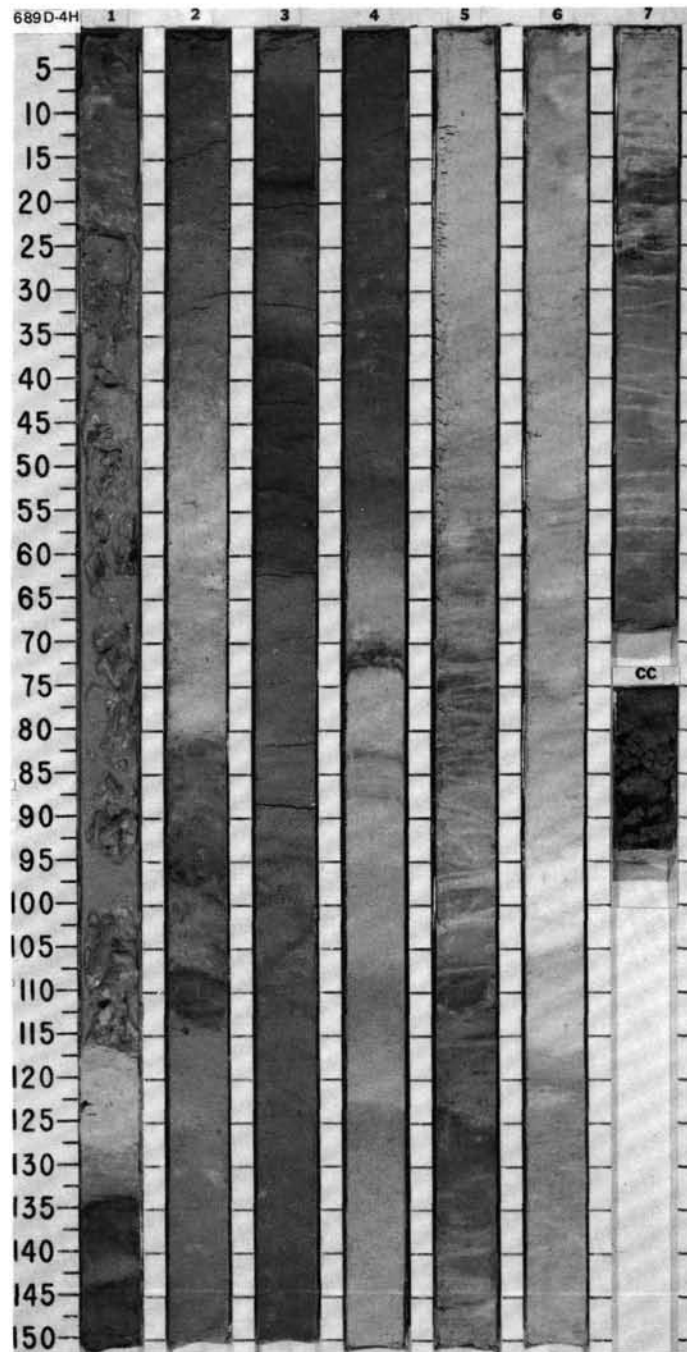


SITE 689 HOLE D CORE 4H CORED INTERVAL 2127.2-2136.9 mbsl; 47.0-56.2 mbsf

TIME-ROCK UNIT	BIOSTRAT. ZONE/ FOSSIL CHARACTER	SECTION	METERS	GRAPHIC LITHOLOGY	DRILLING DISTURB.	SED. STRUCTURES	SAMPLES	LITHOLOGIC DESCRIPTION
	FORAMINIFERS							
	NANNOFOSSILS							
	RADIOLARIANS							
	DIATOMS							
	PALYNOMORPHS							
	PALEOMAGNETICS							
	PHYS. PROPERTIES							
	CHEMISTRY							
		1	0.5 1.0					DIATOM-NANNOFOSSIL OOZE, NANNOFOSSIL-BEARING DIATOM OOZE, NANNOFOSSIL-DIATOM OOZE, and DIATOM OOZE Major lithologies: Diatom-nannofossil ooze, white (2.5Y 8/2) to light brownish gray (2.5Y 6/2). Nannofossil-bearing diatom ooze, light gray (10YR 7/1 to 2.5Y 7/2) to light brownish gray (2.5Y 6/2). Nannofossil-diatom ooze, light gray (10YR 7/2 to 2.5Y 7/2) to pale brown (2.5Y 6/3). Diatom ooze, white (2.5Y 8/2) and light gray (2.5Y 7/2) to light yellowish brown (2.5Y 6/3). Minor lithology: Radiolarian-diatom ooze, light gray (2.5Y 7/2) to light brownish gray (2.5Y 6/2), with a darker layer (grayish brown, 2.5Y 5/2), in Section 7. Bioturbation is minor to moderate. Specific types include halo burrows, vertical burrows, <i>Chondrites</i> , <i>Planolites</i> , and <i>Zoophycos</i> . <i>Zoophycos</i> is particularly abundant in Section 5. Darker layers are present, but with no obvious lithologic color change.
		2						
		3						
		4						
		5						
		6						
		7						
		CC						

SMEAR SLIDE SUMMARY (%):

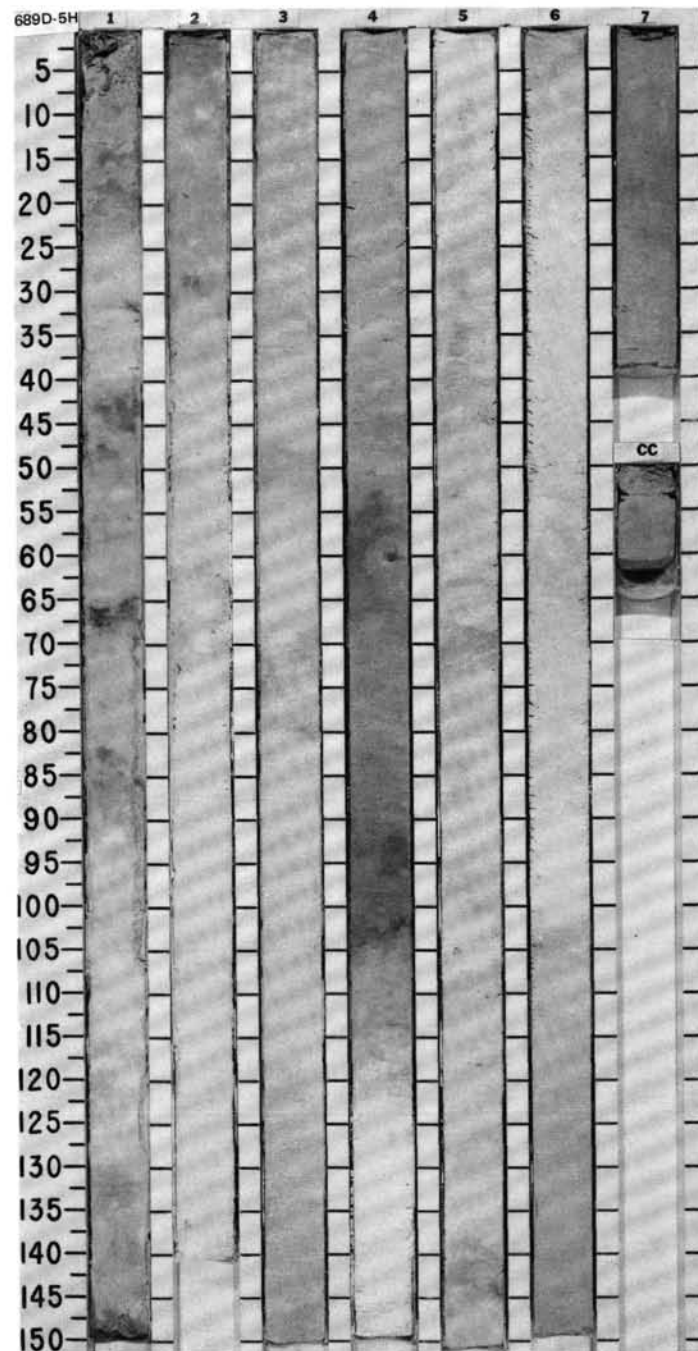
	1, 122 D	2, 96 D	3, 3 D	4, 76 D	5, 10 D	6, 98 D	7, 38 D
COMPOSITION:							
Volcanic glass	—	—	—	—	—	—	5
Accessory minerals	Tr	Tr	Tr	Tr	Tr	Tr	—
Foraminifers	—	—	—	—	—	—	—
Nannofossils	55	10	5	—	45	25	—
Diatoms	40	82	90	95	55	75	50
Radiolarians	5	8	5	5	—	—	45
Silicoflagellates	—	—	—	Tr	—	—	—

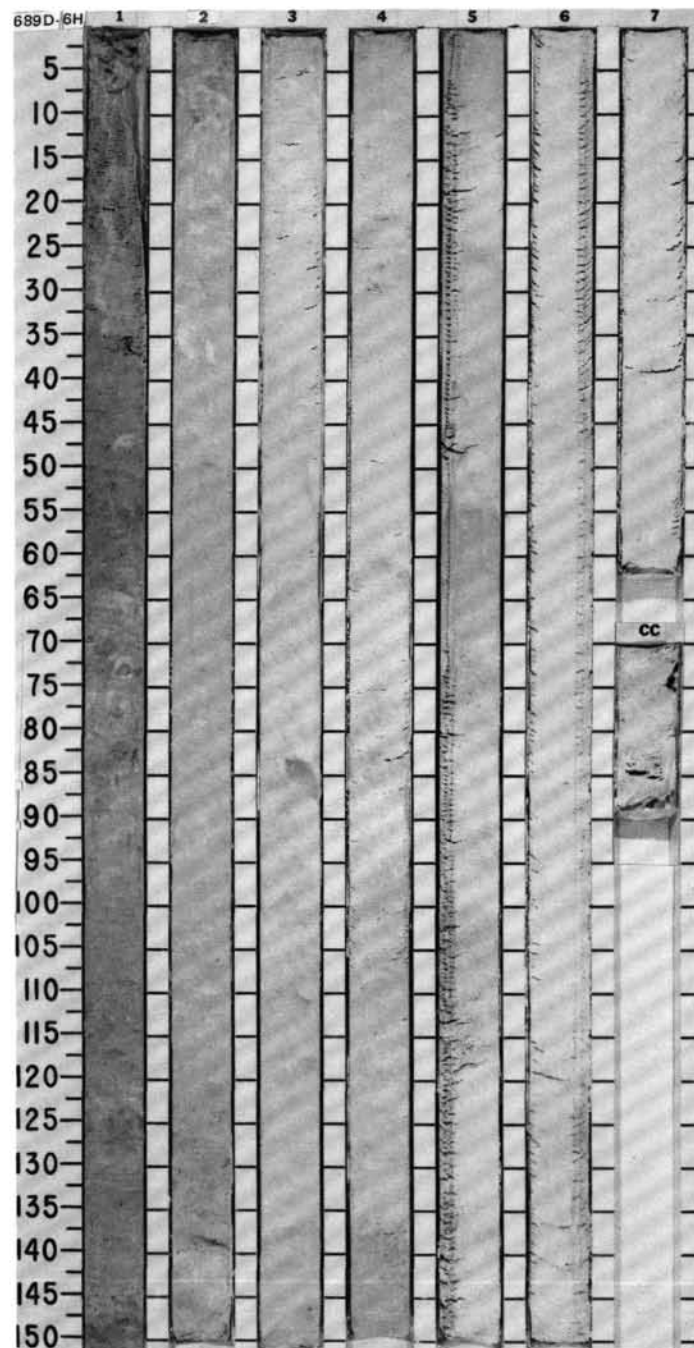


SITE 689

SITE 689 HOLE D CORE 5H CORED INTERVAL 2136.9-2146.6 mbsl; 56.7-66.4 mbsf

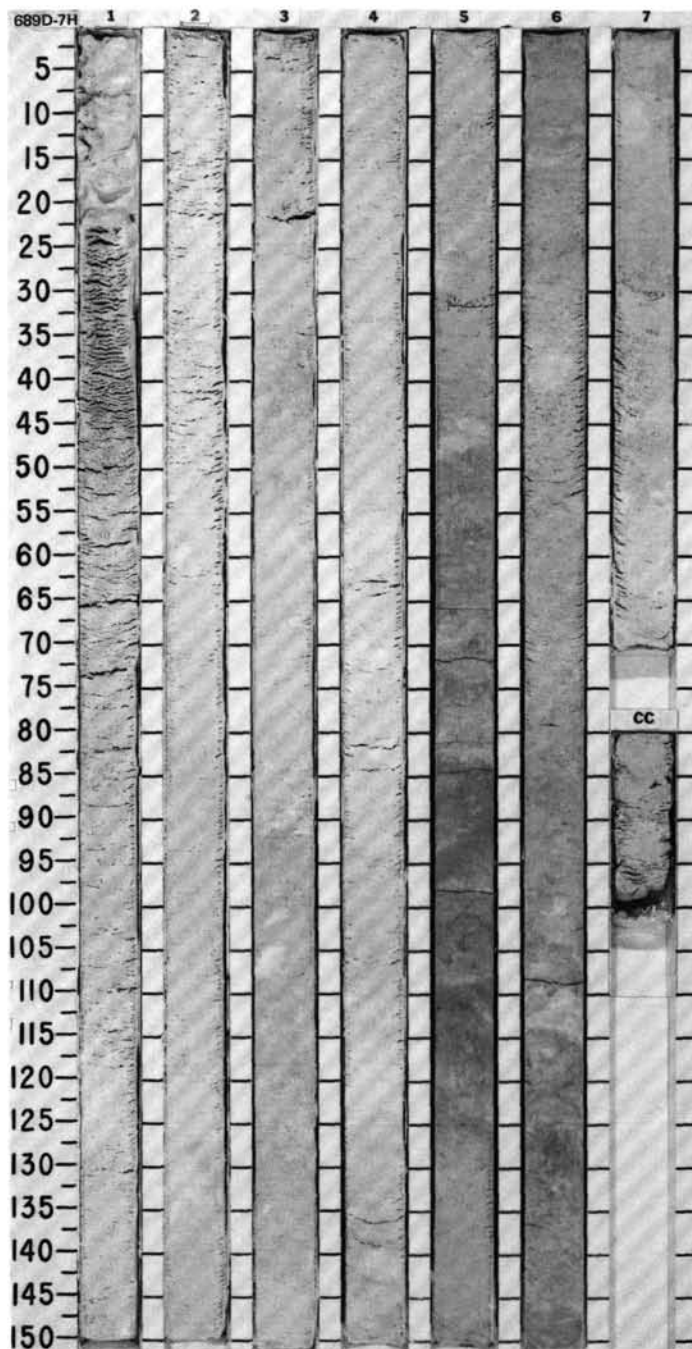
TIME-ROCK UNIT	BIOSTRAT. ZONE/ FOSSIL CHARACTER	FORAMINIFERS	NANNOFOSSILS	RADIOLARIANS	DIATOMS	PALYNOFORMS	PALEOMAGNETICS	PHYS. PROPERTIES	CHEMISTRY	SECTION	METERS	GRAPHIC LITHOLOGY	DRILLING DISTURB.	SED. STRUCTURES	SAMPLES	LITHOLOGIC DESCRIPTION
LOWER MIOCENE	no zone LOWER MIOCENE <i>N. maleinterpretaria - C. rhombicus</i>	F, G A, M C, M B								1	0.5 1.0				* 	

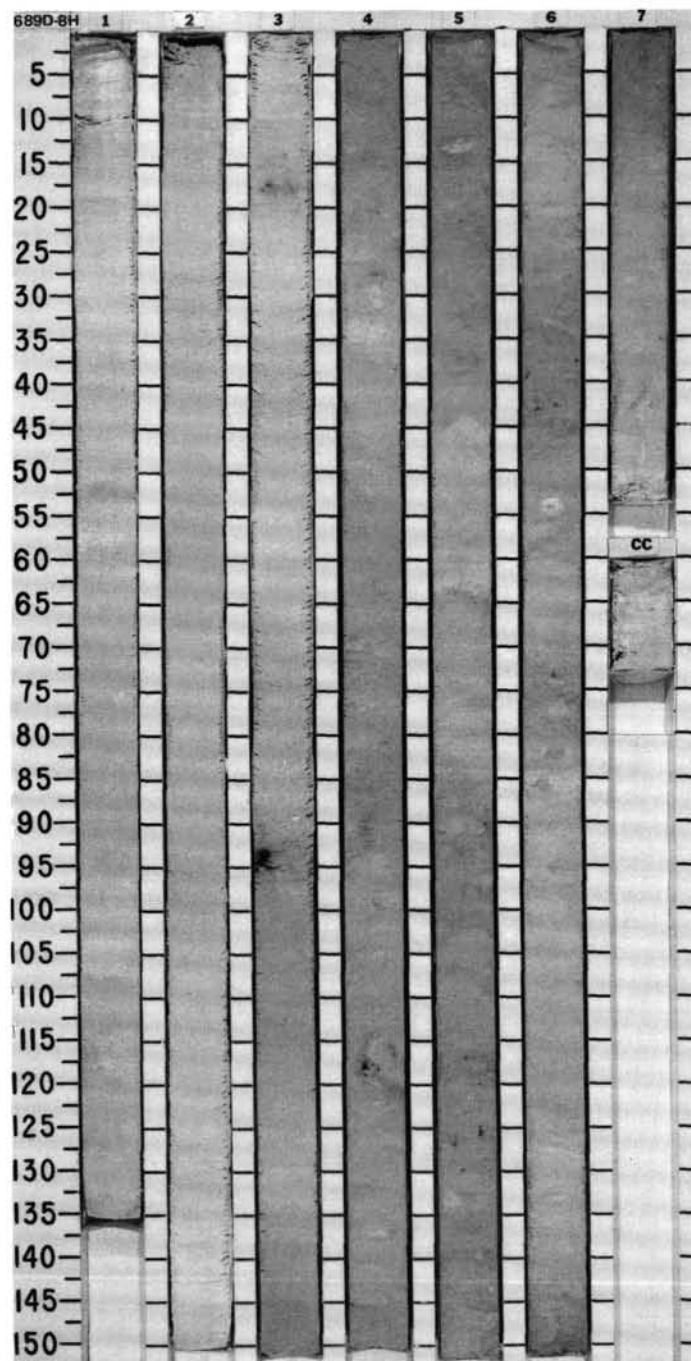




SITE 689 HOLE D CORE 7H CORED INTERVAL 2156.2-2165.8 mbsl; 76.0-85.6 mbsf

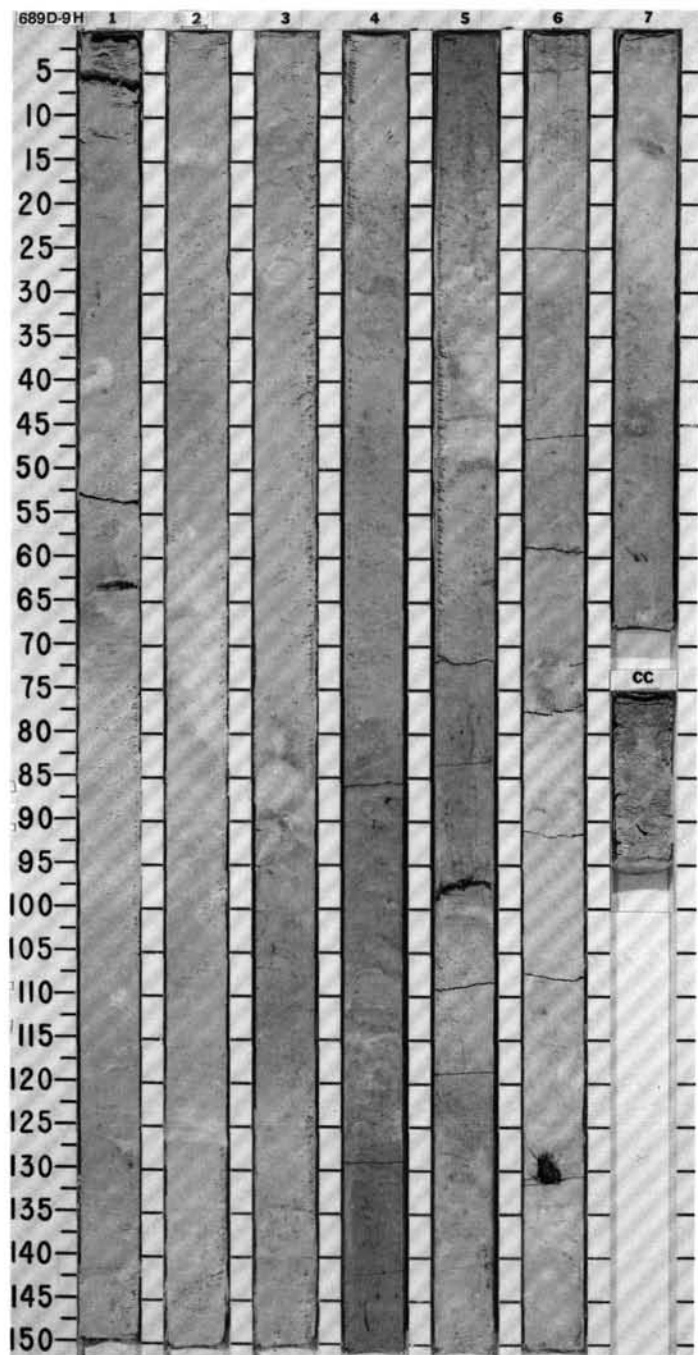
TIME-ROCK UNIT	BIOSTRAT. ZONE/ FOSSIL CHARACTER				PHYS. PROPERTIES	CHEMISTRY	SECTION	METERS	GRAPHIC LITHOLOGY	DRILLING DISTURB.	SED. STRUCTURES	SAMPLES	LITHOLOGIC DESCRIPTION																																																															
	FORAMINIFERS	NANNOFOSSILS	RADIOLARIANS	DIATOMS	PALYNOFORMS	PALEOMAGNETICS																																																																						
UPPER OLIGOCENE													NANNOFOSSIL OOZE and FORAMINIFER-BEARING NANNOFOSSIL OOZE Major lithologies: Nannofossil ooze, white (2.5Y 8/2) to light gray (2.5Y 7/2). Foraminifer-bearing nannofossil ooze, light gray (2.5Y 7/2). Bioturbation is predominantly minor to moderate and includes <i>Planolites</i> and <i>Zoophycos</i> . Small manganese nodules occur in Section 6, 80-90 cm. SMEAR SLIDE SUMMARY (%): <table><tr><td></td><td>1, 50 D</td><td>2, 50 D</td><td>3, 50 D</td><td>4, 50 D</td><td>5, 50 D</td><td>6, 50 D</td></tr><tr><td>COMPOSITION:</td><td></td><td></td><td></td><td></td><td></td><td></td></tr><tr><td>Quartz</td><td>1</td><td>Tr</td><td>Tr</td><td>Tr</td><td>2</td><td>1</td></tr><tr><td>Volcanic glass</td><td>—</td><td>—</td><td>—</td><td>Tr</td><td>Tr</td><td>—</td></tr><tr><td>Foraminifers</td><td>Tr</td><td>Tr</td><td>1</td><td>—</td><td>6</td><td>11</td></tr><tr><td>Nannofossils</td><td>97</td><td>90</td><td>93</td><td>99</td><td>84</td><td>80</td></tr><tr><td>Diatoms</td><td>—</td><td>6</td><td>2</td><td>Tr</td><td>3</td><td>2</td></tr><tr><td>Radiolarians</td><td>—</td><td>2</td><td>3</td><td>1</td><td>7</td><td>7</td></tr><tr><td>Silicoflagellates</td><td>3</td><td>2</td><td>1</td><td>Tr</td><td>—</td><td>Tr</td></tr></table>		1, 50 D	2, 50 D	3, 50 D	4, 50 D	5, 50 D	6, 50 D	COMPOSITION:							Quartz	1	Tr	Tr	Tr	2	1	Volcanic glass	—	—	—	Tr	Tr	—	Foraminifers	Tr	Tr	1	—	6	11	Nannofossils	97	90	93	99	84	80	Diatoms	—	6	2	Tr	3	2	Radiolarians	—	2	3	1	7	7	Silicoflagellates	3	2	1	Tr	—	Tr
	1, 50 D	2, 50 D	3, 50 D	4, 50 D	5, 50 D	6, 50 D																																																																						
COMPOSITION:																																																																												
Quartz	1	Tr	Tr	Tr	2	1																																																																						
Volcanic glass	—	—	—	Tr	Tr	—																																																																						
Foraminifers	Tr	Tr	1	—	6	11																																																																						
Nannofossils	97	90	93	99	84	80																																																																						
Diatoms	—	6	2	Tr	3	2																																																																						
Radiolarians	—	2	3	1	7	7																																																																						
Silicoflagellates	3	2	1	Tr	—	Tr																																																																						
								0.5				*																																																																
								1.0																																																																				
								2				*																																																																
								3				*																																																																
								4				*																																																																
								5				*																																																																
								6				*																																																																
								7				*																																																																
								CC																																																																				



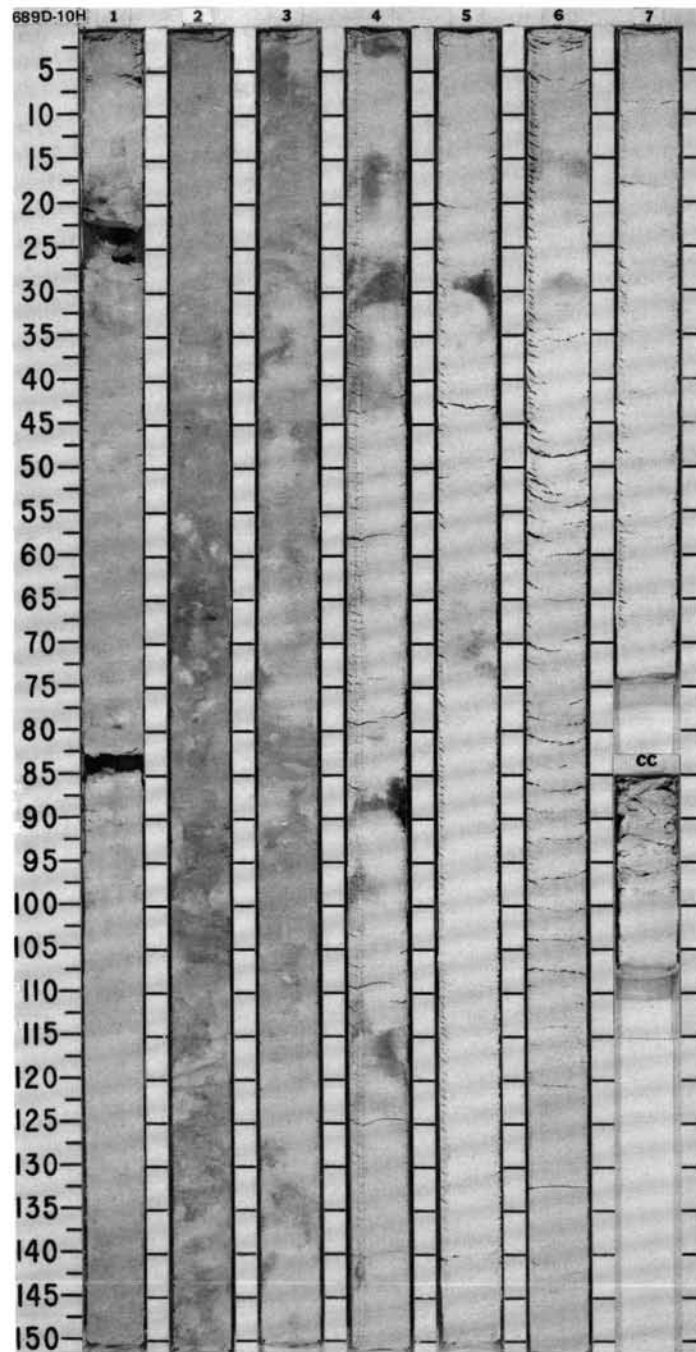
SITE 689

SITE 689 HOLE D CORE 9H CORED INTERVAL 2175.4-2185.0 mbsl; 95.2-104.8 mbsf

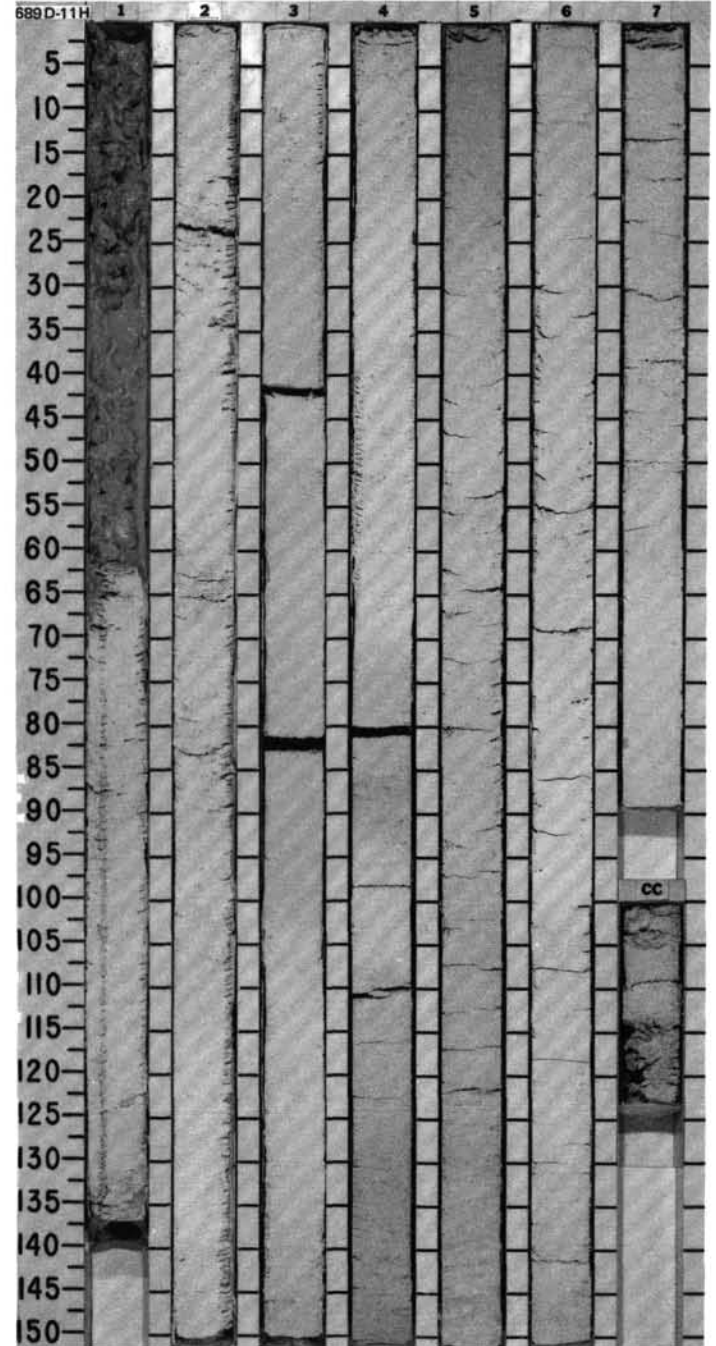
OLIGOCENE									
TIME-ROCK UNIT	BIOSTRAT. ZONE/ FOSSIL CHARACTER								
	FORAMINIFERS	NANNOFOSSILS	RADIODIATARS	DIATOMS	PALYNOFOSPHS				
	PALEOMAGNETICS								
	PHYS. PROPERTIES								
	CHEMISTRY								
	SECTION	METERS	GRAPHIC LITHOLOGY			DRILLING DISTURB.	SED. STRUCTURES	SAMPLES	LITHOLOGIC DESCRIPTION
		0.5							NANNOFOSSIL OOZE
	1	1.0							Major lithology: Nannofossil ooze, white (10YR 8/2), pale brown (10YR 8/3), and light gray (10YR 7/2).
									Moderate bioturbation is present throughout, and includes halo burrows. Color changes are subtle and gradational. Black speckles and a black layer in Section 5, 97 cm, are probably drilling grease.
									SMEAR SLIDE SUMMARY (%):
									1, 50 2, 50 3, 50 4, 50 5, 50 6, 50 D D D D D D
									COMPOSITION:
									Quartz Tr — — — —
									Volcanic glass Tr — — — —
									Foraminifers — 1 Tr 3 1 2
									Nannofossils 100 96 98 93 96 93
									Diatoms Tr Tr 2 2 3 2
									Radiolarians — 2 Tr 2 Tr 3
									Silicoflagellates — 1 — Tr — Tr



TIME-ROCK UNIT	BIOSTRAT. ZONE/ FOSSIL CHARACTER	SECTION	METERS	GRAPHIC LITHOLOGY	DRILLING DISTURB. SED. STRUCTURES	SAMPLES	LITHOLOGIC DESCRIPTION
LOWER Oligocene	FORAMINIFERS NANNOFOSSILS RADIOLARIANS DIATOMS PALYNOPOPHS PALEOMAGNETICS PHYS. PROPERTIES CHEMISTRY	1	0.5 1.0			*	DIATOM-BEARING FORAMINIFER-NANNOFOSSIL OOZE, RADIOLARIAN- AND FORAMINIFER-BEARING DIATOM-NANNOFOSSIL OOZE, RADIOLARIAN- AND FORAMINIFER-BEARING DIATOM-NANNOFOSSIL OOZE, and NANNOFOSSIL-SILICEOUS OOZE
		2				*	Major lithologies: Diatom-bearing foraminifer-nannofossil ooze, white (10YR 8/11, 8/2), and light gray (10YR 7/1). Foraminifer- and radiolarian-bearing diatom-nannofossil ooze, white (10YR 8/1). Radiolarian- and foraminifer-bearing diatom-nannofossil ooze, white (10YR 8/1). Nannofossil-siliceous ooze, white (10YR 8/1). Percentages of the different microfossil groups change gradually as the sediment goes from a dominantly calcareous to a dominantly siliceous ooze downhole.
		3				*	Bioturbation is minor to moderate in the upper three sections and includes halo burrows and <i>Zoophycos</i> .
		4				*	SMEAR SLIDE SUMMARY (%):
		5				*	COMPOSITION:
		6				*	
		7				*	
		CC					
		B					



SITE	689	HOLE	D	CORE	11H	CORED INTERVAL	2194.6-2204.3 mbsl; 114.4-124.1 mbsf
------	-----	------	---	------	-----	----------------	--------------------------------------

[illegible]

[illegible]